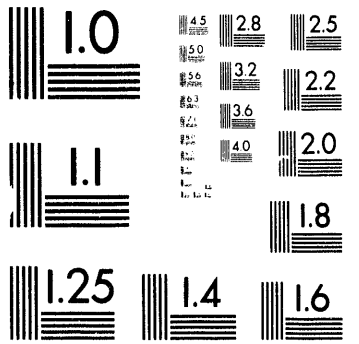
1.0
1.1
1.25
1.4
1.6
1.8
2.0
2.2
2.5
2.8
3.2
3.6
4.0
4.5
5.0
5.6
6.3

1 of 3

LBL-34872

Coordination Chemistry of Two Heavy Metals: I. Ligand Preferences in Lead(II) Complexation, Toward the Development of Therapeutic Agents for Lead Poisoning. II. Plutonium Solubility and Speciation Relevant to the Environment.

Mary Patricia Neu

Ph. D. Thesis

Department of Chemistry
University of California
Berkeley, CA 94720

and

Glenn T. Seaborg Institute for Transactinium Science
Lawrence Livermore National Laboratory
Livermore, CA 94551

and

Nuclear Science Division
Lawrence Berkeley Laboratory
Berkeley, CA 94720

November 1993

MASTER

This research was supported in part by the U.S. Department of Energy through the Glenn T. Seaborg Institute for Transactinium Science, Lawrence Livermore National Laboratory through the U.S. Department of Energy under Contracts W-7405ENG48 (LLNL) and DE-AC03-76SF00098 (LBL).

DISTRIBUTION OF THIS DOCUMENT IS UNLIMITED

Abstract

Coordination Chemistry of Two Heavy Metals:
I. Ligand Preferences in Lead Complexation, Toward the Development of Therapeutic Agents for Lead Poisoning
II. Plutonium Solubility and Speciation Relevant to the Environment

by

Mary Patricia Neu

Doctor of Philosophy in Chemistry

University of California at Berkeley

Professor Darleane C. Hoffman, Chair

The coordination chemistry and solution behavior of the toxic ions lead(II) and plutonium(IV, V, VI) have been investigated. The ligand pK_as and ligand-lead(II) stability constants of one hydroxamic acid and four thiohydroaxamic acids were determined. Solution thermodynamic results indicate that thiohydroxamic acids are more acidic and slightly better lead chelators than hydroxamates, e.g., N-methylthioaceto-hydroxamic acid, $pK_a = 5.94$, $\log\beta_{120} = 10.92$; acetohydroxamic acid, $pK_a = 9.34$, $\log\beta_{120} = 9.52$. The syntheses of lead complexes of two bulky hydroxamate ligands are presented. The X-ray crystal structures show the lead hydroxamates are di-bridged dimers with irregular five-coordinate geometry about the metal atom and a stereochemically active lone pair of electrons. Molecular orbital calculations of a lead hydroxamate and a highly symmetric pseudo octahedral lead complex were performed.

The thermodynamic stability of plutonium(IV) complexes of the siderophore, desferrioxamine B (DFO), and two octadentate derivatives of DFO were investigated using competition spectrophotometric titrations. The stability constant measured for the plutonium(IV) complex of DFO-methylterephthalamide is $\log\beta_{110} = 41.7$.

The solubility limited speciation of ^{242}Pu as a function of time in near neutral carbonate solution was measured. Individual solutions of plutonium in a single oxidation state were added to individual solutions at pH = 6.0, T = 30.0, 1.93 mM dissolved carbonate, and sampled over intervals up to 150 days. Plutonium solubility was measured, and speciation was investigated using laser photoacoustic spectroscopy and chemical methods.

Solubility data show that plutonium(IV) initially falls out of solution, resolubilizes over the next 5 days, and at 22 days the concentration of soluble plutonium is 1.0×10^{-6} M. The plutonium(V) solution has a soluble plutonium concentration of 2.1×10^{-5} M over a time of 53 days and is > 95% PuO_2^+. Plutonium(VI) exhibits the most interesting solution behavior. Immediately after preparation of 1.9 to 3.7×10^{-4} M PuO_2^{2+} solutions, some of the plutonium becomes insoluble and a different soluble species forms, probably $PuO_2(OH)^+$. Within hours PuO_2^+ forms, and within a few days, becomes the dominant soluble species. After several months only 1-2% of the plutonium added initally remains in solution and is essentially all PuO_2^+.

Darleane C. Hoffman

Dedication:

To my mother, Janette,
and to my sisters, Barbara and Diane...

They wondered if I should, and always told me I could.

Table of Contents

List of Figures

List of Tables

Acknowledgements

I have been very privledged to work with many incredible and talented people during my tenure as a graduate student. First and foremost, I thank Professor Darleane Hoffman, an amazingly generous and gifted research director, for her wisdom and guidance. She provides an incomparable model of a kind, strong, dedicated person who can accomplish anything. I will always be grateful for the support and opportunities she has given me. I thank Professor Ken Raymond for his support, patience, and insight, and for allowing me the freedom to learn by doing. I thank the professors at the University of Alaska for teaching me and introducing me to research, especially Professor Richard Stolzberg, my undergraduate research director.

I am indebted to the Hoffman, Nitsche, Russo, Raymond, and Silva research groups for their magnanimity of space, equipment, and experience. I thank all the past and present group members, too numerous to mention inclusively, for befriending me, teaching me, and providing a fertile atmosphere for research. I thank several people whose zeal for science (and life!) is inspirational, and whose support I value highly: Maureen Tortorelli, Rick Russo, Dave Wruck, Greg Klunder, John Andrews, Ann Kinzig, Chris Wilisch, Steve Keller, Margaret Geselbracht, and my Raymond Group Contemporaries: Torin Dewey, Barb Bryan, Tim Karpshin, and Ken Czerwinski. For sharing great times in the outdoors, and introducing me to runnning and ultimate frisbee, I thank Stephanie Robertson, Brad Chmelka, and Joel Gohdes. For encouraging me to run harder and "stay strong", I thank the "Striders", especially Babak Kadkhodyan, Ken Gregorich, Malia Dinnell, and most especially, Christina Hannan, Jill Cartwright and Matt Urdan.

The credit for getting me to finish this research and dissertation belongs to Joel Gohdes whose amazed responses to my doubts always helped me move forward. I will thank him forever for renewing my faith. I thank my brother, Brad, who taught me that academic work is rewarding. And I thank my wonderful parents and family, who give me constant support and encouragement.

I want to thank the scientists with whom I collaborated on some of the projects described herein, and acknowledge their contributions. Professor Kamal Abu-Dari helped me get started in graduate research; and generously synthesized samples of the following compounds for solution thermodynamic studies: N-methylthioacetohydroxamic acid, N-methylthioformohydroxamic acid, m-hydroxy-N-methylthiobenzohydroxamic acid, and 2-pyridinethiol-1-oxide-6-carboxylic acid.

I thank Professor Chis Orvig, who synthesized N-toluyl-*tert*butylhydroxamic acid, and Dr. Susan Barclay, who synthesized N-phenyl-toluylhydroxamic acid, for samples used to make lead(II) complexes. The characterization and structure determination of the compound, tetra(N-phenyltoluylhydroxamato)-di-lead(II) was performed in collaboration with Dr. Andrew Borovik, who synthesized the compound. Victor Christou, George Lucier, and Chad Sofield determined the structure of tetra(μ-N-toluyl-*tert*-butyl-hydroxamato)-tetra(μ-acetato)-tetralead(II) as a X-ray crystallography course requirement. The plutonium(IV)-desferrioxamine project was done in collaboration with Donald W. Whisenhunt, Jr. Samples of the methyl sulfonate salt of desferrioxamine were provided by Nicomed/Salutar; samples of DFOMTA were synthesized and donated by Dr. Jide Xu; and samples of DFOHOPO were synthesized and donated by Dr. Jean-Claude Chambron. I thank Dr. Pat Grant for kindly donating lab space for the plutonium(IV)-desferrioxamine project. I especially thank Dr. Heino Nitsche and Dr. Bob Silva for their help in the initiation and support of the plutonium solubility and speciation project. The photoacoustic spectrometer used in the plutonium speciation project was built in collaboration with Dr. Rick Russo, and Dr. Dave Wruck and Dr. Greg Klunder provided great technical assistance. Dr. Richard Torres wrote the photoacoustic spectra data acquisition programs. Nancy Hannink contributed to setting up the inert atmosphere box and associated equipment. Ray Gatti and Kevin Roberts provided expertise on the plutonium oxidation state distribution/solvent extraction procedures. Kevin Roberts assisted with solvent extractions for the comparison of photoacoustic spectroscopy and extraction methods for the determination of plutonium oxidation state distributions. I thank John Andrews who is always giving of his time and expertise. I thank Dr. Joel Gohdes for encouraging me to do molecular orbital calculations and Ryan Powers for helping me with molecular modeling.

I am thankful to the U.S. Department of Energy's Heavy Element Production Program at Oak Ridge National Laboratory for the ^{242}Pu used in this work. I thank the Glenn T. Seaborg Institute for Transactinium Science for financial support of my graduate research.

Introduction: Coordination Chemistry of Two Toxic Heavy Metals

As the world continues to shrink in mankind's view due to technological advances, and we recognize the interconnectedness of biological systems, one of our greatest challenges is to protect ourselves and our natural resources from the materials we mine or make. For several thousand years man has been using grey, malleable lead, whose physical and chemical properties make it a most versatile material. And in the last several decades man has produced plutonium, whose nuclear properties make it an inherently awesome substance. Unfortunately, both lead and plutonium are potentially extremely harmful, making their utility strongly dependent on our understanding and control of their chemical behavior and environmental distributions. For example, utilization of nuclear power is limited largely by concerns of potential release of radioactivity to the environment and risks associated with fuel use and waste disposal. These issues are being addressed by waste treatment, handling and storage methods development, and radionuclide environmental chemistry research.

This dissertation on the coordination chemistry of two toxic heavy metals has two sections: First is a report of research on compounds that may be useful in removing lead from aqueous solutions. Second is research within two branches of plutonium chemistry relevant to the environment: selective binding of plutonium(IV), and plutonium solubility and speciation under conditions approximating groundwater.

I. Lead(II) Human Toxicity and Coordination Chemistry

Lead Utility and Toxicity. Lead is an extremely prevalent and versatile metal. The Romans used lead extensively, not only for water pipes and cooking utensils, but also in winemaking.[1] Since that time it has been used in: pigments, glazes, plastic stabilizers, brass alloys, crystal making, plumbing, shot, batteries, antiknock fuel additives, ferroelectric materials, lead casting and type setting.[2-4] A grave consequence of lead's utility is its pervasive presence. Lead is found in varying concentrations in wine, paint, pottery, pewter, plaster, old newsprint, cosmetics, dust, tobacco, utensils, food, milk, herbal medicines, water, soil, air, and unfortunately, in the human body.[5,6] Lead is introduced into the body through inhalation, ingestion, and skin penetration.[6] The intake of lead in Roman times is estimated to have varied from about 35 to 250 mg/day[1], compared to estimates of modern daily intake from 0.3 mg/day[1] to 28-38 mg/day[7] generally, and up to 335 mg/day[8] in heavy industrial areas. Body content normally ranges from 100 to 400 milligrams in 70 kg of body weight, increasing with age. Under

normal exposure conditions the body is able to store some lead that enters the body and excrete the balance without adverse health effects. [9]

Lead was one of the first chemical materials to be recognized as hazardous to health under heavy exposure. Nriagu, after reviewing the lifestyle and habits of persons living at the time of the Roman Empire, suggests that the pandemic occurrence of saturntine gout among the upper classes and the eventual decline of the Roman Empire were due to lead poisoning.[10] The field of occupational disease has its origins with craftsman and artisans - potters and painters working with lead have been historically attacked by various ailments. The Greek philosopher Nikander of Colophon in 250 BC first reported the colic and anemia of lead poisoning. And it has been suggested that it was lead poisoning, not schizophrenia or syphilis, that mysteriously disturbed Goya and that it also accounted for van Gogh's insanity. "Both painters were partial to white lead and to the heavily leaded Naples yellow and van Gogh was on at least one occasion seen to actually eat some paint."[11] Amazingly the modes by which people are poisoned by lead have not changed significantly in thousands of years, these are ingestion of veneers or drugs, and industrial exposures. Children eating chunks of peeling paint and slivers of glazed putty or contacting lead-laden soils and adults ingesting lead salts or moonshine prepared in lead-containing stills, or experiencing heavy exposure in their workplace, account for the vast majority of poisoning cases .[1,9,12-14]

When inorganic lead is inhaled it is estimated that between 30-50 percent is absorbed and rapidly enters circulation. Lead absorbed from the gastrointestinal tract passes to the liver and back into the duodenum through the bile, with 10 to 15 percent absorbed into the bloodstream and soft tissue. After absorption, about 50-60 percent of the lead is excreted from the blood through the kidneys at a fairly slow rate.[9,13] Of the remaining lead more than 95% becomes firmly bound to bone, probably to hydroxyapatite, and the rest is distributed to teeth, hair, liver, spleen, brain and kidney. Lead will continue to be excreted via continuous exchange with the soft tissue pool.[1] Gross estimates of the biological half-life of lead are: total body - 5 years, bones - 10 to 20 years, soft tissue - 20 days, and renal system - 1-2 days, with absorption and excretion rates dependent on age, diet and metabolism.[1,7]

Health effects associated with lead toxicity are numerous.[1,2,5,9,12,13,15-18] High levels of lead in the body affect the gastrointestinal, hematopoietic, renal, and nervous systems. Acute effects of extremely high lead levels include gastrointestinal cholic (pale skin, slow pulse, and increased blood pressure), encephalopathy and peripheral nerve damage (more common in children, usually associated with pica) which may lead to seizures, comas, and death. Chronic effects include anemia, headaches, convulsions,

inflammation of the kidneys, certral nervous system disorders (most often associated with alkyl lead poisoning) and brain damage. In both adults and children, most early symptoms of neurotoxicity are nonspecific, including defective memory, irritability, mental dullness, inability to concentrate, fatigue, weakness, nervousness, insomnia and anxiety.[1] Early manifestations are followed by more severe disturbances of the nervous system, gastrointestinal, and haematological and endocrine abnormalities. Arthritis and muscle pain are common in lead intoxication, as are hypertension and/or gout.[1] The peripheral nerves most often injured are the motor nerves supplying the most actively used muscles of the body. Industrial workers, for example, experience forearm weakness and "wrist drop."[5]

The toxicity of lead is due, in general, to its binding of thiol and cellular phosphate groups of numerous enzymes, proteins, and cell membranes.[3,7] Lead inhibits or interferes in the functioning of: δ-aminolevulinic acid (ALA) dehydratase, ferrochelatase, nucleotidase, acetylcholine-esterase, glucose-6-phosphate dehydrogenase, acid phosphatase, ATP-ase, guanase, brain and pancreatic adenylate cyclase, and possibly carbonic anhydrase.[1,12,19-22] It also inhibits protein synthesis, probably by modifying transfer -RNA, and the functions of all enzymes containing cysteine residues, at least to some extent.[1] Lead affects the concentration and turnover rate of the putative neurotransmitters noradrenaline and dopamine[23,24] and inhibits two enzymes involved in norepinephrine metabolism, phenylethanolamine-N-methyltransferase and dopamine-β-hydroxylase.[25] Another effect is the formation of intranuclear acid-fast inclusions within the proximal renal tubular lining cells and hepatocytes. A blue lead sulfide line may appear at the gingival margins in chronic lead intoxication, which is caused by hydrogen sulfide, produced in bacterial degradation, reacting with lead.[1,13]

Diagnosis of lead poisoning relies on high blood content of lead, urinary excretion of lead, free erythrocyte protoporphyrin, or δ-aminolevulinic acid, basophilic stippling of red blood cells, and/or X-rays or [illegible]F measurements indicating lead lines.[1,5,12] Because lead is cleared from the blood rapidly, levels are extremely low in all cases and patients with suspected lead intoxication are given EDTA, so stored lead levels can be estimated. Measured post chelation lead excretion levels above 350 micrograms in 72 hours are considered suggestive of intoxication.[1]

There has been a progressive decline in the lowest observed exposure-effect levels.[17,26-29] The level of lead in blood considered dangerous enough to warrant medical attention in children has declined from approximately 60 μg/dL in the 1960s to 25 μg/dL in 1984[17] to current action levels of one reading of 20 μg/dL or multiple testings of 15μg/dL.[30] It has been extimated that 1.9% of children in the U.S. have blood lead

levels greater than 30 μg/dL, and that greater than 10% of children aged 1-6 in the inner city areas have elevated serum lead concentrations.[1] Despite efforts to curb lead poisoning, the number of children in industrial areas recorded in the lead registry with high blood lead levels[31] and the numbers at risk remain alarmingly high.[32] In the San Francisco Bay Area alone it is estimated that up to 114,500 children may have lead in their bloodstreams exceeding safe levels set by the Environmental Protection Agency.[33] Public outcry based on the low levels which are now considered toxic prompted the Environmental Defense Fund to propose legislative action to curb "an epidemic of childhood lead poisoning."[34] Current lead abatement and soil remediation projects[35,36] will help alleviate lead sources, but the magnitude of the problem ensures it will remain a public health concern for many years.

Current Chelating Therapy Agents. Treatment for lead poisoning includes removal from exposure, minimization of absorption (inactivation of the gastrointestinal tract), and partial elimination of absorbed lead via diuresis, dialysis, and chelation. Prior to the development of chelating agents, 65% of severe cases of lead poisoning had fatal outcomes.[1] The use of chelating agents for lead decorporation in children was presented in the landmark study by Chisolm,[15] and has been reviewed for the treatment of children and adults by others.[1,16,37-39] Ligands often used for lead chelation therapy are shown in Figure 1.

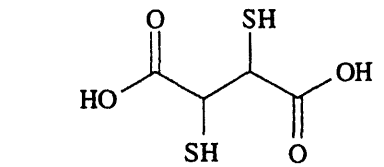

meso-2,3-Dimercaptosuccinic Acid (DMSA)

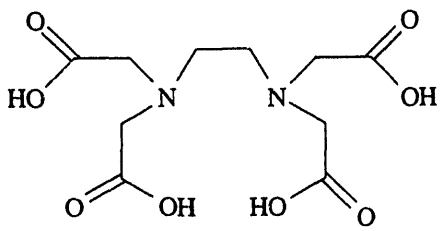

Ethylenediaminetetraacetic Acid (EDTA)
(calcium di-sodium salt used)

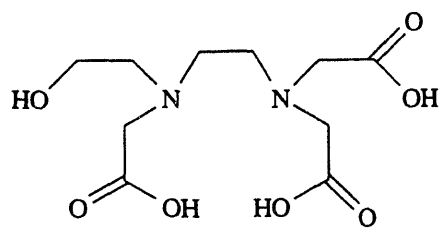

Hydroxyethyl-EDTA
(sodium salt used)

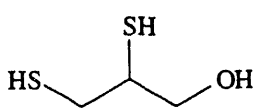

1,2-Dimercaptopropanol
(known as British AntiLewisite, BAL)

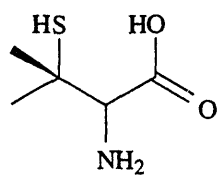

β,β-Dimethyl-D-cysteine
(known as Penicillamine)

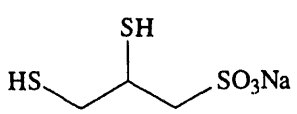

Dimercaptopropanesulfate, DMPS
(sodium salt used)

Figure 1. Chelating agents used in the treatment of lead poisoning.

Ethylenediaminetetraacetic acid (EDTA) is the most widely used therapeutic agent.[40-42] Three hours after EDTA administration the concentration of lead in blood peaks; δ-ALA dehydrase activity is maximal five hours after treatment; and approximately 39% of the body burden of accessible lead is mobilized and excreted in the

urine within 24 hours.[1,43] While EDTA and the hydroxyethyl derivative, HEDTA, are effective in partially removing lead from the body, there are some problems with their use. When administered as the disodium calcium salt, EDTA promotes the excretion of beneficial metal ions: zinc, copper, manganese, and iron.[38,42,44] In fact, animal studies show that virtually no zinc-metallothionein[45] remains in the kidney 24 hours after $CaNa_2EDTA$ injection.[46] EDTA is also reported to have a teratogenic effect.[47] The sources of lead mobilized in response to $CaNa_2EDTA$ treatment are debated (from blood, hemopoietic tissue, extracellular space, spongy bone, bone, etc.).[40,43,48] One study found that the standard $CaNa_2EDTA$ treatment has little impact on critical organs such as the brain and liver, and moreover EDTA may mobilize lead from bone and kidney and deliver it to the brain and liver.[48] Another criticism is that EDTA actually intensifies the inhibition exerted by lead on ALA dehydrase and other sulfhydryl-dependent enzymes.[48]

British AntiLewisite (BAL), 1,2-mercaptopropanol, is another commonly used effective chelating agent with some undesireable side effects. In Europe BAL has apparently been rejected as a lead poisoning treatment agent.[15] When used in North America it is typically given in conjunction with EDTA.[15,49,50] It has been proposed that BAL readily enters red cells and delivers lead to extracellular EDTA, yielding EDTA-Pb for elimination via urine. Chisolm reported that the combined EDTA, BAL treatment was faster, and ALA was excreted at lower levels, than when EDTA was used alone.[15] BAL has a hypertensive effect, apparently due to inhibition of carboxypeptidase. Other side effects include: nausea, vomiting, lacrimation, tachycardia and severe headache.[1,51] Both BAL and EDTA must be administered intravenously, a painful process which precludes outpatient treatment.

A less effective lead removal agent[52], penicillamine, was the only chelator administered orally as of 1988.[53] In a study of 84 treated subjects and 37 controls, Shannon and coworkers found that penicillamine was effective in increasing the excretion of lead. However, 33% of the subjects had an associated adverse reaction and treatment was terminated in 10% of cases.[54] In addition to side affects associated with its use[1,5,54] penicillamine is limited because it cannot be given to patients who are allergic to penicillin.[52]

The most promising orally administered lead chelating agent, *meso*-dimercaptosuccinic acid (DMSA), was first studied in the clinical treatment of lead poisoning in the late 1970s[51,55] and approved for use in humans in 1991.[56] Metabolites of the drug, and not DMSA itself, may be responsible for lead excretion from the body.[57,58] Biotransformation products containing disulfide linkages to plasma protein in the blood, and to L-cysteine in urine, have been recovered.[59] Clinical studies show that

DMSA is effective, and may have fewer and less detrimental associated effects than other chelating agents.[60-66] Graziano and coworkers found effects on a liver enzyme for some subjects in one clinical study[63] and slightly increased excretion of copper and zinc in another.[67] Grandjean and coworkers suggest there may be side effects associated with relatively high doses and/or long treatment schedules.[60] The evaluation of DMSA is ongoing.

Several other compounds have been considered as lead chelating agents, including: dithiocarbamates, sodium dimercaptopropanesulfonate[68], S-adenosyl-L-methionine[69], and N-Acetylcysteine[70,71] and found to be unsuitable. The dithiocarbamates, for example, reportedly remove lead from bone and deliver it to the brain.[72,73] The preventive and therapeutic role of vitamins B and C in lead toxicity has also been investigated.[74-77]

Lead(II) Coordination Chemistry and Our Approach to Ligand Design. Despite the long history of lead poisoning, the vast numbers of people affected, and the problems associated with current pharmaceuticals, the fact remains that there are no therapeutic chelating agents which have been designed specifically for lead(II). In attempting to design new chelating agents we recognize a number of desireable characteristics. The ligand and its lead complex must be soluble and highly kinetically and thermodynamically stable under *in vivo* conditions so the lead complex will form in body fluids and be rapidly excreted through renal or biliary routes. The ligand should be nontoxic, selective for lead(II) over essential cations, especially zinc(II), iron(II,III), manganese(II), and calcium(II), and ideally, synthesized inexpensively and easily, and be appropriate for oral administration. While the ligand attributes described above are nontrivial to achieve, there are clear structural features which are likely to supply them, with the exception of ensured specificity.

Because the lead(II) ion has only s valence electrons, guides used to predict the coordination geometry of d-block metals, such as ligand field stabilization, are not useful.[78] Metal ions may be categorized using the generalized acid-base concept of Lewis as "hard" or "soft" electron pair acceptors[79,80], where the soft atom is of low positive charge, large size and has polarizable outer electrons and the hard atom is of high positive charge, small size and has no easily polarized outer electrons. Typically a soft cation will covalently bond with a donor atom which has low electronegativity, highly polarizable low-lying empty orbitals and is easily oxidized, and a hard cation will form an ionic bond with a donor atom which has high electronegativity, low polarizability, high energy empty orbitals and is hard to oxidize. In contrast to biologically useful harder transition metals, lead(II) is considered a softer or borderline hard/soft cation and should

interact most strongly with softer donor types. The affinity of sulfur and oxygen donors for lead is clearly indicated from the biotoxicity. Hancock and coworkers use relatively soft neutral oxygen donors within macrocycles to increase selectivity for the large lead(II) ion relative to the small zinc(II) ion.[81] Another useful coordination chemistry trend, that five-membered chelate rings are better than six membered rings for most large metal ions,[82] may be used to select for lead(II) over zinc(II).

It is well known that linking functional groups together in a fashion appropriate to make a multidentate ligand, leads to a remarkable enhancement in the thermodynamic stability of metal-ligand complexes formed (the chelate effect).[82,83] Unfortunately, it is not clear how many functional groups and what configuration is optimal for lead(II) since it does not show strongly dominant coordination features like many other cations (four-coordinate, square planar, nickel(II), for example). Indeed, lead(II) complexes have coordination numbers ranging from 3 to 12 and arrangements of these atoms about the lead ion is typically irregular or very distorted.[3,84] Even the simple oxides and hydroxides contain a variety of structural groups including pyramidal PbO_4 in PbO_2[3], a Pb_4O_4 cube in $[Pb_4(OH)_4](ClO_4)_4 \cdot 2H_2O$[85], a distorted tetrahedron with facial capping hydroxyl groups in $[Pb_4(OH)_4]_3(CO_3)(ClO_4)_{10} \cdot 6H_2O$ and $[Pb_4(OH)_4)(ClO_4)_4]$[86], and a remarkable Pb_8O_4 group in $Pb_9O_4Br_{10}$[87]. Lead is most like tin, its immediate congener, however the introduction of inner shell, $4f^{14}$, electrons results in a higher effective nuclear charge affecting the outer shell electrons, and thus a relative increase in ionization potential and shrinkage in size for lead.[88]

One feature found in most tin and many lead solid state structures is the irregular spacing of donor groups about the central metal atom caused by the s^2 pair of valence electrons. Zachariasen first noticed that central atoms with certain numbers of valence electrons seem to be displaced from the centers of their respective coordination polyhedra.[89] The unshared inert pair of electrons were proposed to lie at the root of the geometrical distortion.[90] This stereochemical effect of the electron pair was elaborated by Gillespie and Nyholm who treat the lone pair as a distinct class of electron sets.[91] Lone pairs are generally treated as a ligand in modern molecular models because the lone-pair electrons usually contain considerable bonding and hybrid character.[92] Although the principles of electron pair repulsion can be applied to predict the geometry of tetravalent and simple bivalent compounds, as Harrison points out in his review of group IV metals, "the factors underlying the stereochemistry of tin(II) and lead(II) compounds in the solid state can often be more subtle, and hence not so readily understood."[86]

Armed with some general ideas about what might bind the lead(II) ion and very specific ligand requirements we began to study thiohydroxamates, as subunits which could be encorporated into highly specific lead chelating agents. (Figure 2).

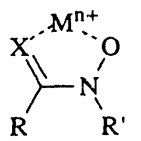

X = S, thiohydroxamate
X = O, hydroxamate

Figure 2. Thiohydroxamate and hydroxamate metal (M^{n+}) chelates. Showing the five-membered chelate ring and the thione/carboxyl ligang structure.

Interest in the chemistry of thiohydroxamic acids grew when the copper complex of N-methylthioformohydroxamic acid was isolated from cultures of *Pseudomonas fluorescens*. and discovered to have antibiotic properties.[93-95] The synthesis, chemical stability, and initial metal complexation chemistry of thiohydroxamic acids had been investigated previously by Nagata and others.[96-98] Bis(thiohydroxamato)copper(II) complexes were shown to have *trans* square planar geometry by Becher et al.[99] using electron spin resonance spectroscopy and by Taylor using X-ray crystallography.[100,101] Several other thiohydroxamate transition metal complexes have been prepared and characterized to investigate the chemistry of the complexes and probe the mechanism of antiobiotic activity (including cobalt(I), chromium(III), and iron(III);[101-104] manganese(IV);[105] ruthenium(III);[106] rhodium(III) and platinum(II)[107]).

The thiohydroxamates contain oxygen and sulfur donor atoms, both of which bond strongly with lead, as illustrated by lead's interference with thiol and phosphate groups in biological systems. Mixed donor atom ligands, like DMSA[108,109] and penicillamine[110], form stable complexes with lead. The "soft" thione group may form complexes with "softer" lead in the presence of "hard" metals, and should be more stable with respect to oxidation and *in vivo* disulfide formation than thiolate groups. Thiohydroxamic acids are water soluble, weakly acidic ligands which should form lead complexes under physiological conditions (pH = 7.4, 37°C, μ = 0.1). Since thiohydroxamates are naturally occurring they may be less toxic and be better tolerated than other chelating ligands.

This work is an initial effort toward developing highly stable, selective, nontoxic lead chelators, focusing on the synthesis, characterization, structure and stability determination of simple hydroxamate and thiohydroxamate ligands and their lead complexes. Hydroxamic acids, oxygen analogs of thiohyroxamic acids, are included in

this research to provide comparison betweeen all oxygen and mixed sulfur, oxygen ligands, and because there is interest in their lead chelating abilities as well. (For example, hydroxamates have been used in lead(II) ion selective electrodes[111] and for the removal of lead and copper from industrial effluents.[112]) Determination of the equilibrium constants for the formation of lead hydroxamate and thiohydroxamate compounds with lead is reported in the first section of Part I, and the synthesis and structural characterization of three hydroxamate lead complexes is presented in the second section of Part I.

References

(1) Ibels, L. S.; Pollock, C. A. *Med. Toxic.* **1986**, *1*, 387.

(2) Moore, M. R.; Campbell, B. C.; Goldberg, A. In *The Chemical Environment*; J. Lenihan and W. W. Fletcher, Ed.; Academic Press: New York, 1977; Vol. 6; pp 64-92.

(3) Greenwood, N. N.; Earnshaw, A. *Chemistry of the Elements*; Pergamon Press: Oxford, 1984.

(4) Widely used lead compounds include: pigments, Pb_3O_4, Ca_2PbO_4, $CaPbO_3$ (red), $PbCrO_4$ (yellow), $PbMoO_4$ (red-orange), PbO (red, orange, or yellow), $2PbCO_3 \cdot Pb(OH)_2$ (white); pottery glaze, $PbSi_2O_5$, battery material, PbO_2, antiknock fuel additives, $Pb(CH_3)_4$, $Pb(CH_2CH_3)_4$; and ferroelectric materials $PbTiO_3$, $PbZrO_3$, $PbNb_2O_6$, $PbTi_2O_6$, $PbO \cdot nFe_2O3$ (n = 6,5,2.5,1,0.5).

(5) Angle, C. R.; McIntire, M. S. *Paediatrician* **1977**, *6*, 204. and references therein.

(6) Ratcliffe, J. M. *Lead in Man and the Environment*; John Wiley & Sons: New York, 1981.

(7) *Lead*; Green, V. A.; Wise, G. W.; Callenbach, J. C., Ed.; Marcel Dekker Inc.: New York, 1978, pp 123.

(8) *Handbook on the Toxicity of Metals*; Tsuchiya, K., Ed.; Elsevier: North Holland, 1985.

(9) Putnam, R. D. *Am. Ind. Hyg. Assoc. J.* **1986**, *47(11)*, 700.

(10) Nriagu, J. O. *New Engl. J. Med.* **1983**, *308*, 660.

(11) Roueché, B. "Annals of Medicine: Cinnabar" In *The New Yorker*; December 8, 1986; p. 94.

(12) *Drug and Chemical Injury-Environmental Pathology*; 7th ed.; Anderson, W. A. D.; Kissane, J. M., Ed.; C. V. Mosby Co.: St. Louis, 1977; Vol. 1.

(13) *Environmental Pathology-Chemical and Drug Injury*; 2nd ed.; Robbins, S. L.; Cotran, R. S., Ed.; W. B. Saunders: Philadelphia, 1979, pp 537.

(14) Allcott, J. V.; Barnhart, R. A.; Mooney, L. A. *J. Am. Med. Assoc.* **1987**, *258(4)*, 510.

(15) Chisolm, J. J. *J. Pediatrics* **1968**, *73*, 1.

(16) Clarkson, T. W.; DiStefano, V. In *Drill's Pharmacology in Medicine*; 4 ed.; J. R. DiPalma, Ed.; McGraw-Hill: New York, 1971; pp 1101.

(17) Davis, J. M.; Svendsaard, D. J. *Nature* **1987**, *329(24)*, 297.

(18) Kazantzis In *Poisoning, Diagnosis and Treatment*; J. A. Vale and T. J. Meredith, Ed.; Update Books: London, 1981; pp 171.

(19) Farkas, W. R.; Stanawitz, T. *J. Inorg. Biochem.* **1989**, *11*, 31.

(20) Lachant, N. A.; Tomoda, A.; Tanaka, K. R. *Blood* **1984**, *63(3)*, 518.

(21) Raghavan, S. R. V.; Culver, B. D.; Gonick, H. C. *J. Toxic. Environ. Health* **1981**, *7*, 561.
and references therein.

(22) Nathanson, J. A. *J. Pharm. Pharmac.* **1977**, *29*, 511.

(23) Silbergeld, E. K.; Chisolm, J. J. *Science* **1976**, *192*, 153.

(24) Moresco, R. M.; Dall'olio, R.; Gandolfi, O.; Govoni, S.; Di Giovine, S.; Trabucchi, M. *Toxicology* **1988**, *53*, 315.

(25) Unni, L. K.; Caspers, M. L. *Biochem. Pharm.* **1984**, *33(13)*, 2149.

(26) Needleman, H. L. *Contemporary Pediatrics* **1988**, *A*, 34.

(27) Thatcher, R. W.; Lester, M. L.; McAlaster, R.; Horst, R. *Environ. Health* **1982**, *37*, 159.

(28) David, O. J.; Hoffman, S.; Kagey, B. *Trace Substances* **1979**, 52.

(29) Marlowe, M.; Errera, J.; Stellern, J.; Beck, D. *J. Orthomol. Psychiat.* **1983**, *132*, 260.

(30) Personal communication, Alameda County Department of Environmental Health, July, 1993.

(31) Schneider, D. J.; Lavenhar, M. A. *Am. J. Public Health* **1986**, *76(3)*, 242.

(32) Kay, J. "Alarming Lead Levels in Children" In *San Francisco Chronicle*; June 26, 1988; p. 1.

(33) Edison, A. "Lead Poisoning Risk to 114,500 Bay Kids" In *San Francisco Examiner*; March 6, 1990; p. 1.

(34) Florini, K. L.; Krumbhaar, G. D.; Silbergeld, E. K. "Legacy of Lead: America's Continuing Epidemic of Childhood Lead Poisoning," Environmental Defense Fund, 1990.

(35) Krishnamurthy, S. *Environ. Prog.* **1992**, *11(4)*, 256.

(36) Peters, R. W.; Shem, L. In *Remediation of Lead-Contaminated Soils*; Proc. Intl. Symp. on Energy, Environ. and Inform. Mgmt.; Chicago, IL; 1992, 3.

(37) See for example: Sahu, S. *Paediatrician* **1977**, *6*, 262.

(38) Garrettson, L. K. In *Clinical Management of Poisoning and Drug Overdose*; L. M. Haddad and J. F. Winchester, Ed.; W. B. Saunders: 1983; pp 649.

(39) David, O. J.; Katz, S.; Arcoleo, C. G.; Clark, J. *Arch. of Environ. Health* **1985**, *40(2)*, 109.

(40) Batuman, V.; Wedeen, R. P.; Bogden, J. D.; Balestra, D. J.; Jones, K.; Schidlovsky, G. *Environmental Research* **1989**, *48*, 70.

(41) Cicchella, G.; Arcangeli, G.; Rizzardini, L. *The Science of the Total Environment* **1988**, *71*, 551.

(42) Thomas, D. J.; Chisolm, J. J. *The Journal of Pharmacology and Experimental Therapeutics* **1986**, *239(3)*, 829.

(43) Flood, P. R.; Schmidt, P. F.; Wesenberg, G. R.; Gadeholt, H. *Arch. Toxicol.* **1988**, *62*, 295.

(44) Victery, W.; Miller, C. R.; Goyer, R. A. *J. Lab. Clin. Med.* **1986**, *107*, 129.

(45) Metallothioneins (MT) are an extensively studied group of heavy metal binding proteins which are produced in response to high levels of metal ions such as cadmium, zinc, mercury, copper, and possibly lead.
A few informative MT references are:
Kojima, Y.; Kägi, J. H. R. *Trends in Biological Science* **1978**, *4*, 90.
Nielson, K. B.; Atkin, C. L.; Winge, D. R. *J. Biological Chemistry* **1985**, *260(9)*, 5342.
Matsumoto, Y.; Okada, Y.; Min, K.-S.; Tanaka, K. *Chem. Pharm. Bull.* **1990**, *38*, 2112.

(46) Miller, C. R.; Zhu, S.; Victery, W.; Goyer, R. A. *Toxicol. and Appl. Pharm.* **1986**, *84*, 584.

(47) Brownie, C. F.; Brownie, C.; Noden, D.; Krook, L.; Haluska, M.; Aronson, A. L. *Toxicol. and Appl. Pharm.* **1986**, *82*, 426.

(48) Cory-Slechta, D. A.; Weiss, B.; Cox, C. *J. Pharm. and Exp. Ther.* **1987**, *243(3)*, 804.

(49) Haust, H. L.; Ali, H.; Haines, D. S. M.; Forret, C. J. *Int. J. Biochem.* **1980**, *12*, 897.

(50) Abu-Melha, A.; Ahmed, N. A.; El Hassan, A. Y. *Tropical and Geographical Medicine* **1987**, *39*, 100.

(51) Friedheim, D.; Graziano, J. H.; Popovac, D.; Dragovic, D.; Kaul, B. *Lancet* **1978**, *12*, 1234.

(52) Chisolm, J. J. *Mod. Treat.* **1971**, *8*, 593.

(53) Beattie, A. D. *Proceedings of the Royal Society of Medicine* **1977**, *70(S3)*,

(54) Shannon, M.; Graef, J.; Lovejoy, F. H. *J. Pediatrics* **1988**, ,

(55) Graziano, J. H.; Leong, J. K.; Friedheim, E. *J. Pharm. and Exp. Ther.* **1978**, *206(3)*, 696.

(56) Nightingale, S. L. *J. Am. Med. Assoc.* **1991**, *265*, 1802.

(57) Rivera, M.; Zheng, W.; Aposhian, H. V.; Fernando, Q. *Toxic. and Appl. Pharm.* **1989**, *100*, 96.

(58) Maiorino, R. M.; Bruce, D. C.; Aposhian, H. V. *Toxic. and Appl. Pharm.* **1989**, *97*, 338.

(59) Aposhian, H. V.; Aposhian, M. M. *Ann. Rev. Pharm. Toxicol.* **1990**, *30*, 279.

(60) Grandjean, P.; Jacobsen, A.; Jorgensen, P. J. *Pharm. and Toxic.* **1991**, *68*, 266.

(61) Bentur, Y.; Brook, J. G.; Behar, R.; Taitelman, U. *Clin/ Toxicol.* **1987**, *25(1&2)*, 39.

(62) Cory-Slechta, D. A. *J. Pharm. and Exp. Ther.* **1988**, *246(1)*, 84.

(63) Graziano, J. H.; Siris, E. S.; LoIacono, N.; Silverberg, S. J.; Turgeon, L. *Clin. Pharmacol. Ther.* **1985**, *37(4)*, 431.

(64) Graziano, J. H.; LoIacono, N.; Meyer, P. *J. Pediatrics* **1988**, *13(4)*,

(65) Kapoor, S. C.; Wielopolski, L.; Graziano, J. H.; LoIacono, N. J. *Toxicol. and Appl. Pharm.* **1989**, *97*, 525.

(66) Mitchell, w. G.; Jones, M. M. *J. Inorg. Nucl. Chem.* **1978**, *40*, 1957.

(67) Graziano, J. H., personal communication, 1990.

(68) Twarog, T. A.; Cherian, M. G. *Bull. Environm. Contam. Toxicol.* **1983**, *30*, 165.

(69) Paredes, S. R.; Fukuda, H.; Kozicki, P. A.; Rossetti, M. V.; Conti, H.; Batlle, A. M. C. *Ecotox. and Environ. Safety* **1986**, *12*, 252.

(70) Banner, W.; Koch, M.; Capin, D. M.; Hopf, S. B.; Chang, S.; Tong, T. G. *Toxicol. and Appl. Pharm.* **1986**, *83*, 142.

(71) Ottenwälder, H.; Simon, P. *Arch. Toxicol.* **1987**, *60*, 401.

(72) Oskarsson, A.; Lind, D. *Acta Pharmacol. Tox.* **1985**, *56*, 309.

(73) Oskarsson, A. *Environ. Res.* **1987**, *44*, 82.

(74) Flora, S. J. S.; Tandon, S. K. *Acta Pharm. and Toxicol.* **1986**, *58*, 374.

(75) Dhawan, M.; Kachru, D. N.; Tandon, S. K. *Arch. Toxicol.* **1988**, *62*, 301.

(76) Saxena, R. K.; Chandel, C. P. S.; Gupta, C. M. *Indian J. Chem.* **1989**, *28A*, 625.

(77) Tandon, S. K.; Flora, S. J. S.; Singh, S. *Bull. Environ. Contam. Toxicol.* **1986**, *37*, 317.

(78) Figgis, B. N. *Introduction to Ligand Fields*; John Wiley & Sons: New York, 1961, pp 351.

(79) Pearson, R. G. *J. Am. Chem. Soc.* **1963**, *85*, 3533.

(80) Pearson, R. G. *Coord. Chem. Rev.* **1990**, *100*, 403.

(81) Hancock, R. D.; Bhavan, R.; Wade, P. W.; Boeyens, J. C. A.; M., D. S. *Inorg. Chem.* **1989**, *28*, 187.

(82) Busch, D. H.; Stephenson, N. A. *Coord. Chem. Rev.* **1990**, *100*, 119.

(83) Schwarzenbach *Helv. Chim. Acta* **1952**, *35*, 2344.

(84) *Structural Inorganic Chemistry*; 5th ed.; Wells, A. F., Ed.; Clarendon Press: Oxford, 1986.

(85) Hong, S. H.; Olin, A. *Acta Chem. Scand.* **1974**, *A28*, 233.

(86) Harrison, P. G. In *Comprehensive Coordination Chemistry*; G. Wilkinson, Ed.; Pergamon Press: Oxford, 1987; Vol. 3; pp 183.

(87) Keller, H. *Angew. Chem. Int. Ed. Engl.* **1983**, *22(4)*, 324.

(88) Huheey, J. E. *Inorganic Chemistry: Principles of Structure and Reactivity*; Harper and Row: New York, 1983.

(89) Zachariasen, W. H. *Phys. Rev.* **1932**, *40*, 917.

(90) Ng, S.-W.; Zuckerman, J. J. *Adv. Inorg. Chem. Radiochem.* **1985**, *29*,

(91) Gillespie, R. J.; Nyholm, R. S. *Q. Rev. Chem. Soc.* **1957**, *11*, 339.

(92) Shustorovich, E.; Dobosh, P. A. *J. Am. Chem. Soc.* **1979**, *101*, 4090.

(93) Egawa, Y.; Umino, K.; Ito, Y.; Okuda, T. *J. Antibiot.* **1971**, *24*, 124.

(94) Itoh, S.; Inuzuka, K.; Suzuki, T. J. *J. Antibiot.* **1970**, *23*, 542.

(95) Shirahata, K.; Hayashi, T.; Matsubara, I. *J. Antibiot.* **1971**, *24*, 140.

(96) Mizukami, S.; Nagata, K. *Chem. Pharm. Bull.* **1966**, *14(11)*, 1249.

(97) Nagata, K.; Mizukami, S. *Chem. Pharm. Bull.* **1966**, *14(11)*, 1255.

(98) Walter, W.; Schaumann, E. *Synthesis* **1971**, *3*, 111.

(99) Becher, J.; Brockway, D. J.; Murray, K. S.; Newman, P. J.; Toftlund, H. *Inorg. Chem.* **1982**, *21*, 1791.

(100) Taylor, D. *Cryst. Struct. Comm.* **1978**, *7*, 237.

(101) Freyberg, D. P.; Abu-Dari, K.; Raymond, K. N. *Inorg. Chem.* **1979**, *18*, 3037.

(102) Abu-Dari, K.; Raymond, K. N. *Inorg. Chem.* **1977**, *16*, 807.

(103) Abu-Dari, K.; Freyberg, D.; Raymond, K. N. *Inorg. Chem.* **1979**, *18(9)*, 2427.

(104) Abu-Dari, K.; Ekstrand, J. D.; Freyberg, D. P.; Raymond, K. N. *Inorg. Chem.* **1979**, *18*, 108.

(105) Pal, S.; Ghosh, P.; Chakravorty, A. *Inorg. Chem.* **1985**, *24*, 3704.

(106) Bhattacharya, S.; Ghosh, P.; Chakravorty, A. *Inorg. Chem.* **1985**, *24*, 3224, and references therein.

(107) Leong, J.; Bell, S. J. *Inorg. Chem.* **1978**, *17(7)*, 1886.

(108) Willes, M. J.; Williams, D. R. *Inorg. Chim. Acta* **1985**, *106*, L21.

(109) Harris, W. R.; Chen, Y.; Stenback, J.; Shah, B. *J. Coord. Chem.* **1991**, *23*, 173.

(110) Doornbos, D. A.; Faber, J. S. *Pharm. Weekblad* **1964**, *99*, 289.

(111) Anuar, K.; Hamdan, S. *Talanta* **1992**, *39(12)*, 1653.

(112) Mendez, R.; Pillai, V. N. S. *Analyst* **1990**, *115*, 213.

II. Plutonium Solubility and Speciation in the Environment

The potential for plutonium dispersion in the biosphere is of importance because it is used in nuclear weapons and power reactors. Plutonium is toxic because of both its chemical and nuclear properties, and is the most prevalent transuranium environmental contaminant. Understanding the migration of plutonium under environmental conditions, including its solubility, chemical speciation, and kinetic and thermodynamic behavior in groundwater is crucial to the solution of radioactive waste disposal and containment problems.

Plutonium in the Environment. With a half-life comparable to the age of the earth, uranium is the heaviest element found in macroscopic quantities in nature.[1,2] Very small amounts of plutonium are naturally occurring: ^{244}Pu has been isolated from a precambrian bastnasite ore mined in California; [3] and ^{239}Pu is produced via neutron capture in ^{238}U in very pure uranium deposits (eq.1).[4] Neutrons from the very small spontaneous fission branch of ^{238}U may be captured, or after moderation the neutrons can also cause fission of ^{235}U (eq.1) which generates additional neutrons. Conditions under which natural nuclear reactors are formed are improbable. The remarkable open-pit uranium mine at Olko, Africa, contains pockets of concentrated ore that at one time achieved all the conditions necessary for a fission chain reaction and which still contain immobilized fission products.[5]

$$^{238}U + {}^{1}_{0}n \longrightarrow {}^{239}U \xrightarrow{\beta^-} {}^{239}Np \xrightarrow{\beta^-} {}^{239}Pu \xrightarrow{\alpha} \qquad (1)$$

Plutonium-238, 239 isotopes were first produced by man in February of 1941 and since that time more than six tons of plutonium have been released to the biosphere.[1] The sources of plutonium include satellite power sources, nuclear weapons, nuclear power reactors, and plutonium production, but most of the plutonium in the atmosphere and ground is from nuclear weapons testing.[1] Fortunately, the release conditions (very high temperature) make it likely that plutonium was dispersed as the oxide form which was deposited in soil and sediments, and it is estimated that less than 1% is resident in the biota.[1] With the ban of atmospheric testing of nuclear weapons by the U.S., U.K. and former U.S.S.R. and improvements in nuclear power reactor design, the future release of plutonium to the environment will depend largely on the containment of materials associated with existing weapons and reactor fuel production, use, and reprocessing, the treatment and disposal of transuranic waste, and weapons testing conducted by countries which do not have test bans. Plutonium waste is composed mostly of the isotopes ^{238}Pu, ^{239}Pu, and ^{240}Pu, which have relatively long half-lives and decay via alpha emission and

^{241}Pu, a shorter lived beta emitter, which decays to ^{241}Am. The nuclear properties of these nuclides are listed in Table 1.

Table 1. Nuclear Properties of Plutonium Isotopes and ^{241}Am Which are Enviromental Contaminants.[6]

Isotope	Emission	Half-life (years)
^{238}Pu	α	87.7
^{239}Pu	α	24,110
^{240}Pu	α	6,563
^{241}Pu	β	14.4
^{241}Am	α	433

Plutonium in Groundwater. The unique chemical properties of plutonium, in particular the number of stable oxidation states, with accompanying disproportionation reactions, and the reactivity with ubiquitous carbonate and hydroxide ions, result in many environmentally important equilibria. Stable solution species of plutonium are the solvated Pu^{3+}, Pu^{4+} and the solvated linear dioxo ions, PuO_2^+, PuO_2^{2+}. The Pu(VIII) oxidation state has been proposed as PuO_5^{3-}, PuO_6^{5-}, $[PuO_4(OH)_2)\beta^-$, and $[PuO_2(OH)_6]^{3-}$ in the classic references by Seaborg and Loveland[1], Cotton and Wilkinson,[7] Greenwood and Earnshaw[8], and Choppin,[9] respectively, but it is reduced in both acidic and basic solutions and, therefore not applicable to environmental studies. Separated by approximately one volt, Pu^{3+}, Pu^{4+}, PuO_2^+, and PuO_2^{2+} may be present in solution simultaneously. Recently Riglet, Robouch, and Vitorge[10] reevaluated existing data, redetermined the redox couples, (Pu^{3+}, Pu^{4+}) and (PuO_2^+, PuO_2^{2+}) and reported the following standard potentials:

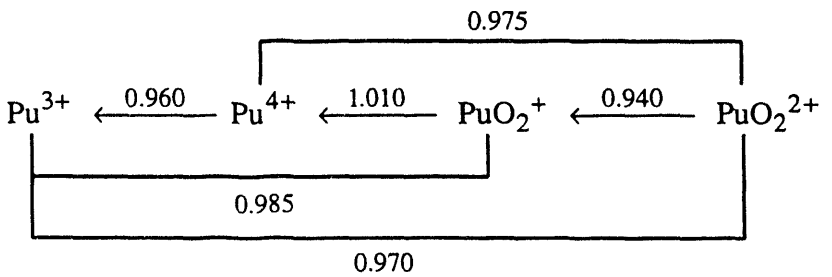

Potentials in volts vs. neutral hydrogen electrode (NHE), in 1 M $HClO_4$, at 25°C

In addition to electron transfer reations, there are a number of disproportionation reactions, (2)-(6) below, which govern the oxidation state distributions.[1,7,11]

$$3Pu^{4+} + 2H_2O \longrightarrow 2Pu^{3+} + PuO_2^{2+} + 4H^+ \quad (2)$$

$$2PuO_2^{+} + 2H^+ \longrightarrow Pu^{4+} + PuO_2^{2+} + H_2O \quad (3)$$

$$2Pu^{4+} + 2H_2O \longrightarrow Pu^{3+} + PuO_2^{+} + 4H^+ \quad (4)$$

$$PuO_2^{+} + Pu^{4+} \longrightarrow PuO_2^{2+} + Pu^{3+} \quad (5)$$

$$3PuO_2^{+} + 4H^+ \longrightarrow Pu^{3+} + 2\,PuO_2^{2+} + 2H_2O \quad (6)$$

The equilibrium quotient for the four dominant species, Pu(III-IV), is 10.7 at 25°C in molar perchloric acid .[12]

$$\frac{\left[PuO_2^{2+}\right]\left[Pu^{3+}\right]}{\left[PuO_2^{+}\right]\left[Pu^{4+}\right]} = 10.7 \quad (7)$$

In general, higher oxidation states (PuO_2^+ and PuO_2^{2+}) are more stable under basic conditions, lower oxidation states (Pu^{3+} and Pu^{4+}) are more stable under acidic conditions, and disproportionations involving bond breaking or bond forming are very slow relative to electron transfer reactions. Under most environmental conditions Pu^{3+} is a less important species because it is oxidixed to Pu^{4+}. Known to disproportionate at high concentrations and in acidic solutions, PuO_2^+ is stable at low concentrations[13] and is the dominant oxidation state of tracer concentrations of plutonium in many natural waters.[14]

The pH of aqueous solutions will not only stabilize certain oxidation states with respect to disproportiation, but will also dictate what ionic or neutral products are formed by the interaction with water. The order of hydrolysis is: $Pu^{4+}>PuO_2^{2+}>Pu^{3+}>PuO_2^+$ and the respective pH values of the onset of hydrolysis are(in order): 0, 4-5, ~6-8, 9-10. The order of hydration entropy, $Pu^{4+}>Pu^{3+}>PuO_2^{2+}>PuO_2^+$ is different because hydrolysis depends on direct interaction with the metal, while hydration depends on electrostatic interaction with the ionic species.[9] The effective charges of the PuO_2^+ and PuO_2^{2+} ions, deduced from the hydrolysis behavior, are ~2.2 and 3.3, respectively.[15] Plutonium(IV) hydrolysis is complicated by the generation of an isoluble polymer whose structure and composition depends on a number of factors, including but not limited to temperature, radiolysis, pH, plutonium concentration, ions present, and time since

formation. Figure 3 is a scheme summarizing Pu^{4+} hydrous polymer chemistry as described by Toth et al. and others.[1,16-18]

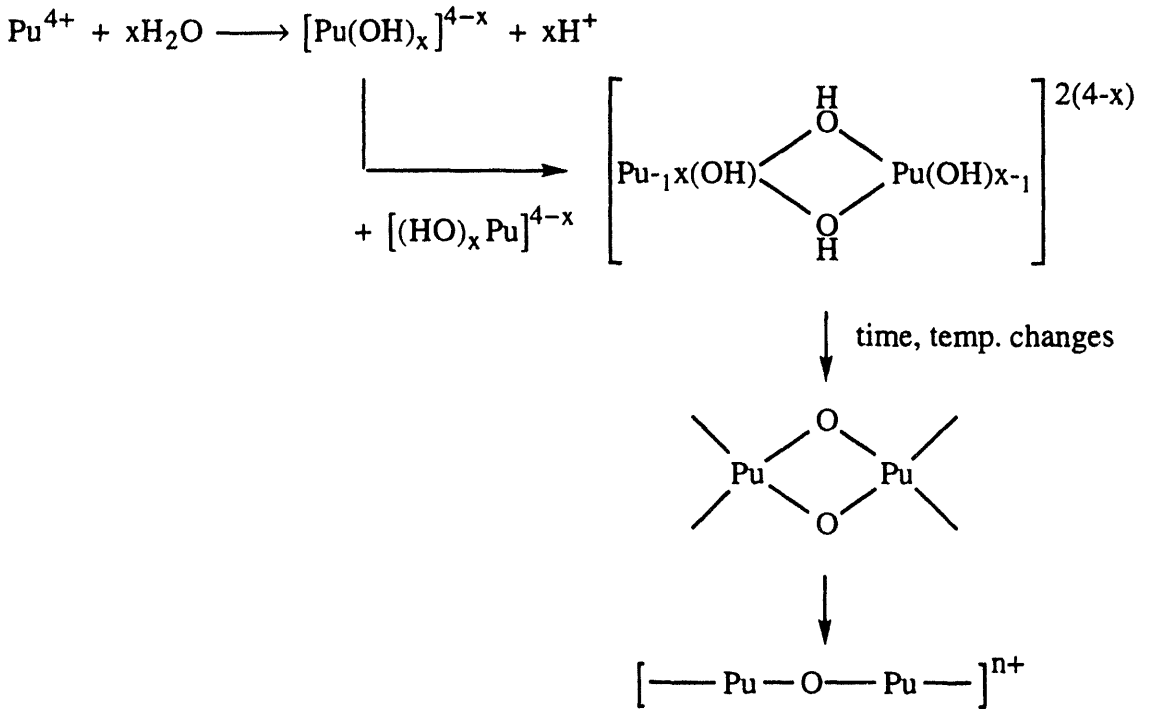

Figure 3. Plutonium hydrous polymer chemistry.

The plutonium ions are "hard" cations and the complexation strength mimics the hydrolysis order given above. Environmentally, waters include numerous ligands (in addition to hydroxide) present at significant concentrations ; among them are carbonate, bicarbonate, phosphate, and the organic acids, fulvates and humates.[2] Plutonium hydrolysis and carbonate equilibria alone consistute a complex aqueous system which is being researched extensively.[9,14,19-22] The speciation (oxidation state, formula, structure) of plutonium in a relatively carbonate-rich solution, which is a model for a specific groundwater, will be discussed in the second section of Part II.

Coordination Chemistry of Plutonium(IV). Plutonium(IV) is the dominant oxidation state at high concentrations of acid and nitrate,[12] conditions common in plutonium production/reprocessing wastes, as exemplified by contents of the underground storage tanks at the facility in Hanford, Washington.[23] Treatment of waste streams prior to disposal and clean-up of transuranic contaminated sites requires separating long-lived plutonium isotopes from solution.

When designing plutonium-specific complexing agents, Raymond and coworkers recognize and use the similarities between Fe^{3+} and Pu^{4+}.[24-28] The charge to ionic radius[29] ratios are almost the same, 0.46 for 6-coordinate Fe^{3+}, 0.42 for 8-coordinate Pu^{4+}, and their hydrolysis constants[30] are similar (eq. 8-11). Plutonium(IV), a "hard" cation, interacts strongly with "hard" donor groups like negatively charged oxygen as illustrated by large hydrolysis constants and the use of DTPA as a therapeutic plutonium decorporation agent.[31] Perhaps the strongest evidence that Fe^{3+} and Pu^{4+} are chemically similar is their transport and storage *in vivo*.[32-34] The Pu-transferrin complex is the principal plutonium binding species in blood plasma[31] and plutonium is stored in ferritin, hemosiderin, bone sialoprotein, and salivary proteins.[35] (Transferrin, ferritin, and hemosiderin are iron transport and storage proteins.[36])

$$Fe(OH)_3 \cdot \longleftrightarrow Fe^{3+} + 3OH^- \qquad K \approx 10^{-38};\ 10^{-12.6} \text{ per } OH^- \qquad (8)$$

$$Fe^{3+} + H_2O \longleftrightarrow Fe(OH)^{2+} + H^+ \qquad K = 0.0009 \qquad (9)$$

$$Pu(OH)_4 \longleftrightarrow Pu^{4+} + 4OH^- \qquad K \approx 10^{-55};\ 10^{-13.7} \text{ per } OH^- \qquad (10)$$

$$Pu^{4+} + H_2O \longleftrightarrow Pu(OH)^{3+} + H^+ \qquad K = 0.0301 \qquad (11)$$

Bacteria and other microorganisms produce siderophores, low molecular weight multidentate "iron carriers", to scavenge the ferric ion from their environment. Iron is solubilized and strongly bound by these highly Fe^{3+}-specific ligands.[37] Two siderophore functionalities, catecholate and hydroxamate groups, along with hydroxypyridinones, which also form strong complexes with the ferric ion,[38] are shown in Figure 4. The tri-hydroxamate siderophore, desferrioxamine B, (DFO, Figure 5) is produced by *streptomyces pilosus* and has a formation constant of $10^{30.6}$ with the ferric ion.[39] By analogy, Pu^{4+} should also be strongly bound by DFO. An important difference between the complexation chemistry of Pu^{4+} and Fe^{3+} is the desired coordination number - Fe^{3+} typically has a coordination number of six, while the larger Pu^{4+} ion is likely to have a coordination number of eight. The addition of a bidentate group to the terminal amine of the hexadentate DFO will yield a ligand which should bind plutonium even more strongly, and provide some selectivity on the basis of octadentate coordination. We are evaluating the thermodynamic stability constants for plutonium complexation by octadentate derivatives of desferrioxamine B as an inital step toward quantitatively removing plutonium from solution in waste treatment or bioremediation schemes.

Two projects in the realm of plutonium environmental chemistry are described in this dissertation: The complexation of plutonium by the iron(III) scavenger desferioxamine B and octadentate derivatives is described in the first section of Part II. An investigation of the solubility and speciation of plutonium in near-neutral carbonate solution is presented in the second section of Part II.

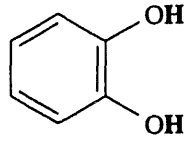

Catechol

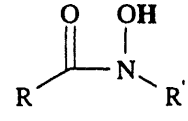

Hydroxamic Acid

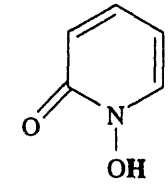

1-Hydroxy-2-(1H)-Pyridinone

Figure 4. Binding groups expected to form strong Pu^{4+} complexes based on known siderophore function and Fe^{3+} stability constants.
Protons released upon metal binding are shown in bold.

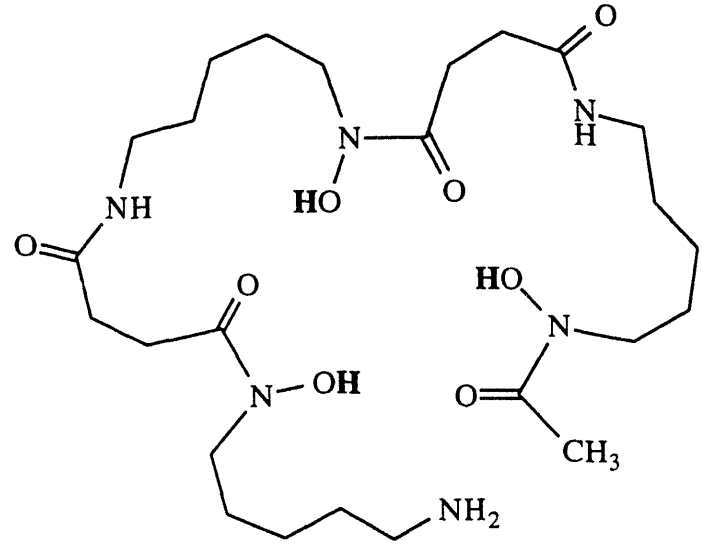

Figure 5. Desferrioxamine B, a naturally occurring siderophore.
Protons released upon metal binding are shown in bold.

References

(1) Seaborg, G. T.; Loveland, W. D. *The Elements Beyond Uranium*; Wiley & Sons: New York, 1990, pp 359.

(2) Hobart, D. E. In *Actinides in the Environment*; Procedings of Robert A. Welch Foundation Conference on Chemical Research XXXIV. Fifty Years with Transuranium Elements; Houston, TX; 1990, 379.

(3) Hoffman, D. C.; Lawrence, F. O.; Mewherter, J. L.; Rourke, F. M. *Nature* **1971**, *234*, 132.

(4) Seaborg, G. T.; Perlman, M. L. *J. Am. Chem. Soc.* **1948**, *70*, 1571.

(5) Cowan, G. A. *Scientific American* **1976**, *235(1)*, 36.

(6) *Table of Isotopes*; 7th ed.; Browne, E.; Dairiki, J. M.; Doebler, R. E.; Shihab-Eldin, a. A.; Jardine, L. J.; Tuli, J. K.; Buyrn, A. B., Ed.; Wiley & Sons: New York, 1978.

(7) Cotton, F. A.; Wilkinson, G. In *Advanced Inorganic Chemistry*; 5th ed.; Wiley: New York, 1988; pp 980.

(8) Greenwood, N. N.; Earnshaw, A. *Chemistry of the Elements*; Pergamon Press: Oxford, 1984.

(9) Choppin, G. R. In *Plutonium Chemistry*; #216 ed.; W. T. Carnall and G. R. Choppin, Ed.; American Chemical Society: Washington, D.C., 1983; pp 213.

(10) Riglet, C.; Robouch, P.; Vitorge, P. *Radiochim. Acta* **1989**, *46*, 85.

(11) Madic, C.; Begun, G. M.; Hobart, D. E.; Hahn, R. L. *Inorg. Chem.* **1984**, *23*, 1914.

(12) Katz, J. J.; Seaborg, G. T.; Morss, L. R. In *The Chemistry of the Actinide Elements*; Chapman and Hall: London, 1986; Vol. 1; pp 499-886.

(13) Nelson, D. M.; Lovett, M. B. *Nature* **1987**, *276*, 599.

(14) Choppin, G. R. *J. Radioanal. Nucl. Chem.* **1991**, *147(1)*, 109.

(15) Choppin, G. R.; Stout, B. E. *Chemistry in Britain* **1991**, *12*, 1126.

(16) Toth, L. M.; A., F. H.; Osborne, M. M. In *Plutonium Chemistry*; #216 ed.; W. T. Carnall and G. R. Choppin, Ed.; American Chemical Society: Washington, D.C., 1983; pp 231.

(17) Wester, D. W. In *Plutonium Chemistry*; #216 ed.; W. T. Carnall and G. R. Choppin, Ed.; American Chemical Society: Washington, D.C., 1983; pp 49.

(18) Kim, J. I.; Kanellakopulos, B. *Radiochimica Acta* **1989**, *33*, 8230.

(19) Kim, J. I.; Lierse, C.; Baumgärtner, F. In *Plutonium Chemistry*; #216 ed.; W. T. Carnall and G. R. Choppin, Ed.; American Chemical Society: Washington, D.C., 1983; pp 317.

(20) Allard, B.; Rydberg, J. In *Plutonium Chemistry*; #216 ed.; W. T. Carnall and G. R. Choppin, Ed.; American Chemical Society: Washington, D.C., 1983; pp 275.

(21) Bennett, D. A.; Hoffman, D.; Nitsche, H.; Russo, R. E.; Torres, R. A.; Baisden, P. A.; Andrews, J. E.; Palmer, C. E. A.; Silva, R. J. *Radiochimica Acta* **1992**, *56*, 15.

(22) The body of work in this area is extensive. The following reference is an actinide solubility study. Nitsche, H.; Müller, A.; Standifer, E. M.; Deinhammer, R. S.; Becraft, K.; Prussin, T.; Gatti, R. C. *Radiochimica Acta* **1992**, *58/59*, 27.

(23) Allen, G. K. "Estimated Inventory of Chemicals Added to Underground Waste Tanks, 1944 through 1975," Energy Research and Development Administration; Atlantic Richfield Hanford Company, ARH-CD-610B, 1976.

(24) White, D. L.; Durbin, P. W.; Jeung, N.; Raymond, K. N. *Journal of Medicinal Chemistry* **1988**, *31*, 11.

(25) Raymond, K. N.; Smith, W. L.; Weitl, F. L.; Durbin, P. W.; Jones, E. S.; Abu-Dari, K.; Sofen, S. R.; Cooper, S. R. In *Specific Sequestering Agents for the Actinides*; ACS Symposium Series, No. 131, Lanthanide and Actinide Chemistry and Spectroscopy; Washington, D.C.; 1979, 143.

(26) Kappel, M. J.; Nitsche, H.; Raymond, K. N. *Inorg. Chem.* **1985**, *24*, 605.

(27) Raymond, K. N. In *Specific Sequestering Agents for Iron and Actinides*; U.S. - Italy International Workshop on Environmental Inorganic Chemistry; San Miniato, Italy, June, 1983; 1985, 331.

(28) Uhlir, L. C.; Durbin, P. W.; Jeung, N.; Raymond, K. N. *J. Medicinal Chem.* **1993**, *36*, 504.

(29) Shannon, R. D. *Acta Cryst.* **1976**, *A32*, 751-767.

(30) Martell, A. E.; Smith, R. M. *Critical Stability Constants;* 1974, 1975, 1977, 1976, 1982,1989 ed.; Plenum: New York; Vol. 1-6.

(31) Taylor, D. M. In *Handbook on the Physics and Chemistry of the Actinides*; A. J. Freeman and C. Keller, Ed.; North-Holland, Elsevier: The Netherlands, 1991; Vol. 6; pp 533.

(32) Boocock, G.; Danpure, C. J.; Popplewell, D. S.; Taylor, D. M. *Radiat. Res.* **1970**, *42*, 381-396.

(33) Stover, B. J.; Bruenger, F. W.; Stevens, W. *Radiat. Res.* **1968**, *33*, 381-394.

(34) Durbin, P. W. *Health Physics* **1975**, *29*, 495-510.

(35) Thorne, M. C., ed. "The Metabolism of Plutonium and Related Elements," International Commission on Radiological Protection, ICRP #48, 1986.

(36) Stryer, L. *Biochemistry;* 2nd ed.; W. H. Freeman and Company: New York, 1981, pp 12.

(37) Matzanke, B. F.; Müller-Matzanke, G.; Raymond, K. N. In *Iron Carriers and Iron Proteins*; T. M. Loehr, Ed.; VCH Publishers: New York, 1989; pp 1-121.

(38) Kontoghiorghes, G. J. *Inorg. Chim. Acta* **1987**, *135*, 145.

(39) Konetschny-Rapp, S.; Jung, G.; Raymond, K. N.; Meiwes, J.; Zähner, H. *J. Am. Chem. Soc.* **1992**, *114*, 2224.

I. Ligand Preferences in Lead(II) Complexation, Toward the Development of Therapeutic Agents for Lead Poisoning

A. Potentiometric Determination of Lead(II) Thiohydroxamate and Hydroxamate Stability Constants

Introduction

Equilibrium constants for metal-ligand complex formation may be used as the measure of the strength of interaction between metals and ligands in solution.[1] This type of thermodynamic data is used to predict or compare: the metal complexing strengths of different donor groups in multidentate ligands, the overall affinity of ligands for a specific metal, and the relative affinities of a specific ligand for a variety of metals. The determination of ligand-lead(II) thermodynamic stability constants for thiohydroxamates (which have one oxygen and one sulfur ligand donor atom) and hydroxamates (all oxygen donors) is described in this section. By interpreting the thermodynamic data, we make some conclusions regarding differences between mixed sulfur and oxygen, and all oxygen donor sets in their affinity for lead(II) and in the nature of metal-ligand species present in solution as a function of pH. The thermodynamic data are compared with published formation constants for these types of ligands with other metals, and with values for ligands used in chelation therapy for the treatment of lead poisoning.

The proton association constants and lead(II) complex formation constants for the thiohydroxamate and hydroxamate ligands shown in Figure 6 were determined. In this procedure the first step is to measure the ligand protonation constants. Subsequently, the ligand protonation behavior in the presence of lead is determined. By measuring the hydrogen ion concentration of a solution containing constant total metal and ligand concentrations as a function of acid or base titrant added, thermodynamic parameters related to metal complexation involving proton transfer may be calculated.[2] The formation constant for lead(II) with N-methylthioacetohydroxamic acid was also determined using a lead-specific electrode. This method is attractive because the free metal ion concentration is measured directly, providing a second method of stability constant determination, independent of the hydrogen ion.

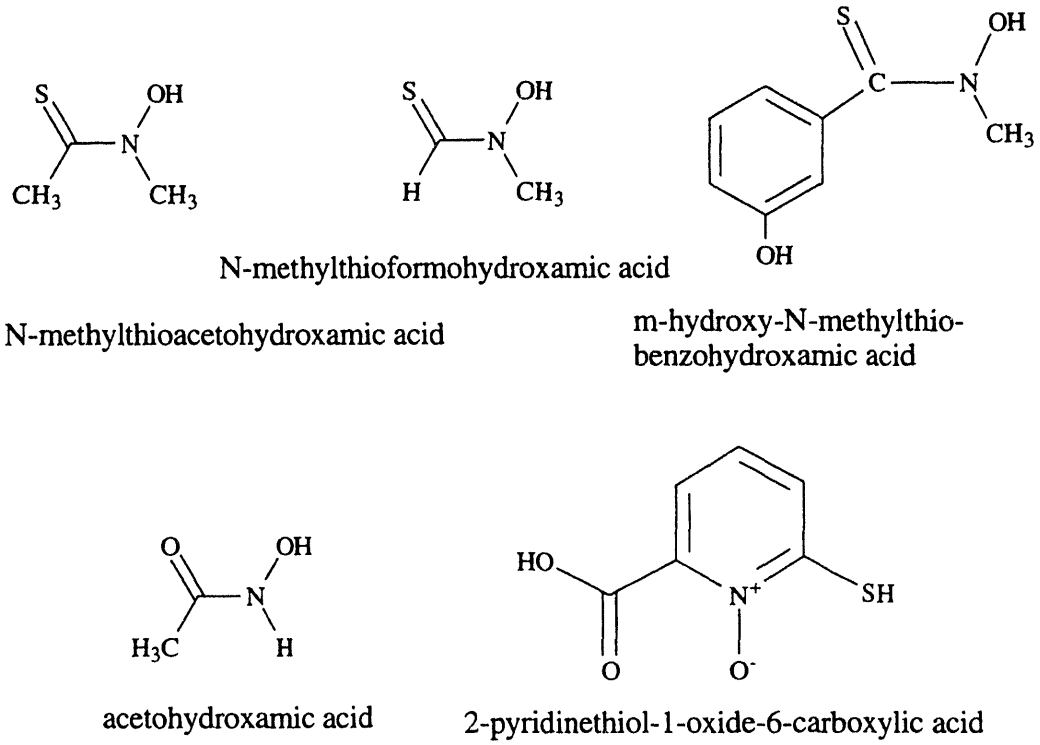

N-methylthioformohydroxamic acid

N-methylthioacetohydroxamic acid

m-hydroxy-N-methylthio-benzohydroxamic acid

acetohydroxamic acid

2-pyridinethiol-1-oxide-6-carboxylic acid

Figure 6. Thiohydroxamate and hydroxamate ligands studied.

Experimental

Potentiometric Titrations

pH Titration Apparatus. Two automated systems were assembled for the potentiometric determination of ligand protonation constants and metal-ligand formation constants. Titrators consisted of Model 655 Dosimat automatic burets equipped with 5 mL buret exchange units, a Fisher Model 925MP or 825 Accumet pH meter with Orion Ross combination pH electrodes, double-walled solution cells maintained at 25.0 ± 0.1°C by Brinkman Lauda K- 2/R constant temperature circulating baths, and a Fountain or IBM Personal Computer interfaced with the autoburet and the pH meter.

Solutions. Solutions were prepared using house deionized, distilled water, which was further deionized using a Millipore cartridge system (resistivity = 18 MΩ), and degassed by boiling for at least 30 minutes under an argon atmosphere. To avoid a decrease in pH due to dissolution of carbon dioxide before and during titrations, solutions were kept under an argon atmosphere which was pretreated by passing it through a Ridox oxygen scavenger (Fisher Scientific) and Ascarite (A.H. Thomas Scientific). Solution

ionic strength was adjusted to 0.100 M by using 0.100 M KNO_3 solution prepared from 99.999% KNO_3 (Aldrich). Titrant solutions were prepared from ampoules of concentrated solutions (Baker Dilut-It). The carbonate-free base (0.1 M KOH) was standardized against potassium hydrogen phthalate, the acid (0.1 M HNO_3) against the standardized KOH solution using phenolphthalein as an indicator. Degassed methanol was prepared by saturating the solution with N_2, followed by three cycles of freezing the solution, evacuating the flask, and thawing under N_2.

The pH electrode for titrations performed in 50% methanol was filled with a 26% methanol, 10% KNO_3 solution; otherwise standard 10% KNO_3 fill solution was used. (26% methanol was used in order to keep the fill and sample solutions as similar as possible, thereby minimizing differences in the electrode junction potentials.) For all experiments the electrode was calibrated in hydrogen ion concentration and p[H] was used, rather than hydrogen ion activity, pH. Immediately prior to each experiment the electrode was calibrated by titrating 2.00 mL of standardized HNO_3 in 25.0 or 50.0 mL of 0.100 M KNO_3 with standardized base. The electrode response in mV, was recorded after each addition of base. The calibration titration data were analyzed using a Marquardt, non-linear least squares refinement program using data in the ranges of -295 to -250 mV and +225 to +295 mV, similar to the treatment described by Leggett.[3] These millivolt ranges correspond to pH ranges of 11.1 to 11.8 and 2.0 to 2.7, respectively, where the electrode response is most linear.[4] Values for the standard electrode potential, E_o, and the electrode slope, S, were used to convert data in millivolts to p[H] for a titration immediately following according to:

$$p[H]_{obs} = (mV_{obs} - E_o) / S \qquad (1)$$

An estimate of the true concentration of the base titrant was also calculated from the calibration data, and used to monitor the integrity of the titrant solution following the method of Gran.[5] A value for pK_w defined in terms of concentration units, was also calculated from the electrode calibration titration data and used in the experimental data analysis.

The lead stock solution used in metal-ligand pH titrations was prepared by dissolving lead(II) nitrate (Aldrich) in distilled, deionized water, and stored under argon. The solution concentration was determined to be 48.86(9) mM by titration with EDTA (Aldrich, gold label, dried overnight) using xylenol orange as an indicator.[6]

Lead(II) standards for lead(II) electrode experiments were prepared as 50% methanol solutions by dilution of 0.1000(5) M lead perchlorate (Orion standard 948206), except the 0.1002 M standard which was prepared by dissolution of lead nitrate (Aldrich 99.999%). The N-methylacetothiohydroxamic acid solution used in the lead(II) electrode

experiments was prepared by dissolving the ligand (0.0604 mg) in 50% methanol (100 mL). All standard and sample solutions were buffered using formate (44.2 mL of 1.00 M formic acid, 5.0 mL of 1.00M sodium hydroxide diluted to 100mL) and adjusted to 0.100 ionic strength using sodium perchlorate.

Ligand Protonation Constants.

Ligand pK_a titrations were performed using approximately 1 mM ligand solution in 0.100 M KNO_3 with a stirring time of 15 sec after each addition of 0.005 to 0.020 mL of titrant. For N-methylthioacetohydroxamic acid and N-methylthioformohydroxamic acid titrations an appropriate volume of a stock ligand solution was added to the titration cell using a calibrated pipet (Gilmont); for acetohydroxamic acid and 2-pyridinethiol-1-oxide-6-carboxylic acid the ligands were added to the titration cell as solids. m-Hydroxy-N-methylthiobenzohydroxamic acid was added to the titration cell as a methanolic solution, yielding a 2% methanol/water titration solution. N-Methyl thioacetohydroxamic acid experiments were done in both water and, as a prelude to lead electrode experiments, 50% methanol/water solution. Typically, 100 to 200 data points were obtained in the pH range 3-11 over approximately 5 hours.

Samples of 2-pyridinethiol-1-oxide-6-carboxylic acid were prepared for infrared spectroscopy in the following manner. The ligand (10 mg) was dissolved in 5.0 mL distilled, deionized water and 0, 0.25, 0.5, 1.0, 1.5, and 2.0 ligand equivalents of 0.1014 M KOH were added to individual solutions. Solution pH was measured using an Orion Ross electrode and the solvent was removed by roto-evaporation (Büchi). Infrared spectra of resulting solids were obtained (KBr pellets) using a Nicolet 5DX FTIR spectrometer.

Lead(II)-Ligand Complex Formation Constants.

Metal-ligand p[H] titrations were typically performed by addition of standardized 1 mM HNO_3 to a ligand titration solution to reach pH ~2.5, followed by the addition of an appropriate amount of standardized lead(II) nitrate solution to yield a lead(II)/ligand ratio of 2.0 to 2.2. Experiments were also carried out for N-methylthioacetohydroxamic acid and acetohydroxamic acid where the lead(II)/ligand ratio was 2.8 to 3.0.

A solid-state electrode selective for lead(II) (Orion) and a double junction Ag/AgCl reference electrode (Orion) were used in determining the formation constant for N-methylthioacetohydroxamic acid. Formic acid was used to buffer 5.47 mM ligand solutions at pH = 3.28.

The lead concentration varied from 1.35 x 10^{-5} M to 1.34 x 10^{-4} M. Aluminum oxide polishing strips (Orion) were used to rejuvenate the electrode surface between any two measurements.

Data Analysis

Data from pH titrations were modeled using the nonlinear least-squares analysis using the program BETA[7-9] (or the updated versions BETA89 and BETA90)[10] in which appropriate equilibrium constants were varied to minimize the residual function

$$R_w = \sqrt{\frac{\sum w(p[H]_{obs} - p[H]_{calc})^2}{\sum w(p[H]_{obs})^2}} \qquad (2)$$

where,

$$1/w = (\sigma_{p[H]})^2 + \left[(\sigma_{vol})^2 \left(\delta_{p[H]}/\delta_{vol}\right)^2\right] \qquad (3)$$

For the equipment used $\sigma_{p[H]}$, the estimated uncertainty in p[H] measurement, was 0.002 and σ_{vol}, the estimated uncertainty in volume of titrant delivered, was 0.003 mL; $\delta_{p[H]}/\delta_{vol}$ is the slope of the titration curve. By using this weighting factor, data where the p[H] is changing rapidly and therefore less accurate are lightly weighted and have less influence on the thermodynamic parameter calculated. The equilibrium constant refinement program is terminated when one of the following criteria is satisfied: 1) all refined stability constants have an estimated error of less than 0.002 log units; 2) the calculated change in the log of the formation constants divided by their corresponding errors is less than 0.05; 3) the goodness of fit (GOF) is not significantly lower than that for the previous refinement cycle. The definition of GOF is given below, where N_o is the number of observations, or p[H] data points, and N_v is the number of variables included in the working model. Generally, GOF values of three or less indicate an exellent fit of the model to the data.

$$GOF = \frac{\sum w(p[H]_{obs} - p[H]_{calc})^2}{N_o - N_v} \qquad (4)$$

Species distribution plots for mM lead(II) and 10 mM ligand solutions were generated using the computer program SPCONC.[11]

Results and Discussion

We found that thiohydroxamic acids bind lead(II) slightly better than hydroxamic acids. The contrast in metal complexing behavior which stems from differences between sulfur (thione) and oxygen (carbonyl) donors, is consistent with the measured protonation constants. The relatively "soft" thiohydroxamate groups have less affinity for the "hard" proton than similar hydroxamic acids--a difference in pK_a of approximately 3 log units. The implication of difference in pK_as is that thiohydroxamic acids will bind lead at a lower pH than hydroxamic acids.

Ligand Protonation Constants

Prior to the determination of metal-ligand formation constants, the ligand acidities in the absence of lead(II) were determined. The hydroxamate and thiohydroxamate ligands studied contain one dissociable proton from the thiohydroxamate (hydroxamate) group; one dissociable proton from a carboxylic acid site in the case of 2-pyridinethiol-1-oxide-6-carboxylic acid; and one dissociable proton from a phenolic site in the case of m-hydroxy-N-methylthiobenzhydroxamic acid. The protonation constants determined are summarized in Table 2. Values of protonation constants listed in the table and discussed herein are weighted averages calculated (root-mean-square) from two or more titrations using the error estimates generated by the data refinement program with an estimate of the uncertainty given in parentheses, except for N-methyl thioacetohydroxamic acid, the ligand for which 7 titrations were done and an average and standard deviation are reported.

The pKa of N-methylthioacetohydroxamic acid was determined to be 5.94(4) in water, and 6.86(4) in 50% methanol. This ligand is much more acidic than its hydroxamate analog, N-methylacetohydroxamic acid, (pK_a = 8.63, μ = 2.0, 25.0°C)[12] reflecting the different inductive effects of sulfur (thione) and oxygen (carboxyl) groups.

The pK_a of N-methylthioformohydroxamic acid was determined to be 5.45(6). The higher pK_a of the aceto- derivative above, by 0.5 log units, is an appraisal of the electron donating effect of the methyl group.

The thiohydroxamate group of m-hydroxy-N-methylthiobenzohydroxamic acid has a pK_a of 5.68(6). Again, the pK_a of the thiohydroxamic acid is much lower than that of the corresponding hydroxamic acid, N-methylbenzohydroxamic acid (pKa = 8.15, μ = 0.1, 25.0°C).[12] The hydroxyl group, with a pK_a of 9.43(6), is more acidic than the hydroxyl group of phenol. This lowering of the pK_a may be attributed to delocalization of the charge on the deprotonated hydroxyl through resonance stabilization provided by

the benzene ring and the thiohydroxamate group. Representative titration curves for pK_a determinations for the three simple thiohydroxamates studied are shown in Figure 7.

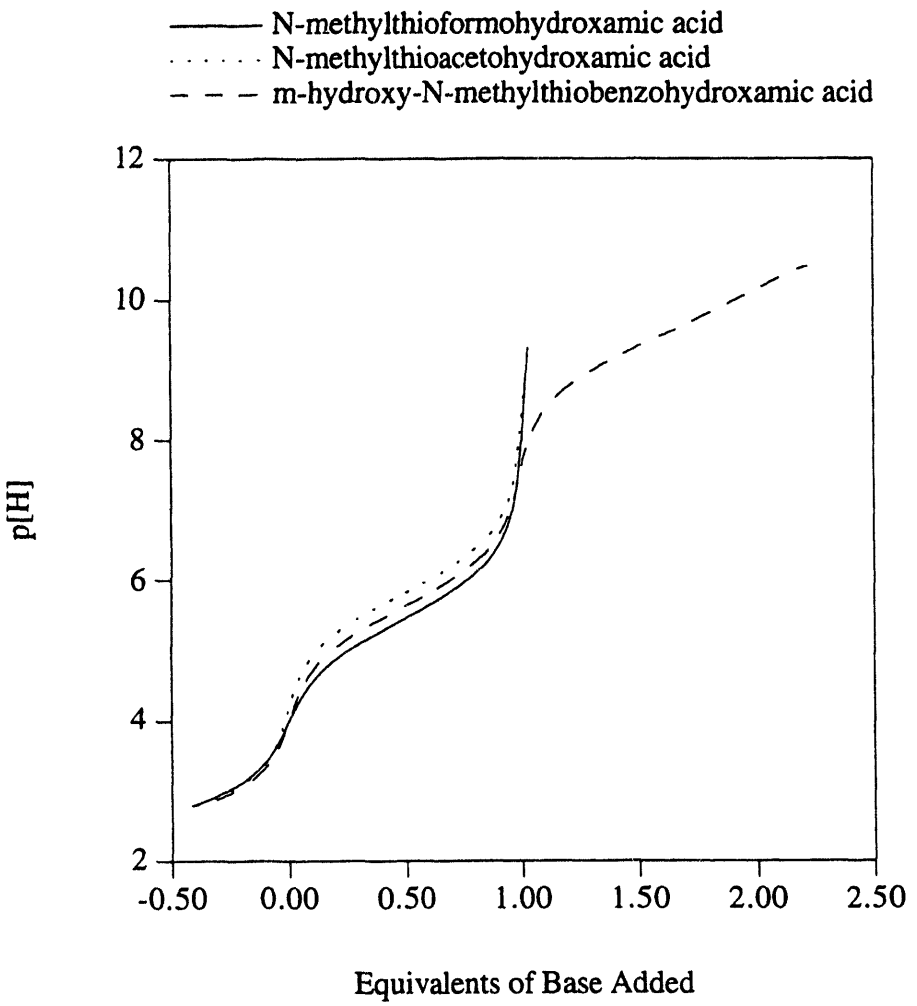

Figure 7. Titration curves for the thiohydroxamate ligands studied. Equivalents of base are defined as (amount of base added)/(amount of ligand present).

The highest pK_a of 2-pyridinethiol-1-oxide-6-carboxylic acid was determined to be 6.43(5) by refinement of titration data from pH 3.7 to 8.0. Ligand precipitation below pH = 3 precludes this method as a means of accurately determining the next lower pK_a, which is approximately 2.3. Tautomeric forms of the ligand can exist (see Figure 9) and there is some ambiguity as to which is predominant--the thione or thiol form.[13,14] A series of infrared spectra were obtained to allow for identification of the tautomeric form(s) of the ligand and unambiguous assignment of pK_as to the ligands' functional groups. Samples of the ligand were treated with increasing amounts of base, (simulating the potentiometric titration shown in Figure 8) and the IR spectra were obtained for samples containing 0, 0.25, 0.5, 1.0, 1.5, and 2.0 equivalents of base. The characteristic stretching frequencies[15] observed and corresponding assignments are summarized in Table 3. A band at 2500 cm^{-1}, indicative of a thiol, appears in the infrared spectrum and shows the tautomeric forms II and III in Figure 9 are dominant and the sulfur group is best described as a thiol, rather than a thione. The disappearance of the characteristic thiol stretch after the addition of less than one equivalent of base and the shift of the characteristic carboxylate stretch from approximately 1700 to 1612 wavenumbers after the addition of more than one equivalent of base indicate the higher pK_a must be assigned to the carboxylate group, while the lower pK_a can be assigned to the thiol. The protonation constant, 6.43, is much higher than that of simple carboxylic acids; this may be explained by intramolecular hydrogen bonding between the carboxyl and pyridinal oxygens, resulting in the formation of a highly stable six membered ring, and resonance stabilization of the singly protonated species. Comparing the N-oxide pK_a with that reported by Sun, et al.[13] for 2-mercaptopyridine-1-oxide, 4.43, provides a measure of 2 log units for the carboxylate group's effect on the acidity of the ligand. The thiolate group is also strongly affected: pK_a of 2.3 for thiol group on 2-pyridinethiol-1-oxide-6-carboxylic acid versus -1.95 for 2-mercaptopyridine-1-oxide.[16]

To provide a comparison of the lead(II) complexing ability of a simple hydroxamate with the thiohydroxamate ligands, acetohydroxamic acid was included in this study. The pK_a of acetohydroxamic acid was redetermined to be 9.34(5), in excellent agreement with the literature value of 9.36.[12] This ligand also follows the trend that hydroxamate pK_as are approximately 3 log units higher than those of corresponding thiohydroxamate; the pK_a of acetothiohydroxamic acid is reported to be 5.58.[17]

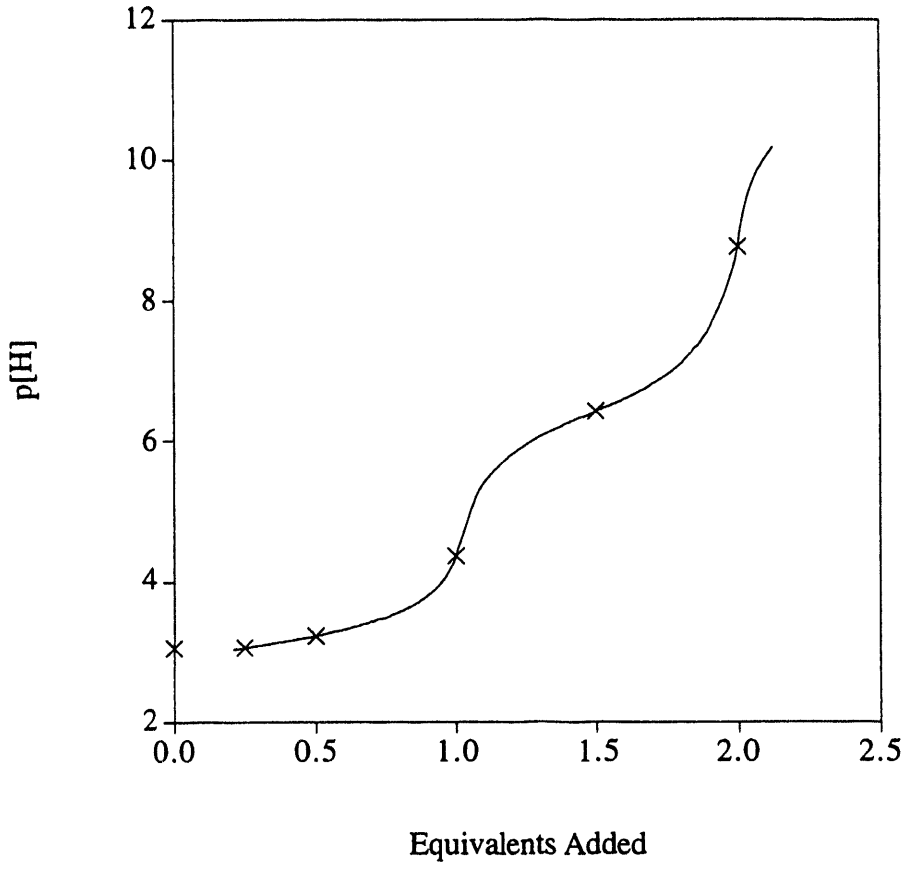

Figure 8. A titration curve for 2-pyridinethiol-1-oxide-6-carboxylic acid. Equivalents of acid are defined as (amount of acid added)/(amount of ligand present). The X symbols superimposed on the curve indicate points where infrared spectra were obtained in the experiment summarized in Table 3.

Table 2.
Summary of Protonation Constants for the Ligands Studied
μ= 0.100 M KNO_3, 25.0°C

Ligand	(thio)hydroxamate pK_a	phenolic pK_a	carboxylate pK_a
N-methylthioacetohydroxamic acid	5.94(4)		
N-methylthioformohydroxamic acid	5.45(6)		
m-OH-N-methylthiobenzohydroxamic acid	5.68(6)	9.43(6)	
2-pyridinethiol-1-O-6-carboxylic acid	6.43(5)		~2.3
acetohydroxamic acid	9.34(5)		
N-methylthioacetohydroxamic acid, 50% MeOH	6.86(4)		

Table 3.
Infrared Spectroscopic Data From a Titration of
2-pyridinethiol-1-oxide-6-carboxylic acid.

Equivalents of Base Added	Characteristic IR Bands (Wavenumbers)	Assignment of Bands
0.00, 0.25	2500; 1678; 1385	SH; C=O; C-O-H
0.50, 1.00	------; 1707; 1380	no SH; C=O; C-O-H
2.00	------; 1612; 1397	no SH; C=O; $C-O^-$

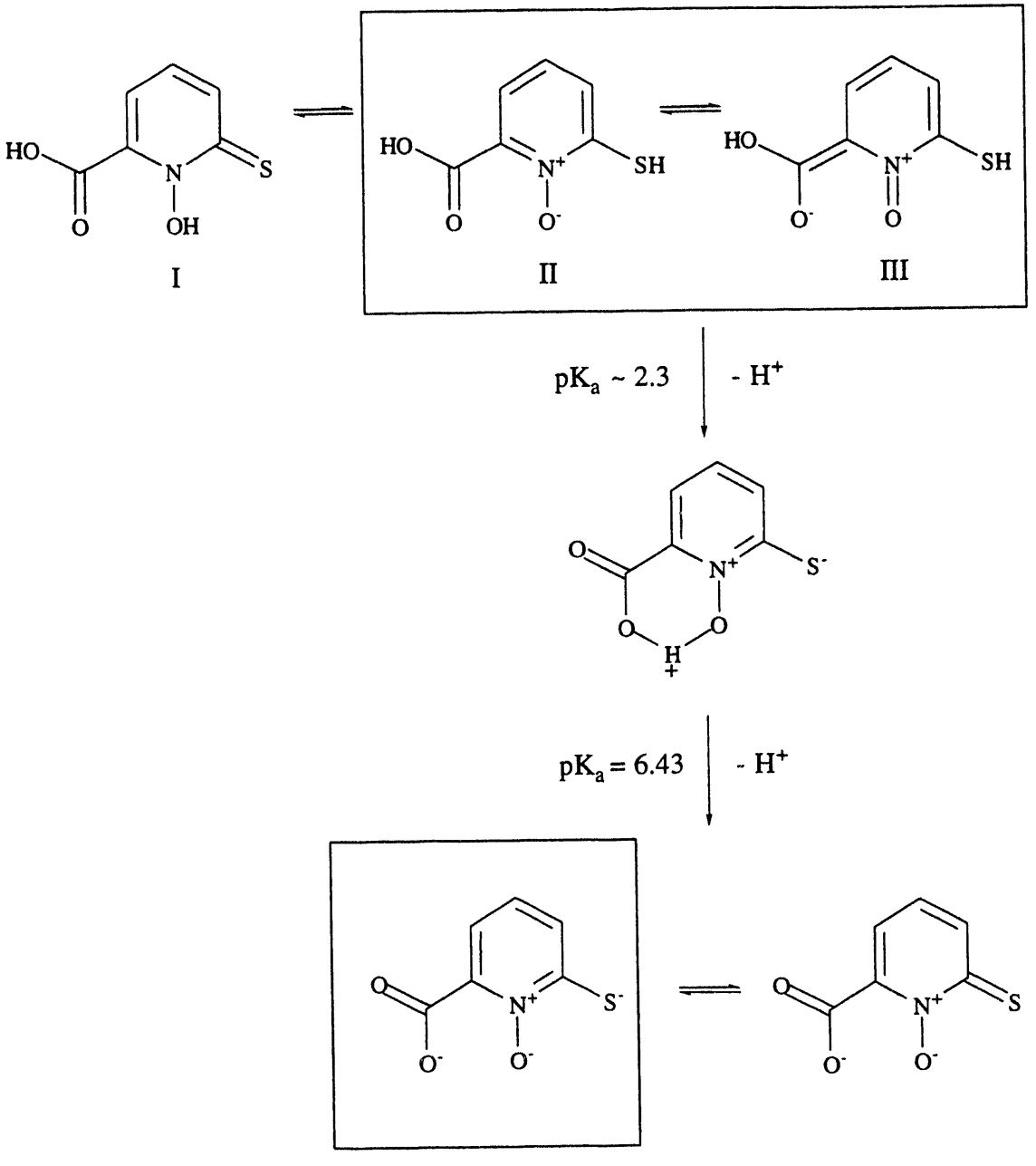

Figure 9. Tautomeric Forms and pK_a Assignments for 2-pyridinethiol-1-oxide-6-carboxylic acid.

Lead(II)-Ligand Stability Constants

Metal-ligand complex formation involves the competition between hydrogen ions and metal ions for ligand donor groups and between solvent and ligand molecules for the metal ion. Complexation equilibria including proton displacement in the pH range of approximately 2-11 may be studied using pH titrations.[1] Calibration of the pH electrode in hydrogen ion concentration, rather than in hydrogen ion activity, allows the use of mass balance equations to quantify the number of unbound protons in solution.[7,18] The equilibrium constants obtained may be compared directly with other constants determined at the same temperature and ionic strength. Typically metal complexation equilibria are presented as formation constants, using the notation $\log\beta_{mlh}$, where β is the constant calculated for the formation of a single species, m is the number of metal atoms in the product, l is the number of ligands in the product, and h is the number of protons.

$$mM + lL + hH \Leftrightarrow M_mL_lH_h \tag{5}$$

$$[M_mL_lH_h] / ([M_mL_{l-1}H_h][L]) \tag{6}$$

Stepwise formation constants, for equilibria involving the addition of a single ligand to a preformed species, are denoted here as Ks with the same mlh indices. (For simplicity, ionic charges are neglected in the equation.)

$$M_mL_{l-1}H_h + L \Leftrightarrow M_mL_lH_h \tag{7}$$

$$K_{mlh} = [M_mL_lH_h] / ([M_mL_{l-1}H_h][L]) \tag{8}$$

Metal complex formation constants were first estimated by inspection of the p[H] titration curves. Refinement of the formation constants was accomplished by building an equilibrium model, beginning with the ligand proton association constants and lead hydrolysis constants[19] as fixed parameters, and sequentially adding probable species with corresponding formation constant estimates as variable parameters. If the refinement converged, the species in that model were temporarily assumed to be significant and were included in subsequent models. New species or formation constant estimates were added to the model until changes did not lead to significant improvements to the fit to the experimental data.

In this work potassium nitrate was used as a background electrolyte, and was assumed to have a negligilbe interation with respect to competition with the ligands for lead(II). To address the possibility of interference from KNO_3 and illustrate the

hydrolysis behavior of lead(II), a species distribution curve was generated based on the stability constants reported for lead(II) nitrate species[12] and hydrolysis constants reported by Sylva and Brown[19] ($\log\beta_{10\text{-}1}$ = -7.86, $\log\beta_{30\text{-}4}$ = -23.91, $\log\beta_{30\text{-}5}$ = -31.75, $\log\beta_{40\text{-}4}$ = -20.40, $\log\beta_{60\text{-}8}$ = -43.38). The species distribution curve shown in Figure 10 may be thought of as a starting point for the aqueous lead(II) ligand equilibria. We found that above pH 4.0 the lead(II) nitrate species are insignificant, and at pH 3.0 approximately 18% of the lead is present as $Pb(NO_3)^+$ and $Pb(NO_3)_2$. This analysis validated our use of potassium nitrate as a noninteracting electrolyte for potentiometric titrations and inclusion of the hydrolysis constants in data refinement input files, although only the $Pb(OH)^+$ hydrolysis product is present in a significant amount below pH 7.

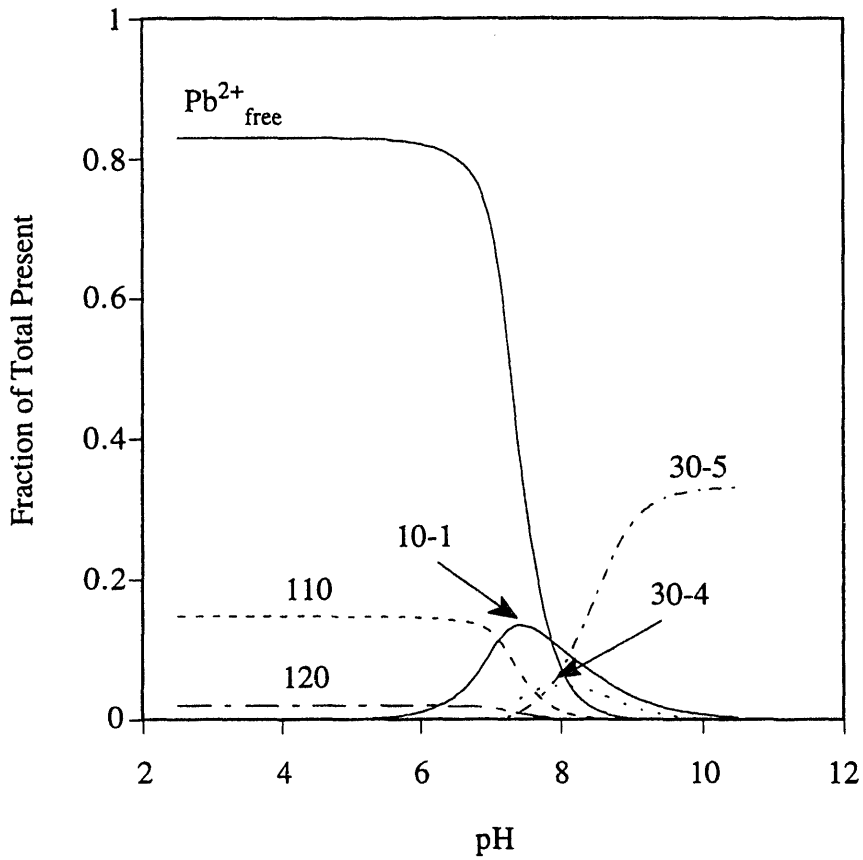

Figure 10. A species distribution curve generated using the stability constants for lead(II) with the nitrate ion[12] and lead(II) hydrolysis constants.[19]

The coordination chemistry of lead(II) includes a variety of coordination numbers and geometries as well as preponderance of polymeric species.[20,21] This suggests an abundance of chemically and structurally reasonable solution species. In this work model building was conducted with a bias toward simplicity, that is monomeric and dimeric species with ligand/lead ratios of 1-3 were considered preferentially. When using p[H] titration data for stability constant determination where the metal concentration is constant, species having the same m/l/h ratios are indistinguishable in mass balance analyses; for example, a lead atom bound by one ligand with one proton associated (a mlh = 1,1,1 species) would show the same p[H] behavior and satisfy the same mass balance role as a dimer where two lead atoms were bound by two ligands with two protons associated (a mlh = 2,2,2 species). Consideration of thermodynamic data obtained using this method should accommodate species which are integer multiples of reported species. High molecular weight oligomers (tetramers, pentamers, etc.) were generally ignored in formation constant refinements, since those species are not expected to be highly water soluble, and titration data where a precipitate was observed were not included in data analyses. Most titrations were performed with a ligand to lead concentration ratio of 2.0-2.2, since the important species were expected to include lead(II) bound by one and two ligands. Considering the possibility of tris ligand-lead species, experiments were also conducted for the representative ligands, N-methylthioacetohydroxamic acid and acetohydroxamic acid, where the ligand-to-lead concentration ratio was 2.8-3.0 .

Lead(II) complexation by N-methylthioacetohydroxamic acid.

Titration curves for N-methylthioacetohydroxamic acid, alone and in the presence of two and three equivalents of lead(II) (Figure 11), show the relative affinities of the thiohydroxamate group for lead(II) compared to the hydrogen ion. The buffer regions centered at 0.5 equivalents, p[H] approximately 4.5 and a single breakpoint at 1 ligand equivalent of base added, suggests the presence of species with integer ratios of l/m. The stepwise formation constants of N-methylthioacetohydroxamic acid with lead(II) were first estimated, and then refined to be log K_{110} = 6.88(4), log K_{120} = 4.04(6) in water. Inclusion of only two metal-ligand species in data analysis models gave excellent fits (GOF = 0.6-2.1) for all experiments, independent of the ligand to metal ratio. Including trishydroxamate variables ($\log\beta_{13x}$) and/or variables corresponding to mixed ligand, hydroxide species ($\log\beta_{11-1}$, $\log\beta_{12-1}$, etc.) yielded unreasonable calculated titration curves and poorer fits to the experimental data. Dimeric species, such as M_2L_3, were also

considered and rejected in the analysis. A species distribution curve generated using these formation constants is shown in Figure 12.

From a single titration in 50% methanol, the corresponding formation constants were determined to be log K_{110} = 7.77, log K_{120} = 4.63 (GOF = 1.49). The 50% methanol titration results were used to establish the conditions appropriate for lead(II)-specific electrode experiments. The higher formation constants show the effect a less protic solvent has on ligand-metal complex formation and can only be compared directly with thermodyamic data obtained in 50% methanol.

Using a lead(II)-specific electrode to measure the concentration of free lead(II) in solution provides an alternative method for determination of stability constants. The β_{120} formation constant for this ligand was too large to determine using an electrode whose sensitivity limit is in the micromolar range. The β_{110} formation constant was determined by measuring the lead(II) concentration in formate buffered ligand solutions to which varying amounts of lead(II) were added. The pH of 2.8 was chosen by considering the expected formation constant, the ligand pK_a, and the lead electrode pH dependent sensitivity limits. Based on the pH titration results in 50% methanol, the only significant equilibrium under these conditions is the formation of the ligand:metal = 1:1 complex, described by the following expressions.

$$\beta_{110} = \frac{[PbL^+]}{([Pb^{2+}][L^-])} = \frac{[Pb^{2+}]_{total} - [Pb^{2+}]_{free}}{\left([Pb^{2+}]_{free}[L^-]\right)} \tag{9}$$

$$[Pb^{2+}]_{free} = \frac{[Pb^{2+}]_{total} - [Pb^{2+}]_{free}}{\left(\beta_{110}[L^-]\right)} \tag{10}$$

$$\log[Pb^{2+}]_{free} = \log\left\{[Pb^{2+}]_{total} - [Pb^{2+}]_{free}\right\} - \log\beta_{110} - \log[L^-] \tag{11}$$

By plotting values of $\log[Pb^{2+}]_{free}$ versus $\log\{[Pb^{2+}]_{total} - [Pb^{2+}]_{free}\}$ for fifteen solution measurements an average $\log\beta_{110}$ value of 6.924(6) was determined. This value is 0.8 log units lower than that obtained from the 50% methanol p[H] titration.

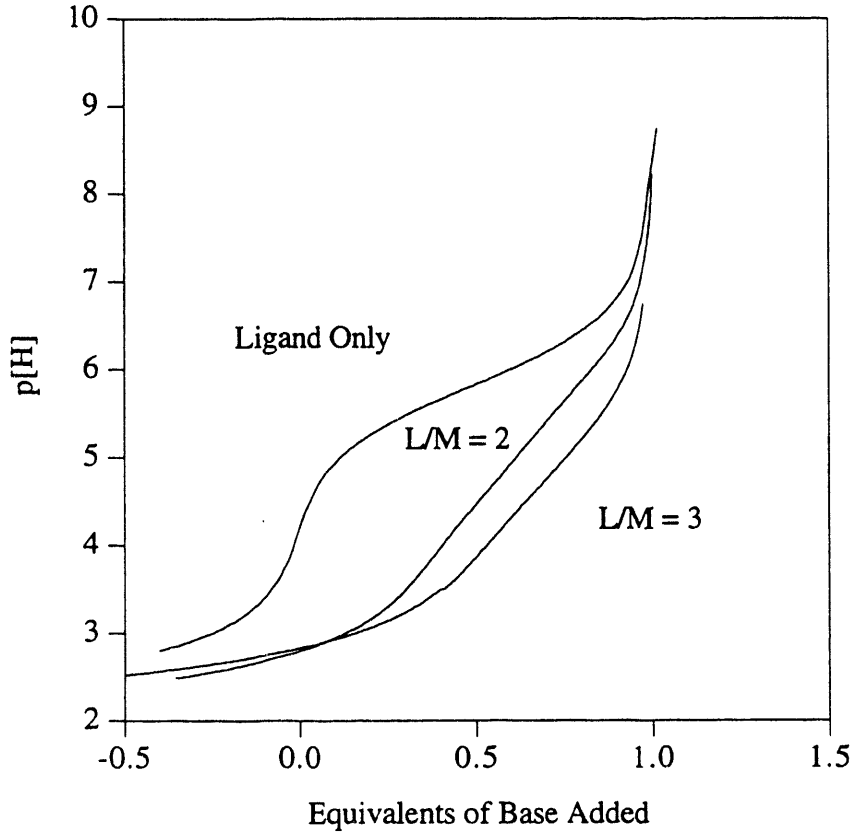

Figure 11. Comparison of p[H] titration curves obtained for N-methylthioacetohydroxamic acid in the absence of lead(II), with a ligand-to-metal ratio of 2, and a ligand-to-metal ratio of 3. Equivalents of base are defined as (moles of base added)/(moles of ligand present).

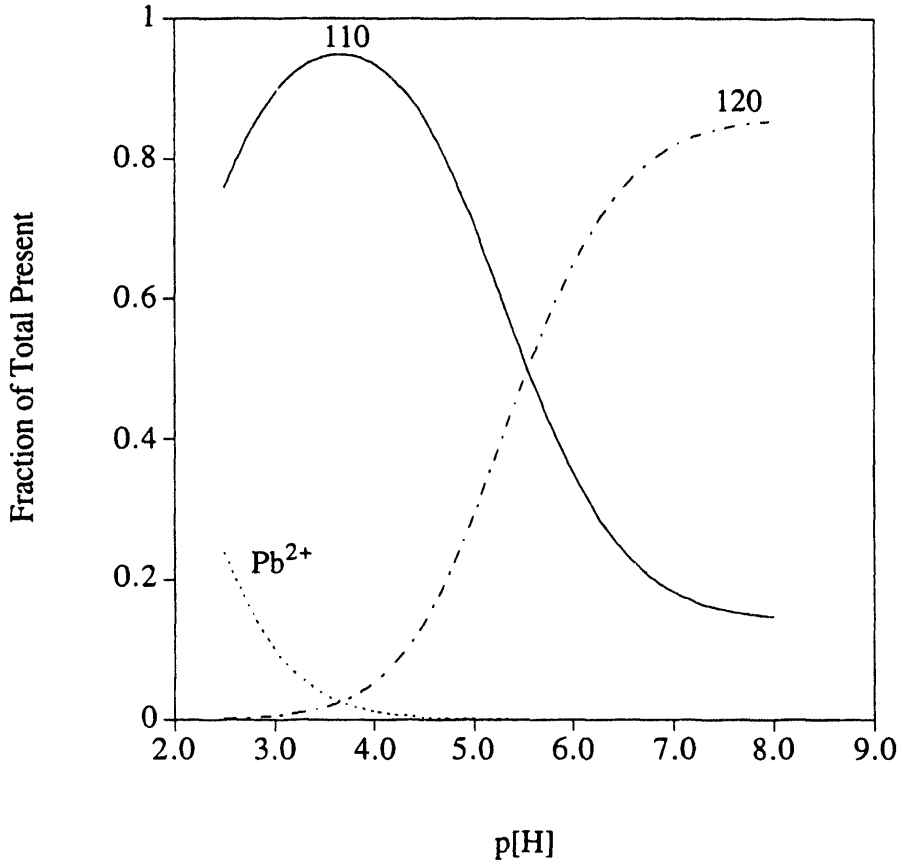

Figure 12. The distribution of lead(II) containing species calculated using the lead(II)-N-methylthioacetohydroxamic acid formation constants listed in Table 4 and [M] = 1.0 mM, [L] = 2.0 mM.

Lead(II) complexation by N-methylthioformohydroxamic acid.

N-methylthioformohydroxamic acid shows solution behavior with lead(II) similar to the aceto-analog, with formation constants of log K_{110} = 5.89(8), log K_{120} = 3.50(8) The rather small formation constants are consistent with the general trend that stronger bases act as stronger ligands.[22] Titration curves for the ligand alone and in the presence of lead(II) are shown in Figure 13. A species distribution curve for the N-methylthioformohydroxamate/lead(II) system is shown in Figure 14

Lead(II) complexation by m-hydroxy-N-methylthiobenzohydroxamic acid.

The solution behavior of m-hydroxy-N-methylthiobenzohydroxamic acid with lead(II) is more complex than the monoprotic ligands discussed above. The titration curve of the ligand in the presence of two equivalents of lead(II) (Figure 15) shows ligand-metal interaction over the entire p[H] range considered. The breakpoint after the addition of one equivalent of base and the greater difference between the ligand only and metal-ligand titration curves from 0 to 1 equivalent of base added compared to that from 1 to 2 equivalents of base suggest the simple model of lead(II) chelated by two thiohydroxamate groups below p[H] = 6 and the dissociation of the two phenolic protons between p[H] 7.5 and 9. This model does not fit the data. A model comprised of a dimer with the indices m,l,h = 233, and corresponding deprotonated species, fit the data almost as well. The model which best fit the data included the following species, shown schematically in Figure 16: m,l,h = 122, 121, 120, 233, and 243. A species distribution plot generated using the stability constants for the best model is shown in Figure 17. However, with a GOF of 14, this model does not was adequately explain the solution behavior. (For comparison, titration data sets for this ligand alone and other ligands, both with and without lead(II), had a GOF of 0.5 to 4.0.) Addition of other reasonable species, including 11x species and the deprotonated forms of the dimers, did not improve the fit. Apparently there are species interconversions with small, but significant equilibrium constants, which we were unable to extract from the available data.

Further experiments must be carried out to elucidate the solution behavior with lead(II); such as titrations with varying ligand/metal ratios and consideration of the m-methoxy derivative of the ligand with lead(II).

Lead(II) complexation by 2-pyridinethiol-1-oxide-6-carboxylic acid.

Addition of lead(II) to aqueous solutions of the 2-pyridinethiol-1-oxide-6-carboxylic acid yielded a precipitate at both high and low pH, preventing study of the metal complex formation equilibria using this method. Based on the insolubility of the lead complex of the pryidinethiol, polymers may be readily formed with this ligand and measuring the complex stability constants will not be straightforward.

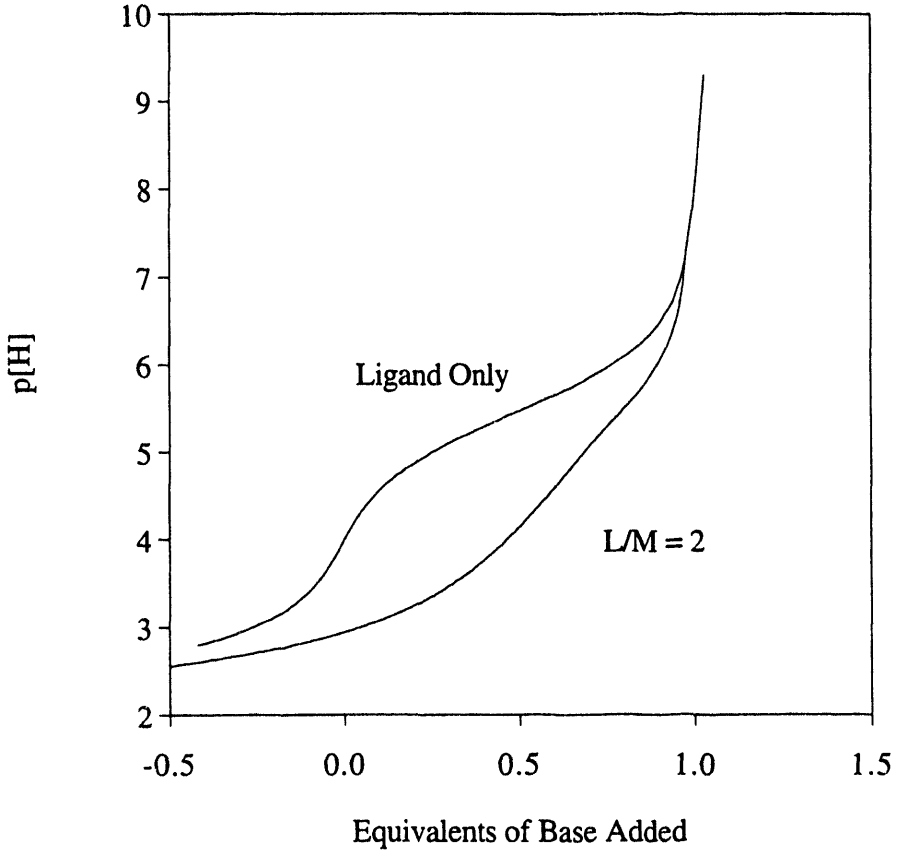

Figure 13. Comparison of p[H] titration curves obtained for N-methylthioformohydroxamic acid in the absence of lead(II) and with a ligand-to-metal ratio of 2. Equivalents of base are defined as (moles of base added)/(moles of ligand present).

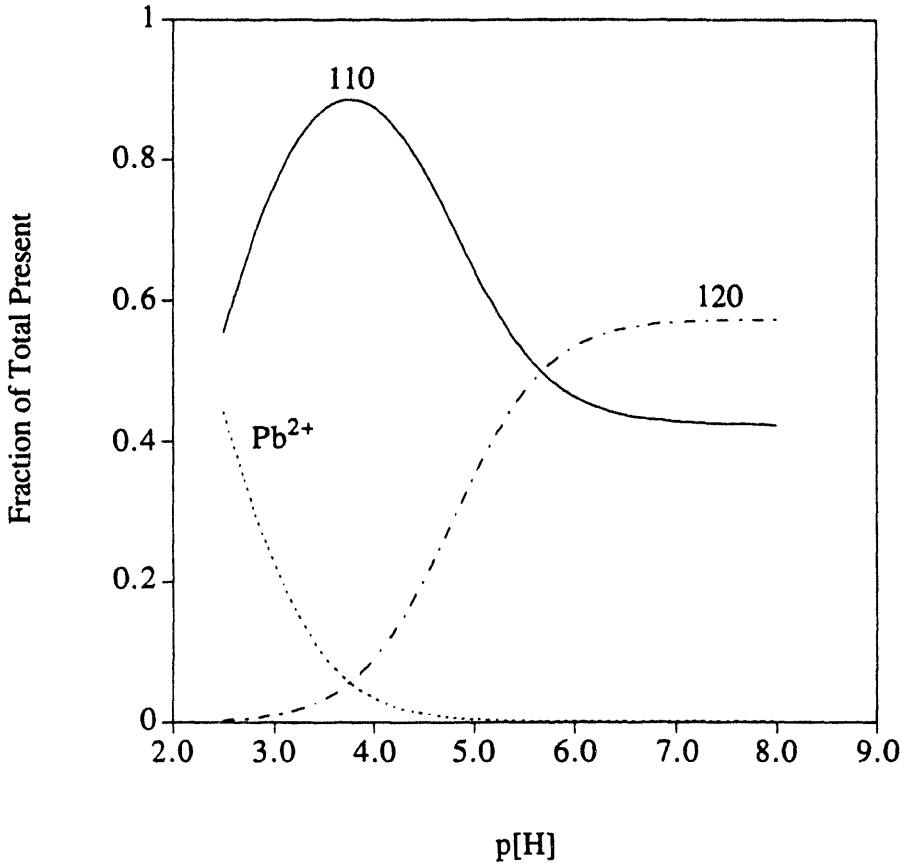

Figure 14. The distribution of lead(II) containing species calculated using the lead(II)-N-methyl-thioformohydroxamic acid formation constants listed in Table 4 and assuming [M] = 1.0 mM, [L] = 2.0 mM.

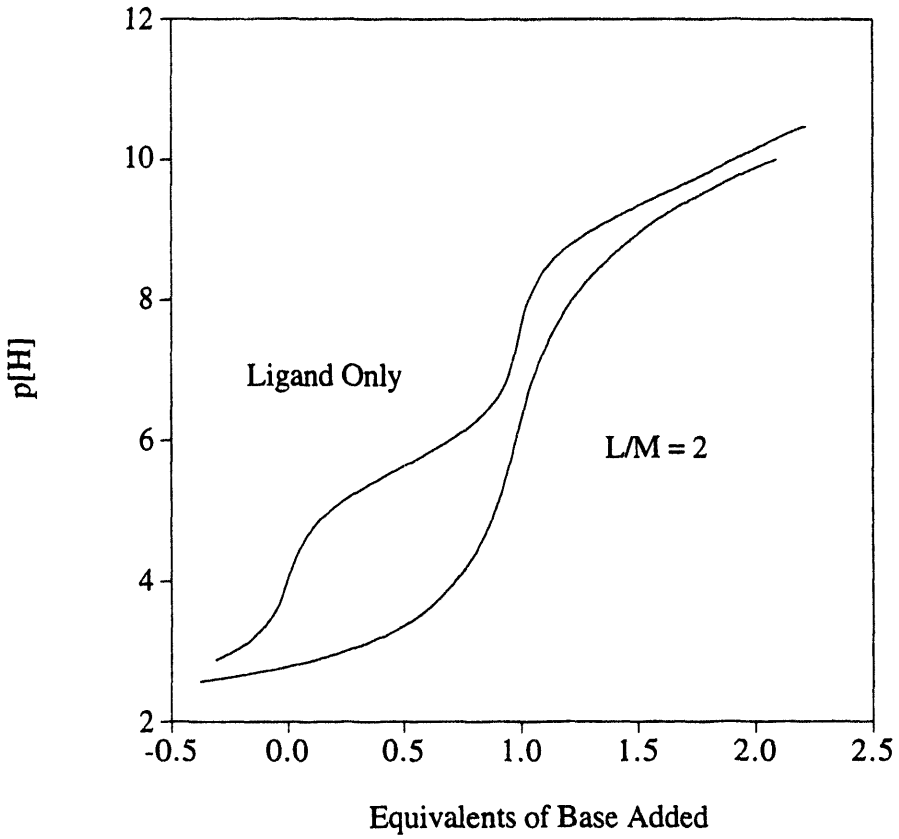

Figure 15. Comparison of p[H] titration curves obtained for m-hydroxy-N-methyl thiobenzohydroxamic acid in the absence of lead(II) and with a ligand-to-metal ratio of 2. Equivalents of base are defined as (moles of base added)/(moles of ligand present).

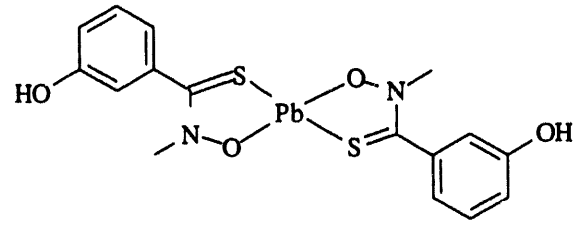

$M_1L_2H_2$ Species

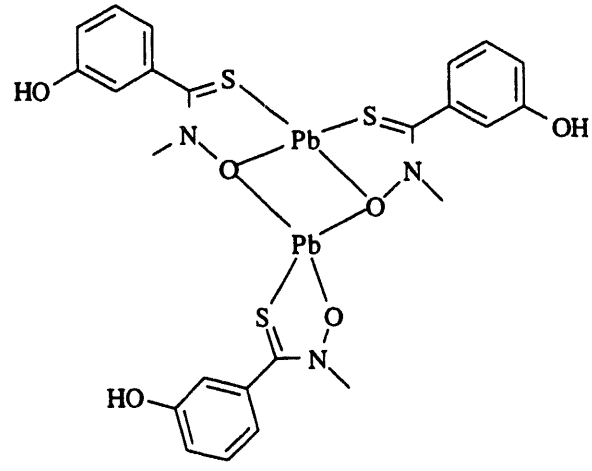

$M_2L_3H_3$ Species

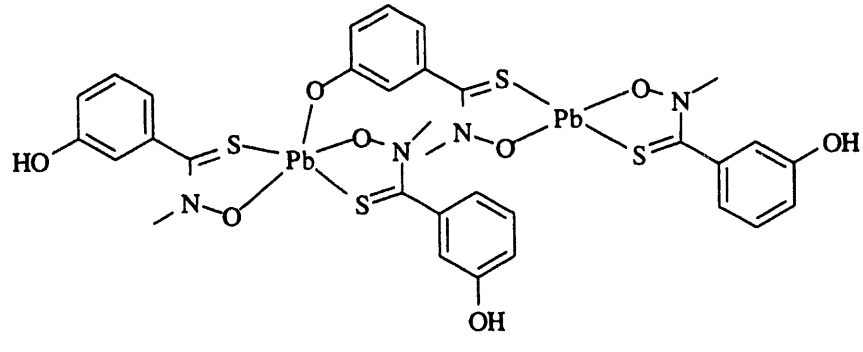

$M_2L_4H_3$ Species

Figure 16. Proposed lead(II) complexes of m-hydroxy-N-methylthiobenzohydroxamic acid[23] included in the data refinement model best approximating p[H] titration data.

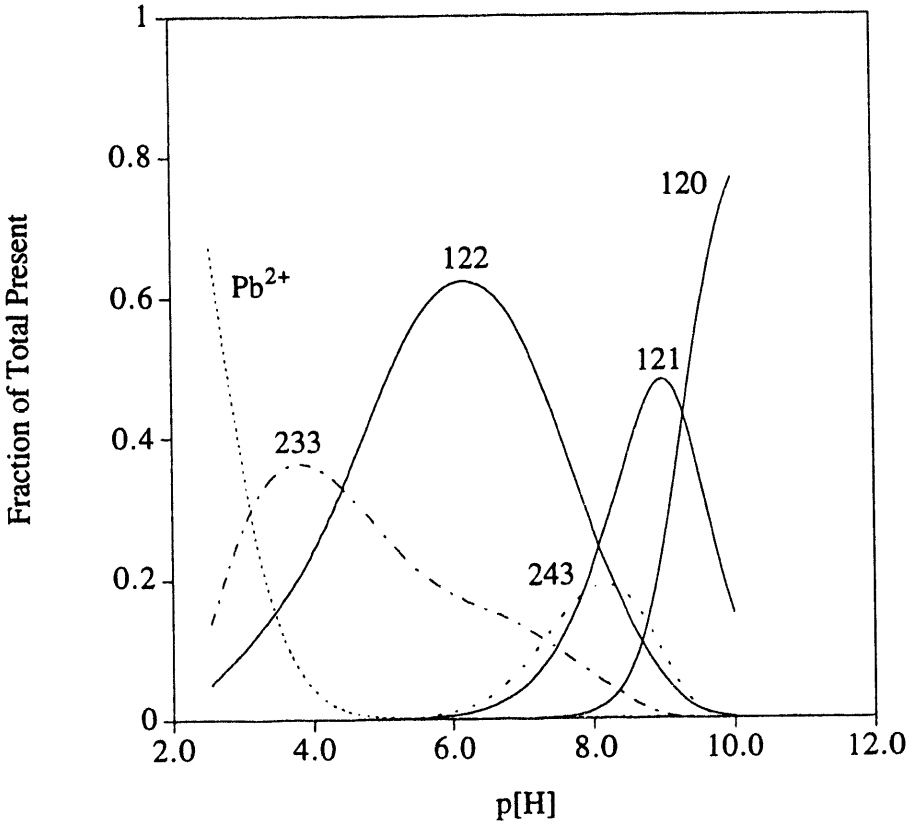

Figure 17. The distribution of lead(II) containing species calculated using the lead(II)-N-methyl-thiobenzohydroxamic acid formation constants listed in Table 4 and assuming [M] = 1.0 mM, [L] = 2.0 mM.

Lead(II) complexation by acetohydroxamic acid.

The formation constants for lead complexes of acetohydroxamic acid were determined, allowing direct comparison of hydroxamate and thiohydroxamate lead(II) binding abilities. Titration curves for the ligand alone and with lead(II) are shown in Figure 19. A breakpoint at 0.35 equivalents of base added, p[H] = 6.2, and four buffer regions at approximately 0.16, 0.63, 0.85, 1.0 equivalents, and p[H] = 4.8, 7.8, 8.9, and 10.0, respectively, were detected in 2:1 ligand to metal titration curves. These features indicated the presence of species with noninteger values of l/m, possibly polymers, and prompted consideration of the following model: m,l,h = 320, 110, 120, and 230. Inclusion of a m,l,h = 12-1 species corresponding to PbL_2OH^-, improved the fit considerably and was included in the final refinement. Other reasonable variables and combinations were input either in place of, or in addition to, the species listed above, but none were accepted. The formation constants were determined to be: $\log\beta_{320}$ = 19.24(6), $\log\beta_{110}$ = 6.34(6), $\log\beta_{230}$ = 19.05(6), $\log\beta_{120}$ = 9.52(8), $\log\beta_{12\text{-}1}$ = -0.68(8); stepwise constants: log K_{110} = 6.34(6), log K_{120} = 3.18(6). Andregg and coworkers[24] previously reported the monomeric formation constants to be log K_{110} = 6.7, log K_{120} = 4.0, but apparently did not consider other species in their analysis. Proposed structures for the polymeric species are shown schematically in Figure 18. Coordination to the lead atom via the two oxygen atoms is assumed based on X-ray crystallographic[25] and infrared spectroscopic[26] studies of other metal complexes.

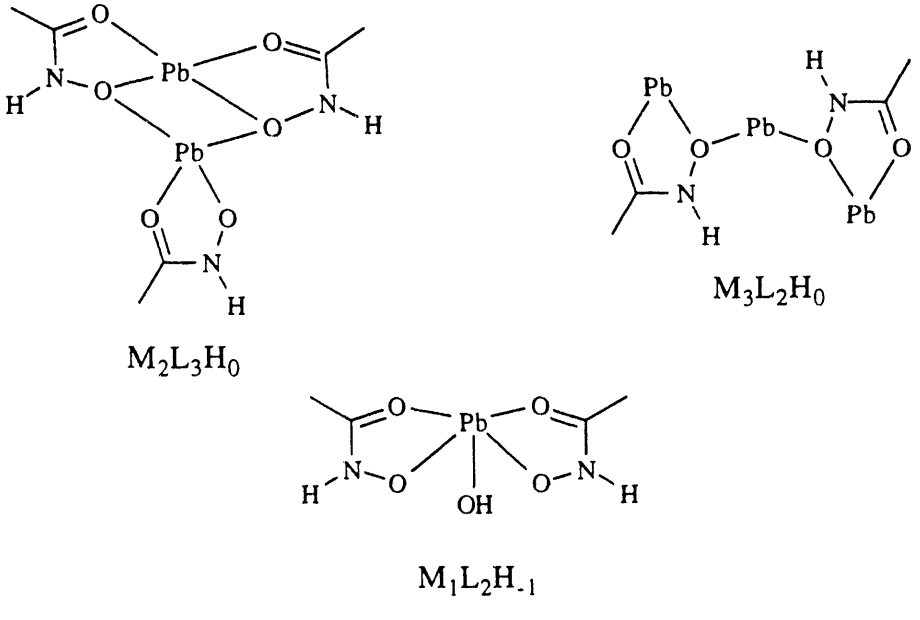

Figure 18. Proposed lead(II)/acetohydroxamate solution species.

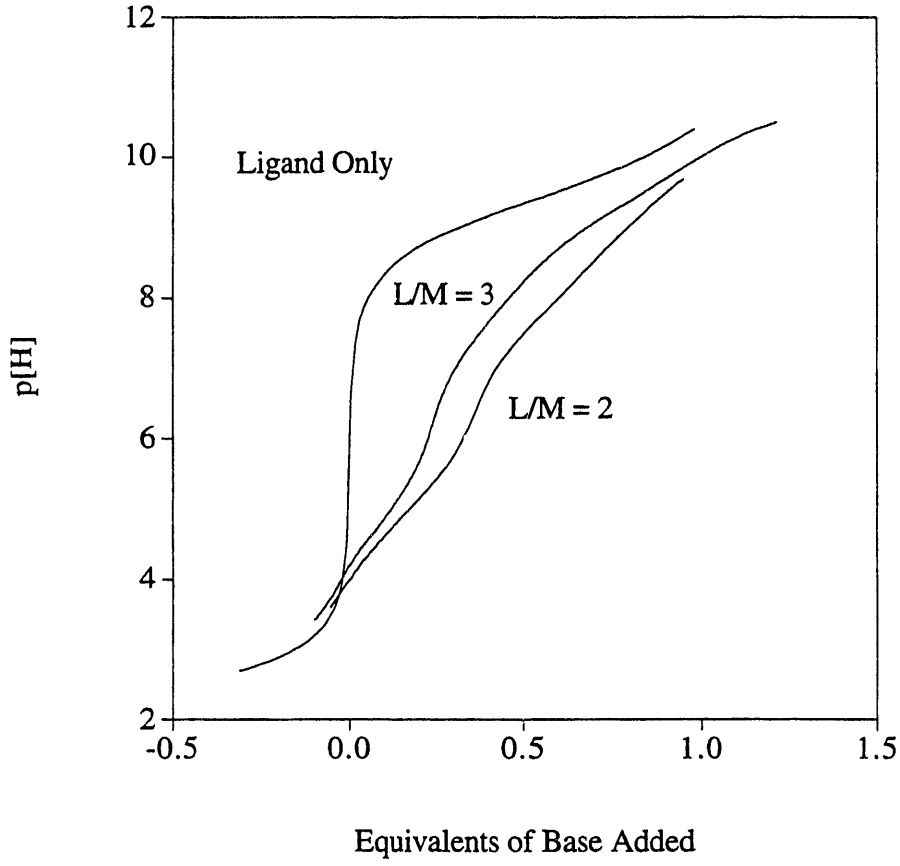

Figure 19. Comparison of p[H] titration curves obtained for acetohydroxamic acid in the absence of lead(II), with a ligand-to-metal ratio of 2, and a ligand-to-metal ratio of 3. Equivalents of base are defined as (moles of base added)/(moles of ligand present).

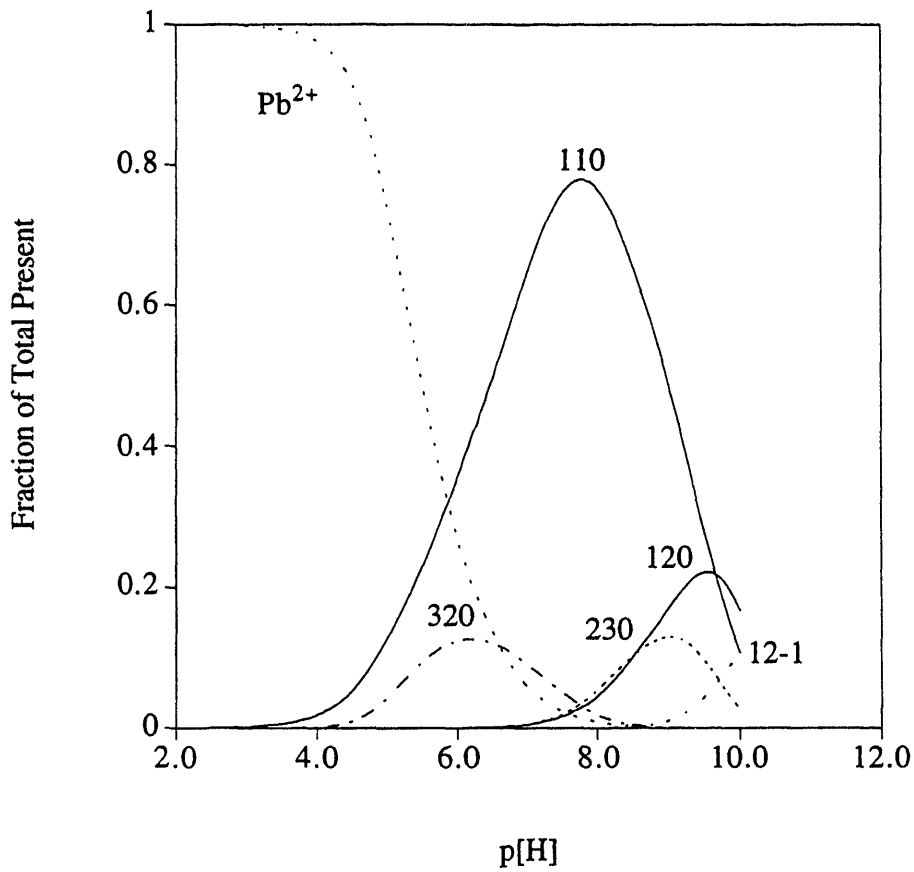

Figure 20. The distribution of lead(II) containing species calculated using the lead(II)-acetohydroxamic acid formation constants listed in Table 4 and assuming [M] = 1.0 mM, [L] = 2.0 mM.

Conclusions

Simple thiohydroxamic acids are lead(II) complexing agents of intermediate strength--stronger than simple carboxylate ligands, like acetate and oxalate; but weaker than thiolates, like cysteine. (Table 4 includes relevant thermodynamic data for these ligands.) Thiohydroxamates are slightly better lead chelators than hydroxamates, based on the metal-complex formation constants determined: N-methylthioacetohydroxamic acid, $\log\beta_{120} = 10.92$; acetohydroxamic acid, $\log\beta_{120} = 9.52$. There was not the expected dramatic increase in stability constant upon replacing a hydroxamate oxygen donor atom with sulfur, like that evidenced by the ligands tartaric acid ($\log\beta_{110} = 3.12$), and the thiol analog, DMSA ($\log\beta_{110} = 17.4$). To extrapolate from benchtop thiohydroxamate thermodynamic data to chelation therapy applicability a fundamental question is: How much metal is uncomplexed by the ligand, and, therefore, remains toxic, under conditions similar to those in biological fluids? In answer, pM values are calculated, where pM is defined as the negative log of the concentration for free metal ion at pH = 7.4, $[Pb^{2+}] = 1\mu M$, $[L] = 10\mu M$. A pM of exactly 6 means the ligand has not bound any of the metal, and the higher the pM value, the less free metal in solution. While the formation constants determined for acetohydroxamic acid with lead(II) are not drastically different than those for thiohydroxamates, thiohydroxamates are more acidic and have higher pM values. For example, N-methylthioacetohydroxamic acid, with a pM value of 7.86, will complex 98% of the lead, and acetohydroxamic acid with a pM value of 6.09, will complex only 19% of the lead under the defining conditions.

When investigating molecules for possible use as *in vivo* chelating agents, the most salient features are the concentration of metal ion which is not complexed by the ligand under physiological conditions, and the selectivity of the ligand for the metal ion of interest. To address the question of selectivity, the formation constants of the ligands with biologically important bivalent and trivalent metals, such as Mg^{2+}, Ca^{2+}, $Mn^{2+/3+}$, Cu^{2+}, $Co^{2+/3+}$, Ni^{2+}, Zn^{2+}, $Fe^{2+/3+}$, must be considered. The stability constants for acetohydroxamic acid with a number of cations are listed in Table 5. These data clearly show that hydroxamates will bind the ferric ion preferentially, unless of course, the iron is already bound to a stronger complexing agent. Unfortunately, there is no similar set of data for a thiohydroxamate ligand. The only thiohydroxamic acid for which several metal stability constants have been measured is N-phenyl-thiobenzohydroxamic acid. Dietzel and Thomas[27] determined the ligand pK_a and several metal complex formation constants in 75% dioxane/water at 30.0°C. While these stability constants, listed in Table 6, cannot be compared directly with the data obtained in water (and at lower temperatures),[28] they illustrate the relative affininty of a thiohydroxamic acid for lead(II) versus comparativly

"hard" pyhsiologically useful metals. For example, the bis-ligand stability constant with lead(II) is nearly eight orders of magnitude greater than with manganese(II). (For acetohydroxamic acid, the bis-ligand stability constant with lead(II) is over two orders of magnitude smaller than with manganese(II)). Mathur and Bhandarie[29] determinded the formation constants of N-phenylthioformohydroxamic acid with trivalent metals, and a number of lanthanides, (Sm, Nd, Gd, Pr, La, Y) in 70% dioxane. They found the Sm(III) complexes were the most stable, with logb values for mlh = 110, 120, and 130 of 6.80, 11.86, 15.51, respectively. These values suggest that there is a smaller difference in the overall complexing strength of thiohydroxamates with bivalent and trivalent cations, than for the hydroxamates. By extension, it is quite likely that thiohydroxamates, in contrast to hydroxamates and other "hard" ligands, would not show the same marked preference for the "hard" ferric ion over lead(II). Thiohydroxamates, as intermediate strength ligands exhibiting some selectivity for the lead ion, are plausible lead(II)-binding subunits of chelation therapy drugs.

Table 4.
Lead(II) Stability Constants Determined
and Published Values for Some Important Ligands† at μ= 0.10, 25.0°C

Ligand	pK_as lh	pK_a	Stability Constants mlh	log β_{mlh}	pM*
N-methylthioacetohydroxamic acid	11	5.94	110	6.88	7.86
			120	10.92	
N-methylthioformohydroxamic acid	11	5.45	110	5.89	6.93
			120	9.39	
m-hydroxy -N-methyl	11	9.43	120	12.32	6.84
thiobenzohydroxamic acid**	12	15.12	121	21.61	
			122	29.70	
			233	48.72	
			243	54.81	
acetohydroxamic acid	11	9.34	110	6.34	6.09
			120	9.52	
			12-1	-0.68	
			230	19.05	
			320	19.24	
acetic acid	11	3.55	110	2.16	6.00
			120	2.91	
			130	3.47	
oxalic acid***	11	3.4	110	4.20	6.06
			120	6.31	
			111	5.63	
tartaric acid***	11	3.97	110	3.12	6.01
	12	6.79			
mercaptoethanol	11	9.40	110	6.7	6.17
			120	8.7	
			340	33.3	
			350	39.8	
cysteine	11	10.4	110	12.3	9.39
	12	18.6	120	18.6	
Penicillamine[30]	11	10.6	110	13.5	10.6
	12	18.5	120	17.4	
(β,β-dimethyl-D-cysteine)	13	20.4			
DMSA[31]	11	10.79	110	17.4	13.44
(2,3-dimercapto succinic acid)	12	19.68			
	13	23.16			
	14	25.87			
EDTA	11	10.2	110	18.0	16.18
(ethylenediaminetetraacetic acid)	12	16.3	111	20.8	
	13	19.0			
	14	21.0			

†Data are from this work (the first four ligands) and Martell and Smith,[12] unless noted.
*pM = -log($[Pb^{2+}]_{free}$) under the conditions: pH = 7.4, $[Pb^{2+}]$ = 1μM, [L] = 10μM
**Estimates
***Lead(II) stability constants were reported for μ = 1.0.

Table 5.

Stability Constants of Acetohydroxamic Acid with Some Important Metals,†
$\log\beta_{mlh}$ in water, under the conditions, μ= 0.10, 25.0°C

hlm	Pb(II)	Cu(II)	Ni(II)	Zn(II)	Mn(II)	Fe(III)
110	6.34	7.89	5.15	5.18	4.0	10.38
120	9.52	14.06	9.18	9.45	6.9	20.28
130			11.68	11.57		27.9
11-1			-4.35	-3.40		
12-1	-0.68	4.44				
230	19.05					
320	19.24					
pM	6.091	6.985	6.007	6.008	6.001	12.700

†Stability constants listed are from:
Pb(II), this work;
Mn(II), 20.0°C, Anderegg and coworkers;[24]
Fe(III), Schuaib and coworkers;[32]
Cu(II), Ni(II), Zn(II), the review by Kurzak, Kozlowski, and Farkas.[26]

Table 6.

Stability Constants of N-phenyl-thiobenzohydroxamic Acid
with Pb(II), Zn(II), and Mn(II)[27]
$\log\beta_{mlh}$ in 75% dioxane, under the conditions, μ= 0.10, 30.0°C

hlm	Pb(II)	Zn(II)	Mn(II)
110	11.3	10.1	6.1
120	20.7	18.6	12.8
pM	8.551	7.076	6.0004

References

(1) Hartley, F. R.; Burgess, C.; Alcock, R. *Solution Equilibria*; Wiley & Sons: Chichester, 1980.

(2) Rossotti, F. C.; Rossotti, H. *The Determination of Stability Constants*; McGraw-Hill: New York, 1961.

(3) *Computational Methods for the Determination of Formation Constants*; Leggett, D. J., Ed.; Plenum Press: New York, 1985.

(4) May, P. M.; Williams, D. R.; Linder, P. W.; Torrington, R. G. *Talanta* **1982**, *29*, 249.

(5) Gran, G. *Analyst* **1952**, *77*, 661.

(6) Vogel, A. I. *Quantitative Inorganic Chemistry;* 3rd ed.; Longmans: London, 1961.

(7) Harris, W. R.; Raymond, K. N. *J. Am. Chem. Soc.* **1979**, *101*, 6534.

(8) Harris, W. R.; Raymond, K. N.; Weitl, F. L. *J. Am. Chem. Soc.* **1981**, *103*, 2667.

(9) Kappel, M. J. Ph. D. Thesis, University of California, Berkeley, 1983.

(10) Franczyk, T. S. Ph. D. Thesis, University of California, Berkeley, 1991.

(11) Scarrow, R. C. Ph. D. Thesis, University of California, Berkeley, 1985.

(12) Martell, A. E.; Smith, R. M. *Critical Stability Constants;* 1974, 1975, 1977, 1976, 1982,1989 ed.; Plenum: New York; Vol. 1-6.

(13) Sun, P.; Quintus, F.; Freiser, H. *Anal. Chem.* **1964**, *36*, 2485.

(14) Scarrow, R. C.; Riley, P. E.; Abu-Dari, K.; White, D. L.; Raymond, K. N. *Inorg. Chem.* **1985**, *24*, 954.

(15) Silverstein, R. M.; Bassler, G. C.; Morrill, T. C. *Spectroscopic Identification of Organic Compounds;* 4th ed.; Wiley & Sons: New York, 1981.

(16) Jones, R. A.; Katritzky, A. R. *J. Chem. Soc.* **1960**, *1960*, 2937.

(17) Mizukami, S.; Nagata, K. *Chem. Pharm. Bull.* **1966**, *14*, 1249.

(18) Martell, A. E.; Motekaitis, R. J. *Determination and Use of Stability Constants*; VCH: New York, 1988.

(19) Sylva, R. N.; Brown, P. L. *J. Chem. Soc. Dalton Trans.* **1980**, *1980*, 1577.

(20) Greenwood, N. N.; Earnshaw, A. *Chemistry of the Elements*; Pergamon Press: Oxford, 1984.

(21) Harrison, P. G. In *Comprehensive Coordination Chemistry*; G. Wilkinson, Ed.; Pergamon Press: Oxford, 1987; Vol. 3; pp 183.

(22) Calvin, M.; Wilson, K. W. *J. Am. Chem. Soc.* **1945**, *67*, 2003.

(23) The stereochemistry of the donor groups about the lead atom may be cis or trans. Crystal structures for both the cis and trans forms of the bis(acetothio-hydroxamato)-nickel(II) complex are described in: Mizukame, S.; Nagata, K. *Coord. Chem. Rev.* **1968**, *3*, 267.

(24) Anderegg, G.; L'Eplattenier, F.; Schwarzenbach, G. *Helv. Chim. Acta* **1963**, *46*, 1400.

(25) Abu-Dari, K.; Freyberg, D.; Raymond, K. N. *Inorg. Chem.* **1979**, *18*, 2427.

(26) Kurzak, B.; Kozlowski, H.; Farkas, E. *Coord. Chem. Rev.* **1992**, *114*, 169. and references therein.

(27) Dietzel, R.; Thomas, P. *Z. Anorg. Allg. Chem.* **1971**, *381*, 214.

(28) As an illustration, the pK_a of N-phenylbenzothiohydroxamic acid in 75% dioxane was reported by Dietzel and Thomas[27] to be 11.5, compared to the pK_a of 5.68 for the thiohydroxamate group of m-hydroxy-N-methylthiobenzohydroxamic acid in water, reported here.

(29) Mathur, S. P.; Bhandari, C. S. *J. Macromol. Sci.-Chem.* **1981**, *A15*, 609.

(30) Doornbos, D. A.; Faber, J. S. *Pharm. Weekblad* **1964**, *99*, 289.

(31) Harris, W. R.; Chen, Y.; Stenback, J.; Shah, B. *J. Coord. Chem.* **1991**, *23*, 173.

(32) Schuaib, N. M.; Marafie, H. M.; Hassan, M. M.; El-Ezaby, M. S. *J. Inorg. Biochem.* **1987**, *31*, 171.

B. Structural Characterization of Lead(II) Hydroxamates

Introduction

When designing metal-specific chelating agents it is advantageous to use the preferred coordination environments of the targeted species as guides. To evaluate the suitability of thiohydroxamates and hydroxamates as subunits of lead sequestering agents, we extended the study of the lead thiohydroxamates and hydroxamates from solution thermodynamic measurements reported in the previous section, to structural characterization. One of the interesting and challenging aspects of attempting to bind lead(II) is the apparent lack of dominant features in known compounds which would warrant rational structural predictions. Lead(II) coordination complexes often contain a large range of metal-ligand distances within the coordination sphere-- a few short lead-ligand distances and other bonds between lead and ligands of similar type up to 0.7Å longer. Coordination numbers ranging from 3 to 10 are found in metal-ligand complexes, with the geometry about the lead atom described as distorted or very distorted from ideal due to the stereochemical activity of the lone pair of electrons. (Examples of lead(II)-ligand solid state structures are described briefly in Table 7.) Lead crystal structures also show a range of molecular aggregation - from monomers and dimers to chain-like structures and three-dimensional nets.

Determining and describing the environment about a lead atom in a solid is not always a straightforward task. The covalent radii used in the "bonding" or "connecting" step of crystallographic data analysis can result in substantial differences in what structural features are detected and reported. One researcher's monomer could be another's monomer with additional long range interactions, or a weakly held dimer, or a chain-like structure. Using a large lead(II) covalent radius in crystallographic data analysis software allows for consideration of all possible interactions, including atoms that are at relatively long distances from the lead atom yet occupy a definite, angularly demanding position within the coordination sphere. The coordination geometry about lead is typically irregular due to the presence of the lone pair of electrons and extended bonding, often making the description of a structure in terms of a regular polyhedron, and comparison of bonding parameters between structures, a challenge.

Table 7.
Coordination Geometries for Selected Lead Complexes.

Compound	C. N.†	Geometry*	Ref.
tris(benzenethiolato)lead(II)	3	trigonal pyramidal	1
lead(II) N,N-diisopropyl-dithiocarbamate	4	pyramidal	2
bis[hydroxolead(II)] 5,5'-azotetrazolediide	5	square pyramidal	3
bis[tris(pyrazolyl)borato]lead(II)	6	octahedral	4
lead(II) monoglycerolate	6	tetragonal pyramidal	5
chloro(2,6-diacetylpyridine disemicarbazone)lead(II)nitrate	6	pentagonal pyramidal	6
bis(oxamato-O,O')lead(II) monohydrate	7	pentagonal bipyramidal	7
bis(2,2',2"-triaminotriethylamine) lead(II) dichloride	8	cubic	8
tris(2,2':6',2"-terpyridine)lead(II) bis(perchlorate)	9	irregular	9
(4,7,13,16,21,24-hexaoxa-1,10-diazabicyclo[8.8.8]hexacosane) lead(II) thiocyanate	10	trigonal-capped hexagonal pyramid	10
$K_2PbNi(NO_2)_6$	12	cubic	11

†Coordination numbers listed reflect the published structure, without further analysis for additional bonding interactions based on positional parameters; however, an effort was made to include examples where the coordination about the lead atom is as listed.

*Geometries are described with respect to the ligand donor atoms. Most are distorted, or very distorted, due to the stereochemically active lone pair of electrons.

Despite the rich structural diversity found in lead(II) compounds, surprisingly few systematic studies have been carried out which would elucidate trends in its coordination chemistry. Harrison and coworkers[12] set out to help rectify this "relative paucity of structural data for lead(II) complexes" by synthesizing and determining the X-ray crystal structures of a series of lead carboxylate compounds including: lead(II) formate, lead(II) acetate trihydrate, lead(II) pentafluorobenzoate bis(methanol) solvate, lead(II)-EDTA hydrate, and di-lead(II)-bis(EDTA) trihydrate. The formate has a three-dimensional structure; the acetate structure contains chains linked by hydrogen bonds to form sheets; the benzoate complex has a linear chain structure; the EDTA monohydrate structure contains isolated monomeric and dimeric units. The lone pair of lead electrons was active in all of the carboxylate structures, based on geometrical deviations from ideal polymorphs, except for the formatecomplex . In the series of carboxylate structures, lead exhibits a preference for eight-coordination, except for the monomeric units in the lead(II)-EDTA complex, which contain seven-coordinate lead; yet the compounds display a variety of stereochemical arrangements about lead and a range of Pb-O bond lengths. Polymer formation was apparently disfavored as the steric bulk of the ligand increased.

Another feature found in many lead crystal structures is evidence for an expanded coordination sphere, described as outer sphere coordination, long-range interactions, or secondary interactions. As an illustration of lead(II) coordination geometries within a single compound and long-range interactions, consider the lead-containing complex cation in triacetato(dichloro)tri-lead(II) tetrachloroaurate(III)[13] where there are three independent lead atoms linked by chloride and acetate ions to form a sheet polymer. Geometric parameters of the complex are listed in Table 8. The coordination about the three lead atoms is described as irregular and, when only the shorter contacts are considered, markedly one-sided due to the effect of the lone pair. There are two sets of distances for a given donor atom type, albeit with seemingly arbitrary bond distance cut-offs for the inner coordination sphere, and coordination numbers for lead ranging from four to nine depending on the Pb-O and Pb-Cl bond distance limits i.e. the sum of ionic radii, lead ionic radius plus chloride or oxygen van der Waal radius, or some other criterion. Another example is the crystal structure of lead with 2,4,6-trinitro-1,3-benzenediol[14] in which the lead coordination number varies from four to eight, including a $[Pb_4(OH)_4]^{4+}$ unit with distorted tetrahedral geometry.

Table 8.
Lead(II) Coordination in triacetato(dichloro)trilead(II) tetrachloroaurate(III).13
An example of bonding variation within a lead crystal structure.

		Inner Coordination Sphere		Longer Contacts	
Atom	C. N.*	Acetate	Chloride	Acetate	Chloride
Pb1	5+3	2.65, 2.43	2.84-3.04	2.72, 3.16	3.39
Pb2	4+4	2.45, 2.49	3.03, 3.04	2.81, 3.00	3.28, 3.41
Pb3	6+3	2.56, 2.61 (chelating) 2.46, 2.60, 2.68, 2.68 (non-chelating)			3.14, 3.48, 3.45

*Coordination number listed as number of inner sphere plus longer contact interactions.

The stereochemical activity/inactivity of the lone pair of electrons in lead complexes is an area of continuing investigation. Recently Reger and coworkers[4] reported the structure of bis[poly(tris)borato]lead(II) and claimed it was the first example of a six-coordinate, main-group, molecular compound in which the lone pair is stereochemically inactive; however, there are structures which conform to idealized octahedral geometry equally well, such as those of hexakis(thiourea)lead(II) perchlorate[15] and hexakis(antipyrine)lead(II) perchlorate.[16] Searching for trends in the activity of the lone pair and metal-complex stability related to donor atom type, Hancock and coworkers successively replaced oxygen donors with nitrogen donors in a macrocyclic ligand and found that when three or four nitrogen atoms are present there is a marked increase in the change of complex stability per nitrogen donor added. This increase was attributed to a change from a stereochemically inactive lone pair with approximately two or fewer nitrogen donors present (and rather ionic bonding) to an active lone pair with more nitrogen donors. However, other data indicate that the activity/inactivity of the lone pair does not depend exclusively on ligand donor atom type or steric effects from ligand size. The sheet-like lead formate structure reported by Harrison[12] contained no evidence for the lone pair. Another simple ligand sheet-like structure, 2-hydroxyethanethiolatolead(II) nitrate[17] where both the nitrate and thiolate act as bidentate ligands and as bridges between lead atoms, provides evidence for the lone pair.

Raymond and Abu-Dari[18] initiated a lead(II) sequestering agent research program (of which this work is a part) by preparing and characterizing lead(II)-thiohydroxamate complexes.

They found the lead(II)-linear thiohydroxamates, bis(N-methylthiobenzo-hydroxamato)lead(II) and bis(N-methylthioacetohydroxamato)lead(II), crystallized as five-coordinate monomers with additional long-range interactions with sulfur and oxygen atoms of adjacent molecules[18] and the lead complex of a cyclic thiohydroxamate, bis(N,N-diethyl-oxo-22(1H)pyridine-thione-6-carboxyamide)lead(II) crystallized as a weakly coupled dimer of five-coordinate lead atoms.[19] Transition metal thiohydroxamate complexes are structurally quite different. In bis(thioacetohydroxamato)-nickel(II) nickel is in *cis* and *trans* square planar configurations,[20,21] and in bis(N-methylthioformohydroxamato) copper(II) the copper atom has *trans* square-planar coordination geometry.[22] Leong and Bell[23] prepared a series of octahedral tris(N-methylthioformohydroxamato)-metal ion substituted complexes, $M(th)_3$ (M(III) = Fe, Co, Cr, Rh) and a series of square-planar bis(N-methylthioformohydroxamate)-metal ion substituted complexes $M(th)_2$ (M(II) = Cu, Ni, Pd, Pt) and characterized them using infrared and UV/visible spectroscopy. Similarly, transition metal hydroxamate complexes[24-26] are octahedral for M = Fe(III), Co(II), Ni(II) and Zn(II), and slightly distorted tetrahedral for Cu(II).

By preparing and structurally characterizing lead hydroxamates the following questions were addressed : How do the complexes differ from other metal-hydroxamtes? How do the hydroxamates compare with the thiohydroxamates in terms of lead coordination? Do the smaller oxygen donor atoms favor oligomer formation and/or higher coordination numbers? What is the effect of ligand substituent bulkiness on coordination number and polymer formation? What role do the lead $6s^2$ electrons play in bonding? Will the lone pair be stereochemically active, and if so, to what extent does it affect the geometry about the lead atom?

To this end lead complexes of three hydroxamic acids have been synthesized and characterized. Crystal structures of the lead complexes of the aryl substituted hydroxamates, N-phenyl-toluyl-hydroxamic acid and N-toluyl-*tert*-butyl-hydroxamic acid along with infrared spectral data, are presented. The geometry and bonding of lead hydroxamates, including molecular orbital considerations, will be described.

Experimental

Synthesis

General. Reagent grade chemicals and solvents were used throughout the syntheses without further purification, unless otherwise noted. Thin-layer chromatography (TLC) was performed using Whatman KGF 250 μm silica on glass plates. Visualization was achieved by iodine vapor. Melting points were taken in open

capillaries with a Büchi apparatus and are uncorrected. Elemental analyses were performed by the Microanalytical Laboratory, College of Chemistry, University of California, Berkeley. Infrared spectra were obtained in KBr pellets, or as Nujol mulls between KBr disks, and were recorded on a Nicolet 5DXB FTIR Spectrometer.

Acetohydroxamic acid. Sodium methoxide (21g, 0.90 mol Na) was added to a solution of hydroxylamine hydrochloride (42g, 0.60 mol) in 300 mL of methanol. Sodium chloride was removed by filtration. The filtrate containing the hydroxylamine was added to ethyl acetate (29 mL, 0.30 mol) in methanol (25 mL) and the mixture was stirred overnight. The methanol/ethyl acetate was removed by rotary-evaporation and the resulting white powder was recrystallized from ethyl acetate/hexane to yield the desired product, mp 87.8 - 89.0°C, lit.: 89-92°C[27] Anal. Calcd. (found) for $C_2H_5NO_2$: C, 32.00 (31.61); H, 6.71 (6.70); N, 18.66 (18.77). IR (cm^{-1}): 3200(s,b), 3053(s), 3000,(s) 2930(m), 2862(w), 1630(s), 1551(m), 1451(m), 1371(m), 1318(m), 1186(w), 1092(s), 1039(w), 993(s), 966(w), 830(w,b), 745(m,b), 650(m), 587(s), 545(m).

Lead complexes of acetohydroxamic acid. A) Lead acetate trihydrate (1.263g, 3.33 mmol) was added to a solution of acetohydroxamic acid (0.500 g, 6.66 mmol) in 20 mL of methanol and the reaction mixture was stirred at 65°C for one hour. As the lead salt slowly dissolved the solution changed from clear, colorless to very pale yellow, followed by precipitation of a white solid . The solution pH was measured to be 5.0 using a combination pH electrode. The solid was isolated by filtration and dried under house vacuum for 12 hours. Recrystallization of the reaction product from hot/cold methanol yielded fine white needles (0.724 g, 2.1 mmol, 64% based on lead) mp 183.0-184.5°C, Anal. Calcd. (found) for $PbC_4H_7NO_4$: C, 14.12 (13.96); H, 2.07 (1.97); N, 4.11 (4.02). IR of lead complex (cm^{-1}): 3436(w,b), 3238(s,b), 3048(w), 2958(w), 2932(w) 2870(w), 2802(w), 2748(w), 2638(w), 1625(s), 1598(s), 1559(m), 1534(s), 1438(m), 1422(m), 1385(m), 1319(s), 1167(w), 1089(s), 1033(w), 988(s), 970(w), 849(w), 712(m), 664(s). IR of lead acetate (cm^{-1}): 3428(w,b), 2965(w), 2928(w), 1576(s), 1522(s), 1409(s), 1341(s), 1045(s), 1022(w), 934(w), 656(s).

B) Lead nitrate (2.206 g, 6.66 mmol) was added to a mixture of triethylamine (1.85 mL, 13.32 mmol) and acetohydroxamic acid (1.00 g, 13.32 mmol) in 30 mL methanol. A fine white precipitate formed immediately, and continued to form as the lead salt dissolved. The reaction mixture was stirred vigorously for 12 hours, after which a white powder was recovered by filtration. Recrystallization of a portion of the powder from hot/cold water yielded thin white needles mp 210.5-211.3°C, Anal. Calcd. (found) for $Pb_2C_{7.5}H_{18}N_3O_{7.5}$: C, 13.15 (13.60, 13.19); H, 2.63 (2.22, 2.46); N, 6.14 (6.78, 6.92). IR of lead complex (cm^{-1}): 3430(m,b), 3231(s), 3055(w), 2939(w), 2875(w),

2770(m,b), 2695(w), 2644(w), 1623(s), 1597(s), 1550(m), 1532(s), 1443(m), 1422(m), 1385(m), 1320(s), 1089(s), 1050(w), 988(s), 970(w), 831(w,b), 719(m), 666(s).

bis(N-phenyl-toluylhydroxamato)-bis(μ-N-phenyl-toluylhydroxamato)-dilead(II)-dimethanol solvate (PbHY1). Dr. Andrew Borovik prepared the lead complex of N-phenyl-toluylhydroxamic acid by adding lead(II) nitrate to a methanolic solution of the hydroxamic acid and one equivalent of triethylamine. Crystals of the compound were obtained by recrystallization of the reaction product from methanol. IR of crystals (cm^{-1}): 3426(m,b), 3062(m), 3035(m), 2922(w), 2867(w), 1612(m), 1582(s), 1541(s), 1513(w), 1491(m), 1457(m), 1420(m), 1311(w), 1292(w), 1278(w), 1184(w), 1150(m), 1116(w), 1054(m), 1037(s), 1025(m), 944(s), 827(s), (m)775(s), 725(s), 697(s), 613(s).

bis(N-toluyl-*tert*-butyl-hydroxamato)-bis(μ-N-toluyl-*tert*-butyl-hydroxamato)dilead(II)·N-toluyl-*tert*-butyl-hydroxamic acid (PbHY2). Lead(II) acetate trihydrate (0.92 g, 2.41 mmol, Aldrich 99.999%) was added in one portion to a methanolic solution of N-toluyltertbutylhydroxamic acid (1.00 g, 4.82 mmol in 30 mL). The pale yellow solution was stirred at about 75° C for 2 hours. Thin layer silica gel chromatography of the reaction mixture showed a single spot with greater retention than the reactant ligand. Methanol was removed using rotary evaporation leaving a pale yellow oil. The yellow oil was dissolved in warm ethanol, which upon cooling yielded small, pale yellow crystals (1.25 g, 1.51 mmol of **2**). The desired lead complex was isolated, along with a hydrogen-bound ligand molecule, via recrystallization from ethanol, mp 132-133 °C. IR of unreacted ligand (cm^{-1}): 3154(s,b), 2955(s) 2871(w), 1596(s,b), 1512(s), 1490(m), 1402(m), 1357(s), 1225(m), 1077(s), 941(w), 883(m), 824(s), 775(m), 580(m), 508(m). IR of lead complex (cm^{-1}): 3187(m,b), 2965(s), 2958(m), 1658(w), 1602(w), 1540(s,b), 1508(w), 1483(m), 1408(s), 1298(w), 1250(w), 1085(m), 975(m), 828(m), 666(m), 565(m). Anal. Calcd. for $Pb_2C_{72}H_{114}N_{62}O_{12}$ (found): C, 52.28 (52.62); H, 5.97 (6.10); N, 5.08 (4.95).

tetra(μ-N-toluyl-*tert*-butyl-hydroxamato)-tetra(μ-acetato)-tetralead(II) (PbHY3). Triethylamine (0.67 mL, 4.82 mmol) was added to a methanolic solution of N-toluyltertbutylhydroxamic acid (1.00 g, 4.82 mmol in 50 mL), after which lead(II) acetate trihydrate (0.92 g, 2.41 mmol, Aldrich 99.999%) was added. The pale yellow solution was stirred at room temperature for 12 hours. The resulting viscous yellow solution was heated to about 75°C, stirred for 20 minutes, then filtered. Small, clear, very pale yellow crystals formed upon cooling of the filtrate and slow evaporation of the solvent. The lead complex was recrystallized from 50% methanol/ethanol. IR of lead complex (cm^{-1}): 3129(w,b), 2969(s), 2925(m), 2869(w), 1653(w), 1643(s), 1607(w),

1538(s,b), 1512(w), 1481(m), 1459(w), 1363(m), 1337(s), 1308(m), 1248(w), 1220(w), 1077(m), 1002(s), 958(s), 947(m), 882(w), 829(m), 824(m), 796(w), 639(w), 580(m), 508(m). Anal. Calcd. for $Pb_2O_8N_2C_{28}H_{38}$(found): C, 35.58 (35.43); H, 4.05 (4.10); N, 2.97(2.74).

X-ray Crystallographic Structure Determinations

General. Suitable crystals were chosen directly, or obtained by cutting larger crystals, and mounted on glass capillaries using epoxy. Data were collected using an Enraf-Nonius CAD-4 four-circle diffractometer equipped with a locally modified low-temperature device. Cell parameters were obtained by least-squares refinement of the angular settings of 24 strong, high-angle reflections well-spaced in reciprocal space. Because there were no systematic absences in precession photographs for all three complexes, the choice of space group was limited, and $P\bar{1}$ (#2) was subsequently determined from structure analysis. Applying θ - 2θ techniques and MoK_α radiation, intensity data (+h, ±k, ±l) were collected. Reflections used for the azimuthal (ψ) scans were located near χ= 90°, and the intensities were measured at 10° increments of rotation of the crystal about the diffraction vector. The intensities of three standard reflections were measured every 1 h of X-ray exposure time. Orientation checks of the same three reflections were performed after every 200 intensity measurements. The raw intensity data were converted to structure factor amplitudes and their esd's by correction for scan speed, background, Lorentz and polarization effects. Atomic scattering factors and anomalous corrections were from International Tables for X-ray Crystallography.[28]

A table summarizing X-ray data collection parameters and crystallographic data is included in Appendix 1. Positional and thermal parameters, intramolecular distances and angles, and ORTEP[29] diagrams for the crystal structures determined are also in Appendix 1. The crystal structures were all in the space group $P\bar{1}$. The inversion related atoms are indicated with primes throughout this section and in Appendix 1.

bis(N-phenyl-toluylhydroxamato)-bis(μ-N-phenyl-toluylhydroxamato)-dilead(II)-dimethanol solvate (PbHY1). The desired complex co-crystallized with methanol solvent molecules, yielding single crystals of a material with the empirical formula, $Pb_2C_{56}H_{58}N_4O_{10}$. The structure of this complex was determined in collaboration with Dr. Andy Borovik. The density of the crystals, d_m was measured by flotation in a mixture of hexane and bromoform. The sample crystal had dimensions 0.40 x 0.30 x 0.20 mm. Cell parameters were obtained by least-squares refinement of the angular settings of 24 strong reflections in the 2θ range $27.2° \leq 2\theta \leq 28.9°$. Intensity data (+h, ±k, ±l) were collected at -117°C in two intervals: $3° \leq 2\theta \leq 45°$ and $45° \leq 2\theta \leq 55°$,

yielding 6262 datum. The intensities of three standard reflections were measured every hour of X-ray exposure time.[30] Reorientation was necessary four times during data collection. Inspection of the list of intensity standards showed a loss of 2.6% for $3°\leq 2\theta \leq 45°$data, and hence a linear decay correction was applied. High angle data showed no indication of decay. An empirical absorption correction was made by the use of ψ-scan data. The correction factors ranged from 74.35 to 99.64%, with an average of 86.68%. The two data sets were merged with a 3.1% intensity correction applied to the high angle data. Redundant data (0 -k l) were removed. The heavy atom positions were established using Patterson methods. The structure was solved and refined via standard full-matrix least-squares and Fourier techniques with a Digital Equipment Micro-Vax 4000 computer using SDP software.[31] A difference Fourier map calculated following anisotropic refinement of all non-hydrogen atoms revealed the positions of all hydrogen atoms. Hydrogen positional and thermal parameters were refined. (Aromatic hydrogens were introduced at fixed positions (C-H distance = 0.95 Å[32], bisecting the C-C-C angles); methyl hydrogens also at fixed positions (C-H distance = 0.95 Å, H-C-H angle = 109.5°) The secondary extinction coefficient was included and refined to 4.5963×10^{-7}.[33] Full matrix least-squares refinement with 447 variables, using 5393 reflections with $(F_o)^2 \geq 3\sigma(F_o)^2$, led to convergence with R = 0.022, R_w = 0.028, S = 1.367. The maximum shift/esd on the final cycle = 0.00 and the largest peak on final difference Fourier map = 0.1.116 e/Å^{-3}.

bis(N-toluyl-*tert*-butyl-hydroxamato)-bis(μ-N-toluyl-*tert*-butyl-hydroxamato)dilead(II)·N-toluyl-*tert*-butyl-hydroxamic acid (PbHY2). Single crystals of the compound were obtained by recrystallization of the reaction product from hot ethanol followed by cooling of the saturated solution. The sample crystal had dimensions 0.3 x 0.3 x 0.2 mm. Cell parameters were obtained by least-squares refinement of the angular settings of 24 strong reflections in the 2θ range $23.2° \leq 2\theta \leq 24.9°$. A total of 4937 intensity data (+h, ±k, ±l) was collected at -77°C, where $3°\leq 2\theta \leq 45°$. The intensities of three standard reflections were measured every 1 h of X-ray exposure time.[34] Reorientation was necessary four times during data collection. Inspection of the list of intensity standards showed a loss of 3.8% for $3°\leq 2\theta \leq 45°$data, and hence a linear decay correction ranging from 1.000 to 1.038 was applied. An empirical absorption correction was made by the use of ψ-scan data. The correction factors ranged from 66.42 to 99.76, with an average of 85.50%. Redundant data (0 -k l) were removed. The structure was solved by Patterson methods using SHELXS-86 software[35], and refined via standard full-matrix least-squares and Fourier techniques. One of the tertiary butyl groups was disordered; it modeled as half occupancy on two sets

of positions. A difference Fourier map calculated following anisotropic refinement of all non-hydrogen atoms revealed the positions of all hydrogen atoms. Positional parameters for a hydrogen atom within bonding distance to two hydroxamic acids (one of which is bound to the lead atom) were refined. The remaining hydrogens were placed in calculated positions and their thermal and positional parameters were constrained to ride on their parent atoms. Aromatic hydrogens were introduced at fixed positions (C-H distance = 0.95 Å, bisecting the C-C-C angles); methyl hydrogens also at fixed positions (C-H distance = 0.95 Å, H-C-H angle = 109.5°) A total of 49 atoms were refined anisotropically; 89 atoms were included in the structure factor calculation. The secondary extinction coefficient[33] was included and refined to 1.0223×10^{-7}. Full matrix least-squares refinement with 443 variables, using 4160 reflections with $(F_o)^2 \geq 3\sigma(F_o)^2$, led to convergence with R = 0.021, R_w = 0.028, S = 1.269. The maximum shift/esd on final cycle = 0.01 and the largest peak on final difference Fourier map = 1.252 e/Å^{-3}.

tetra(μ-N-toluyl-*tert*-butyl-hydroxamato)-tetra(μ-acetato)-tetralead(II) (PbHY3). Single crystals of the compound were obtained by recrystallization of the reaction product from ethanol/methanol. The crystal chosen for the structure determination had the dimensions 0.10 x 0.10 x 0.30 mm. The structure of this complex was determined by the group of students, Victor Christou, George Lucier, and Chad Sofield, to fulfill a requirement of the U.C., Berkeley, Department of Chemistry, X-ray Crystallography course. A total of 4036 intensity data (+h, ±k, ±l) was collected over 21.2 hours at -95°C, where $3° \leq 2\theta \leq 45°$. The intensities of three standard reflections were measured every hour of X-ray exposure time.[36] Reorientation was necessary three times during data collection. Inspection of the list of intensity standards showed a loss of 0.426 per hour, 9.1%, for $3° \leq 2\theta \leq 45°$data, and hence a linear decay correction ranging from 1.000 to 1.048 was applied. An empirical absorption correction was made by the use of ψ-scan data. The correction factors ranged from 72.87 to 99.90, with an average of 88.81%. Redundant data (0 -k l) were removed. The structure was solved by Patterson methods and refined via standard full-matrix least-squares and Fourier techniques . One tertiary butyl group was disordered, and was modeled as half occupancy. A difference Fourier map calculated following anisotropic refinement of all non-hydrogen atoms revealed the positions of all hydrogen atoms. A total of 41 atoms were put in at calculated positions and refined anisotropically; 61 atoms were included in the structure factor calculation. Full matrix least-squares refinement with 350 variables, using 2927 reflections with $(F_o)^2 \geq 3\sigma(F_o)^2$, led to convergence with R = 0.029, R_w = 0.034, S = 1.339. The maximum shift/esd on final cycle = 0.04.

Results and Discussion

Crystal structures of the lead complexes of the aryl substituted hydroxamates, N-phenyl-toluyl-hydroxamic acid and N-toluyl-*tert*-butyl-hydroxamic acid, each show five-coordinate dibridged dimers, with the lead lone pair of electrons stereochemically active. These structures are used along with infrared spectral data, to propose compositions of acetohydroxamato-lead complexes, which crystallized as thin needles unsuitable for single crystal X-ray analysis under a variety of conditions. Molecular orbital calculations were performed, using the structural data obtained for one of the hydroxamate complexes and published data for a pseudo octahedral lead(II) complex, to compare the geometry and bonding of two lead structural types.

When discussing the bonding in lead complexes, ranges of interatomic distances are used to discriminate between different types of interactions. The limiting distance for primary lead-oxygen bonds was chosen to be the 2.85 Å, the sum of the lead and oxygen ionic radii.[37] Other useful lead-oxygen distances used to identify attractive atomic interactions, or secondary bonding are: 3.54Å, the sum of the van der Waal radii; 3.02 Å, the sum of the covalent radius for lead[38] and the van der Waal radius for oxygen[39]; and 2.54Å, the sum of the ionic radii for six coordinate lead and two coordinate oxygen.[37].

Structural Analyses. The N-phenyl-toluylhydroxamato lead complex is dimeric, with five-coordinate, inversion-related lead atoms bridged by two hydroxamate N-bound oxygens. The compound, (bis(N-phenyl-toluylhydroxamato)-bis(μ-N-phenyl-toluylhydroxamato)-dilead(II)-dimethanol solvate) **1** shown in Figure 21, has a planar Pb_2O_2 parallelogram core with angles of 108° (Pb-O4-Pb') and 72°(Pb-O4'-Pb') and a lead-lead interatomic distance of 4.008Å. The coordination geometry about the lead atoms is best described as distorted octahedral with an N-bound oxygen (O2) and the lead lone pair of electrons occupying axial sites (Figure 22). The equatorial oxygen atoms, O1,O3, O4, O4', have a root-mean-square deviation from planar of 0.33Å. Reflecting the repulsive force of the lead lone pair of electrons, the average angle between the axial oxygen and equatorial oxygens is 75.9°, compared to 90° for idealized octahedral geometry. The lead-oxygen bond lengths range from 2.262 to 2.589Å, with the N-bound oxygen atoms which carry a full negative charge forming shorter bonds (2.262 and 2.345Å) than the "carbonyl" oxygen atoms, except for the bridging N-oxygen, the longest Pb-O bond in the compound.

The lead complex with a more bulky hydroxamate ligand, (bis(N-toluyl-*tert*-butyl-hydroxamato)-bis(μ-N-toluyl-*tert*-butyl-hydroxamato)dilead(II)·N-toluyl-tert-butyl-hydroxamic acid), **2** , is also dimeric, with the same gross structure about lead as seen in

compound **1**. A free ligand (not bonded to the lead atom) is connected to the dimer via a hydrogen bond with a chelating hydroxamate N-oxide. Figure 23 is a view of the dimer only. An ORTEP view including all the atoms in the unit cell is included in Appendix 1. The configuration within the Pb_2O_2 core of **2** differs from **1**, with angles of 99.4°(Pb-O4-Pb') and 80.6° (Pb-O4'-Pb'), a lead-lead distance of 3.913Å, and bridging lead-oxygen lengths of 2.815 and 2.392Å. The geometry about the five-coordinate metal centers is again very distorted octahedral with the stereochemically active lone pair occupying the sixth coordination site opposite O4 (toward the reader in Figures 23 and 24). Distortion from ideal octahedral geometry due to dimer formation and lone pair-bond repulsion is illustrated by the variable bond lengths: 2.392 and 2.463Å (C bound oxygens), 2.295, 2.296 and 2.815Å (N bound oxygens), the average of the axial-equatorial angles 77.1° and angles in the lead-ligand equatorial plane of 65.2, 70.7, 88.5, and 125.2°. In contrast to **1**, the equatorial oxygens are essentially planar, with the total deviation in the plane for O1, O3, O4, and O4' of 0.0307Å.

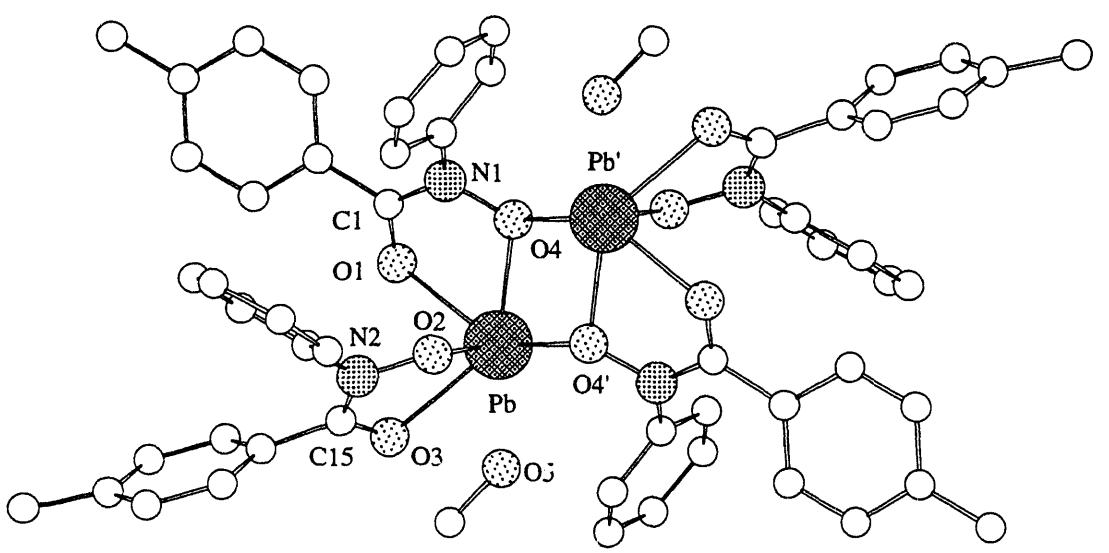

Figure 21. Crystal structure of compound **1**, including the methanol solvent molecules.

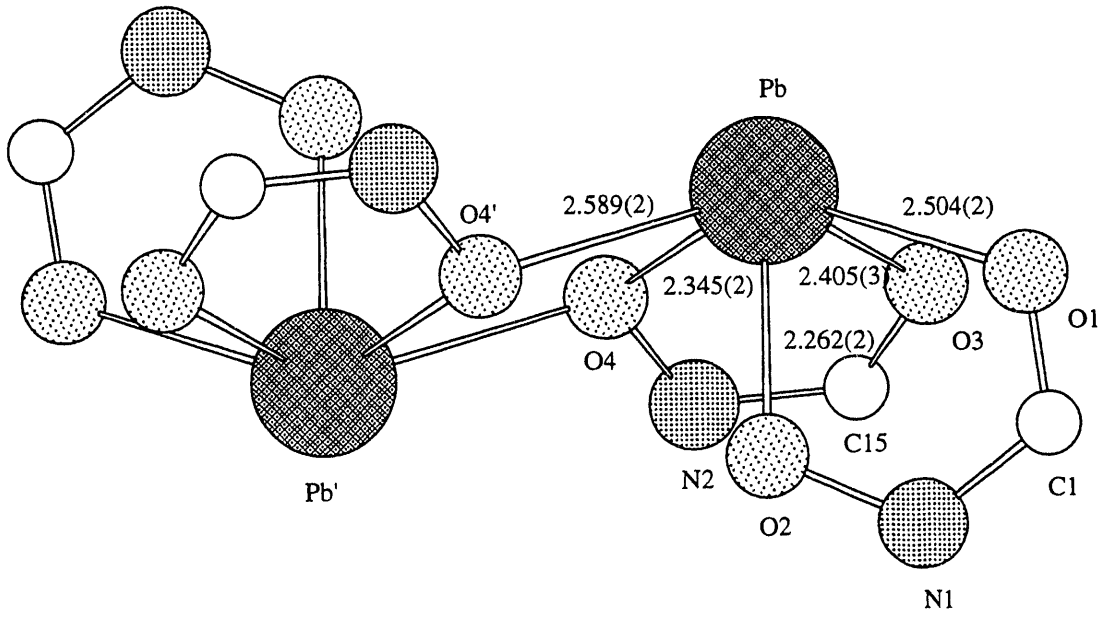

Figure 22. The lead-oxygen dimer core of **1** showing the coordination geometry about the two Pb^{2+} atoms, Pb-O bond lengths, and chelating hydroxamate rings.

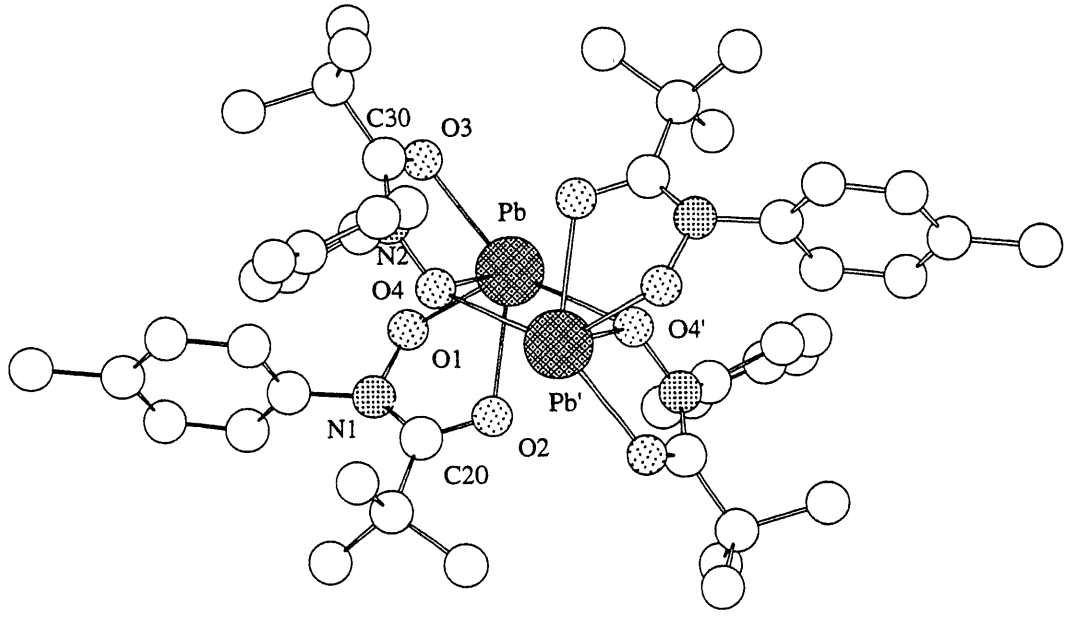

Figure 23. Crystal structure of **2** showing the numbering scheme for the dimer.

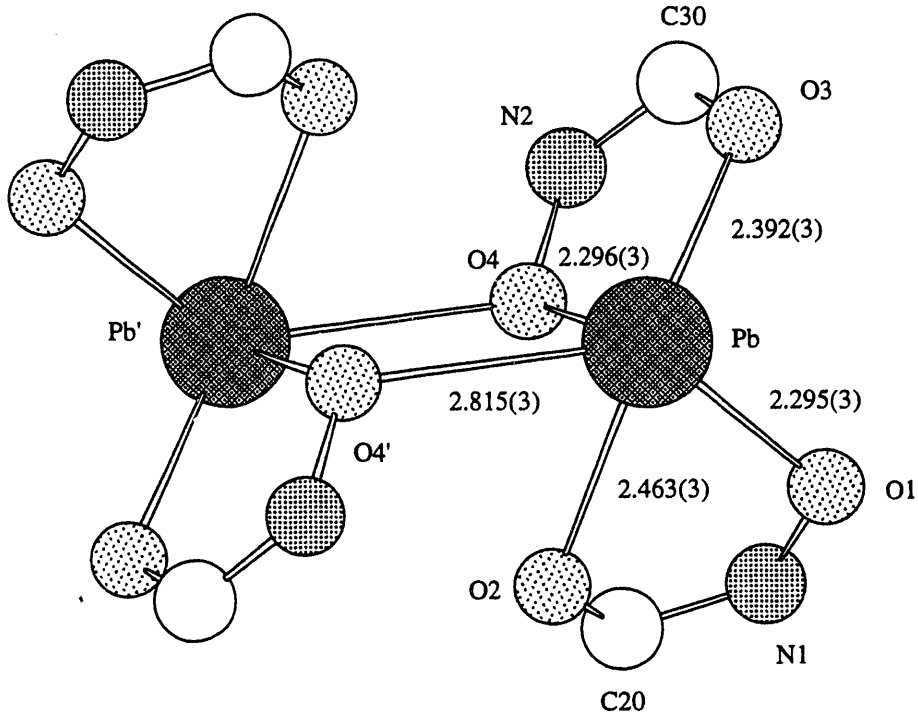

Figure 24. Perspective view of the coordination geometry about the two lead atoms in compound **2**.

When triethylamine was used as a base in the reaction of N-toluyltertbutyl-hydroxamic acid with lead(II) acetate, the product isolated was a tetramer composed of lead-hydroxamate and lead-acetate pieces. The structure of tetra(μ-N-toluyl-*tert*-butyl-hydroxamato)-tetra(μ-acetato)-tetralead(II), **3**, is built up from the asymmetric unit shown in Figure 25. The compound has a five-coordinate dimer with an asymmetric Pb_2O_2 core similar to those seen in the **1** and **2**. In addition, each lead is bonded to two other five-coordinate lead atoms via hydroxamate and acetate bridges. Because the lead-O5 and lead-O3 distances are significantly longer than the sum of the covalent and ionic radii, and the other lead-oxygen bonds in the structure, they are considered secondary bonds, not included in the primary coordination sphere. However, the lead-O5 and lead-O3 distances are substantially shorter than the sum of the van der Waal radii, indicating there is some attractive interaction.

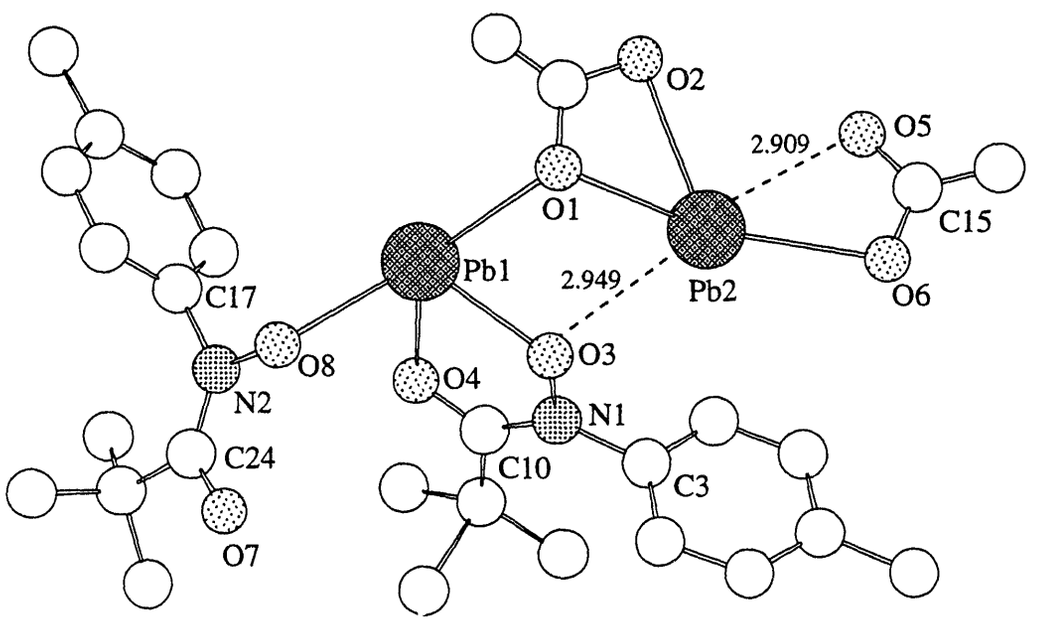

Figure 25. The asymmetric unit in the crystal structure of **PbHY3**. Dashed lines, labeled with lead-oxygen distances in Å, indicate secondary bonding interactions.

The tetrameric units within the solid are loosely linked by O5, the acetate oxygen positioned almost equidistant from Pb2 and Pb1' (2.909 and 2.923Å), resulting in an overall chain-like structure. A piece of the lead-oxygen framework within the crystal structure is shown in Figure 26. There is a similar structure reported in the literature[5] consisting of two six-coordinate diglycerato bridged lead atoms which are also bridged to two other lead atoms. Both the acetate and hydroxamate ligands in **3** are chelating (acetate O1 and O2; hydroxamate O3 and O4) and nonchelating (acetate O5 and O6; hydroxamate O7 and O8). The formation of an eight-membered ring within the tetramer (shown in Figure 27) may have been a contributing force toward polymerization.

Like the dimers in **1** and **2**, two inversion related hydroxamate N- bound oxygen atoms bridge the lead atoms, Pb1 and Pb1', in the structure of **3**. The configuration within the dimer core is similar to **1** with angles of 111.4° (Pb-O3-Pb') and 68.6° (O3-Pb-O3') and a lead-lead distance of 4.058Å. The average axial-equatorial angle, $O3_{ax.}$-Pb-$O_{eq.}$, is 79.7°, the root mean square deviation of the equatorial atoms (O1, O3', O4, O8) from planar is 0.576Å, and the bridging lead-oxygen bond lengths are 2.357 and 2.554Å. The coordination geometry about the two other lead atoms in the tetramer, inversion-related Pb2 and Pb2', is also distorted octahedral, with the lone pair of electrons and the oxygen, O7, occupying axial sites. The average axial-equatorial angle, is 74.1°and the root mean square deviation from planar for the equatorial oxygen atoms is 0.122Å. The coordination spheres of both lead atoms include oxygen atoms, O3 and O5 at interacting distances (less than the sum of the lead and oxygen van der Waal radii and greater than the discretionary primary bond limit, 2.85Å.) The oxygen, O3, is linked to three lead atoms, Pb1, Pb1', and Pb2, within the unit cell at 2.357, 2.554, and 2.949Å, respectively. There is precedence for multibridged lead-oxygen topology in lead oxides structures[40], in adamanta-(μ_4-oxo-hexakis)μ-triphenylsiloxy)-tetralead(II)[41] where the lead-oxygen framework is an adamantane configuration, and $TlPb_8O_4Br_9$[42] , a thallium compound which contains OPb_4 tetrahedra.

Both acetate ligands bind Pb2 asymmetrically: the bond lengths Pb2-O5, Pb2-O6; Pb2-O1, Pb2-O2 are 2.909, 2.688; 2.566, 2.689Å, respectively. Interestingly, the shortest Pb2 acetate bond is to O1 which bridges Pb1 and Pb2, while the longest is to O5 which links Pb1' and Pb2. Lead oxygen bonds in other acetate-containing crystal structures are generally shorter, ranging from 2.43 to 2.74Å in lead trihydrate[12,43] and from 2.37 to 2.8Å in mixed ligand complexes. [13,44,45] The $O_{acetate}$-lead-$O_{acetate}$ bite angles, 45.07 and 48.58°, are small relative to other structures (49.3-51.9°).[12,13,43-45]

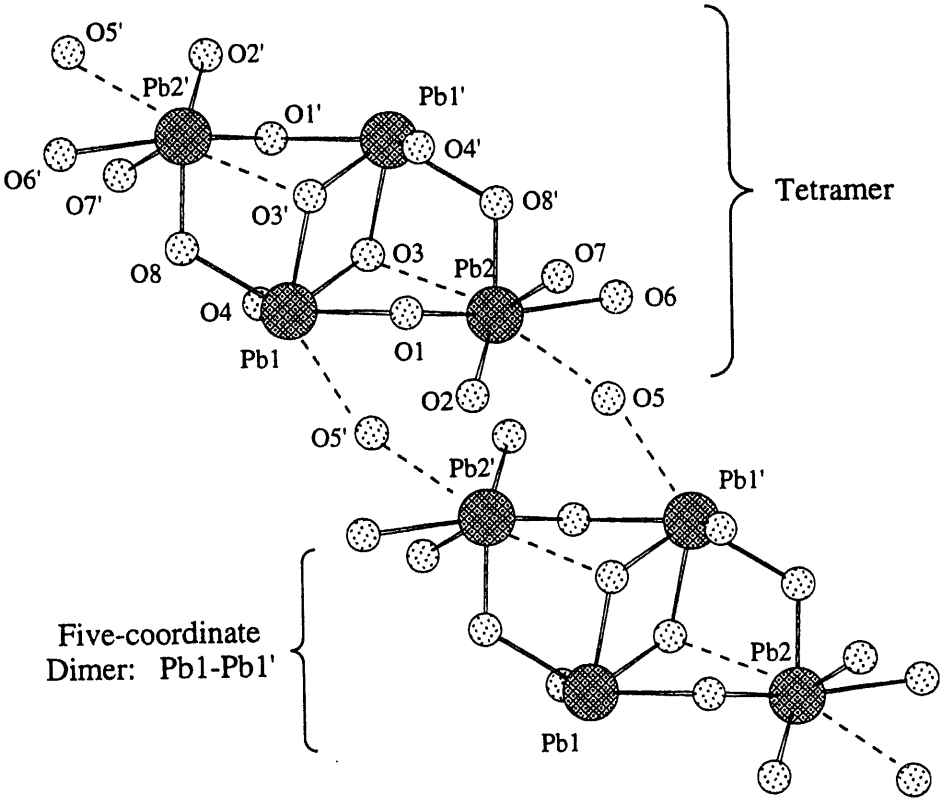

Lead-Lead and Lead-Oxygen Distances

Atom 1	Atom 2	Distance (Å)	Atom 1	Atom 2	Distance (Å)
Pb1	Pb1'	4.058(1)	Pb1'	Pb2	4.152(1)
Pb1	Pb2	4.229(1)	Pb2	Pb2'	3.859(1)
Pb1	O4	2.303(8)	Pb2	O8'	2.276(7)
Pb1	O3	2.357(7)	Pb2	O7	2.292(7)
Pb1	O8	2.518(7)	Pb2	O1	2.566(8)
Pb1	O3'	2.554(6)	Pb2	O6	2.688(7)
Pb1	O1	2.743(7)	Pb2	O2	2.689(8)
Pb1	O5'	2.923(8)	Pb2	O5	2.909(8)
			Pb2	O3	2.949(7)
			Pb2'	O5	3.238
			Pb2'	O2	3.595

Figure 26. The Lead-Oxygen bonding in the crystal structure of compound **3** including a five-coordinate lead dimer within loosely linked tetramers. Interactions where lead-oxygen distances are greater than 2.85 Å are indicated by dashed lines.

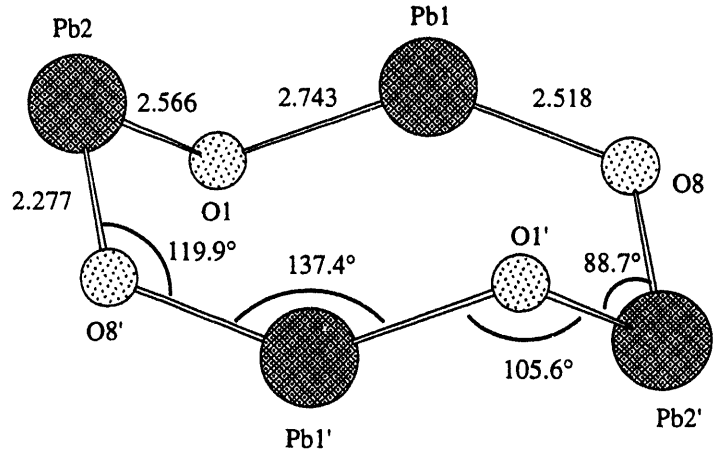

Figure 27. An eight membered ring within the crystal structure of **3**.

Extended structures in which ligand oxygen atoms bridge two more lead atoms range from long range interactions as seen in compound **3** and numerous other crystal structures[46] to dimers, tetramers, and chain-like structures.[47] There is very similar tetrameric structure containing five-coordinate dibridged lead atoms, a dithiocarbamate lead complex where the lead atoms are also monobridged to another lead atom.[48] Dimeric structures like those adopted by lead complexes of the relatively basic hydroxamates **1**, **2**, and **3** are fairly common. Di-bridged lead(II) dimers with lead atoms separated by 3.8-4.1Å have been reported for several other oxygen donor, coordination compounds; for example: lead(II) disaccharinate monohydrate[49]bis(oxamato-O,O')lead(II) monohydrate,[7] 2,4,6-trinitro-1,3-benzenediol monohydrate a lead(II),[50], O-ethylxanthato-quinolin-8-olato-lead(II),[51], and diaquopyridine-2,6-dicarboxylato lead(II) pyridine-2,6-carboxylic acid monohydrate[52]. The configuration of five coordinate lead dimer also occurs in the thiolate complex, lead(II) 1,1-dicyanoethylene-2,2-dithiolate.[53] Although the donor atoms (2S, N, 2O) in the O-ethylxanthato-quinolin-8-olato-lead(II),[51] differ from the hydroxamates, the geometry about the five-coordinate lead atoms is similar, including an unsymmetrical Pb_2O_2 core with Pb-O bond distances of 2.296(5) and 2.548(4)Å, a Pb-O-Pb' angle of 112°, and a Pb-Pb' contact distance of 4.023Å compared to the hydroxamate Pb_2O_2 core in **2** where the Pb-O lengths are 2.345(2) and 2.589(2), the angle Pb-O-Pb' is 109°, and the Pb-Pb' distance is 4.008Å.

The pyridine-2,6-dicarboxylato-lead structure contains a similar asymmetric Pb_2O_2 unit with corresponding core bond distances of 2.52(2) and 2.73(2), and an angle of 112°. (Longer bond distances are expected for this compound since the lead atoms are six-coordinate having distorted pentagonalbipyramidal geometry about the lead with the lone pair occupying one site.) The average of the apical angles in the pentagonalbipyramid is 77°, compared to the corresponding average for the hydroxamate complexes, 77.6°.

There is a large range of lead-oxygen distances in the lead hydroxamate dimers, from 2.26 to 2.95Å. Intramolecular distances and angles for the three dimers in the crystal structures, **1**, **2**, and **3**, are summarized in Table 9. The average bond distances for lead with N-bound oxygens in the three structures, 2.431Å, and for lead with C-bound oxygens, 2.393Å indicate strong lead coordination by anionic oxygen donors (~2.4Å is typical for comparable ligands, for example lead antipyrine[16]). In lead complexes where there are several atoms within bonding distance of the lead atom there are typically a few very short bonds and the remaining bonds are longer than average. This trend is evident when in the N-toluyl-*tert*-butyl-hydroxamate lead structures **3** where there are 7 oxygen atoms within 3.0Å of lead and the lead-oxygen distances for C-bound oxygen atoms are quite short, 2.292 and 2.303Å. It is suprising that the analogous lead-oxygen distances in **2** where there are 5 oxygen atoms are longer (2.463 and 2.392Å). The lead-oxygen distances for C-bound oxygens are comparable to those within lead thiohydroxamates -- 2.407Å for the thiopyridinone[19], 2.383Å for the N-methyl thiobenzo[18], and 2.448Å for the N-methyl thioaceto[18] complex.

The lead coordination geometry is, not suprisingly, unlike that observed for early transition metal (chromium(III), iron(III), cobalt(II), nickel(II), copper(II), zinc(II)) hydroxamate structures. There is a five-coordinate iron complex, chlorobis(N-methylbenzothiohydroxamato)iron(III)[54] which has pseudo-square-pyramidal geometry with the chl e apical; but most metals are four or six coordinate with essentially regular geometry. The large size of lead(II) makes the hydroxamate bite angles smaller than bite angles in transition metal complexes, such as iron(III) and zinc(II). For example, the average bite angle of the hydroxamates in the lead structures, 66.8°, is significantly smaller than hydroxamate bite in the tris benzohydroximato chromium(III) and iron(III) complexes.[55] The bite angles for the benzohydroxamate are 78.1 and 77.9° in the crystal structure of (ethylenediamine)zinc(II) benzohydroxamate hydrate.[25,26] Zinc is in a slightly distorted octahedral environment where the average of the angles about zinc is 90.2°and all the bond distances zinc-oxygen bond distances were within 0.02 Å of eachother.

Table 9.
Intramolecular Distances (Å) and Angles (°) for Hydroxamato-Lead Dimers.

1

Pb-Pb'	Pb-O*	bridging Pb-O*	C-N	Pb-O Core Angles	Bite Angles
4.008	2.262 (N) 2.405 (C) 2.504 (C)	2.345 (N) 2.589 (N)	1.337 1.329	108.5 71.5	66.8 66.7

Ax.-Eq. Angles		Dihedral Angles	
O2-Pb-O1	66.8	(O1, Pb,O2)/(O3,O2,Pb)	80.3
O2-Pb-O3	85.3	(O1, Pb,O2)/(O4,O2,Pb)	147.4
O2-Pb-O4	82.3	(O4, Pb,O2)/(O3,O2,Pb)	67.0
O2-Pb-O4'	69.3	(O4', Pb,O2)/(O1,O2,Pb)	139.6
		(O4', Pb,O2)/(O3,O2,Pb)	140.1
		(O4', Pb,O2)/(O4,O2,Pb)	73.0

2

Pb-Pb'	Pb-O	bridging Pb-O	C-N	Pb-O Core Angles	Bite Angles
3.9133	2.295 (N) 2.392 (C) 2.463 (C)	2.296 (N) 2.815 (N)	1.335 1.323	99.4 80.6	65.2 67.3

Ax.-Eq. Angles		Dihedral Angles	
O4-Pb-O1	89.2	(O1, Pb,O4)/(O3,O4,Pb)	88.7
O4-Pb-O3	67.3	(O1, Pb,O4)/(O4',O4,Pb)	136.7
O4-Pb-O4'	80.6	(O1, Pb,O4)/(O2,O4,Pb)	64.0
O4-Pb-O2	71.2	(O2, Pb,O4)/(O3,O4,Pb)	152.7
		(O2, Pb,O4)/(O4',O4,Pb)	72.6
		(O3, Pb,O4)/(O4',O4,Pb)	134.6

3

Pb1-Pb1'	Pb1-O*	bridging Pb-O*	C-N	Pb-O Core Angles	Bite Angles
4.058	2.303 (C)	2.357 (N) 2.554 (N) 2.517 (N) 2.743 (ac)	1.357	111.4 68.6	67.9

Ax.-Eq. Angles		Dihedral Angles	
O3-Pb1-O1	70.4	(O1,Pb1,O3)/(O8',O3,Pb1)	134.4
O3-Pb1-O3'	68.6	(O1,Pb1,O3)/(O4,O3,Pb1)	159.6
O3-Pb1-O4	67.9	(O3',Pb1,O3)/(O8',O3,Pb1)	57.0
O3-Pb1-O8	111.8	(O4,Pb1,O3)/(O8',O3,Pb1)	66.0
		(O3',Pb1,O3)/(O4'O3,Pb1)	123.0
		(O3',Pb1,O3)/(O1,O3,Pb1)	77.4

* The donor atom type is indicated in parentheses where C = hydroxamate C-bound oxygen, N = hydroxamate N-bound oxygen, hy =hydroxamate, and ac = acetate.

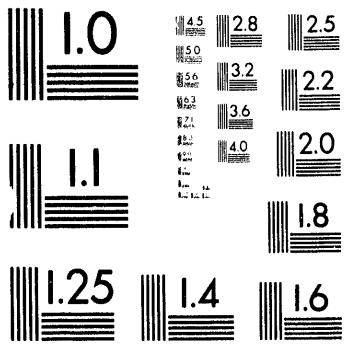
1.0
1.1
1.25
1.4
1.6
1.8
2.0
2.2
2.5
2.8
3.2
3.6
4.0
4.5
5.0
5.6
6.3
7.1

2 of 3

Table 10.
Intramolecular Distances (Å) and Angles (°) within the tetramer in compound **3**.

Pb-Pb	Pb2-O*	bridging Pb2-O*	C-N	Pb-O Core Angles	Bite Angles*
Pb1-Pb2 4.229	2.293 (C)	2.277 (N)	1.303	88.7	45.1 (ac)
Pb1'-Pb2 4.152	2.688 (ac)	2.566 (ac)		119.9	48.6 (ac)
Pb2'-Pb2 3.859	2.689 (ac)			137.4	
	2.910 (ac)			105.6	
	2.949 (N)				

Ax.-Eq. Angles		Dihedral Angles	
O7-Pb2-O8	68.866	(O8,O7,Pb2)/(O1,Pb2,O7)	92.1
O7-Pb2-O1	81.079	(O1,O7,Pb2)/(O2,Pb2,O7)	49.3
O7-Pb2-O2	73.772	(O2,O7,Pb2)/(O5,Pb2,O7)	84.8
O7-Pb2-O6	72.557	(O5,O7,Pb2)/(O6,Pb2,O7)	45.6
		(O6,O7,Pb2)/(O8,Pb2,O7)	88.2

*The donor atom type is indicated in parentheses where C = hydroxamate C-bound oxygen, N = hydroxamate N-bound oxygen, hy =hydroxamate, and ac = acetate oxygen.

The main group metal hydroxamate complexes which would be most comparable to the lead structures are tin(II) complexes; but no crystal structures have been reported. Harrison, King and coworkers[56] have published structures of a number of monohydroxamate alklytin(IV) compounds. In the structure of O-trimethylstannyl-N-phenyl-N-benzoylhydroxylamine the geometry at two independent tin atoms is very distorted trigonal bipyramidal; the Sn-O bond lengths are 2.263 and 2.392Å, axial, and 2.152 and 2.064Å, equatorial. The hydroxamate bite angles (O-Sn-O) are 71.1 and 70.7° and the SnONCO rings are planar.

Bond distances in free and metal-bonded hydroxamates reflect delocalization of electron density within the O-C-N-O group and the changes upon metal complexation. Bond distances for an isolated hydroxamic acid, N-(4-methylphenyl)acetohydroxamic acid,[57] and N-toluyl-*tert*-butyl-hydroxamic acid bound to hydrogen and lead in compound **2** are listed in Table 11. The hydoxamates have an average C-N bond distances of 1.32-1.37Å corresponding to a bond order of 1.5 compared with the nitrogen single bond to the hydroxamic acid substituents, ~1.44Å, and the C-N double bond distance of 1.27-1.29Å.[58] The C-O bond distance increases by 0.03Å and C-N bond distance decreases by ~0.03Å upon bonding to lead; the difference in the N-O distance is insignificant.

Table 11.
Hydroxamate Bond Distances (Å)

Structure	N-O	C-O	C-N
N-(4-methylphenyl)acetohydroxamic acid (MPA)[57]	1.400(3)	1.239(3)	1.356(3)
N-toluyl-*tert*-butyl-hydroxamic acid, H-bonded, **2**	1.402(5)	1.222(6)	1.366(6)
N-toluyl-*tert*-butyl-hydroxamic acid, Pb-bonded, **2**	1.396(4) 1.397(5)	1.250(5) 1.250(6)	1.323(6) 1.335(6)

Infrared spectroscopy. Shifts in the IR spectra from the free hydroxamic acids to the lead complexes are similar to those observed for thiohydroxamate lead complexes.[18] Infrared spectral bands for acetohydroxamic acid and N-toluyltertbutylhydroxamic acid were assigned by comparison with those reported for formohydroxamic acid[59] listed in Table 12. The OCN bands in the free ligand spectrum, 1596, 1512, 1077, and 824 cm^{-1} are observed at 1602, 1508, 1085, and 1540, 1483, 1040, and 828 cm^{-1} in **2** which contains both a hydrogen bonded ligand molecule and chelating hydroxamates, and at 1538, 1481, 1038, and 824 cm^{-1} in **3** which contains only lead-bound hydroxamates. The IR spectrum of **1** has a band at 3426 cm^{-1}, assigned to the methanol which cocrystallized with the lead-hydroxamate molecule, but is otherwise similar to the spectra of **2** and **3** with OCN bands at 1541, 1491, 1037, and 827 cm^{-1}. Bands in the IR spectrum of **2** assigned as NH and OH stretching modes at 3187 and 2965 cm^{-1}, versus 3154 and 2955 cm^{-1} in the free ligand spectrum, illustrate the shift due to hydrogen bonding. The IR spectrum of **3** has bands at 2969, 2925, and 1337 cm^{-1} corresponding to bands seen in the lead acetate spectrum at 2965, 2928, and 1341 cm^{-1}.

Using infrared spectral data and the crystal structures determined for **1**, **2** and **3** the composition and probable structures for the lead complexes of acetohydroxamic acid, **A** and **B** may be proposed. The product from the reaction of lead acetate and acetohydroxamic acid, **A**, has an atomic composition which is consistent with PbL_1Ac_1 while the product from the reaction of lead nitrate with acetohydroxamic acid in methanol, using triethylamine as a base, **B**, has an atomic composition which is consistent with $Pb_2L_3 \cdot 1.5MeOH$ (L = acetohydroxamic acid, Ac = acetate). Infrared bands assigned to OCN are at 1625, 1534,1089, 831cm^{-1} for compound **A** and 1623, 1532, 1089, 849 cm^{-1} for compound **B** compared to 1630, 1551, 1092, and 830 cm^{-1} for the free ligand. The IR spectrum of **A** also shows bands at 2958, 2932, 1559, 1385, and 1033 cm^{-1} which can be assigned to lead chelating acetate by comparison to the spectra for lead acetate and **3** ($Pb_2L_2Ac_2$, where L = N-toluyl*tert*butyl-hydroxamic acid, Ac = acetate).

The IR spectrum of **B** contains a band at 3430 cm^{-1} which can be assigned to methanol by comparison to the spectra for **1** (Pb_2L_4 • MeOH, where L = N-phenyl-toluylhydroxamic acid).

Table 12.
Selected Infrared Bands for Hydroxamic Acids (cm^{-1})

Band Assignment		Hydroxamic Acids		
Stretching	Bending	Formo-[59]	Aceto-	N-toluyl*tert*butyl-
NH		3202	3200	3154
OH		3123	3053	2955
OCN		1647	1630	1596
OCN & NH		1572	1551	1512
	OH	1425	1451	1402
OCN & NH		1262	1186	1225
OCN & NH .		1102	1092	1077
NO		985	993	941
OCN & CN		837,828	830	824
	NH	756	745	775

Molecular orbital calculations. The irregular geometry about the lead atom in most crystal structures, presumably induced by the lone pair of electrons, raises the question: What is the role of the lead $6s^2$ electrons in bonding? A number of studies have been carried out recently on the structural evidence of the lone-pair effect of the subvalent metal cations.[60] Burdett and Lin[61], for example, showed that the lone-pair effect of red PbO is a result of a distortion of the CsCl-type structure giving rise to a mixing of the 6s orbital of Pb and p-type orbitals located on oxygen. On the other hand, PbS, where the anion is larger and much less electronegative, crystallizes in an undistorted sodium chloride lattice with the valence electrons of lead residing in the stereochemically inert 6s orbital.

To contemplate the bonding contribution of the lead $6s^2$ electrons, extended Hückel molecular orbital calculations were performed for two discrete configurations about lead: the irregular geometry depicted in the lead hydroxamate structures reported here, and for comparison, slightly distorted octahedral geometry reported for the lead antipyrine complex. The calculations were performed using the software package CACAO[62] which is based on molecular orbital calculation methods created by Hoffmann and coworkers.[63] The calculations include only valence orbitals, that is the filled d orbitals on lead are assumed to be insignificant in the bonding. Positional parameters for the structural models, shown in Figure 28, were taken from the crystal structures of (bis(N-toluyl-*tert*-butyl-hydroxamato)-bis(μ-N-toluyl-*tert*-butyl-hydroxamato)dilead(II) (**2**), and hexakis(antipyrine)lead(II) perchlorate.[16] To simplify the calculations, without significantly changing the molecular orbitals involved in lead bonding, the toluyl and *tert* butyl substituents on the hydroxamate were replaced by methyl groups, and the phenyl ring on the antipyrine was replaced by a hydrogen atom.

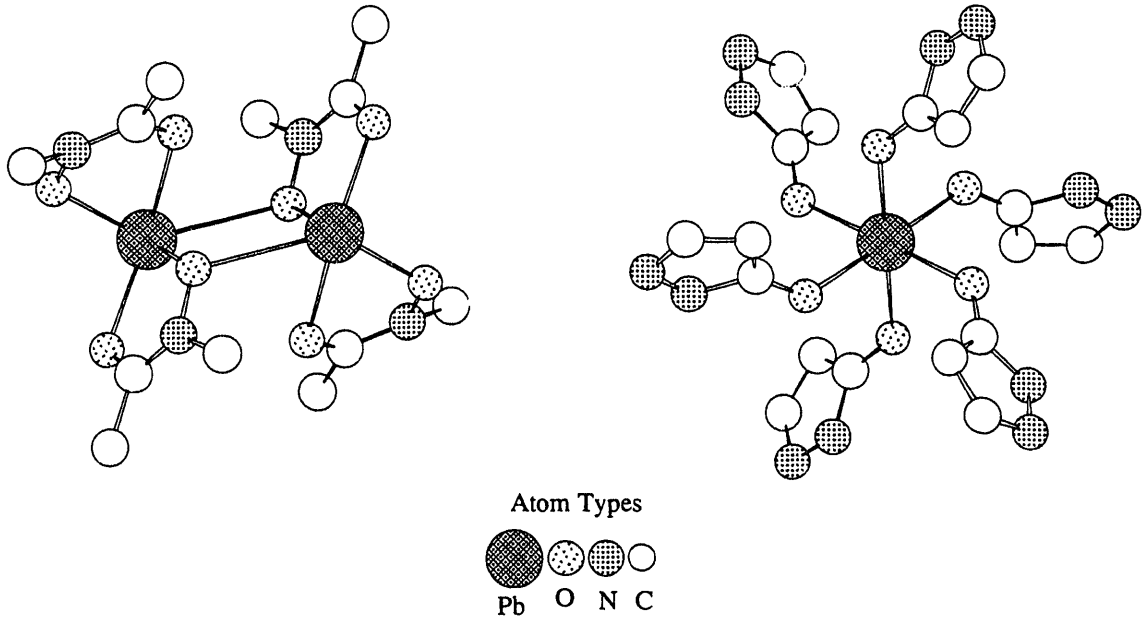

Figure 28. Structural models of two geometries found in lead(II) complexes based on lead hydroxamate structures (left) and hexakis(antipyrine)lead(II) perchlorate (right).[16]

Results for the lead hydroxamate compound show the lead s and p orbitals combine to form hybrid orbitals and the pair of electrons highest in energy occupy a sp orbital. The lead lone pair of electrons occupy the HOMO (highest occupied molecular orbital) shown in Figure 29. The HOMO is antibonding with respect to lead-lead interaction and nonbonding with respect to the other atoms, with the following atomic composition (percent contribution, atom, orbital): 18%, Pb1, s; 20% Pb1, p_z; -18%, Pb2, s; 20%, Pb2, p_z; 2% each O s and p; and all other atomic orbitals contributing less than 2%. The next highest occupied molecular orbital, by 0.397 eV, is the corresponding bonding combination, the lead atoms' lone pairs, which was composed of: 17%, Pb1, s; 20% Pb1, p_z; 18%, Pb2, s; -21%, Pb2, p_z; 3% each O p_z; with all other atomic orbitals contributing less than 2%. The sp character of the HOMO is consistent with the crystal structure data which show the second shortest lead oxygen bond in **3** and the shortest lead oxygen bonds in **1** and **2** are opposite the lone pair of electrons. The four lowest unoccupied molecular orbitals (LUMOs) are π-antibonding, composed of N and C atomic orbitals, and the lowest also has some Pb p_y character. Highest occupied and lowest unoccupied orbitals calculated for the lead hydroxamate molecule are shown in Figure 29. The effective charges calculated for the atoms within the chelate ring were: Pb, +1.226; $-1.13 \leq O \leq -0.96$; $+0.24 \leq N \leq +0.26$; and $+0.92 \leq C \leq +0.97$, indicating both the N-oxide and carbonyl oxygens carry a full negative charge in the hydroxamate complex.

a)

b)

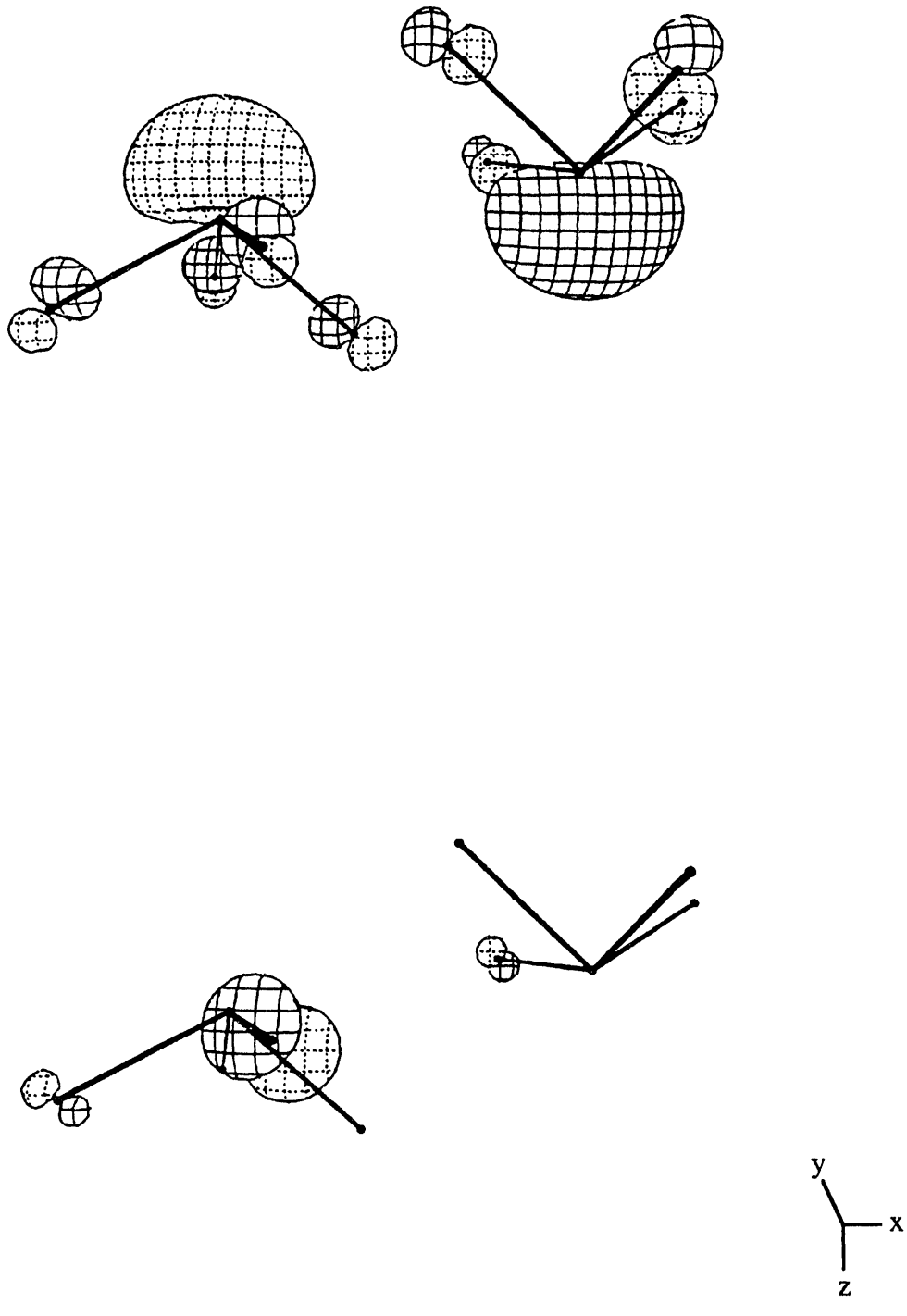

Figure 29. Calculated molecular orbitals in the lead(hydroxamate), Pb_2L_4, structure type
a) The highest energy occupied orbital; Pb-Pb antibonding.
b) The lowest energy unoccupied orbital; Pb p_y and N-C antibonding.
Note: Solid and dashed lines indicate orbitals of opposite signs.

Results for the "antipyrine" complex are quite different; most importantly, there is no indication of s,p mixing, and the lone pair of electrons which resides in the HOMO is essentially the lead s orbital. The HOMO, an antibonding orbital with 47% Pb s orbital content and less than 3% of any other atomic orbital, is 6.5-7.8 eV lower in energy than three molecular orbitals which are predominantly lead p orbitals (67-70% Pb p). Four bonding molecular orbitals have significant contribution from the lead s orbital, two of which are lead-oxygen orbitals. These orbitals are 6-8 eV lower in energy than the HOMO and have lead s orbital contributions of 3, 9, 9, and 12%. The LUMO is basically an antipyrine π antibonding orbital. Highest occupied and lowest unoccupied orbitals calculated for the lead "antipyrine" molecule are shown in Figure 30. The effective charges calculated for the atoms within the chelate ring are: Pb, +1.619; $-1.12 \leq O \leq -1.11$; $-0.07 \leq N \leq +0.002$; and $+0.75 \leq C \leq +0.76$.

Molecular orbital (MO) calculations for the two structures, represented in Figure 28, show there is no mixing of the lead s and p orbitals when there are six oxygen atoms equidistant, in pseudo octahedral geometry, about the metal atom; and when there are five oxygen atoms arranged in an irregular geometry about each lead atom of a dimer, there is substantial s p mixing, and the HOMO is a Pb-Pb antibonding orbital, essentially the two lone pairs of electrons.

a)

b)

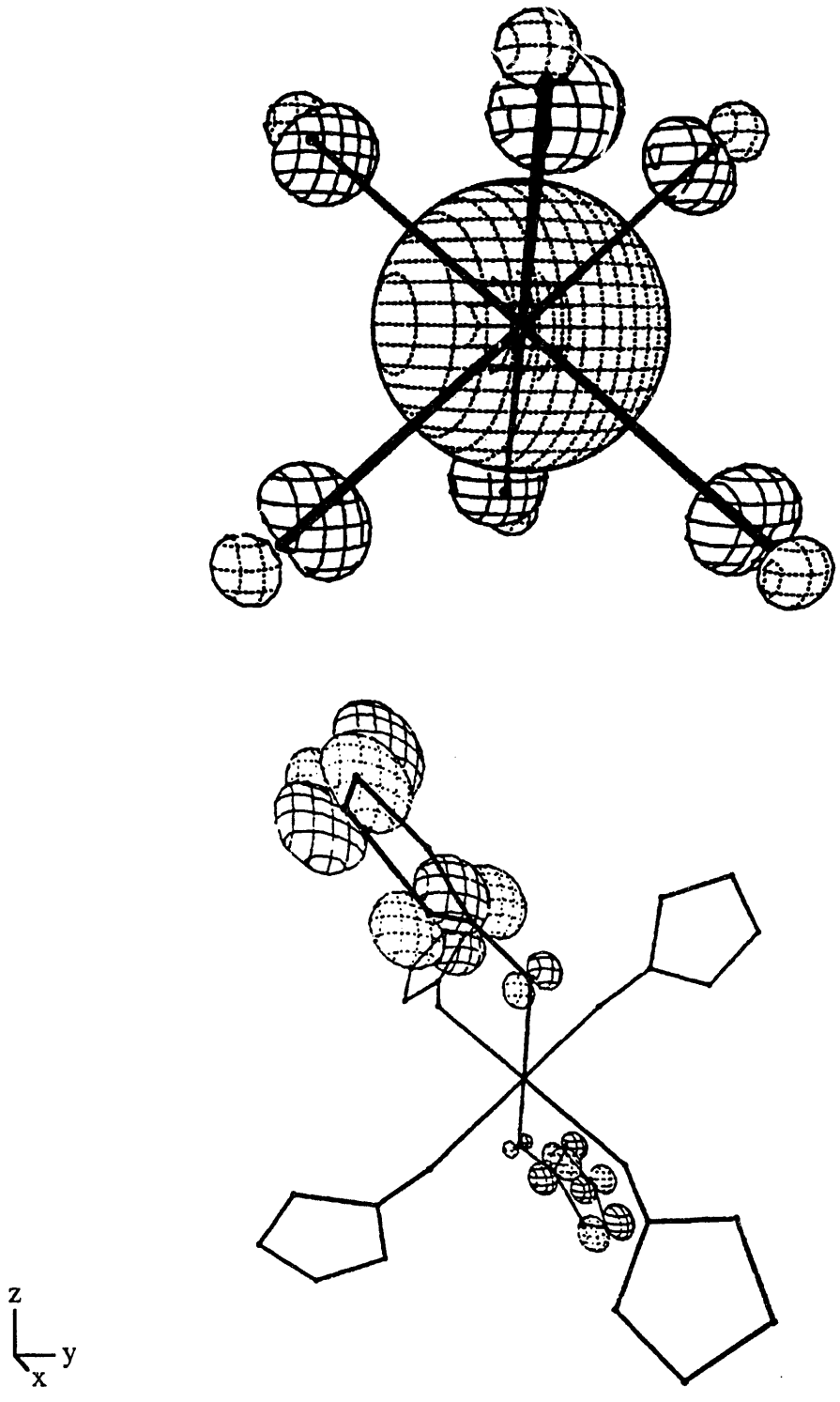

Figure 30. Calculated molecular orbitals in the lead hexa-antipyrine structure type
a) The highest energy occupied orbital; Pb-O antibonding.
b) The lowest energy unoccupied orbital; ligand π antibonding.
Note: Solid and dashed lines indicate orbitals of opposite signs.

Conclusions

The hydroxamic acid ligands studied form polymeric lead complexes under the reaction conditions used. The lead hydroxamate solid state structures elucidated are helpful in understanding solution data. Specifically, the structures determined, and presented in this section, add credibility to the solution structures proposed for the acetohydroxamato-lead species in the previous section.

A major reason for preparing and characterizing lead(II)-hydroxamate complexes was to provide a comparison for lead(II)-thiohydroxamate complexes. Lead complexes of linear thiohydroxamate have been described as monomers[18]; the "cyclic" thiohydroxamate, bis(N,N-diethyl-1-oxo-22(1H)pyridine-thione-6-carboxamide)lead(II) is a weakly held dimer.[19] The lead thiohydroxamates are thought to be monomers in solution as well because the UV/VIS and NMR spectra change with solvent polarity, perhaps indicating open sections in the coordination sphere. Comparing the lead hydroxamates and lead thiohydroxamates, the more basic hydroxamates bridge two lead atoms quite readily and the lead-lead distances in the crystal structures are very similar. (Recall from the previous section, the hydroxamates have pK_as around 9, while the thiohydroxamates have pK_as around 6.) Lead is essentially four coordinate in the thiohydroxamate structures and five coordinate in the hydroxamate structures, suggesting that smaller oxygen donors do result in higher coordination numbers (although in acetothiohydroxamate compound there is a fifth oxygen from a neighboring molecule at 2.880Å). The properties and structures of the hydroxamates and the thiohydroxamates may provide insight to specific ligand properties which lead to monomer or polymer formation. The hydroxamate ligands in the structurally characterized compounds were bulky, yet the lead complexes are dimeric, indicating the steric hinderance supplied by the large substituents neither reduces the coordination number of lead, nor predicates monomer formation. In fact, there are examples where polymer formation would not be hindered by the steric bulk of the ligand and the product is monomeric, i. e., lead(II) D-gluconate is a six-coordinate monomer with distorted octahedral geometry.[64] The extent of polymerization appears to depend on a combination of ligand basicity and steric bulk. The lead acetohydroxamato reaction products were much less soluble than the larger hydroxamates complexes and the linear thiohydroxamate lead complexes, suggesting the acetohydroxamate complexes were polymeric. The hydroxypyridinone appears to be a ligand in which the combined basicity and size result in a lead complex, bis(N,N-diethyl-1-oxo-22(1H)pyridine-thione-6-carboxamide, which is just at the monomer/polymer division.

The lone pair of electrons is stereochemically active in all the lead (thio)hydroxamic complexes characterized, and drastically affects the geometry about the lead atom. Molecular orbital calculations indicate there is 6s, 6p mixing, and the lone pair of electrons occupy a nonbonding sp hybrid orbital in the five-coordinate, very distorted octahedral, (thio)hydroxamic complexes.

Conclusions Regarding Ligand Preferences in Lead(II) Complexation

There are many desirable ligand properties to be considered when designing potential therapeutic chelating agents: water solubility, low molecular charge, synthetic feasibility, *in vivo* tolerance etc., but arguably the most important characteristic that inorganic chemists can pursue is metal ion selectivity. Ethylenediamine-tetraacetic acid is effective in removing lead from the human body[65]; however, the polycarboxylate is very attractive to zinc and other metal ions as well as lead, compromising EDTA's practical utility. We chose to consider the thiohydroxamates as a class of ligands under the hypothesis that "softer" donor atoms and mixed S and O binding groups would form stronger bonds with lead. Indeed, the stability constants reported in the previous section show that lead thiohydroxamates are slightly more stable complexes than lead hydroxamates.

The structural data for lead complexes, including the hydroxamates and thiohydroxamates, show some trends which may be exploited for selectivity producing features. We know that the lone pair of electrons is almost always stereochemically active, dictating irregular geometry about the lead atom. There are numerous crystal structures where the lead atom is held by several ligand donor atoms in a distorted octahedral fashion with the lone pair filling a large portion of the coordination sphere.[66] Polymer formation, as exemplified by the hydroxamate dimers reported here, is common, and almost certain when the ligands are basic and have low denticity. Dean, et al. suggested[67] that aggregation through the sulfur might be a general feature of lead(II)-thiolate complexes in the solid state, but there are examples to the contrary e.g., the 2-mercaptoethanol structure reported by Jackson and Hancock.[68]

Ligand attributes which are likely to yield a highly stable, monomeric lead complex include: recognition of the lone pair of electrons, mixed donor atom types, relatively high denticity, small bite angles, and relatively high acidity. Direct interaction with the lone pair using a Lewis acid group could increase selectivity for lead, but is difficult to build into a ligand so that the group is likely to be perfectly poised for bonding. Alternatively, the lone pair could be recognized indirectly.

If a ligand is preformed for binding in a rigid irregular geometry with an open coordination site, lead is more likely to adopt the configuration than hard sphere cations, and will probably be complexed preferentially. Penicillamine a therapeutic lead-chelating agent [69], could be coupled with a thiohydroxamic acid to make a very promising ligand. The crystal structure of the 1:1 lead(II), D-penicillamine complex shows the ligand acting as a tridentate chelator and an oxygen and a sulphur of neighboring molecules forming two weak bonds to lead.[70] A thiohydroxamic acid linked to the penicillamine primary amine could replace the weakly bound oxygen and sulfur atoms in the structure. The lead complex of a ligand containing these two groups should have a high formation constant, based on logβ for the 1:1 D-penicillamine, lead(II) species, 13.5[71] and logβ for the 1:1 N-methylacetothiohydroxamate, lead(II) species, 6.88.[72] An additional incentive to derivatize penicillamine is to attempt to elliminate the penicillin-like allergic reaction which discourages its use *in vivo*.[69,73]

A prototype ligand where penicillamine and N-methylacetothiohydroxamic acid are joined by a 2-ethyl-benzyl group is shown as a lead complex in Figure 31. The structure was generated using the molecular dynamics software package, CAChe[74], and lead-donor atom bond distances and from the lead-penicillamine[70] and bis(N-methylacetothiohydroxamato)lead [18] crystal structures. The lead-nitrogen bond was fixed at 2.55 Å in the energy minimization based on the lead-nitrogen distance in lead isopropylxanthate-pyridine where the lead is five-coordinate is 2.55Å.[75] The tertiary amine nitrogen in 2-(morpholin-4-yl)ethanethiolatolead(II) nitrate has a bond distance with lead of 2.61Å.[76]) Lead-thiohydroxamate bond angles were fixed; but the lead-penicillamine angles were not reported by Freeman,[70] and therefore were allowed to vary in the energy minimization.

Based on minimization results for a structure where penicillamine and N-methylthiohydroxamic acid were bonded to lead and the groups were not linked together, the nitrogen-lead-thiohydroxamate sulfur angle was fixed at 85° in structures where the two groups were connected. A simple link is desirable to retain the water solubility of the two constituents and hold them at a distance suitable for bonding to one lead atom. A five-carbon chain spacing between the penicillamine nitrogen and the thiohydroxamate carbon was determined to be appropriate; then a benzene ring was added to make the ligand more rigid. The relatively inflexible ligand should force irregular geometry about a complexed metal.

Intramolecular angles and molecular energy terms computed for structures containing the 2-ethyl-benzyl linker and the less restraining five carbon chain linker were nearly identical, suggesting the gain in rigidity was not offset by an increase in strain energy. Ideally the thiohydroxamate group would be planar; the minimum energy structure the deviation from planar for (S,C,N,O) is 0.030Å. The bond distances and angles in the minimum energy structure of the prototype ligand-lead complex emulate trends in lead structural data asserting the ligand will readily conform to the preferred geometry of lead(II).

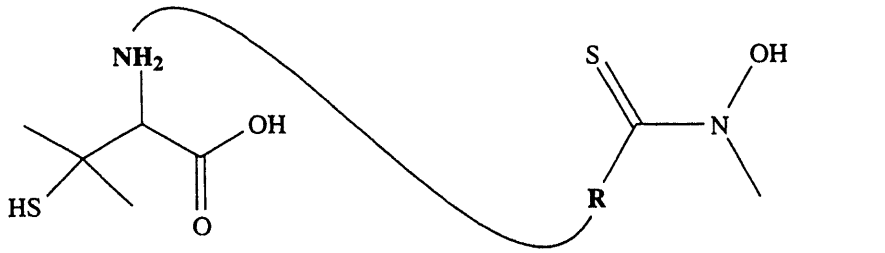

Penicillamine N-methyl thiohydroxamic Acid

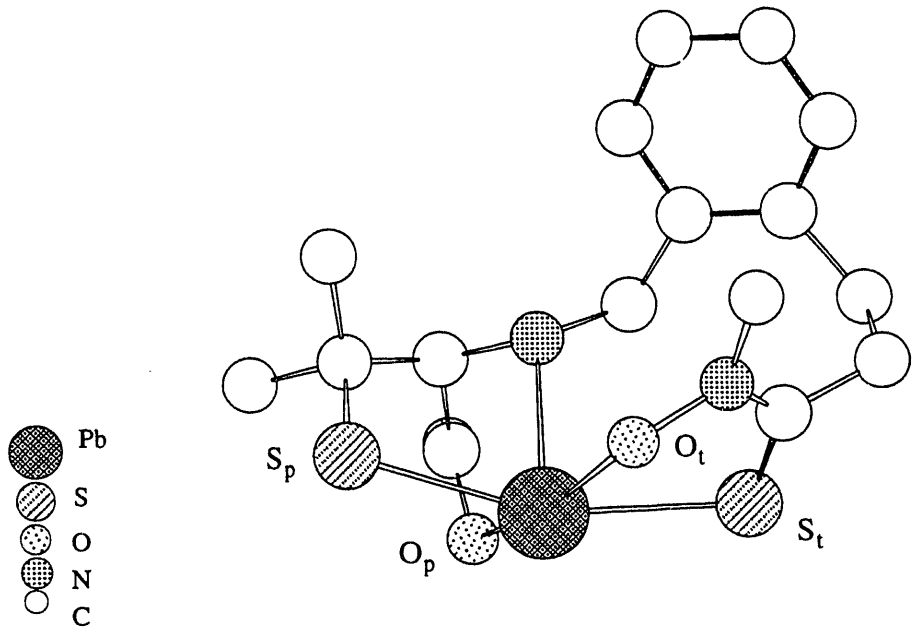

Bond Distances	(Å)	Bond Angles	(°)
Pb-N	2.550	S_t-Pb-S_p	161.3
Pb-O_p	2.444	O_t-Pb-O_p	162.2
Pb-S_p	2.716	N-Pb-O_p	73.5
Pb-O_t	2.374	N-Pb-S_p	77.8
Pb-S_t	2.744	N-Pb-O_t	90.0
		N-Pb-S_t	85.0

Figure 31. The minimum energy structure of a prototype ligand-lead complex where penicillamine and N-methylacetothiohydroxamic acid are joined by a 2-ethyl-benzyl group.

References

(1) Christou, G.; Folting, K.; Huffman, J. C. *Polyhedron* **1984**, *3(11)*, 1247.

(2) Ito, T.; Iwasaki, H. *Acta Cryst.* **1980**, *B36*, 443.

(3) Pierce-Butler, M. A. *Acta Cryst.* **1982**, *B38*, 2681.

(4) Reger, D. L.; Huff, M. F.; Rheingold, A. L.; Haggerty, B. S. *J. Am. Chem. Soc.* **1992**, *114*, 579.

(5) Keller, H. L.; Riebe, H. J. *Z. Anorg. Allg. Chem.* **1987**, *550*, 102.

(6) Koziol, A. E.; Palenik, G. J.; C., P. R. *Inorg. Chim. Acta* **1986**, *116*, L51.

(7) Skoulika, S.; Michaelides, A.; Aubry, A. *Acta Cryst.* **1988**, *C44*, 808.

(8) Miyamae, H.; Yoshinari, K.; Hihara, G.; Nagata, M. *Acta Cryst.* **1988**, , 1528.

(9) Kepert, D. L.; Patrick, J. M.; Skelton, B. W.; White, A. H. *Aust. J. Chem.* **1988**, 157.

(10) Metz, B.; Weiss, R. *Inorg. Chem.* **1974**, *13(9)*, 2094.

(11) Ng, S.-W.; Zuckerman, J. J. *Adv. Inorg. Chem. Radiochem.* **1985**, *29*,

(12) Harrison, P. G.; Steel, A. T. *J. Organomet. Chem.* **1982**, *239*, 105.

(13) Jones, P. B.; Schelbach, R.; Schwarzmann, E.; Thone, C. *Acta Cryst.* **1988**, *C44*, 1198. $[Pb_3(acetato)_3Cl_2]^{2-}$.

(14) Pierce-Butler, M. A. *Acta Cryst.* **1984**, *C40*, 63.

(15) Goldberg, I.; Herbstein, F. H. *Acta Cryst.* **1972**, *B28*, 400.

(16) Vijayan, M.; Viswamitra, M. A. *Acta Cryst.* **1966**, *21*, 522.

(17) Clegg, W.; Abrahams, I. L.; Garner, C. D. *Acta Cryst.* **1984**, *C40*, 1367.

(18) Abu-Dari, K.; Hahn, F. E.; Raymond, K. N. *J. Am. Chem. Soc.* **1990**, *112*, 1519.

(19) Abu-Dari, K.; Karpishin, T. K.; Raymond, K. N. *Inorg. Chem.* **1993**, *32*, 3052.

(20) Sato, T.; Shiro, M.; Koyama, H. *J. Chem. Soc. B, Phys. Org.* **1968**, , 125.

(21) Sato, T.; Shiro, M.; Koyama, H. *J. Chem. Soc. B, Phys. Org.* **1968**, , 989.

(22) Becher, J.; Brockway, D. J.; Murray, K. S.; Newman, P. J.; Toftlund, H. *Inorg. Chem.* **1982**, *21*, 1791.

(23) Leong, J.; Bell, S. J. *Inorg. Chem.* **1978**, *17(7)*, 1886.

(24) Kurzak, B.; Kozlowski, H.; Farkas, E. *Coord. Chem. Rev.* **1992**, *114(2)*, 169, and references therein.

(25) Göttlicher, S.; Ochsenreiter, P. *Chem. Ber.* **1974**, *107*, 391.

(26) Göttlicher, S.; Paulus, H. *Chem. Ber.* **1982**, *115*, 393.

(27) *Merck Index*; 10 ed.; Windholz, R., Ed.; Merck & Co.,Inc.: Rathway, NJ, 1983.

(28) *International Tables for X-ray Crystallography*; Kynoch Press: Birmingham, 1974; Vol. I-IV.

(29) Johnson, C. K. *ORTEP, A Thermal Ellipsoid Plotting Program*, Report ORNL-5138, Oak Ridge National Laboratory, Oak Ridge, TN, 1976.

(30) The reflections used for intensity and orientation standards were (5 -3 -4), (1 2 -8) and (0 7 -5).

(31) Function minimized was:
$\dot{S}_w(|F_o|-|F_c|)^2$, $w = 1/s^2(F_o)$, $s(F_o^2) = [s_o^2(F_o^2) + p(F_o^2)^2]^{1/2}$; p factor = 0.03.

(32) Churchill, M. R. *Inorg. Chem.* **1973**, *12*, 1213.

(33) Zachariasen, W. H. *Acta Cryst.* **1963**, *16*, 1139.

(34) The reflections used for intensity and orientation standards were (2 5 7), (6 -4 0) and (3 -6 1).

(35) Sheldrick, G. "SHELXS-86," Institut fur Anorganische Chemie der Universitat, 1986.

(36) The reflections used for intensity and orientation standards were (7 3 2), (1 -1 -8) and (-5 -4 1).

(37) Shannon, R. D. *Acta Cryst.* **1976**, *A32*, 751-767.

(38) Pauling, L. *The Nature of the Chemical Bond;* 3rd ed.; Cornell U. P.: Ithaca, 1960.

(39) Bondi, A. *J. Phys. Chem.* **1964**, *68(3)*, 441.

(40) Greenwood, N. N.; Earnshaw, A. *Chemistry of the Elements*; Pergamon Press: Oxford, 1984.

(41) Gaffney, C.; Harrison, P. G.; King, T. J. *J. Chem. Soc., Chem. Comm.* **1980**, , 1251.

(42) Keller, H. *Angew. Chem. Int. Ed. Engl.* **1983**, *22(4)*, 324.

(43) Bryant, R. G.; Chacko, V. P.; Etter, M. C. *Inorg. Chem.* **1984**, *23*, 3580.

(44) Nardelli, M.; Fava, G.; Branchi, G. *Acta Cryst.* **1960**, *13*, 898. mono-thiourea-lead(II) acetate.

(45) Shin, Y.-G.; Hampden-Smith, M. J.; Kodas, T. T.; Duesler, E. N. *Polyhedron* **1993**, *12(12)*, 1453. $Pb(O_2CCH_3)_2$(18-Crown-6)•3H2O.

(46) See for example, the crystal structure of bis(10-methylisoalloxazine)lead(II) perchlorate tetrahydrate where the lead is strongly bonded to four oxygen atoms (distances < 2.7 Å), and weakly bonded to two oxygen atoms (3.2-3.7 Å) and one nitrogen (2.99Å) atom in:
Yu, M. W.; Fritchie, C. J. *J. Chem. Soc. Dalton* **1975**, 377.

(47) An illustrative example is: *catena*-μ-[aquabis(phenoxyacetato-O)lead(II)-bis(phenoxyacetato)lead(II)] , a chain-like structure made up of monobridged six and seven coordinate dimeric units with long range Pb-O interactions (2.87 and 2.96Å), reported in: Mak, T. C. W.; Yip, W.; O'Reilly, E. J.; Smith, G.; Kennard, C. H. L. *Inorg. Chim. Acta* **1985**, *100*, 267.

(48) Bharadwaj, P. K.; Arbuckle, B. W.; Musker, W. K. *Inorg. Chim. Acta* **1988**, *142*, 243.

(49) Jovanovski, G.; Hergold-Brundic, A.; Kamenar, B. *Acta. Cryst* **1988**, *c44*, 63.

(50) Pierce-Butler, M. A. *Acta. Cryst.* **1984**, *C40*, 1364.

(51) Hardin, S. G.; Healy, P. C.; Mumme, W. G.; White, A. H.; Winter, G. *Aust. J. Chem.* **1982**, *35*, 2423.

(52) Beveridge, K. A.; Bushnell, G. W. *Can. J. Chem.* **1979**, *57*, 2498.

(53) Hummel, H. U.; Meske, H. *Z. Naturforsch* **1987**, *43b*, 389.

(54) Berry, K. J.; Clark, P. E.; Murray, K. S.; Raston, C. L.; White, A. H. *Inorg. Chem.* **1983**, *22(26)*, 3928.

(55) Abu-Dari, K.; Ekstrand, J. D.; Freyberg, D. P.; Raymond, K. N. *Inorg. Chem.* **1979**, *18*, 108.

(56) Harrison, P. G.; King, T. J.; Molloy, K. C. *J. Organometal. Chem.* **1980**, *185*, 199, and references therein.

(57) Dietrich, A.; Powell, D. R.; Eng-Wilmot, D. L.; Hossain, M. B.; van der Helm, D. *Acta Cryst.* **1990**, *C46*, 816.

(58) Waite, M. G.; Sim, G. A. *J. Chem. Soc. B* **1971**, , 752.

(59) Orville-Thomas, W. J.; Parsons, A. E. *J. Mol. Spectrosc.* **1958**, *2*, 203.

(60) Hummel, H.; Meske, H. *J. Chem. Soc. Dalton Trans.* **1989**, , 627.

(61) Burdett, J. K.; Lin, J. H. *Acta Cryst.* **1981**, *B37*, 2123.

(62) Mealli, C.; Proserpio, D. M. *J. Chem. Ed.* **1990**, *67*, 399.
The package contains an udpated version of the program SIMCON reported: Hoffmann R.; Lipscomb W.N. *J. Chem. Phys.* **1962**, *36*, 2179, 3489. Ammeter, J. H.; Burgi, H. B.; Thibeault, J. C.; Hoffmann R. *J. Am. Chem. Soc.* **1978**, *100*, 3686.

(63) Ammeter, J. H.; Bürgi, H. B.; Thibeault, J. C.; Hoffmann, R. *J. Am. Chem. Soc.* **1978**, *100(12)*, 3686, and references therein.

(64) Lis, T. *Acta Cryst.* **1984**, *C40*, 374.

(65) Chisolm, J. J. *Environmental Health Prespectives* **1990**, *89*, 67.

(66) See for example, the crystal structure of lead(II) isopropylxanthate-pyridine reported in: Hagihara, H.; Yoshide, N.; Watanabe, Y. *Acta Cryst.* **1969**, *B23*, 1775, and the lead hydroxamate structure reported herein.

(67) Dean, P. A. w.; Vittal, J. J.; Payne, N. C. *Inorg. Chem.* **1984**, *23*, 4232.

(68) Jackson, G. E.; Hancock, R. D. *Polyhedron* **1982**, *1*, 838.

(69) Chisolm, J. J. *J. Pediatrics* **1968**, *73*, 1.

(70) Freeman, H. C.; Stevens, G. N.; Taylor, I. F. *J. Chem. Soc., Chem. Comm.* **1974**, 366.

(71) Doornbos, D. A.; Faber, J. S. *Pharm. Weekblad* **1964**, *99*, 289.

(72) Stability constant results reported in the first section of Part I of this dissertation.

(73) Garrettson, L. K. In *Clinical Management of Poisoning and Drug Overdose*; L. M. Haddad and J. F. Winchester, Ed.; W. B. Saunders: 1983; pp 649.

(74) CAChe "Molecule Editor and Molecular Mechanics," CAChe Scientific, Inc., 1991.

(75) Hagihara, H.; Yoshida, N.; Watanabe, Y. *Acta Cryst.* **1969**, *B25*, 1775.

(76) Dance, I. G.; Guerney, P. J. *Aust. J. Chem.* **1981**, *34*, 57.

II. Plutonium Solubility and Speciation Relevant to the Environment

A. Complexation of Plutonium(IV) by the Siderophore, Desferrioxamine B, and Two Octadentate Analogs

Introduction

Actinide waste treatment and containment methods often include steps where it would be desirable to use a highly selective complexing agent to remove plutonium from solution. Reducing the volume of high-level waste that requires storage in a geologic repository and clean up of actinide contaminated soils are two areas of concern at sites operated by the Department of Energy. The development of new approaches to plutonium separation would benefit technologies to solve these problems. Solutions likely to be encountered contain a variety of either naturally occurring ligands and organic acids, or chemicals added during industrial processes, or both. Therefore the chosen complexing agent should selectively and strongly complex plutonium(IV) in the presence of large excesses of metal ions such as aluminum(III) and sodium(I) and anions such as nitrate and ethylenediaminetetraacetate.

We are investigating the solution thermodynamics of the potentially plutonium(IV)-selective complexing agents, desferrioxamine B (DFO), and octadentate derivatives of DFO, DFO-methyl-terephthalamide (DFOMTA) and DFO-1,2-hydroxypyridinone (DFOHOPO). The schematic structures of these three ligands are shown in Figure 32. Because DFO binds the ferric ion over a large pH range (1-12)[1] and Fe^{3+} and Pu^{4+} display similar ligand preferences, DFO should complex Pu^{4+} strongly. Desferrioxamine is produced commercially for the treatment of iron overload,[2,3] making it readily available for practical use. The octadentate derivatives should be even better at binding plutonium because Pu^{4+} forms complexes with higher coordination numbers,[4] adopting dodecahedral, D_{2d}, geometry.[5] Desferrioxamine B has been shown to solubilize plutonium from a hydrous plutonium(IV) oxide,[6] and both DFO and DFOHOPO have been tested for their capacity to remove plutonium from laboratory animals, and found to be effective.[5,7] Results from animal studies indicate that in some poisoning cases DFOHOPO would be preferred over DTPA, the current therapeutic plutonium chelating agent. [8] Both DFOHOPO and DFOMTA were included in this research because they have different solubility and acid/base properties and may be suitable for removing Pu^{4+} from solutions having different compositions.

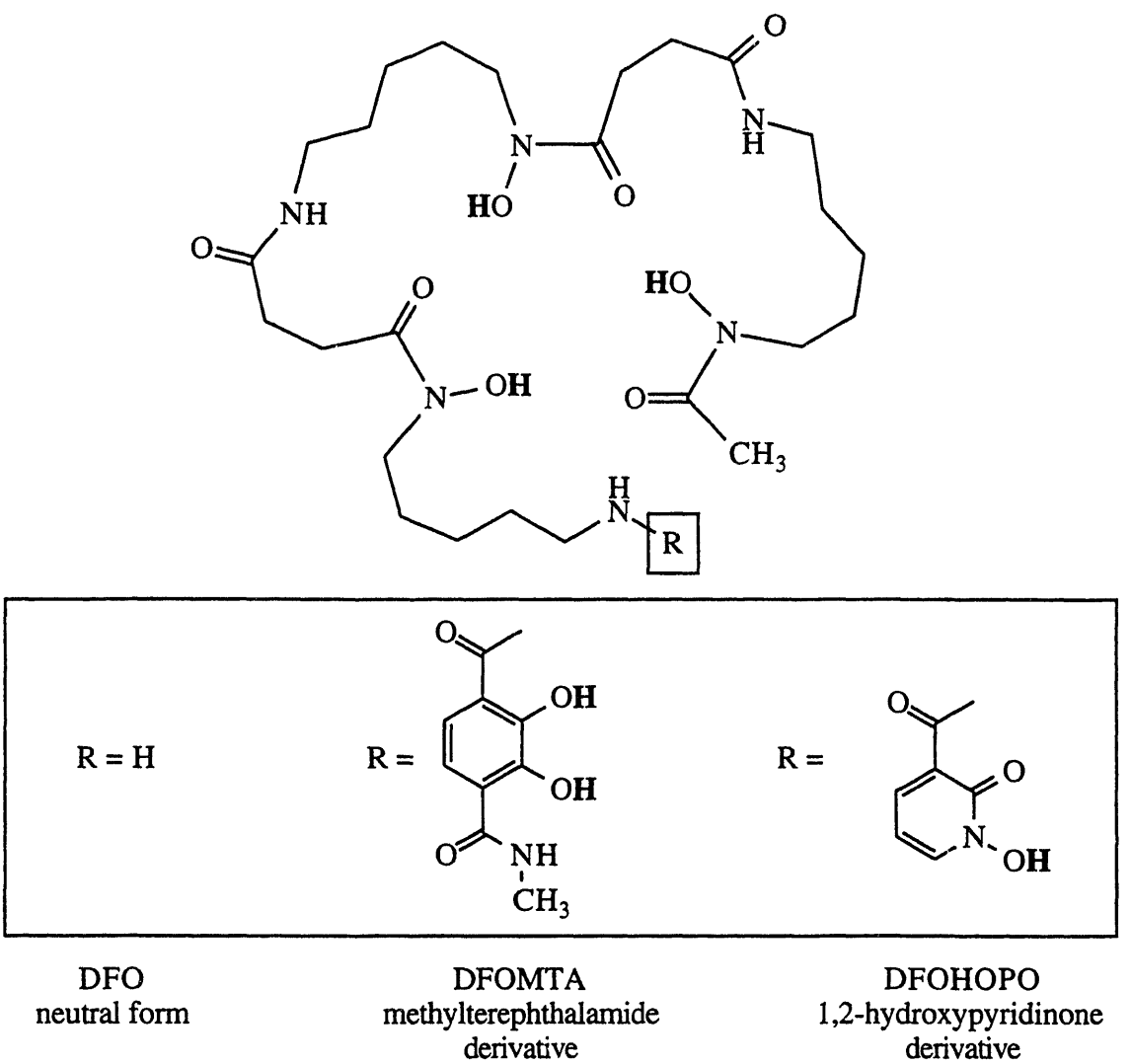

Figure 32. Desferrioxamine B and two octadentate analogs prepared by derivatization of the terminal amine group.[9] Protons released upon metal binding are shown in bold.

To investigate the utility of DFO and synthetic deriviatives as moeties applicable in plutonium separation methods, we measured the stability of the plutonium(IV)-ligand complexes formed in solution. Before metal-ligand formation constants can be measured, the ligand acidity in the absence of metal ions must be known. The pK_as and Fe^{3+} stability constants of DFO[1], DFOMTA and DFOHOPO[9], have been determined previously and are listed in Table 13. The catechol group has a higher negative charge and is more basic than the hydroxypyridinone group, therefore, the Pu^{4+}complex with DFOMTA is expected to be stronger than the Pu^{4+} complex with DFOHOPO. Because

the stability constants were expected to be quite large, the concentration of uncomplexed ligand or metal over the pH range 2-12 was assumed to be too low to measure directly and the competition spectrophotometric titration[10] method was used. In this method, outlined in Scheme 4.1, the competition equilibrium constant, K_{comp}, is measured and used to calculate the formation constant of interest. In this research, metal complex and ligand absorbance spectra were measured as a function of pH, concentration of ligand, and concentration of the competing ligand, EDTA, to determine the thermodynamic stability constants of DFO, DFOMTA, and DFOHOPO with Pu^{4+}. The octadentate ligand UV/visible absorbance bands and ligand to metal charge transfer bands, with molar absorbtivities two to three orders of magnitude greater than uncomplexed plutonium(IV), were used to follow the equilibria.

The stability constant notation described in the first section of Part I is used here with a modification to include the competing ligand: $\beta_{mll'h}$ is the equilibrium constant corresponding to the formation of a solution species with the composition $Pu_mL_lEDTA_{l'}H_h$ from the free ions. Because the DFO terminal amine is protonated in the pH range studied, the notation L refers to that monoprotonated species; for DFOMTA and DFOHOPO, L represents the fully deprotonated species.

Table 13. Known protonation and Fe^{3+} complex stability constants of DFO, DFOMTA and DFOHOPO.

Ligand	DFO	DFOMTA	DFOHOPO
pK_as			
hydroxamate	9.70 9.03 8.30	9.71 9.24 8.58	9.71 9.18 8.50
substituent catechol or hydroxypyridinone		11.1 6.22	4.92
log of the formation constant for the Fe^{3+} complex (L:M = 1:1)	30.6	34.8	30.7

Equilibrium of Interest:

$$M + L \underset{}{\overset{K_1}{\rightleftharpoons}} ML$$

Competition Equilibria:

$$MA + L \overset{K_{comp}}{\rightleftharpoons} ML + A$$

$$M + A \overset{K}{\rightleftharpoons} MA$$

In this work:

L = DFO, DFOMTA, or DFOHOPO; A = EDTA

$K_1 = K_{comp}K$; K = Pu-EDTA formation constant

$K_1 = \beta_{1100}$; $K = \beta_{1010}$

Scheme 4.1. Competition method used for the determination of metal-ligand complex stability constants. (For simplicity, protons and molecular charges are not included.)

Experimental

Spectrophotometric Titrations

General. The plutonium used throughout was ^{242}Pu, originally obtained as $^{242}PuO_2$ from the U.S. Department of Energy's Heavy Element Production Program at Oak Ridge National Laboratory. It was dissolved in acid by W. Kot of the actinide group at Lawrence Berkeley Laboratory and supplied as a 6 M HCl solution. Alpha and gamma spectroscopic analyses indicated the plutonium was 99.85% ^{242}Pu by mass; the remainder was $^{238\text{-}240}Pu$, and ^{241}Am. The methane sulfonate salt of desferrioxamine was

generously provided by Nicomed/Salutar as Desferal®, samples of DFOMTA was synthesized and donated by Dr. Jide Xu, and DFOHOPO was synthesized by Dr. Jean-Claude Chambrane. Ethylenediaminetetraacetic acid was purchased as the disodium salt from Aldrich (gold label, 99.999%). Concentrated perchloric acid (Mallinckrodt, Vycor, double distilled) was used in plutonium stock solution preparations, and 1.00 M and 0.10 M $HClO_4$ titration solutions were prepared by dilution. Hydroiodic acid used in anion exchange procedures was either (Aldrich, 99.99%) or freshly distilled from reagent grade solution (Baker Analytical), to which hydrazine (Aldrich) was added as a preservative. Nitric acid was reagent grade (Baker Analytical). Sodium hydroxide solutions were prepared by dilution of concentrate (Baker, Dilut-It) or used as purchased (Baker Analytical, 0.100M, carbonate-free). Standard buffers, pH = 4.01, 7.00, and 10.00 were purchased or prepared from concentrates (Fisher, N.I.S.T. certified). Dowex AG 1-X8, 100-200 mesh, anion exchange resin (Biorad) was pretreated by preparing a suspension and removing very fine particulates, followed by conversion to the chloride form using concentrated HCl (Fisher). All chemicals were used as received, unless otherwise noted, and all solutions were prepared using deionized, distilled water, which was further deionized by a Millipore cartridge system.

Titration Equipment. Combination pH electrodes with Ag/AgCl internal references (Beckman or Cole Parmer), used for all titrations, were calibrated using N.I.S.T. certified buffer solutions. Ultraviolet/visible spectra are background corrected and were measured using a Cary (Model 2300) or a Guided Wave, fiber optic (Model 200) spectrophotometer. A custom-made Teflon-capped, 4 mL reservoir, 1 cm path length, quartz cuvette was used with the Cary spectrophotometer, and a standard 1.4 mL thick-walled quartz, 1 cm path length, quartz cuvette was used with the Guided Wave spectrophotometer. Spectra were collected with a 0.5 nm step size using the Guided Wave spectrophotometer; those collected using the Cary spectrophotometer had a resolution of 0.2 nm.

Solutions. Aliquots of the solution provided by the actinide group at LBL were purified using anion exchange chromatography to separate $PuCl_6^{2-}$ from fission products and other cationic contaminants.[11] Conversion to the perchlorate form was accomplished by fuming with concentrated HNO_3 followed by fuming with $HClO_4$ three times. The final solutions were approximately 0.1 M in $HClO_4$. The plutonium concentration was determined using liquid scintillation counting and alpha spectroscopic analysis. Electrochemical preparations of Pu^{3+}, Pu^{4+}, and PuO_2^{2+} were performed in a three electrode quartz electrolysis cell with a platinum grid working electrode, platinum auxiliary electrode, and Ag/AgCl reference electrode (207.5 mV vs. NHE, neutral

hydrogen electrode). The potential was supplied by a Princeton Applied Research Model 264A Polarographic Analyzer/Stripping Voltammeter. The oxidation state purity was verified spectrophotometrically by comparison with previously reported spectra.[12] Plutonium(IV)-EDTA titration solutions were prepared in an argon atmosphere, as needed, by electrochemically reducing an aliquot of the PuO_2^{2+} stock solution (-0.110V vs. Ag/AgCl) to Pu^{3+}, adding Na_2EDTA as a solution or solid and either aerobically or electrochemically oxidizing the solution (+0.160V vs Ag/AgCl) to Pu^{4+}-EDTA. The Pu^{3+}-EDTA oxidation was followed spectroscopically, and judged to be complete by comparison with the reported Pu^{3+}-EDTA and Pu^{4+}-EDTA UV/visible spectra.[13] Additional details of single oxidation state plutonium solution preparation and nuclear and optical spectroscopic analyses are in the next section of Part II.

Data Analysis. The Fortran program FINDCOMP [14] was used to estimate the number of absorbing species in solution from the spectrophotometric titration data. Plutonium complexes thought to be present and corresponding formation constants, along with the known ligand pK_a's, Pu^{4+}-EDTA stability constants[13], and Pu^{4+} hydrolysis constants[15], constituted the solution equilibria model. The model was refined and evaluated using the spectral componentization and least-squares minimization program, REFSPEC[16]. Molar absorptivities and formation constants for each unknown species were varied incrementally using least-squares residual minimization until preset error limits, on the order of spectroscopic noise, were met. Component spectra generated by REFSPEC were compared with the original data to verify the validity of the chemical equilibrium model and the calculated formation constants. Species distribution curves were generated using the calculated formation constants and the program SPCONC[14].

Plutonium-DFOMTA-EDTA Spectrophotometric Competition Titrations. A total of five data sets was used to determine the Pu^{4+}-DFOMTA stability constants, under the following conditions: $[Pu^{4+}]$ = 0.15-0.21 mM, T = 23±2°C, and μ = 0.22±2 M. In four of the experiments the DFOMTA:Pu^{4+} ratio was 1:1, while a single titration was done using a ratio of 2:1. In all experiments EDTA was present in excess, with the EDTA:Pu^{4+} ratio ranging from 79:1 to 118:1. Each titration data set consisted of 10 to 17 solution absorbance spectra (300 to 600 nm) where the pH was adjusted, using $HClO_4$ and NaOH solutions, from an initially measured pH around 7.5 to 2.8. The lower pH limit is dictated by the precipitation of H_4EDTA. At the end of two titrations, the pH was increased and spectra were measured to verify the reversibility of the equilibria and the chemical stability of the ligand. Absorbance values for all spectra were within 0.4 to 1.0 absorbance units, with uncertainties of approximately ±0.005 absorbance units.

Plutonium-DFOHOPO-EDTA Spectrophotometric Competition Titrations. Three titration data sets were collected to determine the Pu^{4+}-DFOHOPO stability constants under the conditions: $[Pu^{4+}]$ = .12-.20 mM, T = 23±2°C, and μ = 0.22±2 M. The experiments were performed with DFOHOPO:Pu^{4+} ratios of 1:1, and excess EDTA, with EDTA:Pu^{4+} ratios of either 77:1 or 121:1. Each titration data set consisted of 14 to 25 solution absorbance spectra (300 to 600 nm) where the measured pH was varied from 7.5 to 2.3. Absorbance values were less than 1.3 absorbance units, with uncertainties of approximately ±0.005 absorbance units.

Results and Discussion

Plutonium (IV)-Desferrioxamine Solution Chemistry. The stability constant for the plutonium(IV)-DFO complex has been reported by Jarvis and Hancock[17] to be $\log\beta_{110} = 30.8$. However, while this value may correspond to the true stability constant for the complex, the method by which it was determined is suspect. Specifically, the stability constant was calculated from acid titration data, a method which requires measurement of a spectrum of uncomplexed Pu^{4+}, but the reported spectrum is inconsistent with published spectra for the free ion. Spectrophotometric titration experiments performed to determine formation constants for plutonium(IV)-DFO complexes, both by the method referred to above, and using EDTA as a competing ligand, yielded results from which stability constants could be calculated, but did not provide a reproducible equilibrium model and corresponding formation constants. Ultraviolet/visible spectra of free Pu^{4+} and DFO are included in Appendix 2, along with spectrophotometric titration data and a brief discussion of the experimental methods used to determine plutonium(IV)-DFO stability constants.

An estimate of the stability constant for the plutonium(IV)-DFO complex, $\log\beta_{110}$, may be obtained using the correlation for highly charged metals between first hydrolysis constants and formation constants with ligands containing negatively charged oxygen donor atoms described by Hancock and Martell.[18] Using the linear correlation for DFO, shown in Figure 33, the formation constant with Pu^{4+} is estimated to be, $\log\beta_{110} = 31.8$. This estimation does not account for differences stemming from coordination numbers, six versus eight, for example. Nor does the estimation extend to speciation--the Pu^{4+}-DFO complex may be $[Pu(DFO)(OH)(H_2O)]$, $[Pu_2(DFO)_2(OH)_4]$, or some other species.

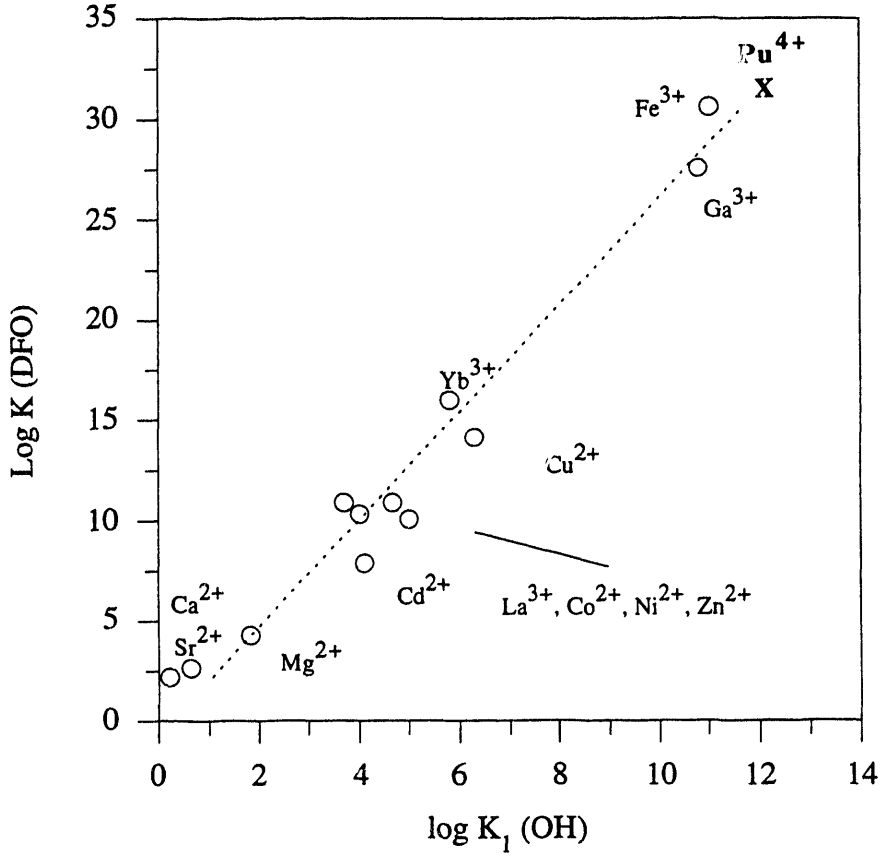

Figure 33. Correlation between 1:1, DFO to metal, formation constants and first hydrolysis constants used to estimate the stability constant for Pu^{4+}-DFO. First hydrolysis constants and formation constants are from Martell and Smith[19], except for the Ga^{3+}-DFO constant which is from reference 20.

Stability Constants of Plutonium (IV) with a Methylterephthalamide Derivative of Desferrioxamine B. The stability constant of the plutonium(IV) DFOMTA complex complex was determined to be $\log\beta_{1010} = 41.7(2)$ by competition spectrophotometric titration using EDTA. This stability constant is 15-20 orders of magnitude larger than the plutonium thenoyltrifluoroacetone [19] and EDTA[13] complexes, indicating that DFOMTA would remove plutonium from these common ligands, even when they are present in large excess.

A Pu/DFOMTA/EDTA titration data set is shown in Figure 34, and corresponding component spectra for the species included in the data analysis model used to calculate the stability constants are shown in Figure 35. When complexes with EDTA and DFOMTA simultaneously bound to Pu were included in the equilibrium model, the residual error was much larger, supporting the assumption that there was a true competition reaction where EDTA was displaced by DFOMTA. Above pH 6 the ligand is fully deprotonated, presumably bound to Pu^{4+} in an octadentate fashion. Spectral changes below pH 6, when compared with data for the ferric complex suggest the catecholate group is protonated first; the first pK_a for the complex was calculated to be 5.9(1). The second pK_a, below pH 2.9, is too low to be determined using the data acquired. The spectral changes observed during the Pu/DFOMTA/EDTA titrations were similar to those observed for the spectrophotometric titration of the free ligand, which shows the ligand has an absorbance maximimum at 358 nm with a molar absorptivity of 40,000 when the three hydroxamates and one catechol site are protonated and an absorbance maximum at 336 nm with a molar absorptivity of 27,000 when the ligand is fully protonated.[9] This similarity was used to identify the fully protonated ligand only species, H_5DFOMTA, when modeling the spectrophotometric titration data. A species distribution diagram for the Pu(IV)/DFOMTA system is shown in Figure 36.

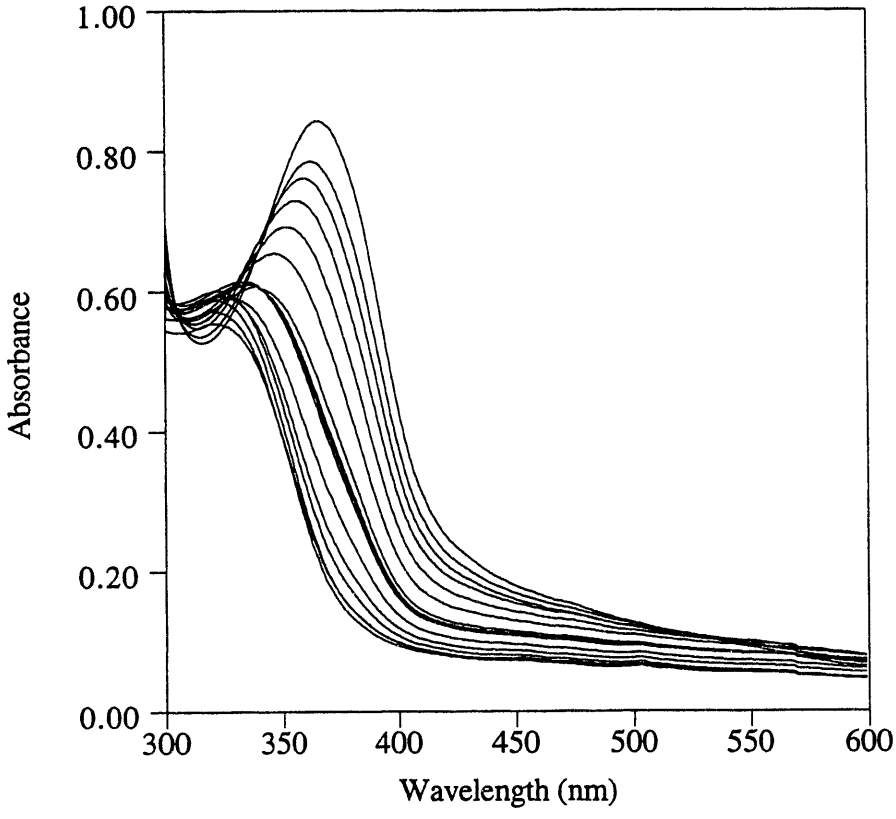

Figure 34. Spectral data from a spectrophotometric competition titration for Pu^{4+} with DFOMTA in the presence of excess EDTA, where [Pu] = 0.212 mM, [DFOMTA] = 0.210 mM, [EDTA] = 17.1 mM, and the absorbance maximum shifted to lower wavelength as the pH is decreased from pH 7.1 to 2.8.

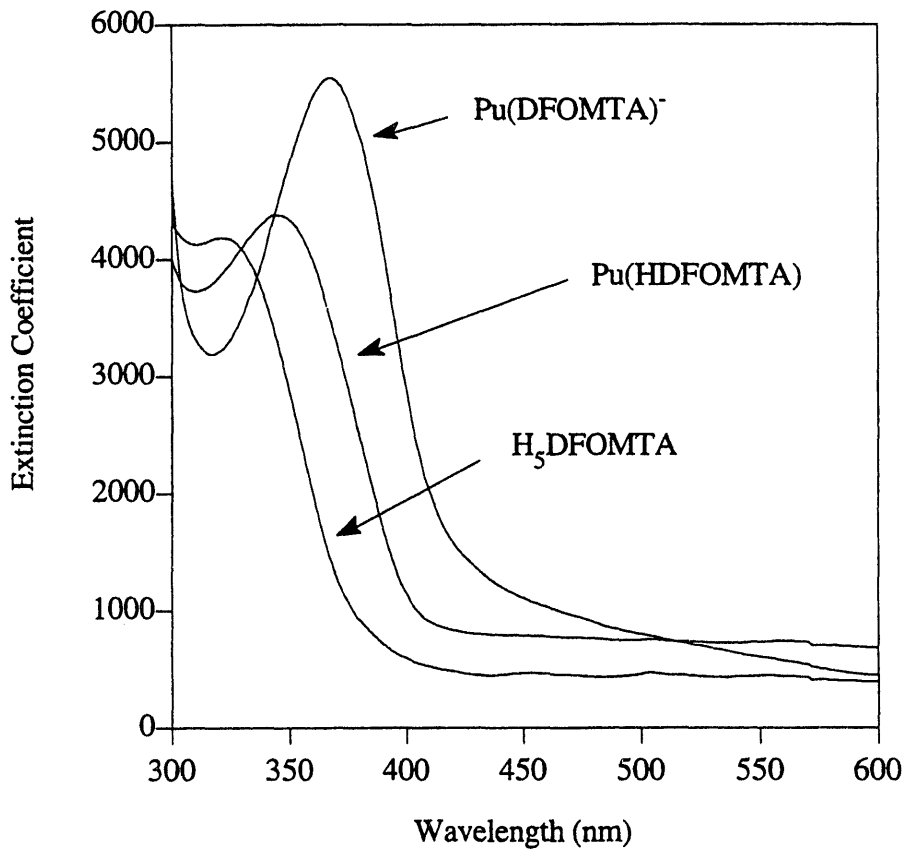

Figure 35. Component spectra generated from spectrophotometric data for the titration of Pu^{4+} with DFOMTA in the presence of excess EDTA (shown in Figure 34).

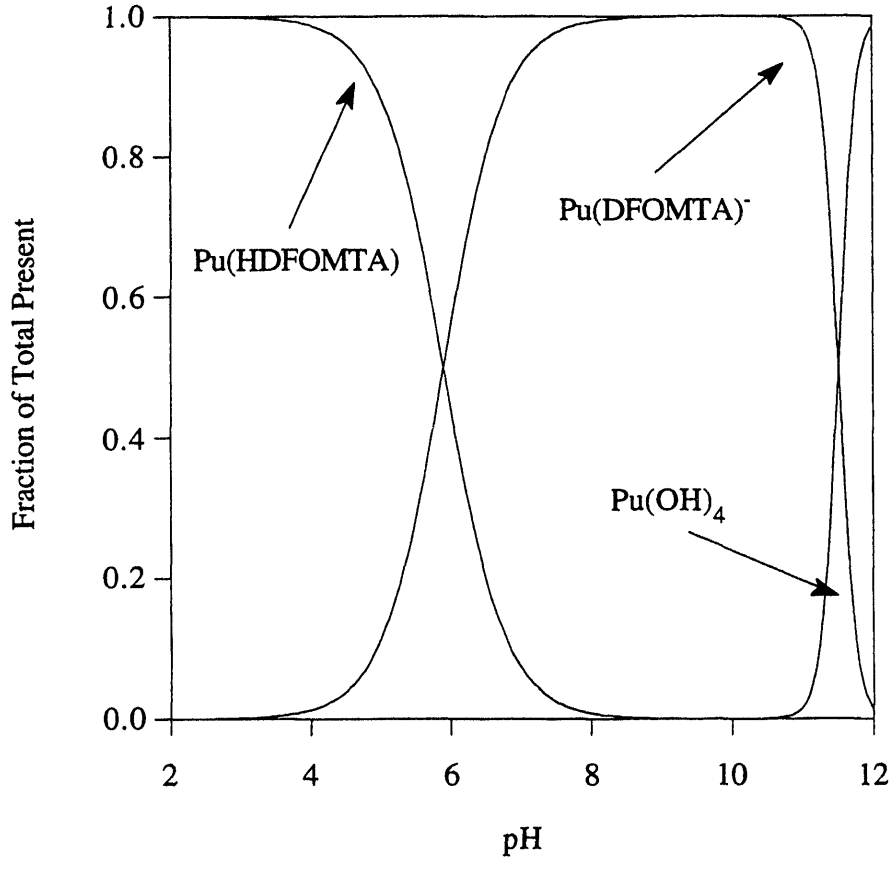

Figure 36. The distribution of Pu^{4+}/DFOMTA species calculated using the stability constants $\log\beta_{1100} = 41.7$, $\log\beta_{1101} = 47.6$, the Pu^{4+} hydrolysis constants reported by Baes and Mesmer[15], and assuming $[Pu^{4+}] = 1.0\ \mu M$, $[DFOMTA] = 10.0\ \mu M$.

Stability Constants of Plutonium (IV) with a Hydroxypyridinone Derivative of Desferrioxamine B, DFOHOPO. The equilibrium constant for the formation of a one to one Pu^{4+}-DFOHOPO complex could not be calculated from the spectrophotometric competition titration data. A model which fit three titration data sets, one of which is shown in Figure 37, is based on a mixed ligand, or ternary species, where both DFOHOPO and EDTA are bound to Pu^{4+}.

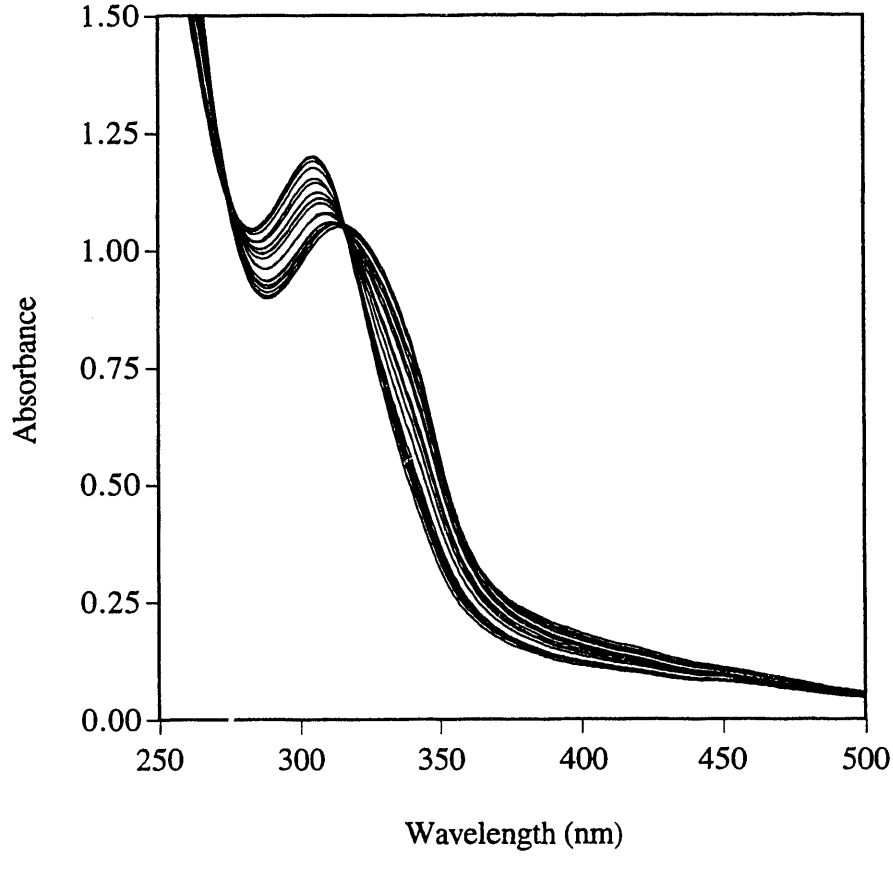

Figure 37. Spectrophotometric competition titration data for DFOHOPO with Pu^{4+} where [Pu] = 0.197 mM, [DFOMTA] = 0.216 mM, [EDTA] = 15.26 mM, showing the absorbance maximum is shifted to higher wavelength as the pH is decreased from 7.4 to 2.3.

Stability constants for the mixed ligand metal complex, $\log\beta_{1111} = 55.0$ (invariant in the model refinement) and $\log\beta_{1112} = 59.9(3)$, corresponding to a pK_a for the mixed species of 4.9(3), were calculated using REFSPEC. Component spectra generated using this equilibrium model are shown in Figure 38. By comparing the component extinction coefficient spectra with the spectrum of the fully protonated DFOHOPO[9], which shows an absorbance maximium at 306 nm ($\varepsilon = 63{,}000$), we find the mll'h = 1112 species corresponds to two of DFOHOPO functionalities being protonated (the hydroxypyridinone, and one of the hydroxamates). An upper limit for the formation constant for the Pu^{4+}-DFOHOPO complex was calculated to be $\log\beta_{1100} = 36.3$ using the program SPCONC with formation constants for Pu^{4+}-EDTA and the mixed ligand species.

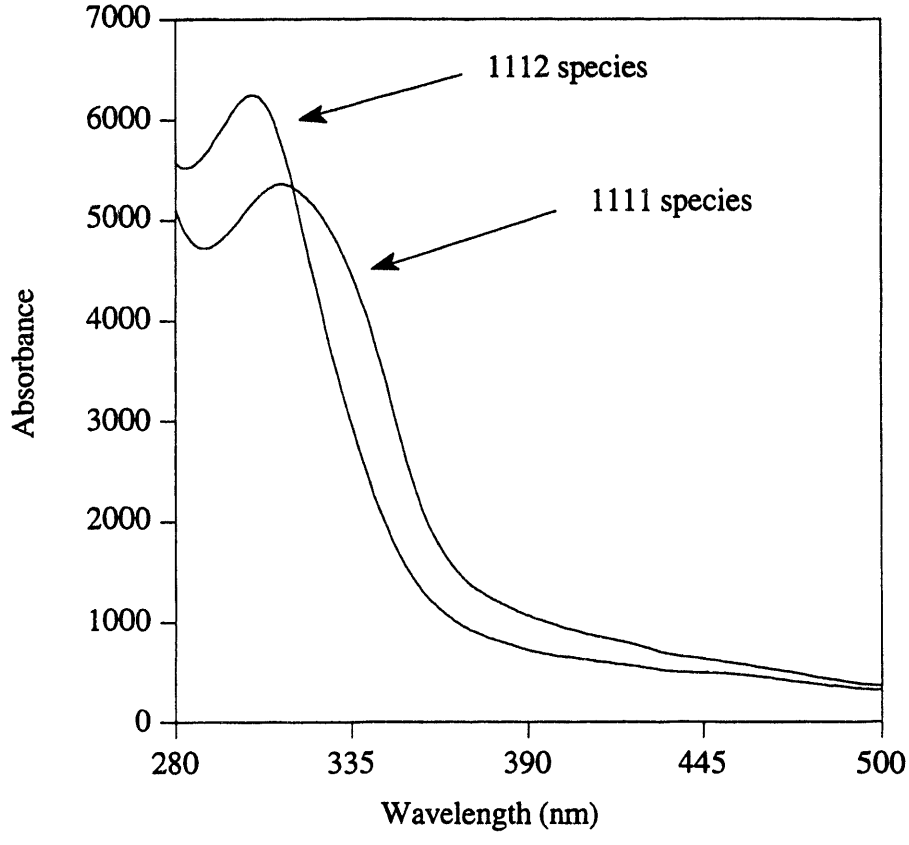

Figure 38. Component spectra generated from spectrophotometric data for the titration of Pu^{4+} with DFOHOPO in the presence of excess EDTA (shown in Figure 37).

Conclusions

We have achieved a first step in the development of plutonium complexing agents which could be incorporated into waste treatment schemes. Removal of Pu^{4+} from aqueous solutions may well be accomplished by using derivatives of DFOMTA or DFOMTA which have been modified for use in phase based separations, e.g., organic-aqueous, or liquid-solid extractions. The large formation constants for the Pu^{4+} complexes of DFO and the two derivatives, DFOMTA and DFOHOPO, listed in Table 14, show the ligands strongly bind Pu^{4+} and may be useful in separations applications where common complexing agents and many di- and trivalent cations are present. However, the current "extended siderophore" approach, derivatization of a hexadentate siderophore by the addition of a bidentate catechol group, has the unfortunate practical limitation that the ligands will bind the ferric ion preferentially. The species distribution curve for equimolar DFOMTA, Fe^{3+}, and Pu^{4+}, Figure 39, shows that even though the stability constant for DFOMTA-Pu^{4+} complex is larger than the Fe^{3+} complex, the ligand will bind Fe^{3+} preferrentially. However, if a competing ligand is present, which binds the ferric ion relatively strongly, DFOMTA will complex Pu^{4+}. This practical scenario, where DFOMTA could be added to a solution containing EDTA, Pu^{4+}, and Fe^{3+}, is modeled in Figure 40. Based on the formation constants determined, even when 100 times more Fe^{3+} is in solution than Pu^{4+}, if EDTA is also present, at twice the concentration of Fe^{3+}, 85% of the DFOMTA present is in the Pu^{4+} complex form. Furthermore, a practical separation scheme could be devised where Fe^{3+} and Pu^{4+} are simultaneously removed from a solution by DFO and Pu^{4+} is isolated by subsequent treatment with an octadentate DFO derivative.

It is unlikely that a simple modification of a natural product whose sole function is to sequester iron will yield a complexing agent specific for plutonium. This is not to say there is no combination of four siderophore-like subunits (catechols, hydroxamates, hydroxypyridinones, phenols, etc.) which could be combined to make a ligand selective for Pu^{4+} over Fe^{3+} in a certain pH range, only that starting with a hexadentate ligand which has evolved in nature as an iron seeker, it is unlikely that displacement of Fe^{3+} and one or two protons accompanied by complexation of Pu^{4+} would be favored thermodynamically. The interactions to compare are the bond strength of the most basic donor group of an octadentate ligand with a proton, versus with Pu^{4+}, which is already bound by six or seven donor groups. There may also be a ligand with appropriate basicity to exploit the differences in the hydrolysis behavior of the two cations.

Table 14. Stability constants of desferrioxamine B and the octadentate derivatives, DFOMTA and DFOHOPO, with plutonium(IV) and iron(III).

Ligand	mlh	Pu^{4+} $\log\beta_{mlh}$	Fe^{3+} $\log\beta_{mlh}$†
DFOMTA	110	41.7(2)	34.8
	111	47.6(1)	44.0
DFOHOPO	110	36.3*	30.6
	111		37.9
DFO	110	31.8*	30.6
EDTA (for comparison)	110	25.6	25.0
	111	28.2	

†Stability constants for Fe^{3+} with DFO and EDTA are from Martell and Smith[19], with DFOMTA and DFOHOPO are from Hou, et al.[9]

*Estimates: Pu^{4+}-DFO estimated from the linear free energy correlation shown in Figure 33; Pu^{4+}-DFOHOPO estimated from competition spectrophotometric titration data.

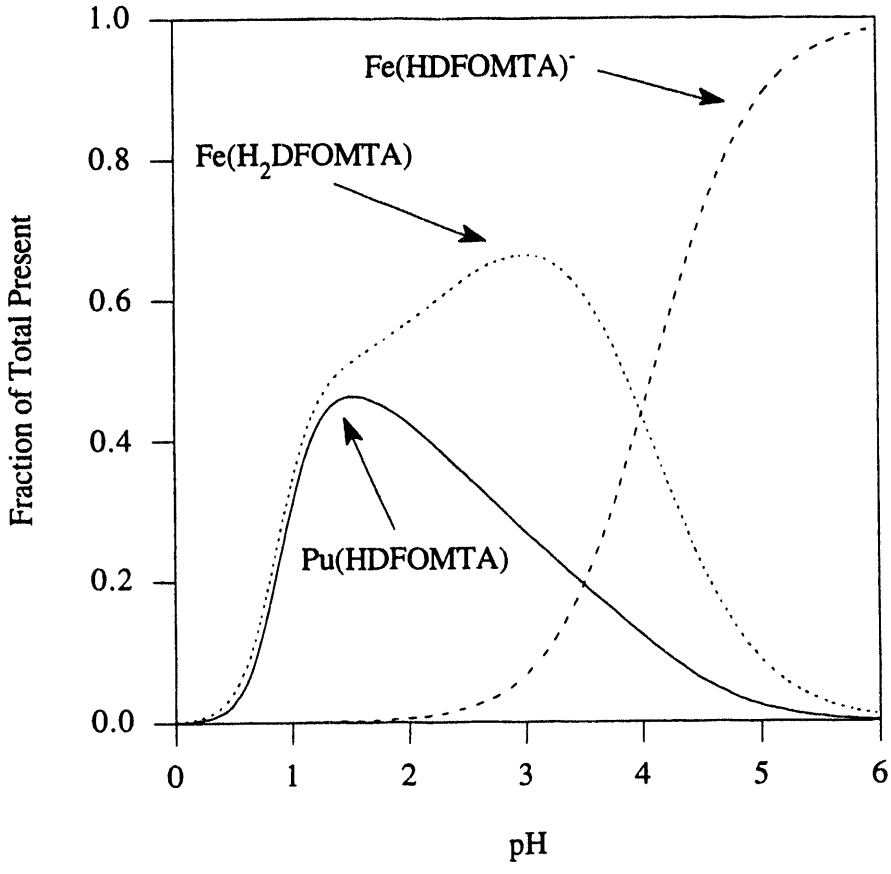

Figure 39. The distribution of Fe, Pu, DFOMTA species calculated using the stability constants listed in Table 14 and the metal hydrolysis constants reported by Baes and Mesmer[15], assuming $[Pu^{4+}] = [Fe^{3+}] = [DFOMTA] = 1.0\ \mu M$.
(Only DFOMTA containing species are shown)

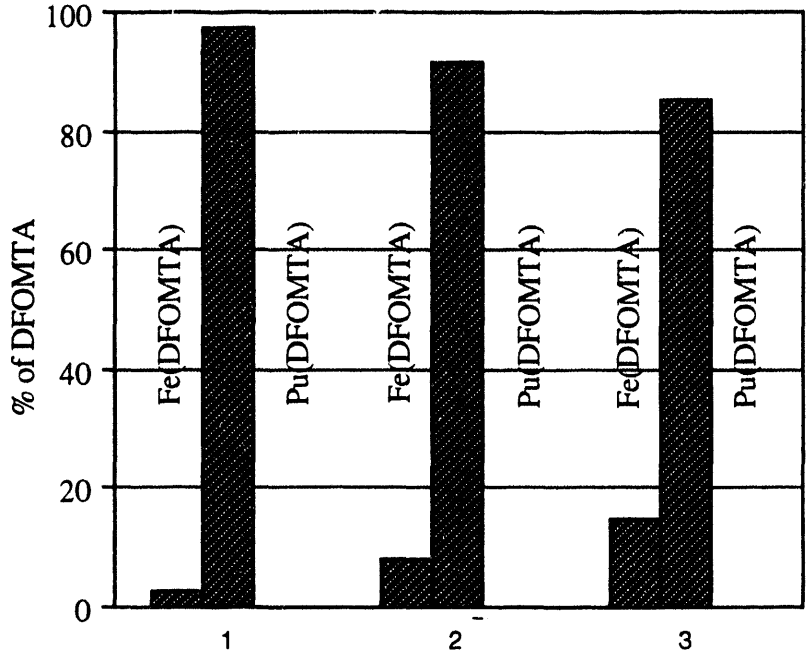

Figure 40. The selectivity of DFOMTA for Pu^{4+} over Fe^{3+} in the presence of EDTA at pH = 6.0, calculated, using the measured stability constants listed in Table 14, for $[Pu^{4+}]$ = [DFOMTA] = 1.0×10^{-5} M: 1) $[Fe^{3+}] = 1.0 \times 10^{-5}$ M, [EDTA] = 1.0×10^{-4} M 2) $[Fe^{3+}] = 1.0 \times 10^{-4}$ M, [EDTA] = 3.0×10^{-4} M 3) $[Fe^{3+}] = 1.0 \times 10^{-3}$ M, [EDTA] = 2.0×10^{-3} M.

To enhance selectivity for Pu^{4+} over Fe^{3+}, we must move beyond the charge-to-size ratio considerations used to choose the hard negatively charged oxygen donor atom type. One approach would be to build in geometrical recognition; however, designing and synthesizing a rigid ligand, preformed to adopt a dodecahedral metal-binding configuration, could be problematic. Selectivity may also be accomplished using the principles developed for solvent extraction systems where the higher charge and larger size of plutonium could be exploited. Alternatively, Pu^{4+} could be removed from a solution through the formation of another species, i.e., pretreatment of the solution to form $PuCl_6^{2-}$, followed by specific recognition of the anion or removal of interfering cations.

References

(1) Schwarzenbach, G.; Schwarzenbach, K. *Helv. Chim. Acta.* **1963**, *46*, 1390.

(2) Barry, M.; Flynn, D. M.; Letsky, E. A.; Risdon, R. A. *Br. Med. J.* **1974**, *2*, 16.

(3) Ackrill, P.; Ralston, A. J.; Day, J. P.; Hooge, K. C. *Lancet* **1980**, *2*, 692.

(4) Katz, J. J.; Seaborg, G. T.; Morss, L. R. In *The Chemistry of the Actinide Elements*; Chapman and Hall: London, 1986; Vol. 1; pp 499-886.

(5) Raymond, K. N.; Smith, W. L.; Weitl, F. L.; Durbin, P. W.; Jones, E. S.; Abu-Dari, K.; Sofen, S. R.; Cooper, S. R. In *Specific Sequestering Agents for the Actinides*; ACS Symposium Series, No. 131, Lanthanide and Actinide Chemistry and Spectroscopy; Washington, D.C.; 1979, 143.

(6) Brainard, J. R.; Strietelmeier, B. A.; Smith, P. H.; Langston-Unkefer, P. J.; Barr, M. E.; Ryan, R. R. *Radiochim. Acta* **1992**, *33*, 357.

(7) White, D. L.; Durbin, P. W.; Jeung, N.; Raymond, K. N. *Journal of Medicinal Chemistry* **1988**, *31*, 11.

(8) Stradling, G. N.; Gray, S. A.; Moody, J. C.; Hodgson, A.; Raymond, K. N.; Durbin, P. W.; Rodgers, S. J.; White, D. L.; Turowski, P. N. *Int. J. Radiat. Bio.* **1991**, *59(5)*, 1269.

(9) Hou, Z.; Whisenhunt, D. W., Jr.; Jide, X.; Raymond, K. N. , submitted to J. Am. Chem. Soc.

(10) Angelici, R. J. In *Synthesis and Technique in Inorganic Chemistry*; Saunders: Philadelphia, 1977; pp 108.

(11) Hoffman, D. C. In *Collected Radiochemical and Geochemical Procedures*; 5th ed.; J. Kleinberg, Ed.; Los Alamos, NM, 1989; Vol. Report No. LA-1721; pp 194.

(12) Cohen, D. *J. Inorg. Nucl. Chem.* **1961**, *18*, 211.

(13) Cauchetier, P.; Guichard, C. *Radiochimica Acta* **1973**, *19(3)*, 137.

(14) Scarrow, R. C. Ph. D. Dissertation Thesis, University of California, Berkeley, 1985.

(15) Baes, C. F.; Mesmer, R. E. *The Hydrolysis of Cations*; Wiley-Interscience: New York, 1976.

(16) Turowski, P. N.; Rodgers, S. J.; Scarrow, R. C.; Raymond, K. N. *Inorg. Chem.* **1988**, *27*, 447.

(17) Jarvis, N. V.; Hancock, R. D. *Inorg. Chim. Acta* **1991**, *182*, 229.

(18) Hancock, R. D.; Martell, A. E. *Chem. Rev.* **1989**, *89*, 1875.

(19) Martell, A. E.; Smith, R. M. *Critical Stability Constants;* 1974, 1975, 1977, 1976, 1982,1989 ed.; Plenum: New York; Vol. 1-6.

(20) Borgias, B.; Hugi, A. D.; Raymond, K. N. *J. Am. Chem. Soc.* **1989**, *28*, 3538.

B. Plutonium Speciation in Near-Neutral Carbonate Solution

Introduction

Currently, nuclear power and other uses of radionuclides in the U.S. are limited by the public concern about long term containment and disposal of long-lived radioactive waste. Several countries adopted the waste management strategy of long term storage in underground repositories which have suitable geologic stability and are isolated from population centers. The U.S. Department of Energy, authorized by the Nuclear Waste Policy Act of 1983 and the NWPA Amendments of 1987, is characterizing a site at Yucca Mountain, a formation located within the Nevada Weapons Test site, as a potential repository site.[1] Chemical and geochemical studies of the interaction of radionuclides with solids and solutions native to the site are being carried out in order to predict radionuclide migration in the event that engineered barriers are breached and waste is leached from the waste form.[2,3] Because spent nuclear fuel and transuranic wastes contain long-lived plutonium isotopes, it is important to understand factors controlling the migration of plutonium under site-specific conditions, including the kinetic and thermodynamic behavior. The environmental fate of plutonium depends on the concentration and oxidation state present in the original waste form, the ambient temperature and pressure, the surrounding mineral composition, and the goundwater composition--pH, Eh, concentrations of ions and organic matter.[4-6]

Laboratory solubility and speciation studies, although they are not performed on the waste isolation time scale (hundreds of thousands of years), can provide data and boundary conditions for geochemical computer modeling studies and further radiochemical research. Specifically, the measured concentration, oxidation state distribution, chemical composition, and chemical structure of soluble plutonium in groundwater samples taken from Yucca Mountain, or approximating solutions, can be used to predict sorption behavior, transport modes, and migration distances, and provide experimental data corresponding to relatively simple cases which computer software and database packages must be able to reproduce.

Nitsche[6] has proposed the following criteria for thermodynamically meaningful solubility studies: 1) solution equilibrium conditions, 2) accurate solution concentrations, 3) a well-defined solid phase, and 4) knowledge of the speciation/oxidation state of the soluble species at equilibrium. Reliable solubility and speciation data are therefore obtained when each chemical parameter is carefully controlled and monitored, all species, including the gas, solution, and solid forms, are characterized fully, and all ambient

conditions are varied systematically. Ideally, the equilibrium solubility and speciation of a radionuclide should be measured both from oversaturation, where an amount of element in excess of the solubility product is added to a solution, and from undersaturation, where a single well-characterized solid is allowed to dissolve, and the results should be consistent.

Groundwaters in the vicinity of Yucca Mountain contain a number of ionic species. The compositions of Yucca Mountain groundwaters, and of water from a specific well at the Nevada Test Site, labelled J-13, are listed in Table 15. In 1985, Nitsche and Edelstein[7] reported their determination of Pu^{4+}, PuO_2^+, and PuO_2^{2+} solubilities in water from the J-13 well at pH = 7.0. They also measured the final oxidation state distributions, using a combination of rare earth fluoride coprecipitation and TTA (thenoyl-trifluoroacetone) and MIBK (methyl-isobutyl-ketone) extractions. The results of their study are summarized in Table 16. The authors reported that their results were somewhat surprising, and presented the following conclusions: 1) Regardless of the initial oxidation state, the only significant solution species present at steady state were PuO_2^+ and PuO_2^{2+}, present at a 2:1 ratio, except in the initially Pu^{4+} experiment, where the was 1:1. 2) The effect of radiolysis from Pu decay should be investigated. (A mixture of ^{238}Pu (4.61 % by mass) and ^{242}Pu (95.39 % by mass) was used in the experiments.) Because the oxidation state distributions were determined only at the end of the solubility experiments, it is not known when, or by what reactions, the equilibrium composition is reached.

Table 15. Water Compositions at Yucca Mountain: Composition Range is from by Daniels et al.[8] and the J-13 Composition is from Ogard and Kerrisk.[9]

Species	Range (mM)	J-13 (mM)
Na^+	2 - 10	9.96
K^+	0.03 - 0.3	0.14
Ca^{2+}	0.02 - 2	0.29
Mg^{2+}	0.002 - 1	0.07
Li^+	0.007 - 0.06	
Fe^{3+}	0.0002 - 0.0009	
Mn^{2+}	0.0002 - 0.0005	
Al^{3+}	0.0001 - 0.001	
Si^{4+}	0.7 - 1	
SiO_2		0.19
Carbonate (tot.)		2.81
HCO_3^-	1 - 12	
Cl^-	0.1 - 1	0.18
F^-	0.05 - 0.2	0.11
SO_4^{2-}	0.2 - 1	0.19
PO_4^{3-}		0.00125
NO_3^-	0.01 - 0.2	
O_2	0.06 - 0.2	
pH	6.9 - 7.7	7.0
Eh (mV)	600 - 800	700
Ionic Strength		~3

Table 16. Solubility and Speciation of Plutonium From Oversaturation in Well J-13 Groundwater at pH = 7.0, 25°C, Determined by Nitsche and Edelstein.[7]

Initial Species	Solubility (M), Time	Oxidation State Distribution		
		+3, +4, and p	+5 and +6	+5
Pu^{4+}	$1.6 \pm 0.2 \times 10^{-6}$, 50 days	2 ± 3 %	98 ± 3 %	40 ± 5%
PuO_2^+	$8 \pm 3 \times 10^{-6}$, 48 days	0 ± 2 %	100 ± 2 %	68± 6%
PuO_2^{2+}	$3 \pm 2 \times 10^{-5}$, 49 days	2 ± 2 %	98 ± 2 %	67± 6%

To provide a comparison for J-13 groundwater results, and address some of the questions raised by Nitsche and Edelstein, we investigated the solubility and speciation of ^{242}Pu in a 1.93 mM total carbonate solution at pH 6.0, 30°C. The aqueous solution serves as a model for groundwater, but contains only carbonate, bicarbonate and hydroxide ligands, and $NaClO_4$ as a background electrolyte, compared with the numerous ions in the J-13 water. The pH of 6 was chosen to simulate natural waters, yet monitor a solution acidic enough to avoid highly insoluble hydrolysis products, thereby accommodating spectroscopic analysis. We attempted to minimize the potential for radiolysis effects by using ^{242}Pu. Plutonium solutions of a single oxidation state, Pu^{4+}, PuO_2^{+}, and PuO_2^{2+}, were prepared electrochemically, and separate aliquots were added to individual pre-equilibrated carbonate solutions and monitored as a function of time for periods of 3 weeks to 5 months. All experiments were performed at pH = 6.0(1), T = 30.0(2), P_{CO_2} = 5.71(6)%, with 0.100 M sodium perchlorate as an electrolyte. Solution temperature and pH were controlled via a computer-linked solution control system modeled after the "pH-stat" developed by Nitsche and coworkers.[10] An overpressure of CO_2 in argon was maintained throughout the experiments. The concentration of soluble plutonium was determined by liquid scintillation counting of aliquots of the plutonium-carbonate solutions. Spectral regions containing characteristic optical absorbance bands for Pu^{4+}, PuO_2^{+} and PuO_2^{2+} were monitored to investigate the speciation of the soluble plutonium. To provide a comparison of chemical extraction and spectroscopic methods of analysis, the distribution of soluble plutonium between oxidation states of several solutions was also determined using a combination of liquid-liquid extractions.

The optical absorbance spectra of plutonium ions contain broad, relatively intense bands due to 5f → 6d transitions and ligand to metal charge transfer, and more narrow, weaker bands due to parity, or LaPorte, forbidden 5f → 5f transitions allowed because of ligand field distortions.[11] Established characteristic absorbance bands, listed in Table 17, can be used to measure solution concentrations of plutonium (III-VI).

Table 17. Characteristic Absorbance Bands of Plutonium Ions in Perchloric Acid.[12]

Wavelength (nm)	Molar absorptivity ($M^{-1}cm^{-1}$)			
	Pu^{3+}	Pu^{4+}	PuO_2^{+}	PuO_2^{2+}
600	39	2	2	1
470	3	58	2	9
569	34	4	19	2
830	5	14	4	550

Because the concentration of soluble plutonium under typical environmental conditions is near or below the detection limits of conventional absorbtion spectrometers, the significantly more sensitive photoacoustic spectroscopy (PAS) was used.

The photoacoustic spectroscopic process is shown schematically in Figure 33. This process and its application are described thoroughly in reviews by Tam[13] and Braslavsky and Heibel.[14] In photoacoustic spectroscopy, photons are used to excite molecules from the ground state to an excited state, and an acoustic wave, generated by thermal expansion from heat released to the bulk solution via the radiationless relaxation of excited state molecules, is detected. The method is a more direct and sensitive technique than conventional absorption spectroscopy, which depends on the difference between incident and transmitted radiation. The use of laser photoacoustic spectroscopy for the measurement of actinide speciation was first described by Schrepp et al.[15] and has been used fairly extensively in the last decade.[16-20] For possible exposure, contamination and solution instability reasons, it is desirable to measure solution spectra in an inert atmosphere box. A photoacoustic spectrometer, modeled after the spectrometer developed by Russo and coworkers,[21,22] was assembled to allow for remote measurements.

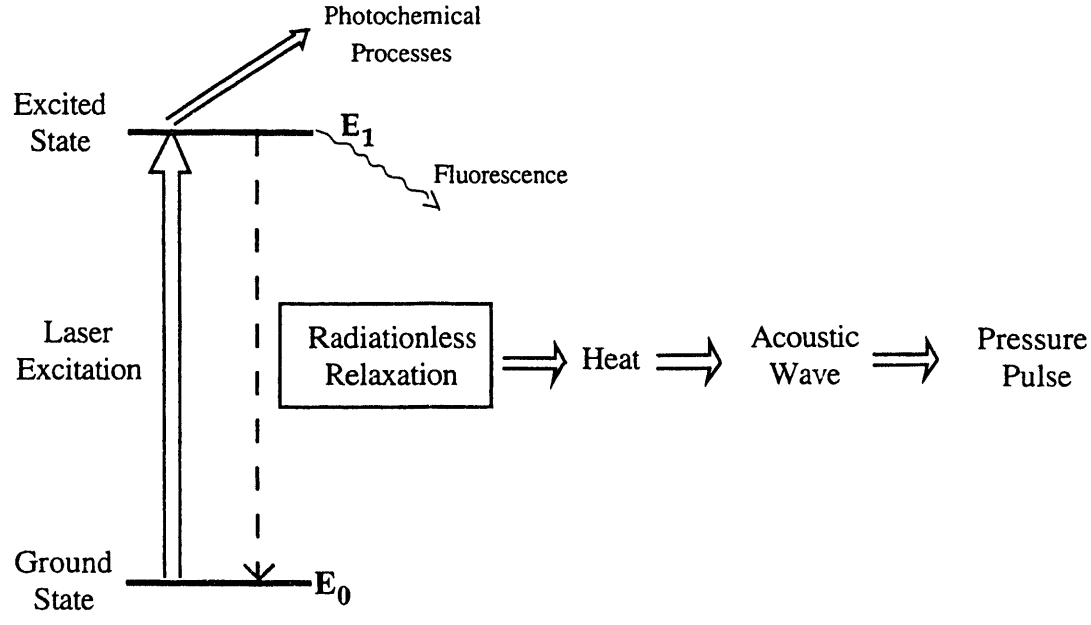

Figure 33. The photoacoustic process used to measure absorbance spectra.

Optical spectroscopy can be used to identify and quantify absorbing species, but like all analytical methods, it is useful only when the analyte concentration exceeds the limit of detection. Chemical extractions are also used to quantify individual oxidation states present in solutions less than 10^{-5} M, in plutonium.[23] Because nuclear decay counting methods are used to determine the concentration of plutonium in separated phases, extraction methods are much more sensitive than even the most sophisticated spectroscopic techniques used currently. However, chemical extractions are destructive, may disturb the solution composition, and separations are typically based on the oxidation state of plutonium, not on the chemical form, or coordination environment, of the ion.

We used a group of extractions employing di-(2-ethylhexyl)-orthohosphoric acid (HDEHP), and either thenoyltrifloroacetone (TTA) or 4-benzoyl-3-methyl-1-phenyl-2-pyrazolin-5-one (PMBP), shown schematically in Figure 34, to separate the soluble plutonium into groups. The overall method, developed by Nitsche and coworkers [23] and summarized in Figure 35, is based on well-established chemistry.[24-29] Both TTA and PMBP extract by chelation and at pH = 0 will extract Pu^{4+} into an organic phase. By adding dichromate, Pu^{3+} is oxidized to Pu^{4+} and also extracted into the organic phase.[24,27,28] The chelating agents PMBP and TTA have similar extraction chemistry, but PMBP is reportedly more efficient than TTA, and is more resistant to decomposition.[30] We performed separate experiments using TTA and PMBP to verify that these two extracting agents produce the same separation. Strongly acidic HDEHP acts as a "liquid cation exchanger," and at pH = 0 removes Pu^{4+} and PuO_2^{2+} from an aqueous solution; in the presence of dichromate HDEHP extracts Pu^{3+}, Pu^{4+}, PuO_2^{+}, and PuO_2^{2+}, leaving only polymeric Pu(IV) (Pu_p) in the aqueous phase.[26,29] Although it may be thermodynamically possible to oxidize Pu^{4+} to PuO_2^{+} and PuO_2^{2+} in the extraction procedures and achieve different separations, the kinetics of these bond forming reactions are very slow and no significant oxidation will occur for many hours.[31] By measuring the relative amounts of plutonium in each phase of the four individual separations using liquid scintillation counting, the percent of each oxidation state can be calculated.

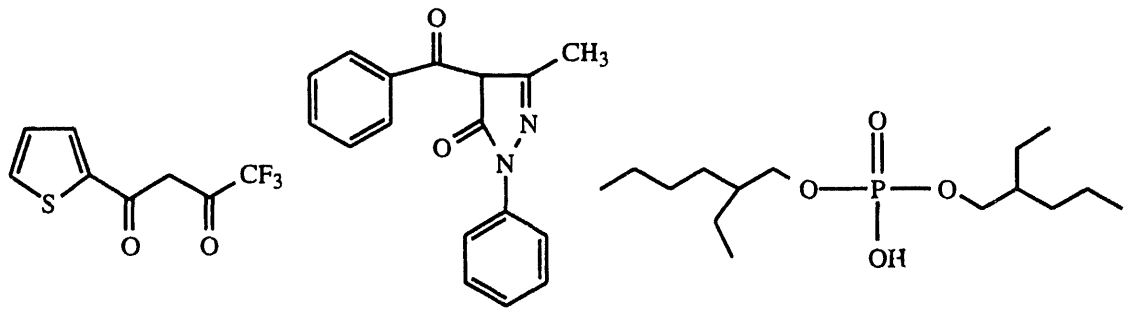

TTA PMBP HDEHP

Figure 34. Extracting agents used in combination to determine the distribution of soluble plutonium among different oxidation states.

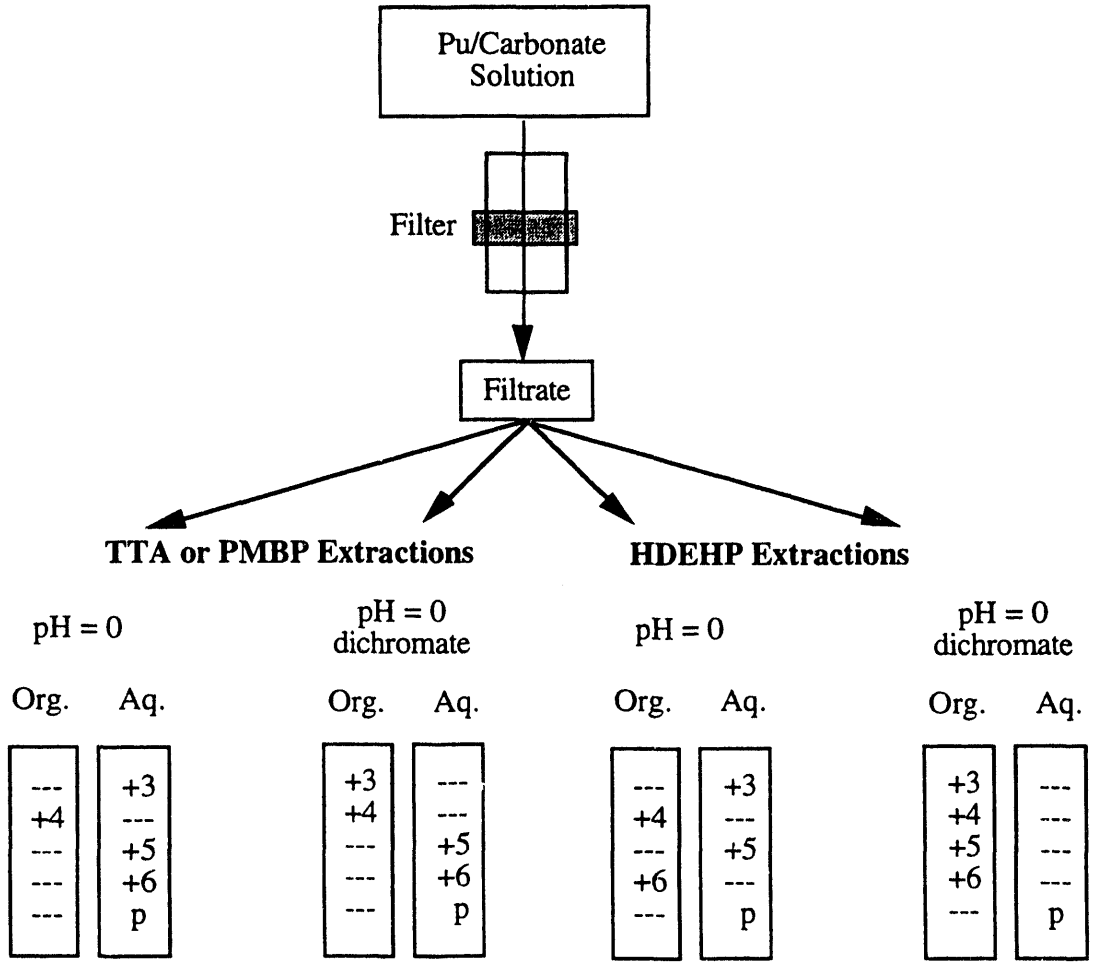

Figure 35. The separation scheme used to determine the distribution of soluble plutonium among oxidation states, Pu (III, IV, V, VI, and p), where p represents Pu^{4+}/hydroxide/oxide polymeric material small enough to pass through the filter.

Experimental

General. All chemicals were used as received, unless otherwise noted, and all solutions were prepared using house distilled, dionized water, which was further deionized by a Millipore cartridge system. Sodium perchlorate solutions were prepared by dissolving the solid ($NaClO_4$, dehydrated, 99.99%) in degassed, deionized distilled water. Rare earth solutions of Nd^{3+} and Dy^{3+}, used as spectroscopic standards in the quantification of plutonium species, were prepared from the oxide salts. Liquid scintillation counting (LSC) was accomplished using a Beckman, Model 5300, LS spectrometer and Ecolite$^+$ scintillation cocktail. Alpha spectra were obtained using either an AlphaKing spectrometer, or a Tennelec spectrometer (Nucleus Model PCAII-1000) equiped with a Si detector, variable pulse generator, (Model TC257-2000-ES-SNA), and a NIM bin power supply (Model TB4/TC911). The electrochemical equipment, the Guided Wave spectrometer, and the acid, base, buffer, and ^{242}Pu, HCl stock solutions, used throughout are described in the previous section, vide infra.

Plutonium Solutions. Stock solutions were prepared as needed by purifying an aliquot of the ^{242}Pu, 6 M HCl, stock solution referred to above, using anion exchange chromatography.[32] Typically, a glass column approximately 4 mm x 12 filled with a Dowex AG 1x8, 100-200 mesh resin, pretreated with concentrated HCl, was used to purify $PuCl_6^{2-}$. The plutonium was removed from the column, via reduction to Pu^{3+} with HI, fumed with HNO_3, and then converted to a perchlorate media by treatment with fuming $HClO_4$ in an inert atmosphere box. The chemical oxidation step was performed using a simple, small-volume distillation apparatus to which four interconnected scrubber bottles were linked. The first three collection bottles contain distilled water; the last contains a saturated KOH solution to trap the $HClO_4$ driven off of the plutonium solution, via precipitation of $KClO_4$.

The composition of the plutonium used was reported previously by Bennett[33], and verified using α and γ pulse height analysis of an aliquot of the stock solution. The calculated solution composition is summarized in Table 18. The chemical purity of the source plutonium was verified by spark emission spectroscopy.[34]

Table 18. Pulse Height Anlaysis of an Aliquot of the Plutonium Stock Solution Used.

Peak Identification	Energy[35] (keV)	atom %
Alpha		
^{242}Pu	4,901	99.85
^{239}Pu	5,161	0.120
^{238}Pu	5,498	0.048
Gamma		
^{241}Am	59.6	0.01
^{241}Pu	149	0.029

Single oxidation state solutions were prepared electrochemically as needed by applying a fixed potential to a Pt mesh working electrode to an aliquot of a ^{242}Pu, 0.1 M $HClO_4$, stock solution until the residual current was less than 10 μA. Solutions containing only Pu^{3+} or only PuO_2^{2+} were prepared using an applied voltages (vs an Ag/AgCl reference electrode) of -0.110 V, or 1.100V, respectively. Solutions of only Pu^{4+} were obtained by oxidizing a Pu^{3+} solution, using an applied potential of +0.900 V. Solutions of pure PuO_2^{+} were prepared by adding base (KOH, or NH_4OH) to a PuO_2^{2+} solution until the measured pH was 3, then applying a potential of +0.70 V. The oxidation state purity was verified spectrophotometrically, and the concentration was determined by comparison with previously reported spectra.[12] Standard solutions were prepared by diluting stock solutions and measuring the concentration using LSC, and/or α spectroscopy of thin samples on Pt foils.

Solubility/Speciation Experiments. The oversaturation solubility/speciation experiments were conducted in an argon atmosphere glove box using custom-made Teflon solution cells. An oxygen analyzer (Teledyne, 316AX) fed by a circulating pump (Markson, J-15947) inside the glove box was used to verify that the amount of O_2 present was not significant--typically 18-30 ppm. Experiments were initiated by the addition of an appropriate volume of single oxidation state plutonium solution to a 0.100 M $NaClO_4$ solution, which had been pre-equilibrated with 5.71% CO_2 in Ar (Alphagas, certified), and an amount of base required to neutralize the acid in the plutonium stock solution. The experimental solutions studied are listed in Table 19.

Table 19. Solutions Used to Measure Plutonium Solubility and Speciation. Solutions were 0.100 M in $NaClO_4$, and Maintained at pH = 6.0(1), 30.0(2)°C with an Overpressure of 5.71% CO_2 in Ar.

Initial Species	Initial Concentration (M)	Duration of Experiment (days)
Pu^{4+}	4.70×10^{-5}	25
PuO_2^{+}	2.51×10^{-5}	52
PuO_2^{2+}	1.63×10^{-4}	43
PuO_2^{2+}	2.42×10^{-4}	120
PuO_2^{2+}	3.68×10^{-4}	150

To ensure that the total carbonate concentration remained constant (at 1.93×10^{-3} M calculated, total dissolved carbonate), a slight overpressure (approximately 7 inches of water) of the water-saturated CO_2/Ar gas, was maintained over solutions for the duration of each experiment using a custom-made manometer. Solution pH was measured using a combination electrode (Beckman, Model 39532), and a digital pH meter (Markson, Model 95). Saturated NaCl/AgCl was used as an electrode fill solution in place of KCl/AgCl to prevent clogging of the junction by $KClO_4$. The electrode was standardized with the National institute of Standards and Technology traceable buffers of pH 4.00 and 7.00 (25°C, EM Science). Addition of 0.100 M, CO_2-free, NaOH or $HClO_4$ to adjust the pH of individual solutions was accomplished using two high pressure pumps (Ranin, Rabbit-HP) and two valve selectors (Eldex, SV-3) fitted with Teflon tubing, 0.015" i.d. at the delivery site. The solution temperature was controlled using a custom-made heating block and interface, and monitored using a thermistor thermometer (Omega, L-08502-2), equipped with pyrex and stainless steel probes (Omega, L-08436, 08446) which were placed in a blank solution and the heating block.

Each time a solution was sampled for analysis, a phase separation was performed on an aliquot of the plutonium solution using Centricon-30 centrifugal filters, which contain a YM-type membrane with a calculated pore size of 4.1 nm, and a high speed centrifuge (Savant, HSC 10K). Each filter was presaturated immediately before use with at least 500 µL of the experimental solution to be separated, thereby preventing errors due to sorption of plutonium species on the membrane. A second aliquot was then filtered and used for analysis. The filter pretreatment volume was arrived at by comparison with similar plutonium/hydroxide/carbonate solubility studies.[36] Throughout this work "soluble plutonium" includes the amount of colloidal Pu^{4+} polymer material, or any other solid suspended in solution, which is small enough to pass through the membrane filter.

Laser Photoacoustic Spectroscopy. Laser photoacoustic spectra were obtained remotely using the spectrometer system represented in the block diagram in Figure 36.

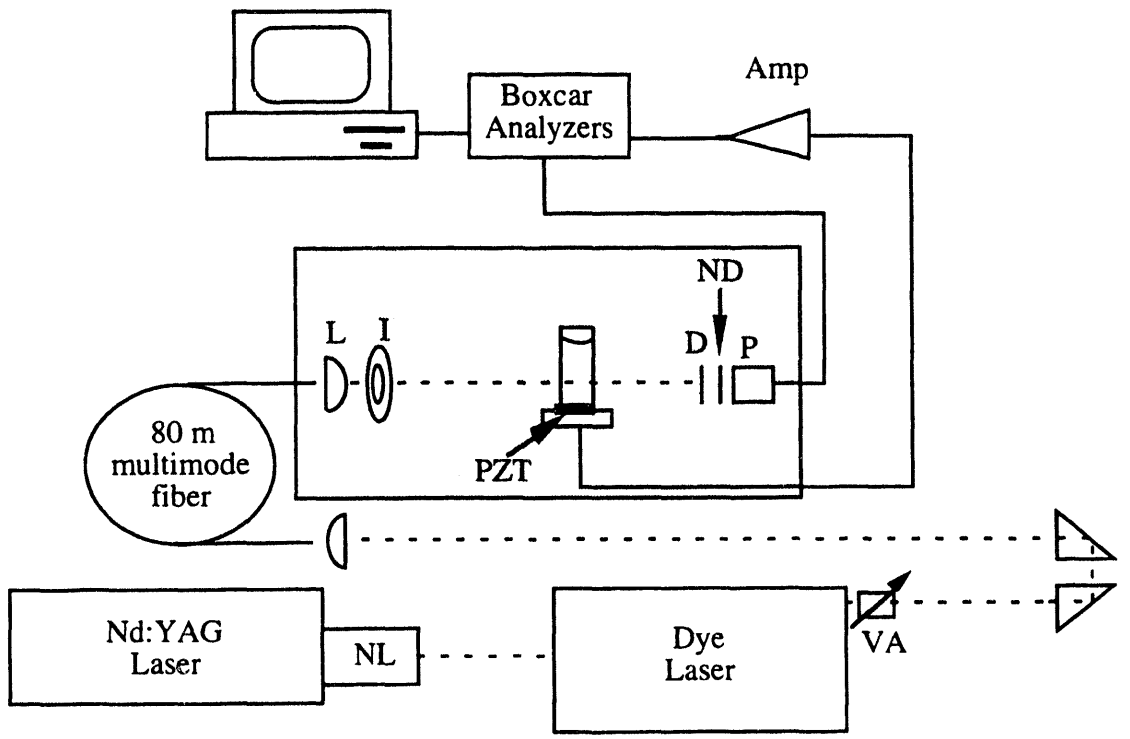

Figure 36. A schematic representation of the remote laser photoacoustic spectrometer used to measure plutonium conentrations of solutions in an inert atmosphere box. Components within the shaded area are enclosed in the glove box, all others are in the laser laboratory. Components include: NL, nonlinear optics (harmonic generator and beam separator); VA, variable attenuator; L, focusing lens; I, iris; PZT, piezoelectric transducer; D, diffuser; ND, neutral density filter; PD, photodiode; and AMP, amplifier.

The beam from a pulsed Nd:YAG laser (Spectra Physics, DCR-3G), operating at 20Hz, is used as an excitation source to pump the dye laser (Quanta Ray DCR-3/PDL). The second and third harmonic of the YAG laser, used to access different wavelength ranges, are obtained using the harmonic generator (Spectra Physics HG-2) and harmonic separator (Spectra Physics PHS1). A variable attenuator (NRC, 9355) is used to adjust the output enengy of the dye laser to a level appropriate for coupling into the optical fiber, typically 60 mW, measured using a power meter (Scientech, 365) just before the fiber. A 35-mm quartz plano-convex lens (Oriel) is used to launch the laser light into the multimode optical fiber, which has a core diameter of 600μm (Fiberguide).

Originally, a 10X microscope objective was used to collimate and focus the light from the fiber and direct it into a 1 cm quartz cuvette (NSG Precision Cuvette), but the standard cuvette was replaced by a smaller volume, thick-walled, 1 cm pathlength cuvette which requires tighter focusing of the laser light. A plano-convex lens (Oriel, f=25) is used to focus the beam entering the cuvette to approximately 2 mm, followed by an iris to remove stray light. The laser height giving the optimum photoacoustic signal was determined to be 14 mm from the base of the cuvette. The piezoelectric transducer (PZT), a piezoelectric, lead-zirconate-titanate, disc (Vernitron, type 5A, 1.5 cm x 6 mm), is physically coupled to the cuvette via a 1 cm cylindrical quartz rod. The electric signal from the PZT is amplified by a charge-sensitive preamplifier (Ortec 142C) in the glove box, then further amplified and conditioned by a spectroscopy amplifier (Ortec 570) with a 1 μs shaping time. A boxcar integrator (Stanford Research Systems; SR250) with a 900 ns gate, delayed approximately 40 μs to select the portion of the acoustical pulse from the analyte and avoid the signal due mostly to the cuvette,[37] is used for gated detection. The optimum gating time was determined by measuring "on peak" and "off peak" photoacoustic signals with the analyte of interest in the cuvette and looking at their difference.

To correct for variations which arise from the laser dye gain and pulse-to-pulse variations in the laser energy a filter/photodiode (PD) assembly is used to collect the beam exiting the cuvette. The assembly consists of a diffuser and neutral density filters (Ealing, 26-6510) placed in front of the photodiode (United Detector Technology, PIN-10DFP) to reduce the intensity of the light hitting the photodiode to levels within the linear response range. A 9V battery was used to power the photodiode, and a bias box was used to apply a reverse bias so the photodiode would respond only when the light generated an input signal large enough to overcome the bias. A boxcar integrator (Stanford Research Systems; SR250) with a 20 ns gate, delayed approximately 1 μs, is used for detecting the PD signal.

Boxcar sensitivities were adjusted to maximize PZT and PD signals, and both boxcar input filters were set to >10 kHz. Components in the inert atmosphere box, including the lens, iris, PD assembly, and the solution cell/PZT assembly (fixed in a custom-made aluminum box), were mounted on a translational rail and placed at optimal positions to maximize the analyte signal. Signals were observed using a Tektronix, Model 11402, digitizing oscilloscope. Spectra are measured by stepping the dye-laser monochromator (Spectra Physics, grating drive MCI) by 0.2 or 0.3 nm intervals over the desired wavelength range and averaging the PZT and PD signals from 100 laser pulses at each wavelength.

An IBM-PC controls the monochromator through an IEEE-488 interface (National Instruments, Model GPIB-PC2A) using an A/D-I/O board (Data Translation, Model DT-2801A). All spectra presented were acquired in a single-beam arrangement with off-line background subtraction, where the "photoacoustic signal" is actually the photoacoustic signal divided by the photodiode signal. Three replicate spectra were measured, background corrected, then averaged; unless the time between solution sampling was very short and the first two spectra were not significantly different, then two spectra were used. Photoacoustic spectra were viewed and manipulated using the sprogram Spectra-Calc.[38] The laser dyes (Exciton) used to access various wavelength ranges are listed in Table 20. Approximately 1 gram of 1,4-diazobicyclo(2,2,2)octane was added to each liter of dye solution to extend their useable lifetime.[39]

Plutonium concentrations were calculated from the peak heights of the analyte compared with the peak heights of plutonium standards of the same oxidation state or standard Nd^{3+} or Dy^{3+} perchloric acid solutions.

Table 20. Laser Dyes Used, and Corresponding Wavelength Ranges and Characteristic Cationic Plutonium Absorbance Bands.

Laser Dye (Exiton)	Wavelength Range (nm)	Characteristic Absorbance	Concentration (mg/L)	
			Oscillator	Amplifier
3rd Harmonic Pump	(354 nm)			
LD466	455-485	Pu^{4+}, 470	180	74
C540A	540-590	PuO_2^{+}, 569	1550	620
2nd Harmonic Pump	(531 nm)			
R590	554-580	PuO_2^{+}, 569	115	17
DCM	605-670	PuO_2^{2+}, 615	175	24
LDS821	810-840	PuO_2^{2+}, 830	125	32.5

Solvent Extractions. A 0.025 M solution of 4-benzoyl-3-methyl-1-phenyl-2-pyrazolin-5-one in xylene was obtained by dissolving the solid (PMBP) (Aldrich , 99%). Thenoyltri-floroacetone (TTA), (Alfa Products, M. Thiokol, Inc.) was recrystallized twice from cyclohexane before being dissolved in xylene to make a 0.50 M solution.

Di(2-ethylhexyl)orthophosphoric acid (HDEHP, Aldrich) was dissolved in toluene to make a 0.50 M solution. Sodium dichromate dihydrate (Mallinckrodt, analytical grade) was dissolved in 1 M HCl to make a 4.0 mM $Cr_2O_7^{2-}$ solution. Concentrated HCl (Ultrex II, Baker) was used to acidify each filtrate to pH = 0, and to prepare solutions of 1 M HCl. To minimize disturbing the oxidation state distribution, the four extraction methods were carried out independently, as suggested in Figure 43. All extraction experiments were completed in less than thirty minutes, to avoid errors due to disproportionation. Extractions were performed using 500 µL of organic and aqueous solutions; the composition of which are listed in Table 21.

Table 21. The Composition of the Four Biphasic Extraction Mixtures used to Separate Different Oxidation States of Plutonium.

Solution #1	Solution #2	Solution #3	Solution #4
458 µL Pu filtrate 42 µL 12 M HCl	433 µL Pu filtrate 42 µL 12 M HCl 25 µL 4 mM $Cr_2O_7^{2-}$	458 µL Pu filtrate 42 µL 12 M HCl	433 µL Pu filtrate 42 µL 12 M HCl 25 µL 4 mM $Cr_2O_7^{2-}$
0.025 M PMBP or 0.50 M TTA in xylene	0.025 M PMBP or 0.50 M TTA in xylene	0.50 M HDEHP in toluene	0.50 M HDEHP in toluene

After mixing each aqueous phase in centrifuge cones, the organic phase, presaturated with an equal volume of 1 M HCl, was added; each biphasic solution was mixed vigorously for two minutes using a vortex mixer, then the solutions were centrifuged at high speed (~5000 g) for one minute. Each organic phase was transferred to individual scintillation vials containing 20 mL of LSC cocktail. A second extraction was performed immediately and the organic phases were combined with the respective first extraction samples. The remaining aqueous phases, and one 1 M HCl wash were then transferred to individual vials containing 20 mL of LSC cocktail. All samples were analyzed for plutonium using a Beckman, Model 5300, LS spectrometer Standards for each fraction were prepared by spiking samples of identical chemical composition with activity obtained from a 2.7×10^{-4} M plutonium stock solution verified through absorption spectrophotometry. A comparable amount of activity was used in making the standards to ensure accurate measurement of the chemical quenching associated with the different fractions. Background samples were also prepared to subtract from the fractions that contained low levels of activity.

Results and Discussion

A fiber optic laser photoacoustic spectrometer was built and used to measure plutonium solution spectra. The transmission effeciency, measured through the optical components, fiber, and cuvette is approximately 55% at 575 nm. A typical photoacoustic signal, detected using the lead zirconate disc PZT and amplified, is shown in Figure 36. Conventional absorbance spectra, and laser photoacoustic spectra of characteristic bands obtained remotely using the spectrometer, of Pu^{3+}, Pu^{4+}, PuO_2^{+}, and PuO_2^{2+} in perchlorate acid, are shown in Figures 37-40.

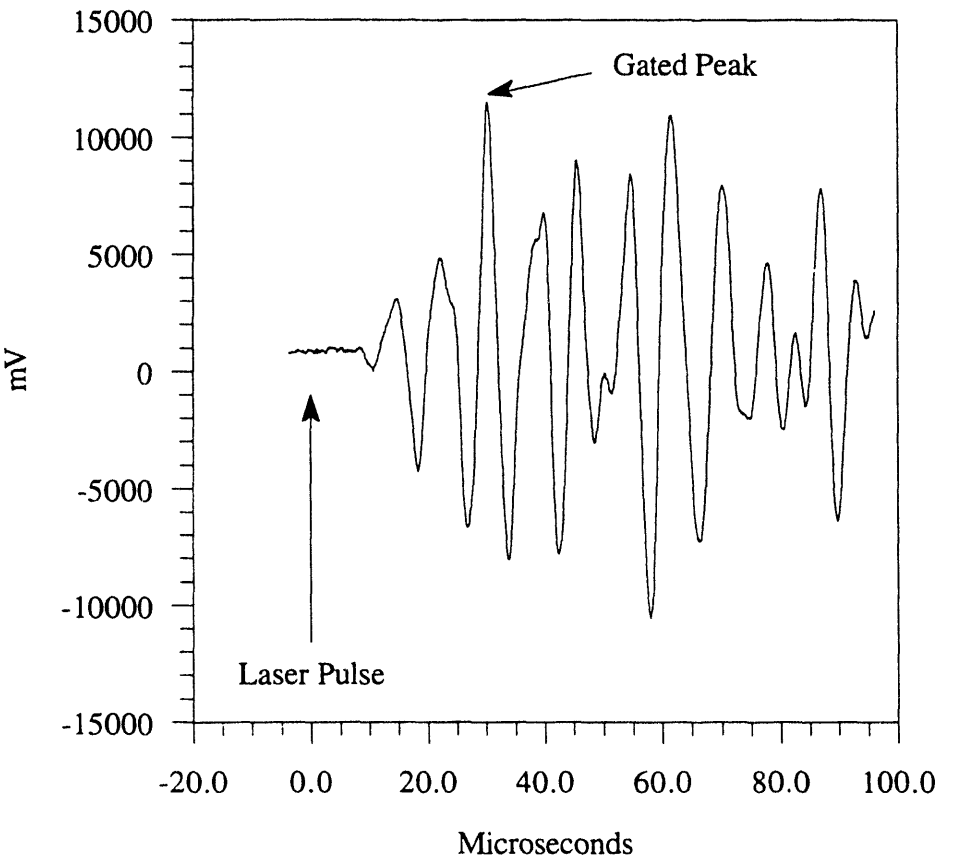

Figure 36. A representative amplified signal from the piezioelectric transducer disc, which is physically coupled to a 1.4 mL quartz cuvette via a 1 cm quartz rod.

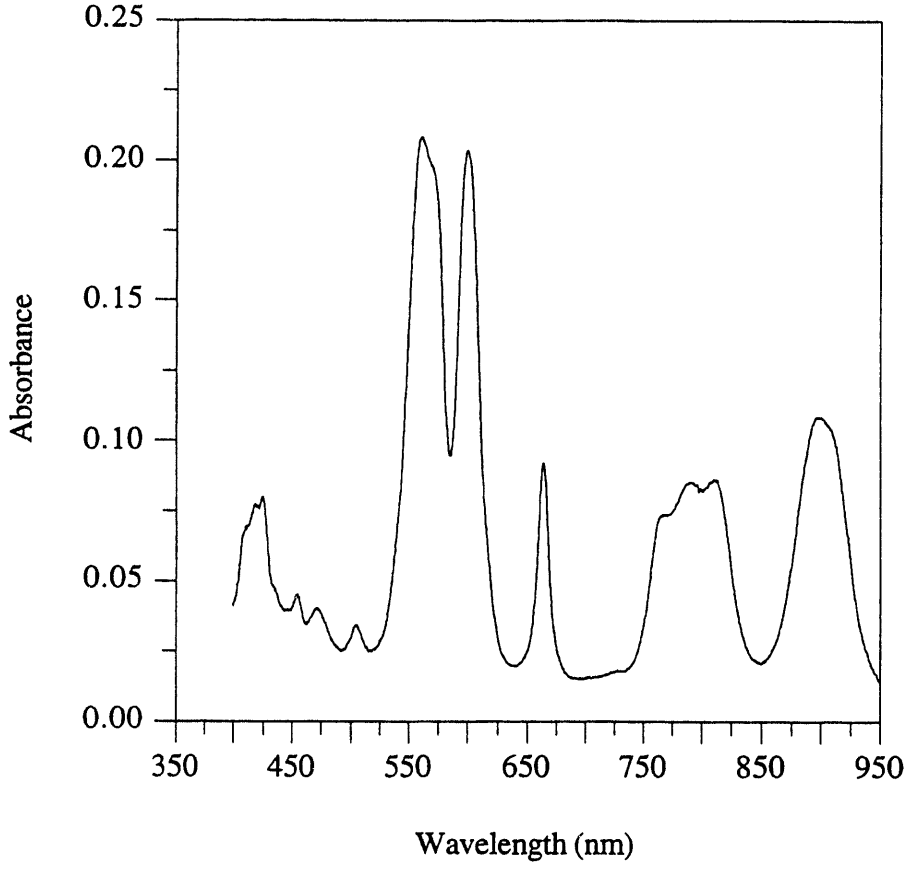

Figure 37. A conventional absorbance spectrum of 5.31 x 10^{-3} M Pu^{3+} in 0.1 M $HClO_4$ measured using a Guided Wave, fiber optic, spectrophotometer.

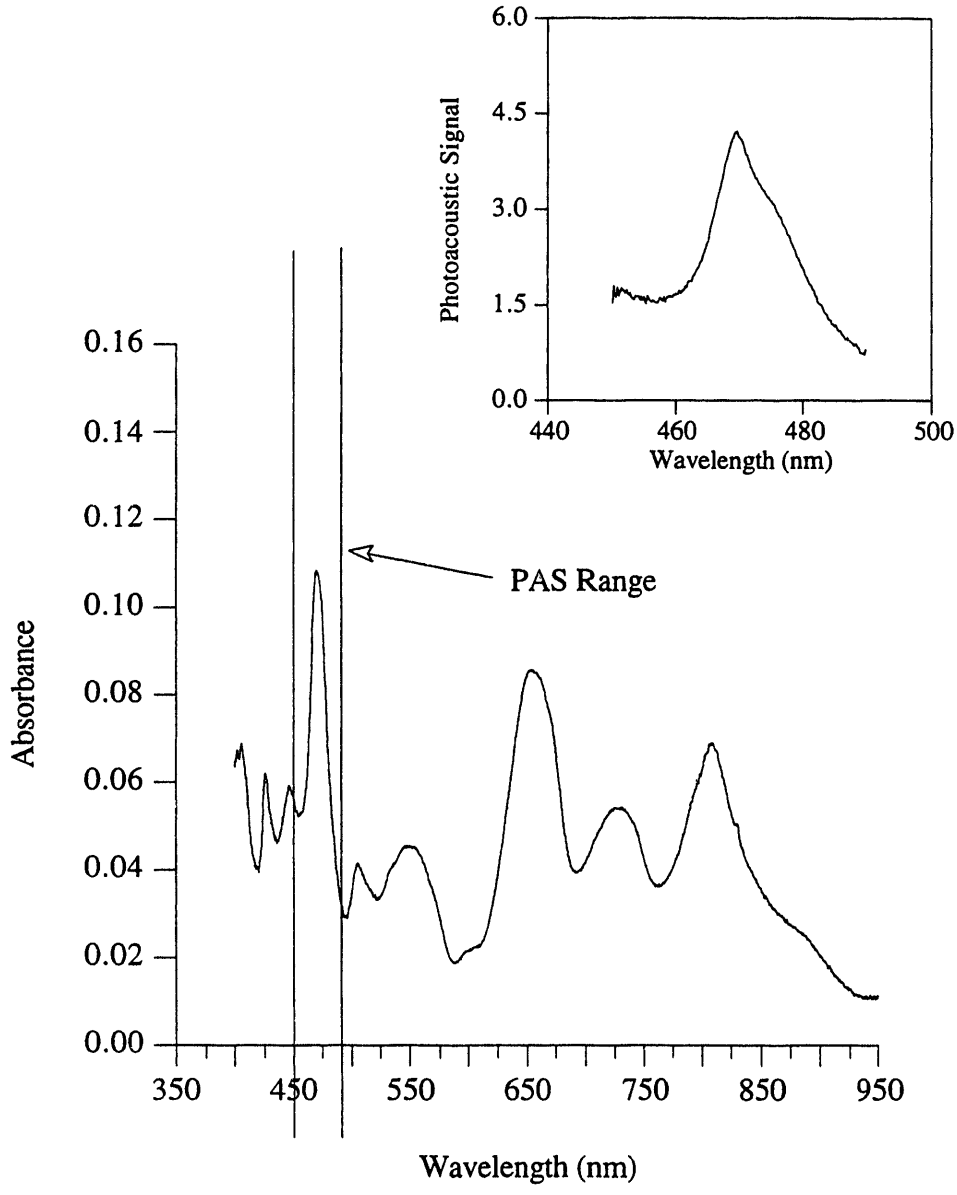

Figure 38. Absorbance spectra of Pu^{4+}: the bottom spectrum is a conventional absorbance spectrum of 1.96 x 10^{-3} M Pu^{4+} in 0.1 M $HClO_4$ measured using a Guided Wave, fiber optic, spectrophotometer; the upper spectrum is a photoacoustic spectrum of 1.96 x 10^{-5} M Pu^{4+} in 0.1 M $HClO_4$ measured using the spectrometer described herein with the laser dye LDS466.

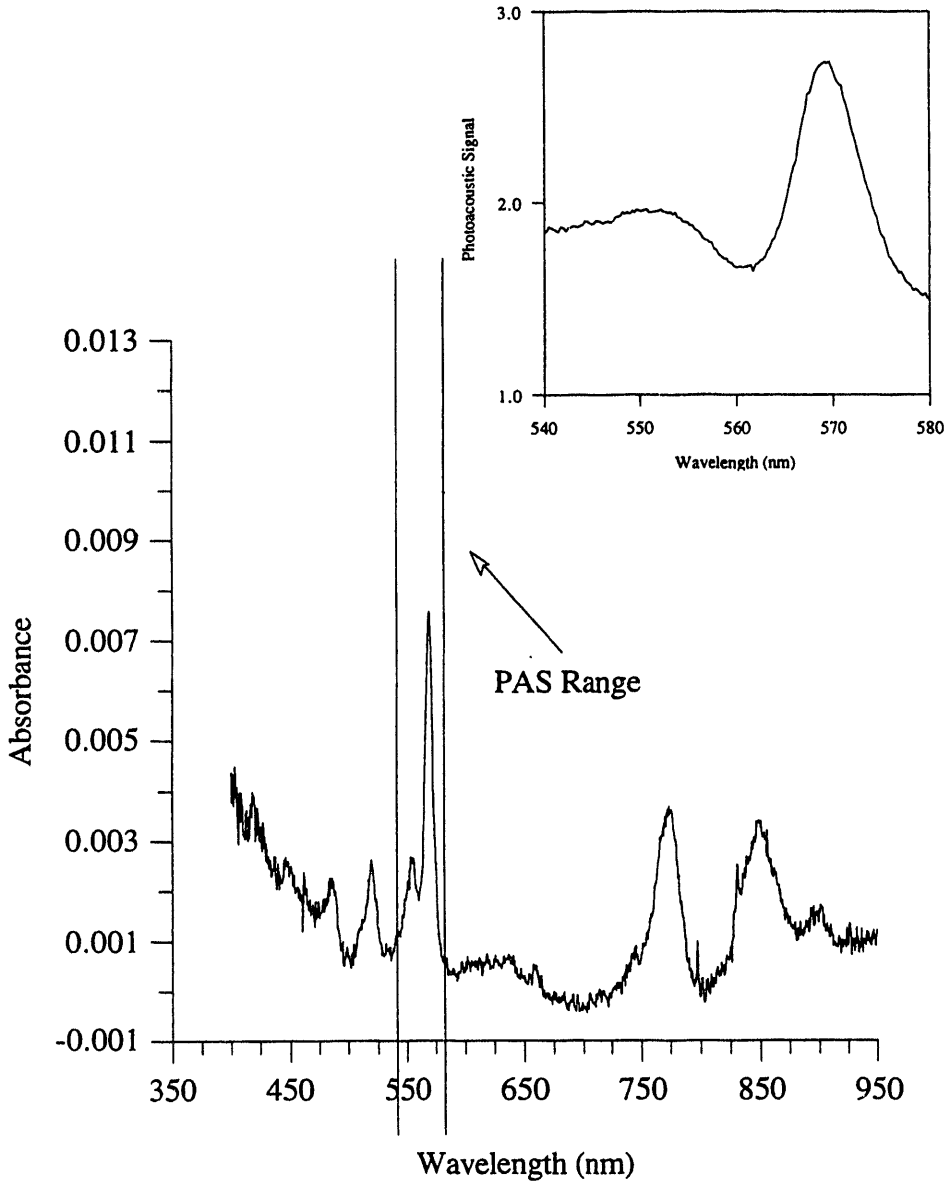

Figure 39. Absorbance spectra of PuO_2^+: the bottom spectrum is a conventional absorbance spectrum of 3.98 x 10^{-4} M PuO_2^+ in 0.1 M $HClO_4$ measured using a Guided Wave, fiber optic, spectrophotometer; the upper spectrum is a photoacoustic spectrum of 1.11 x 10^{-5} M PuO_2^+ in 0.1 M $HClO_4$ measured using the spectrometer described herein with the laser dye C540.

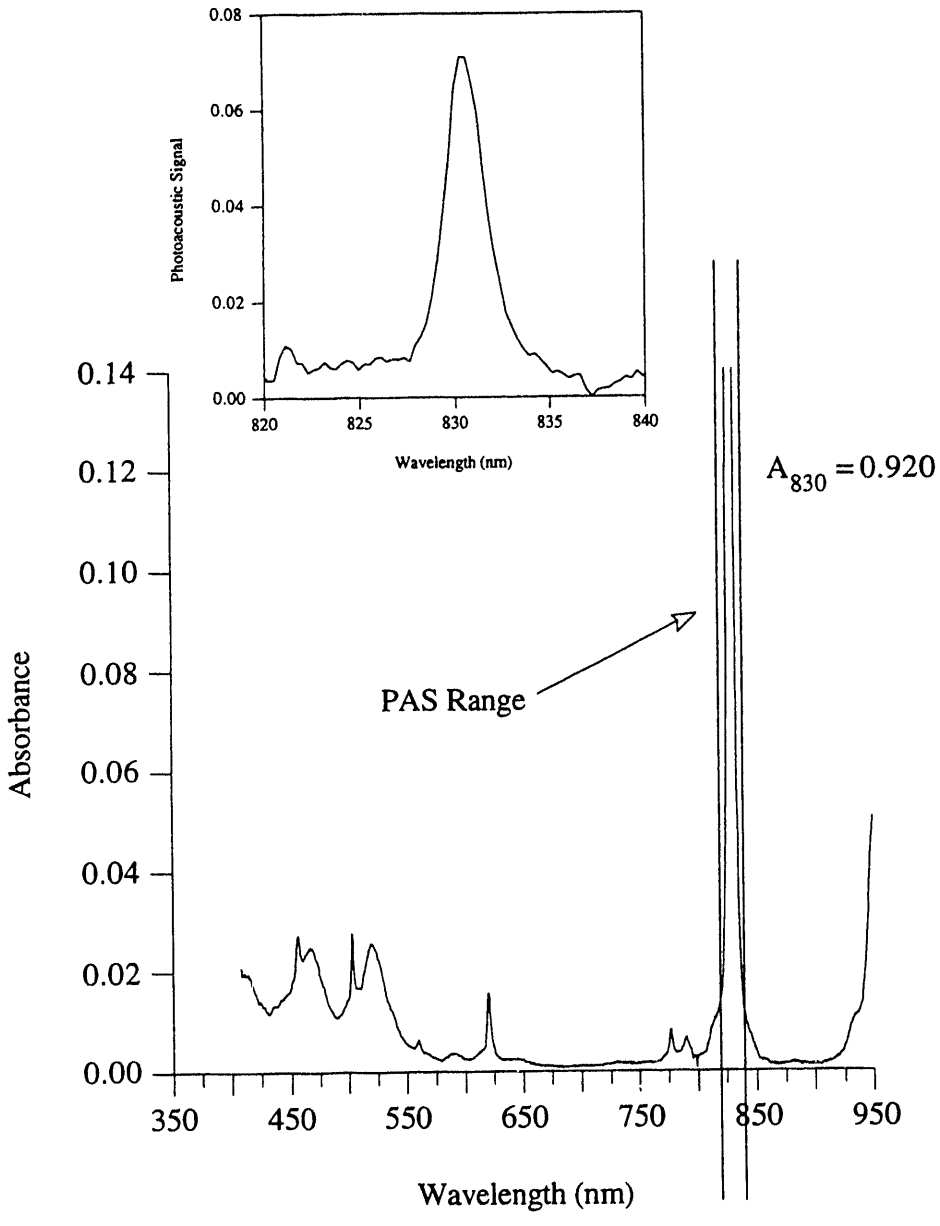

Figure 40. Absorbance spectra of PuO_2^{2+}: the bottom spectrum is a conventional absorbance spectrum of 2.43 x 10^{-3} M PuO_2^{2+} in 0.1 M $HClO_4$ measured using a Guided Wave, fiber optic, spectrophotometer; the upper spectrum is a photoacoustic spectrum of 1.45 x 10^{-6} M PuO_2^{2+} in 0.1 M $HClO_4$ measured using the spectrometer described herein with the laser dye LDS821.

Plutonium(IV) Solubility and Speciation

Plutonium(IV) rapidly precipitates under the conditions studied, as illustrated by the solubility curve shown in Figure 50. The plutonium precipitated rapidly, dropping from the initial concentration of 4.75 x 10^{-5} M to a solution concentration of 4.1(6) x 10^{-8} M after 6 days, then appeared to be resolubilized over the next 5 days. Uncertainty in the solubility measurements are due largely to errors incurred when a single aliquot of the experimental solution is used to determine the solution concentration. An estimate for this error, 10%, was obtained by measuring the concentrations of replicate samples of the Pu^{4+} experimental solution using LSC. Points defining the solubility curves are plotted with 15% error bars reflecting the sampling error and smaller errors propagating from standard solution concentrations and counting uncertainties.

The concentration of soluble plutonium at the end of the experiment, after 22 days, was 1.0(3) x 10^{-6} M. Spectroscopic identification and quantification of the soluble species was not possible at this low concentration. Photoacoustic spectra measured in the range 455-485 nm in the first week of the experiment showed a very large absorbance over the entire range, which was highest at the lower wavelength, and decreased almost linearly with higher wavelength over the range investigated. These very intense photoacoustic signals and high absorbance values are consistent with, but not definitive for, $Pu(IV)_p$ formation. After 10 days, photoacoustic spectra measured in the ranges 455-485 nm and 540-590 nm were indistinguishable from blank solutions; therefore the concentration of the free ions Pu^{4+} (λ_{max} = 470 nm) and PuO_2^+ (λ_{max} = 569 nm) were below the detection limits of approximately 5 x 10^{-7} M and 5 x 10^{-6} M, respectively. A green, moss-like, precipitate was observed in the Teflon solution cell, but was not characterized.

The short duration of the Pu^{4+} experiment was due to rapid use of the experimental solution. The conventional 3.5 mL, 1 cm square cuvette initially used for PAS measurements necessitated the use of relativly large volumes of the solution for each measurement. The cuvette, PZT assembly, and optical components in the glove box were replaced with a 1.4 mL thick-walled cuvette, associated optical components, and PZT detector assembly, which were used for all of the PuO_2^+ and PuO_2^{2+} experiments.

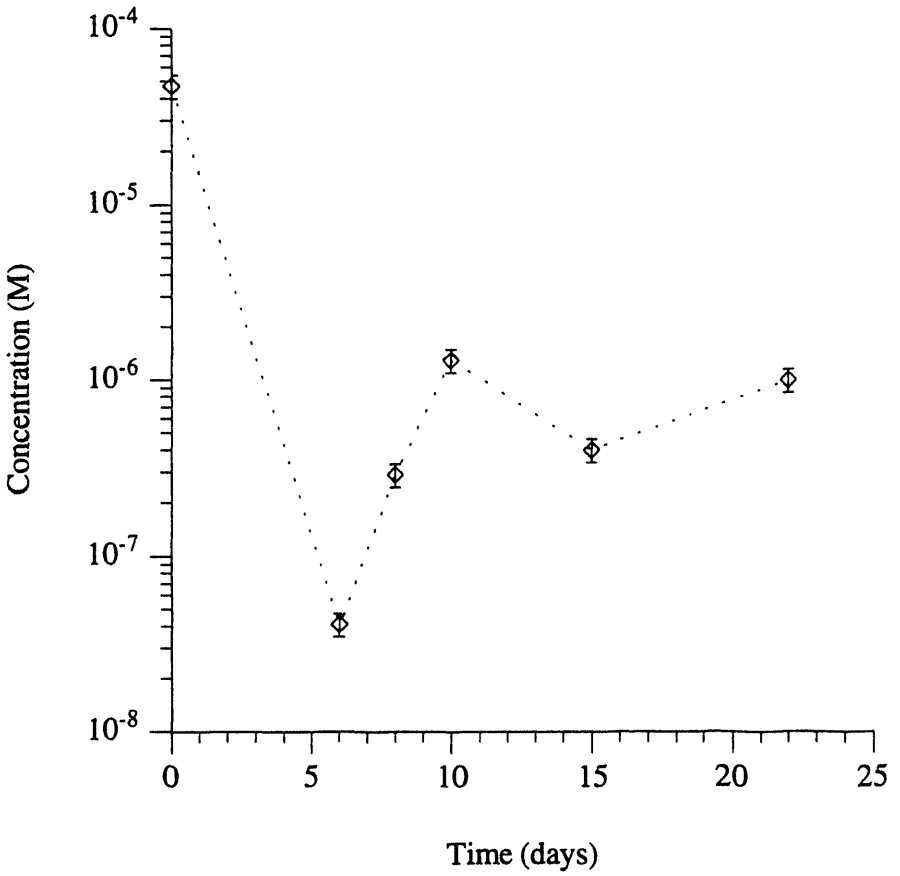

Figure 41. The solubility curve obtained for Pu^{4+}, with an initial concentration of 4.75 x 10^{-5} M, and maintained at 1.93 mM total carbonate , pH = 6.0(1), T = 30.0(2)°C.

Plutonium(V) Solubility and Speciation

A plutonium(V) solution, with an initial concentration of 2.51 x 10^{-5} M had a soluble plutonium concentration of 2.1(1) x 10^{-5} M after 53 days. Both the solubility curve, shown in Figure 42, and photoacoustic spectra measured at several times during the experiment, shown in Figure 43, indicate that changes in the soluble fraction were minimal. At the end of the experiment, the soluble plutonium was determined to be 95 ±5% PuO_2^+ from spectroscopic analysis using PuO_2^+ standards. Photoacoustic spectra of the experimental solution filtrate and PuO_2^+ standard solutions, and a linear regression curve of the 569 nm peak heights are shown in Figure 44.

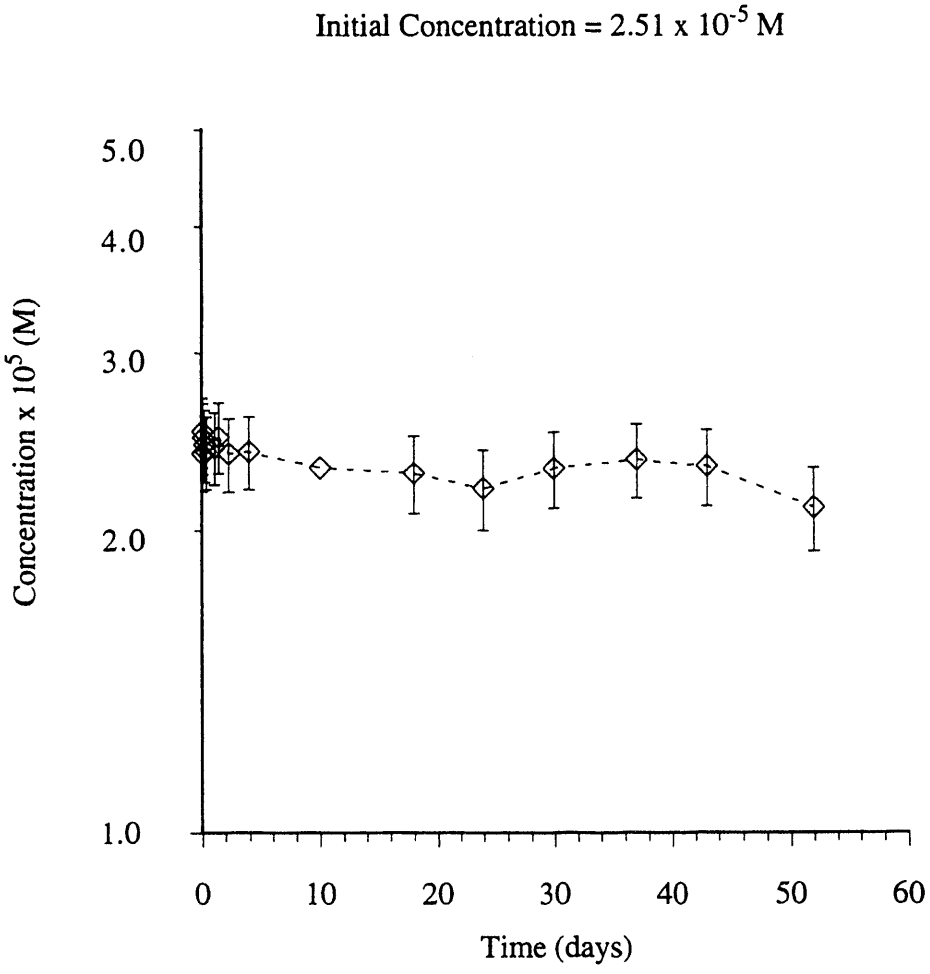

Figure 42. The solubility curve obtained for a PuO_2^+ solution, with an initial concentration of 2.51 x 10^{-5} M, and maintained at 1.93 mM total carbonate solution, pH = 6.0(1), T = 30.0(2)°C.

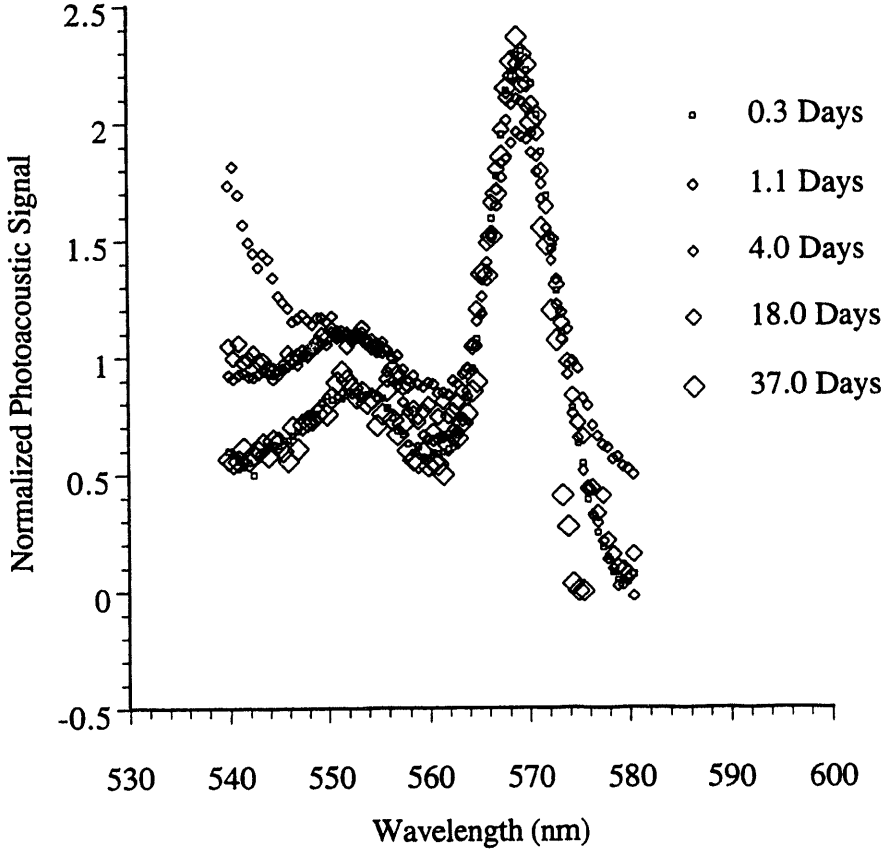

Figure 43. Photoacoustic spectra measured during the PuO_2^+ solubility experiment, showing minimal changes in the PuO_2^+ absorbance band, centered at 569 nm, over the duration of the experiment.

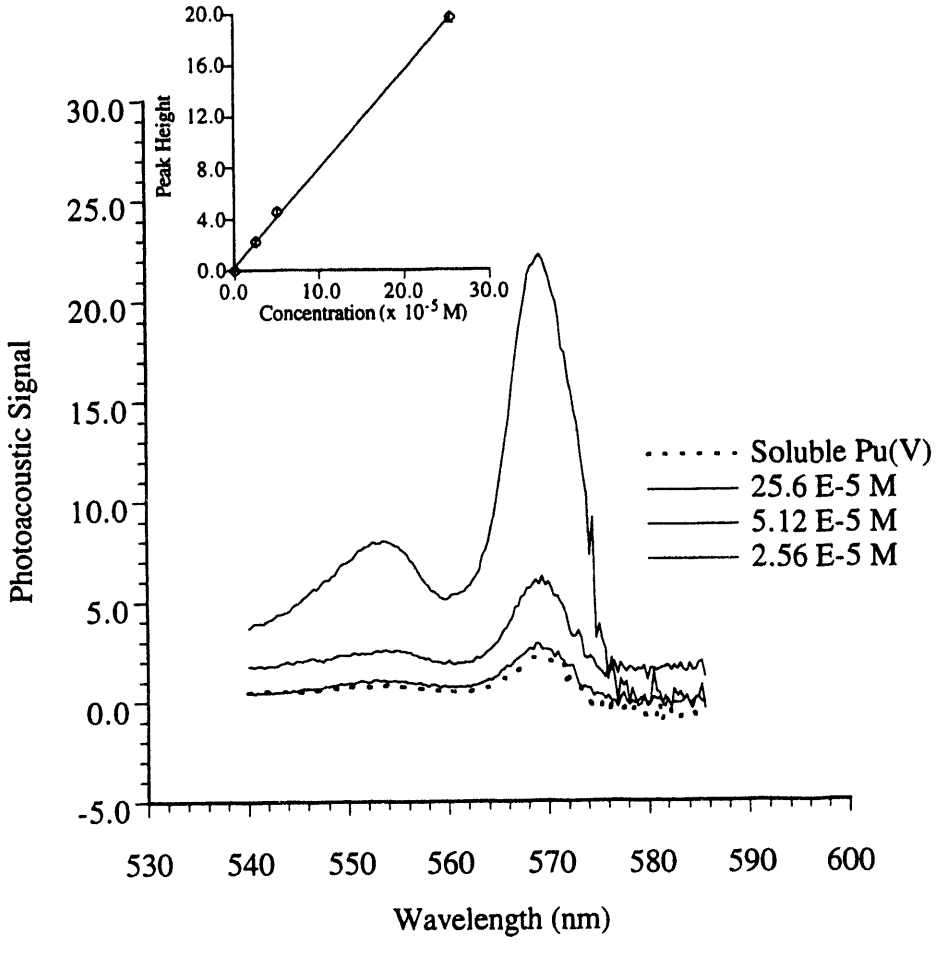

Figure 44. Photoacoustic spectra of the PuO_2^+ solution filtrate and PuO_2^+ standard solutions measured at the end of the solubility experiment (after 52 days) and the linear regression curve of 569 nm peak heights.

Because the solution filtrate was determined to be 95 ± 5% PuO_2^+, there may be another species present at a concentration of up to 2.2 x 10^{-6} M. Absorbance spectra in the wavelength ranges 605-680 nm and 810-845 nm were measured to search for evidence of soluble PuO_2^{2+} and/or PuO_2^{2+} hydrolysis products. The photoacoustic spectra of the soluble fraction, shown in Figures 45 and 46, contained an absorbance band at approximately 661 nm, but no discernable peaks in the longer wavelength range, 810-845 nm. (Aqueous PuO_2^{2+} solution spectra contain absorbance bands at 622 and 830 nm for the solvated ion, which typically shift upon complexation. The detection limits for plutonium(VI) species based on absorbance bands in the 810-845 nm region are typically lower than at lower wavelengths, due to the strong absorbance of water.) The absorbance band at approximately 661 nm was not useful for quantitative analysis due to its ill-defined shape and unknown identity. Okajima, Reed, and coworkers,[40] in their determination of plutonyl hydrolysis constants using a 2.6 x 10^{-4} M PuO_2^{2+} solution, reported absorbance bands centered at 622 nm and 632 nm when the pH was 4.6 and 4.9, which they identified as corresponding to the free ion and the hydrolysis product PuO_2OH^+, respectively, and an unassigned band at 638 nm when the pH was 6.0. However, these researchers and others[41] report significant changes in the solution spectra depending on the plutonium concentration, age of solution, and pH, thus the species corresponding to the band at 661 nm may, or may not, be the same as the species Okajima et al. observed with an absorbance maximum at 638 nm.

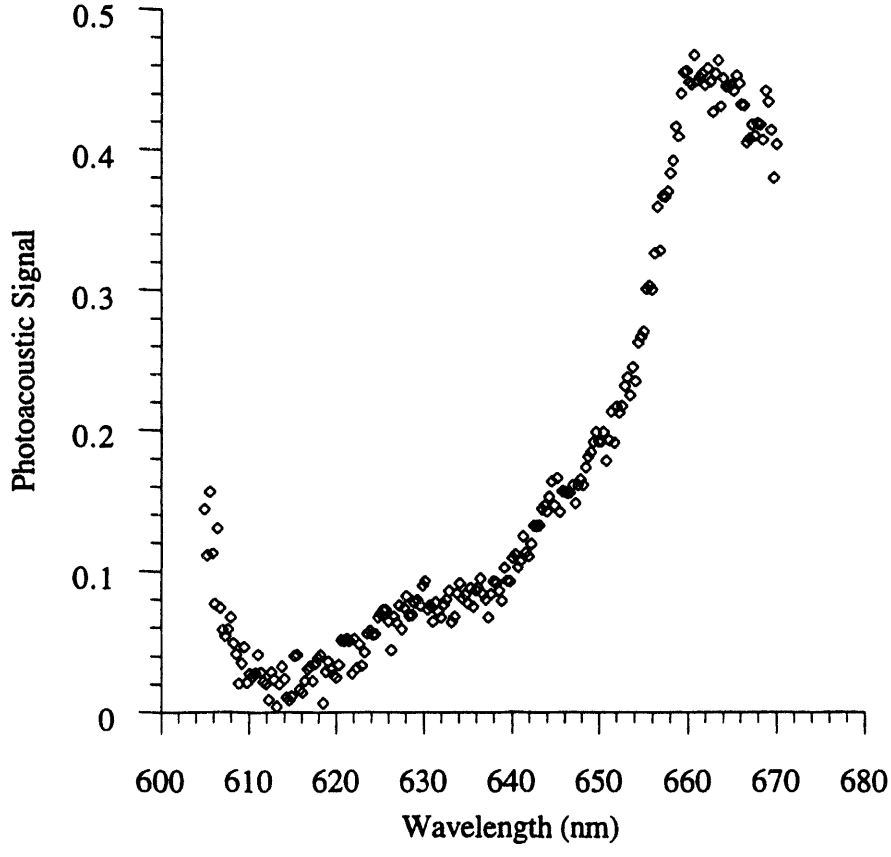

Figure 45. Photoacoustic spectra of the mostly PuO_2^+ solution filtrate measured at the end of the PuO_2^+ solubility experiment (after 52 days) containing an absorbance band which may correspond to a PuO_2^{2+} species.

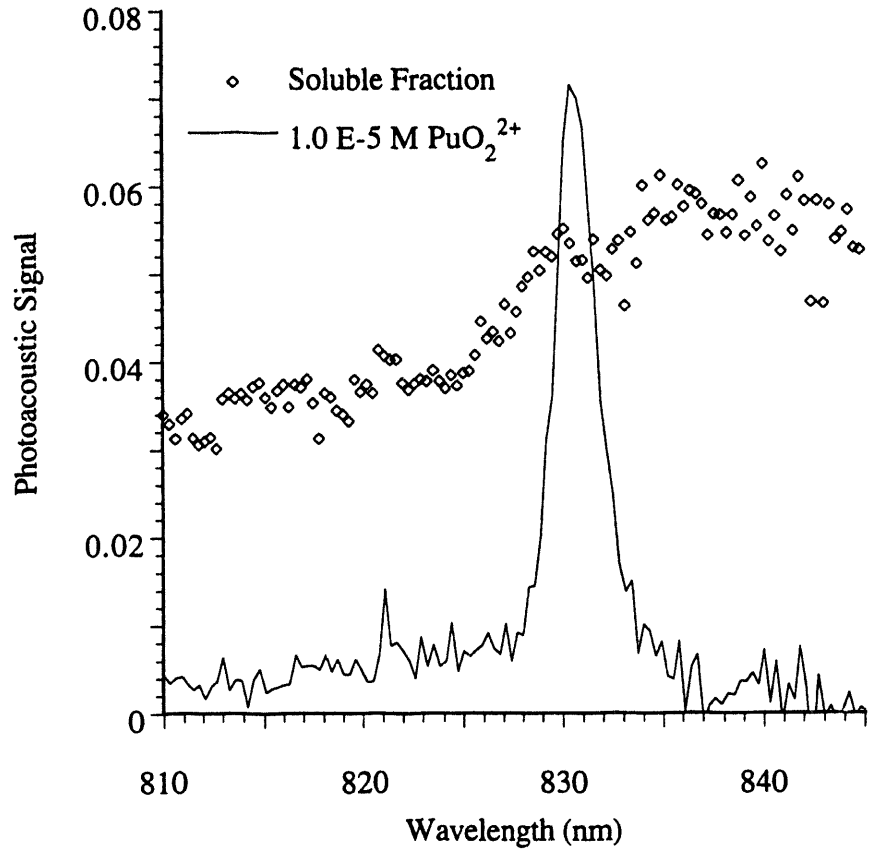

Figure 46. Photoacoustic spectra of the PuO_2^+ solution filtrate (diamonds), measured at the end of the solubility experiment (after 52 days) and, for comparison, a 1.0 x 10^{-5} M PuO_2^{2+} (solid line), showing the characteristic absorbance band at 831 nm.

Plutonium(VI) Solubility and Speciation

Three separate PuO_2^{2+} solubility experiments were conducted with the initial concentrations of 1.86, 2.40, and 3.68 x 10^{-4} M. The solubility curves obtained for the separate experiments are shown in Figure 56.

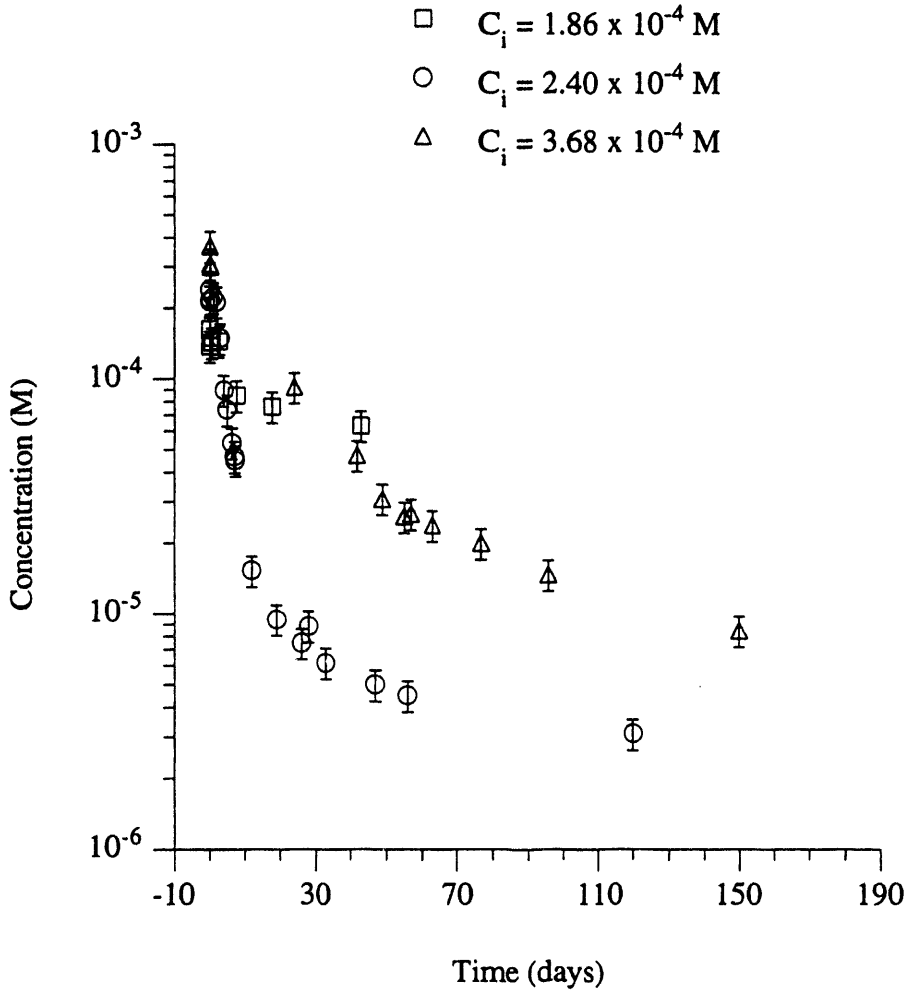

Figure 56. Solubility curves obtained for initially pure PuO_2^{2+} solutions, which had initial concentrations (C_i) of 1.86, 3.68, and 2.40 x 10^{-4} M, and maintained at 1.93 mM total carbonate, pH = 6.0(1), T = 30.0(2)°C.

Plutonium(VI) Solubility and Speciation Experiment 1. The speciation behavior of the soluble plutonium in the solution which was initially 1.86 x 10^{-4} M PuO_2^{2+} was monitored for 43 days. The concentration of soluble plutonium was measured to be 6.3(9) x 10^{-5} M, or 34% of the plutonium initially added to the solution, at the end of the experiment.

A photoacoustic spectrum from 815 to 840 nm measured at 2 hours contained a weak band at 831 nm, presumably corresponding to the small amount of free PuO_2^{2+}. A photoacoustic spectrum of the soluble fraction, from 815 to 840 nm, measured 18 hours after the plutonium was added to the preequilibrated carbonate solution is shown in Figure 48. The characteristic absorbance band for aqueous PuO_2^{2+} at 831 nm was not present, but there is an absorbance band centered at a higher wavelength (determined to be centered at 840.8 nm in a separate experiment). The absorbance band probably corresponds to a PuO_2^{2+}/hydroxide species based on the plutonyl hydrolysis behavior,[31,40,41], and oxidation state distribution measurements presented later in this section. Photoacoustic spectra, in the region 555-580 nm, measured during the experiment to determine the concentration of PuO_2^{+} present are shown in Figure 49 The solubility curve for the plutonium solution and the concentrations of PuO_2^{+} in the solution calculated from the photoacoustic spectra are shown in Figure 50. The percentage of soluble plutonium which was PuO_2^{+} varied from 58% at 18 hours to 100% at 17 days, and 87% after 43 days (Table 22). In an attempt to indentify the other species present a conventional spectrum was measured over the wavelength range, 500 to 900 nm. Because the absorbance values are so low, it is impossible to extrapolate meaningful speciation information from the spectrum, shown in Figure 51; however, three absorbance bands are suggested in the spectrum at approximately 570, 770, and 835 nm.

Table 22. Fraction of Soluble Plutonium Which was PuO_2^{+} in a Solution Initially 1.86 x 10^{-4} M PuO_2^{2+}, 0.100 M $NaClO_4$, Maintained at pH = 6.0(1), T = 30.0(2), P_{CO_2} = 5.71%

Time (days)	Fraction PuO_2^{+} (%)
0.75	58
2.75	68
7.75	100
17.75	82
43.0	87

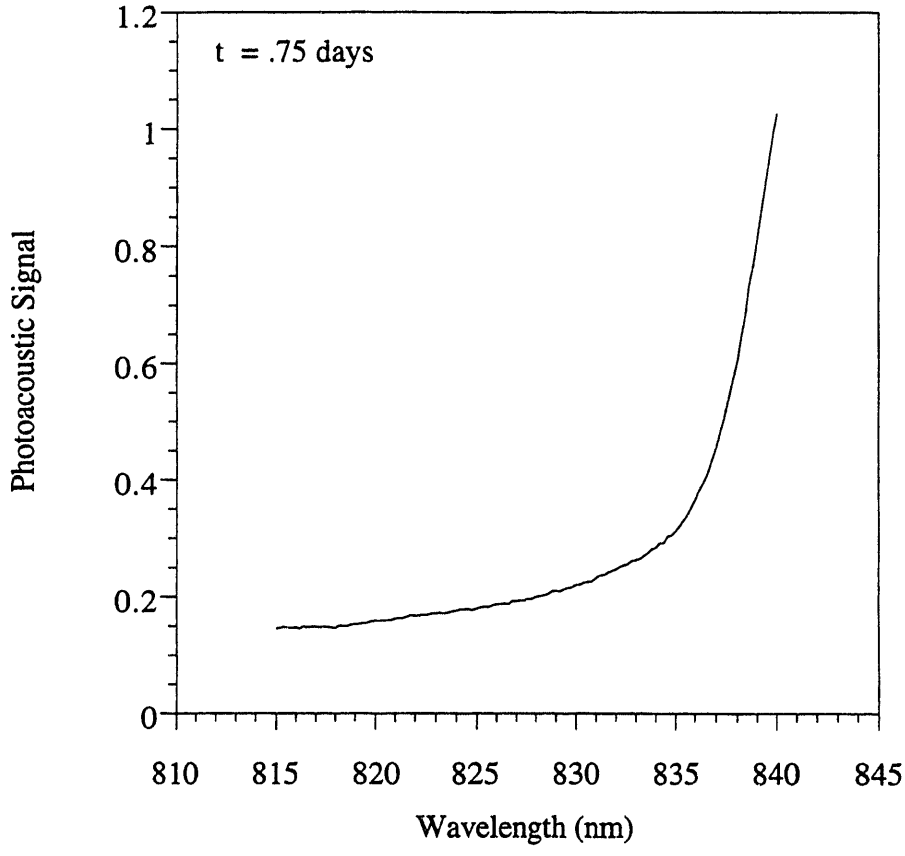

Figure 48. A photoacoustic spectrum of the soluble fraction of a plutonium solution, initially 1.86 x 10^{-4} M PuO_2^{2+}, and maintained with 1.93 mM total carbonate at pH = 6.0(1), T = 30.0(2)°C, measured after 18 hours.

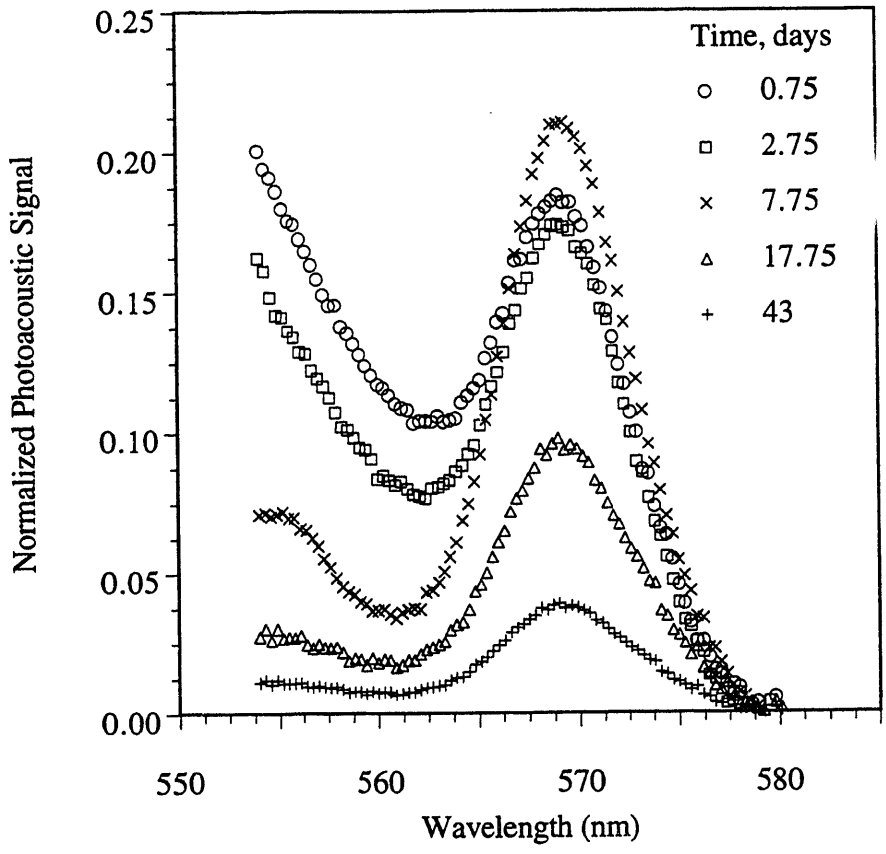

Figure 49. Photoacoustic spectra of the soluble fraction of a plutonium solution, initially 1.86 x 10^{-4} M PuO_2^{2+}, and maintained with 1.93 mM total carbonate at pH = 6.0(1), T = 30.0(2)°C, showing the change in the absorbance band, corresponding to PuO_2^{+}, as a function of time.

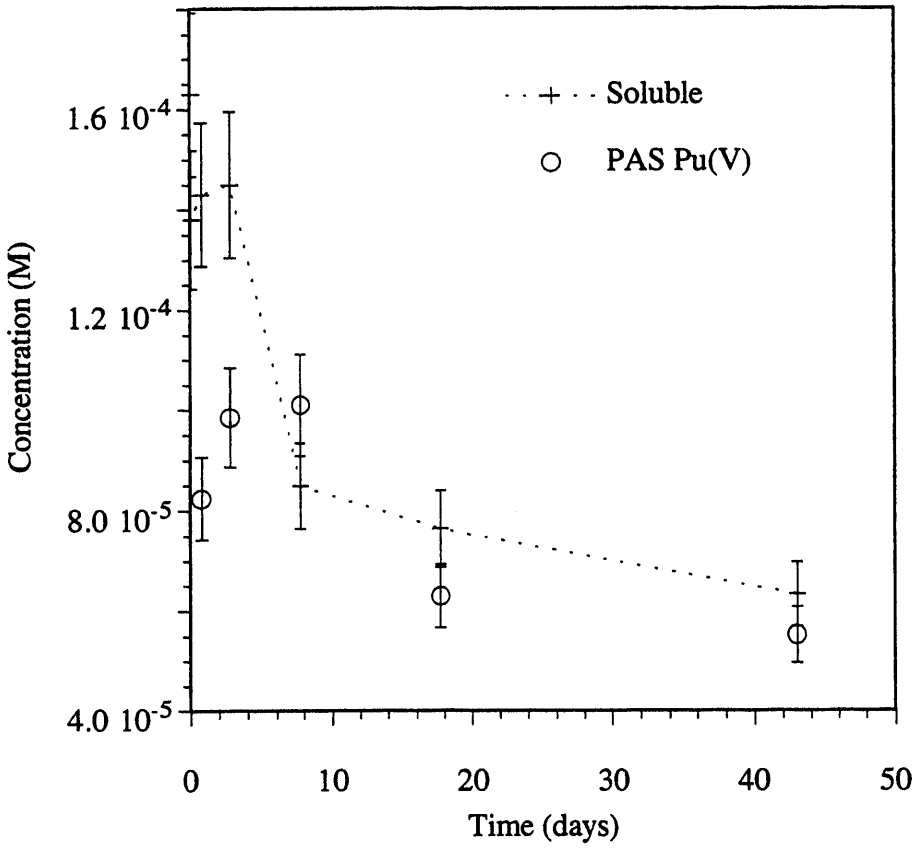

Figure 50. The solubility curve obtained for a plutonium solution initially 1.86 x 10^{-4} M PuO_2^{2+} (+ with dashed line), and the concentrations of PuO_2^{+} (circles) in the solution calculated from the photoacoustic spectra shown in Figure 49.

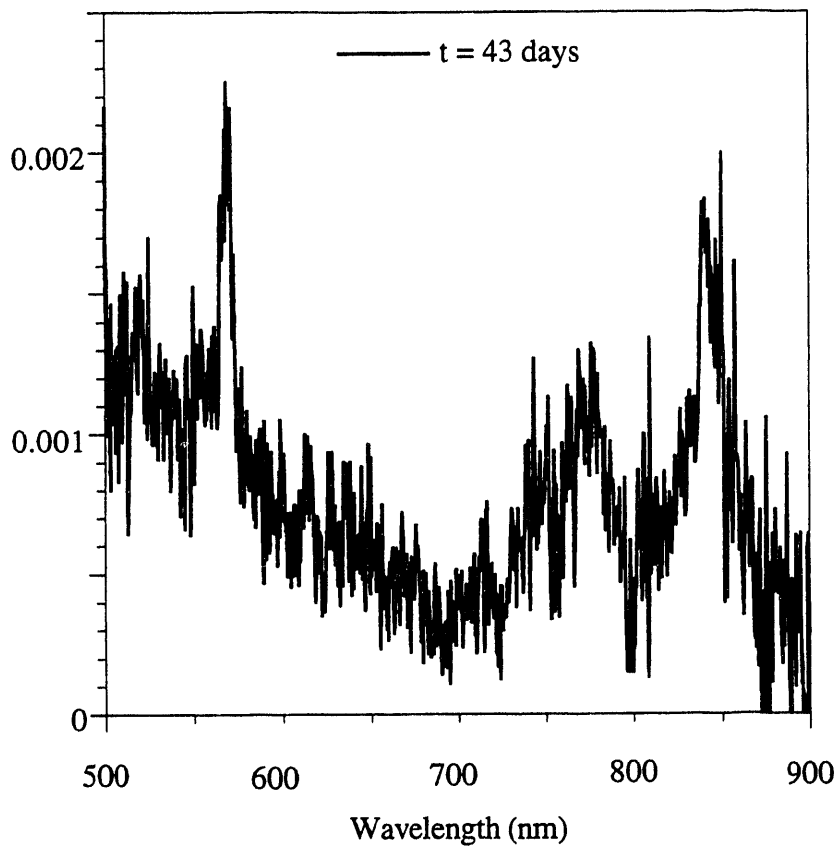

Figure 51. A conventional absorbance spectrum of the soluble fraction of a plutonium solution, initially 1.86 x 10^{-4} M PuO_2^{2+}, and maintained at 1.93 mM total carbonate, pH = 6.0(1), T = 30.0(2)°C for 43 days.

Plutonium(VI) Solubility and Speciation Experiment 2. The solubility and speciation behavior of the solution which was initially 3.68 x 10^{-4} M PuO_2^{2+} was monitored for 150 days. The concentration of soluble plutonium at the end of the experiment was measured to be 8.5(1.3) x 10^{-6} M, or 2.3% of the plutonium initially added to the solution, at the end of the experiment.

Conventional absorbance spectra of the soluble fraction were measured after 7 hours and 24 days; these spectra are shown in Figure 52. In the spectrum measured at 7 hours, there are several bands, the strongest of which is centered at 840.8 nm. The soluble fraction was determined to be 84%, or 2.5 x 10^{-4} M, Pu(VI) at this point in the solubility/speciation study from chemical extraction experiments. Note that Pu(VI) refers to plutonium in the +6 oxidation state, not necessarily the single species PuO_2^{2+}, or $PuO_2(OH)^+$. If the absorbance band centered at 840.8 nm (A = 0.072 Abs.) is assumed to correspond to a single mononuclear species, the molar absorptivity of this species is approximately 284 Abs.*$cm^{-1}M^{-1}$. Using this molar absorptivity for the Pu(VI) species, the concentration was determined to be 2.6 x 10^{-6} M, or 84% of the soluble plutonium. The spectrum measured after 24 days shows the band at 840.8 nm has decreased in intensity to approximately 0.001 Abs.. There is also an absorbance band with roughly the same intensity at 569 nm, corresponding to PuO_2^+.

Photoacoustic spectra in the spectral region 555-580 nm, shown in Figure 53, measured during the experiment allowed for the determination of the PuO_2^+ concentration at several times. The percentage of soluble plutonium which was PuO_2^+ was: 14% at 7 hours, 75% at 24 days, and 93-100% on days 57, 63, 77, and 96 (Table 23).

Table 23. Fraction of Soluble Plutonium Which was PuO_2^+ and a Pu(VI) Species in a Solution Initially 3.68 x 10^{-4} M PuO_2^{2+}, 0.100 M $NaClO_4$, Maintained at pH = 6.0(1), T = 30.0(2), P_{CO_2} = 5.71%.

Time (days)	Fraction PuO_2^+ (%)	Fraction Pu(VI) (%)
0.30	14	84
24.0	75	not determined
57.0	95	"
63.0	100	"
77.0	93	"
96.0	100	"

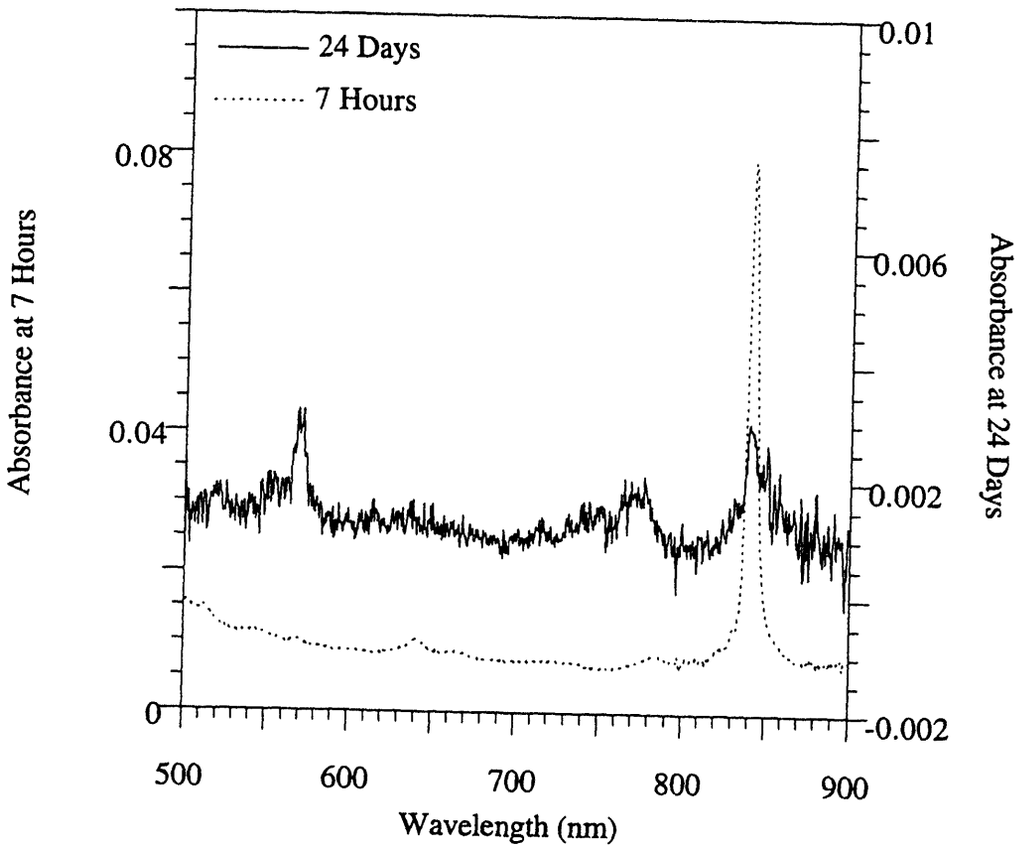

Figure 52. Conventional absorbance spectra of the soluble fraction of a plutonium solution, initially 3.68 x 10^{-4} M PuO_2^{2+}, maintained at 1.93 mM total carbonate, pH = 6.0(1), T = 30.0(2)°C.

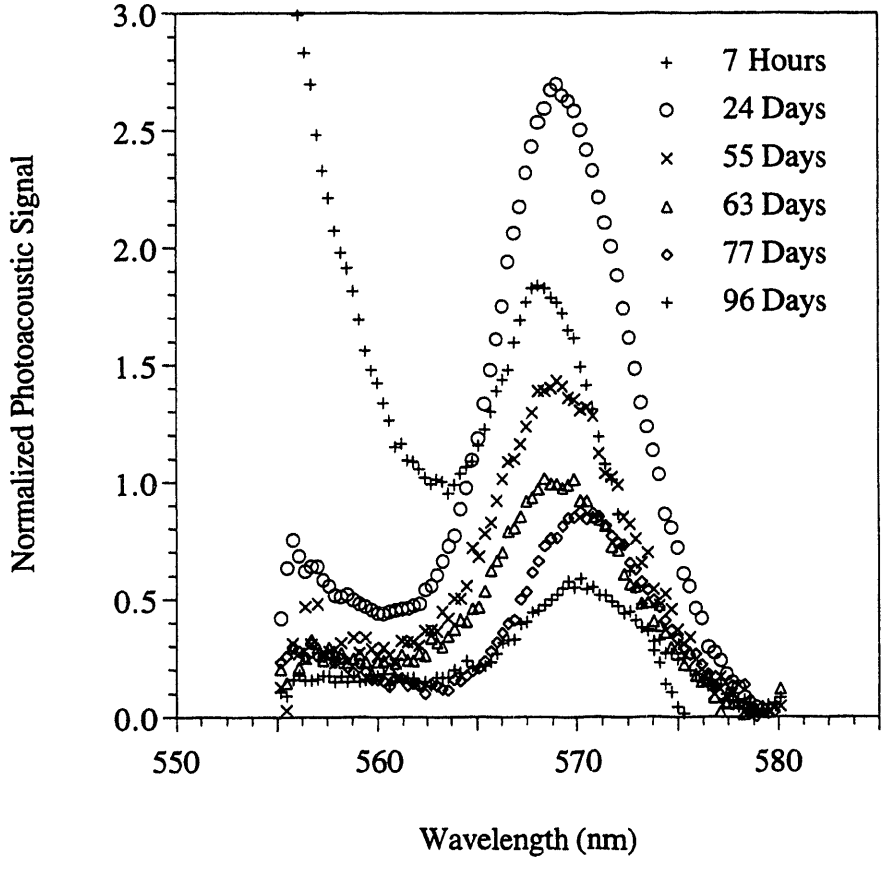

Figure 53. Photoacoustic spectra of the soluble fraction of a plutonium solution, initially 3.68 x 10^{-4} M PuO_2^{2+}, maintained at 1.93 mM total carbonate, pH = 6.0(1), T = 30.0(2)°C, showing the change in the absorbance band corresponding to PuO_2^{+} as a function of time.

Plutonium(VI) Solubility and Speciation Experiment 3. The speciation behavior of the soluble plutonium in the solution which was initially 2.40 x 10^{-4} M PuO_2^{2+} was monitored for 120 days. The concentration of soluble plutonium at the end of the experiment was measured to be 3.1(5) x 10^{-6} M, or 1.3% of the plutonium initially added to the solution, at the end of the experiment.

Conventional absorption spectra of the solution filtrate were measured during the first week of the experiment to monitor the disappearance of the band with a maximum at 840.8 nm. These spectra, along with a plot showing the change in the height of the peak at 840.8 nm, are shown in Figure 54. The concentration of soluble Pu(VI) was calculated using the absorbance values at 840.8 nm, as described above for the PuO_2^{2+} experiment 2. Using conventional spectral data, the concentration of soluble Pu(VI) was determined to decrease slightly in the first two days, from 1.8 x 10^{-4} to 1.6 x 10^{-4} M, and accounted for 84 to 75% of the total soluble plutonium. On days 3,4, and 5 the Pu(VI) concentration accounted for 63, 43, and 28%, of the soluble plutonium, respectively, and decreased from 9.3 to 2.0 x 10^{-5} M. Photoacoustic spectra, in the spectral region 830-870 nm, measured after 7 and 24 days are shown in Figure 55. The concentration of soluble Pu(VI) was calculated to be 1.2 x 10^{-5} M at 7 days, accounting for 26% of the soluble plutonium; at 28 days there was no peak corresponding to the Pu(VI) species.

Photoacoustic spectra, in the region 555-580 nm measured to determine the concentration of PuO_2^{+} present are shown in Figure 56. The concentration of PuO_2^{+} increased during the first day of the experiment and decreased over the first 66 days from 6.0 x 10^{-5} to 4.5 x 10^{-6} M. On the first day of the experiment PuO_2^{+} accounted for approximately 23% of the soluble plutonium; on days 6 and 7 the fraction of soluble plutonium which was PuO_2^{+} was 76 and 77%, respectively. The solubility curve for this experiment, including concentrations of species thought to be present, is shown Figure 57. The speciation over the duration of the experiment is summarized in Table 24.

Table 24. Fraction of Soluble Plutonium Which was PuO_2^+ and a Pu(VI) Species in a Solution Initially 2.40 x 10^{-4} M PuO_2^{2+}, 0.100 M $NaClO_4$, Maintained at pH = 6.0(1), T = 30.0(2), P_{CO_2} = 5.71%.

Time (days)	Fraction PuO_2^+ (%)	Fraction Pu(VI) (%)
0.04		84
0.08		80
0.17	28	79
1.00	23	76
2.00		77
3.10		63
4.10		43
5.00		28
6.30	67	
7.00	63	26
28.00	100	
33.00	100	
47.00	100	
66.00	100	

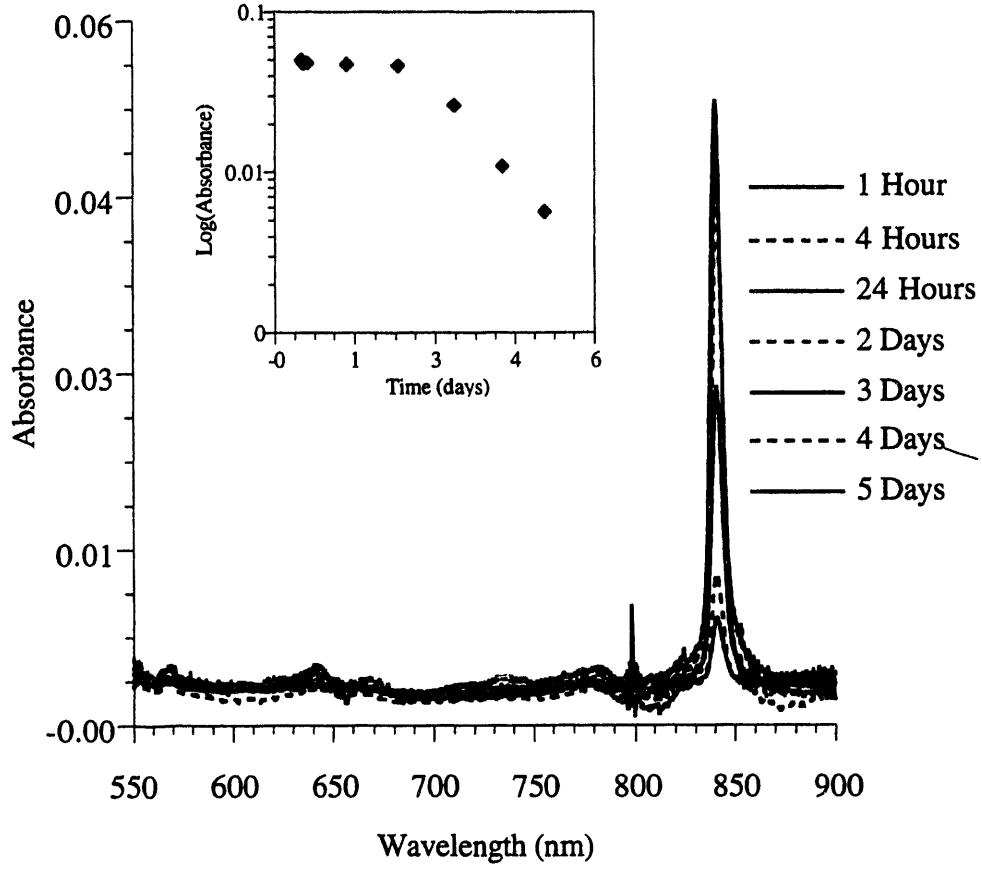

Figure 63. Conventional absorbance spectra of the soluble fraction of a plutonium solution, initially 2.40 x 10^{-4} M PuO_2^{2+}, maintained at 1.93 mM total carbonate, pH = 6.0(1), T = 30.0(2)°C. The plot in the upper left shows the decrease in intensity of the absorbance band at 840.8 nm, proposed to correspond to a PuO_2^{2+} hydrolysis product.

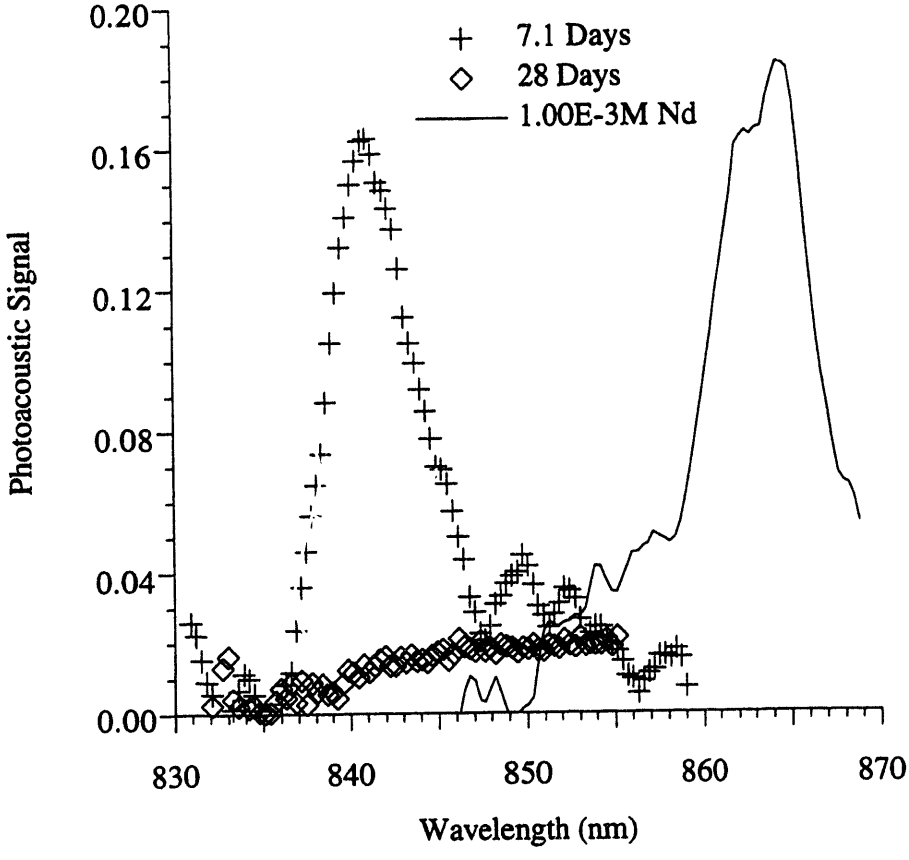

Figure 64. Photoacoustic spectra of the soluble fraction of a plutonium solution, initially 2.40 x 10^{-4} M PuO_2^{2+}, maintained at 1.93 mM total carbonate, pH = 6.0(1), T = 30.0(2)°C, showing the change in the absorbance band at 840.8 nm, as a function of time. Included in the figure is a spectrum of a 1.00 x 10^{-3} M Nd^{3+}, 1.0 M perchloric acid solution used as a standard.

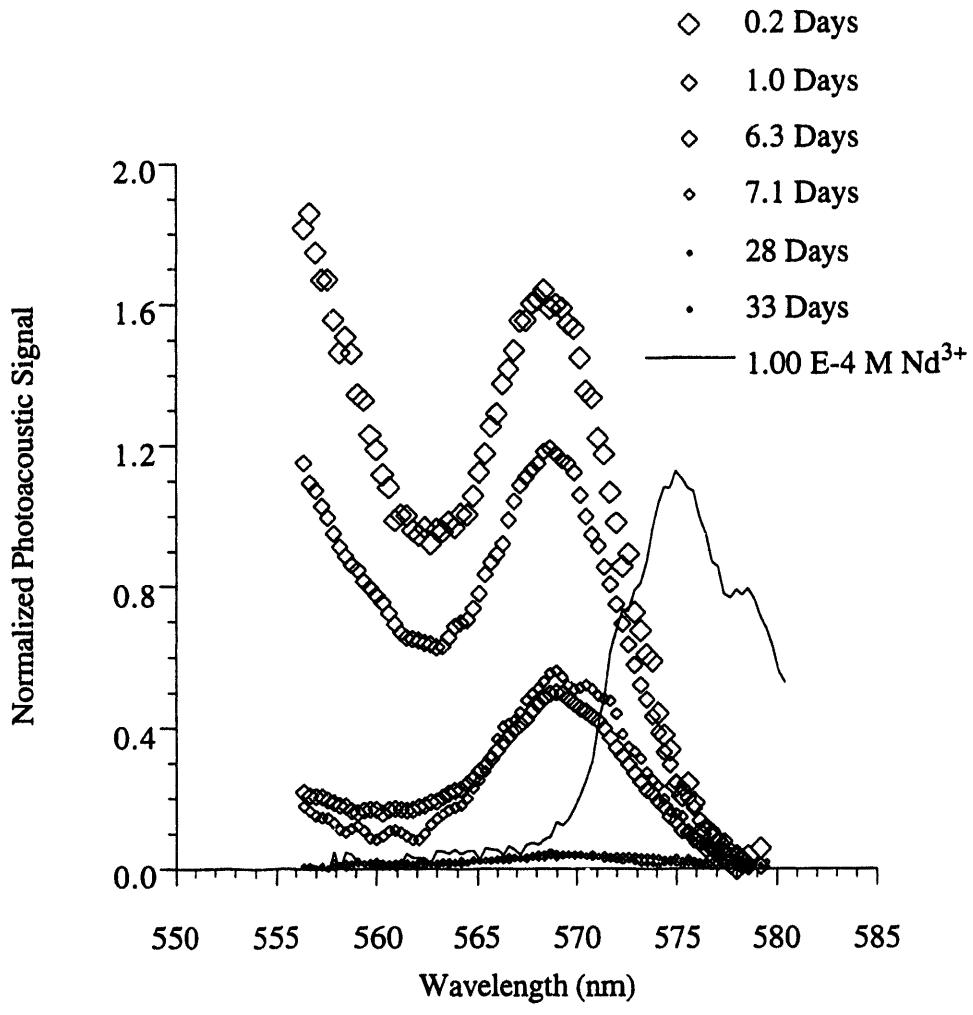

Figure 65. Photoacoustic spectra of the soluble fraction of a plutonium solution, initially 2.40 x 10^{-4} M PuO_2^{2+}, maintained at 1.93 mM total carbonate, pH = 6.0(1), T = 30.0(2)°C, showing the change in the absorbance band corresponding to PuO_2^{+} as a function of time. Included in the figure is a spectrum of a 1.00 x 10^{-4} M Nd^{3+}, 1.0 M perchloric acid solution used as a standard.

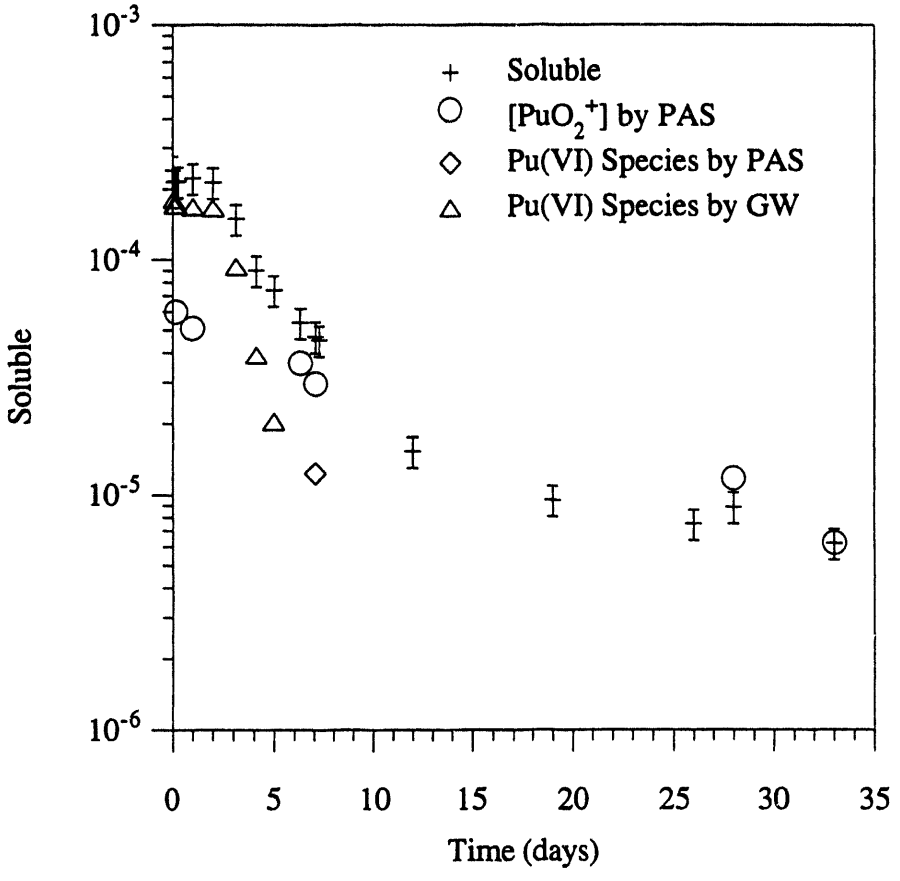

Figure 66. The solubility curve obtained for a plutonium solution initially 2.40 x 10^{-4} M PuO_2^{2+} (+), and the concentrations of PuO_2^{+} (circles) in the solution calculated from the photoacoustic spectra shown in Figure 65. The other points marked correspond to the concentration of a Pu(VI) species calculated from photoacoustic spectra (diamonds) and conventional spectra measured using a Guided Wave spectrophotometer (triangles), assuming the band corresponds to a single mononuclear species.

Plutonium Oxidation State Distributions Determined Using Chemical Extractions

The distribution of soluble plutonium among the stable oxidation states was determined using the extracting agents, HDEHP (di-(2-ethylhexyl)-orthophosphoric acid), PMBP (4-benzoyl-3-methyl-1-phenyl-2-pyrazolin-5-one), and TTA (thenoyltri-floroacetone). For a solution, initially 2.52 x 10^{-5} M PuO_2^+, oxidation state distributions were determined three separate times, twice on day 52 of the solubility experiment, and a third time, one day later. The results calculated from the chemical extraction data are listed in Table 25.

Table 25. Results From Three Separate Oxidation State Determinations for a Solution Which was Initially 2.52 x 10^{-5} M PuO_2^+, and Had a Concentration of Total Soluble Plutonium of 2.1 x 10^{-5} M at the When the Extractions Were Performed.

Oxidation State	Relative Amount (in percent)		
	First Determination	Second Determination	Third Determination
Pu(III)	1.11	1.22	0.84
Pu(IV)	0.38	0.71	0.61
Pu(V)	95.34	89.92	95.30
Pu(VI)	2.95	8.07	3.12
Pu(IV)-polymer (< 4.1 nm)	0.22	0.18	0.14

Essentially no solid plutonium material remained after the initial phase separation--the relative amount of Pu(IV)-polymer found was no more than 0.2 percent. The primary species present in solution is Pu(V), accounting for 95 percent of the soluble plutonium. The second most abundant oxidation state is Pu(VI), at a fraction of approximately three percent. Both Pu(III) and Pu(IV) are present in insignificant amounts. The second determination showed slightly different results for the relative amounts of Pu(V) and Pu(VI), even though only two hours passed between the first and the second sets of oxidation state determinations. Twenty-four hours passed before the third analysis was performed, and the results from the last determination are virtually identical to those obtained from the first analysis. The small difference between the first two sets of determinations may be due to disruption of the solution equilibrium caused by opening the reaction vessel for sampling. The short time between the first two determinations was probably not long enough to restore equilibrium in the system; however, by allowing the solution to stand over night, equilibrium was restored, and the oxidation state distribution returned to that found in the first determination.

From this set of experiments we conclude that plutonium oxidation states can be determined using the extraction methods at concentrations near 10^{-5} M with an error of about five percent.

On both days, a portion of the solution filtrate was immediately acidified and transferred to a scintillation vial to determine the total aqueous plutonium concentration. A standard solution prepared identically, whose concentration was verified by absorption spectrophotometry, was used as a counting standard to normalize the LS counting data. The samples from the two days provided the concentrations: 2.22×10^{-5} M and 2.18×10^{-5} M; yielding an average concentration of $2.20 \pm 0.02 \times 10^{-5}$ M. If 95% of the soluble plutonium is Pu(V), then the Pu(V) concentration is 2.1×10^{-5} M.; and at 3%, the Pu(VI) concentration is $\sim 7 \times 10^{-7}$ M.

Chemical extractions were performed on three other "solubility solutions" following the procedure decribed above. The results of all the chemical extraction oxidation state determinations are summarized in Table 26.

Table 26. Plutonium Oxidation State Distributions Determined for Plutonium Solubility Solutions Using a Combination of Chemical Extraction Methods.

Initial Species, Concentration (M)	Time Since Experiment Initiated	Distribution	Concentrations of Oxidation States (M)
PuO_2^+, 2.51 x 10^{-5}	52 days	Total Soluble	2.1(3) x 10^{-5}
		6	6(1) x 10^{-7} (3%)
		5	2.0(3) x 10^{-5} (95%)
		4	~1 x 10^{-7}
		3	~1 x 10^{-7}
		p	<1 x 10^{-8}
PuO_2^{2+}, 3.68 x 10^{-4}	7 hours	Total Soluble	3.1(3) x 10^{-4}
		6	2.6(3) x 10^{-4} (84%)
		5	4.7(5) x 10^{-5} (15%)
		4	~5 x 10^{-7}
		3	~4 x 10^{-7}
		p	<1 x 10^{-8}
PuO_2^{2+}, 2.42 x 10^{-4}	5 days	Total Soluble	7.4(3) x 10^{-5}
		6	5.1(3) x 10^{-5} (70%)
		5	2.3(3) x 10^{-5} (30%)
		4	<1 x 10^{-8}
		3	<1 x 10^{-8}
		p	<1 x 10^{-8}
PuO_2^{2+}, 2.42 x 10^{-4}	7 days, 2hrs.	Total Soluble	4.7(3) x 10^{-5}
		6	1.2(1) x 10^{-5} (75%)
		5	3.5(3) x 10^{-5} (25%)
		4	<1 x 10^{-8}
		3	<1 x 10^{-8}
		p	<1 x 10^{-8}

Comparison of Results: Photoacoustic Spectroscopy vs. Chemical Extractions

Chemical extractions and photoacoustic spectroscopy have compare favorably as methods of oxidation state distribution determination. Results obtained for the determination of PuO_2^+ in solutions initially containing only PuO_2^+ or only PuO_2^{2+} are summarized in Table 27. The two methods are in excellent agreement.

Results obtained for the determination of Pu(VI) in solutions initially containing only PuO_2^{2+} are summarized in Table 28. This comparison is marred by the uncertainty of the spectroscopic measurements which stems from the equivocal identitification and molar absorptivity of the solution species corresponding to the absorbance band centered at 840.8 nm. Given the uncertainty in the spectroscopic measurements, the concentrations determined using the two methods are in surprisingly good agreement. Two of the three determinations are identical, and one shows a difference of approximately 60%.

This study clearly show there are advantages to each analytical method. Valuable information about the speciation may be obtained using spectroscopy, which is not limited to oxidation state distribution. For example, PuO_2^{2+} and $PuO_2(OH)^+$ have significantly different absorption spectra, but behave equivalently in the extraction scheme. Predictions of the solution behavior, such as sorption proporties of the soluble plutonium will differ depending on which of the two species is thought to be present. However, at a miniumum, the number, identity, and molar absorptivities of the solution species must be known to allow for quantitative spectroscopic measurements. In addition, methods which rely on nuclear counting for detection (including the extraction procedure used) are far more sensitive than even the most sophisticated spectroscopic methods available.

Table 27. Results of Extractions and Photoacoustic Spectroscopy for the Determination of PuO_2^+

Original Plutonium Concentration (M)	Concentration of Soluble Plutonium (M)	Concentration of PuO_2^+ Chemical Extractions	Concentration of PuO_2^+ Photoacoustic Spectra
2.51×10^{-5}, PuO_2^+	$2.1(3) \times 10^{-5}$	$2.0(3) \times 10^{-5}$	$2.1(1) \times 10^{-5}$
2.42×10^{-4}, PuO_2^{2+}	$4.7(3) \times 10^{-5}$	$3.5(4) \times 10^{-5}$	$4.0(2) \times 10^{-5}$

Table 28. Results of Extractions and Photoacoustic Spectroscopy for the Determination of the Concentration of Soluble Pu(VI). (GW Refers to Data Collected Using a Conventional Spectrometer, and PAS Refers to Data Collected Using the Photoacoustic Spectrometer Described Herein.)

Original Plutonium Concentration (M)	Concentration of Soluble Plutonium (M)	Concentration of Pu(VI) Chemical Extractions	Concentration of Pu(VI) Spectroscopically*
3.68×10^{-4}, PuO_2^{2+}	$3.1(3) \times 10^{-4}$	$2.6(3) \times 10^{-4}$	$\sim 2.6 \times 10^{-4}$ (GW)
2.42×10^{-4}, PuO_2^{2+}	$7.4(3) \times 10^{-5}$	$5.1(3) \times 10^{-5}$	$\sim 2.0 \times 10^{-5}$ (GW)
2.42×10^{-4}, PuO_2^{2+}	$4.7(3) \times 10^{-5}$	$1.2(1) \times 10^{-5}$	$\sim 1.2 \times 10^{-5}$ (PAS)

The concentration of Pu(VI) was calculated using the absorbance at 840.8 nm, assuming a single mononuclear species, which has a molar absorptivity of 284 Abs.$cm^{-1}M^{-1}$. Because of these assumptions no errors are listed with the concentrations.

Conclusions Regarding Plutonium Solubility and Speciation

The uncomplexed ion, PuO_2^+, is the dominant species in solution a few days after 10^{-4} to 10^{-5} M plutonium(V) or plutonium(VI) is added to the near-neutral solution used to model a natural groundwater (pH = 6.0(1), T = 30.0(2), P_{CO_2} = 5.71%). Table 29 is a summary of the solubility and speciation behavior observed for five plutonium solutions.

When plutonium(IV) is introduced to the solution, the plutonium initially falls out of solution, dropping from 4.75×10^{-5} M to 4.1×10^{-8} M after 5 days, then resolubilizes over the next 5 days. The concentration of soluble plutonium after 22 days is 1.0×10^{-6} M. Due to the relatively low solubility, the soluble species were could not be identified using absorbance spectroscopy.

Plutonium(V) is stable in the solution and has a soluble concentration of $2.1(1) \times 10^{-5}$ M over a time of 53 days. The soluble plutonium is >95% PuO_2^+ based on photoacoustic spectroscopic data.

Plutonium(VI) shows the most interesting solution behavior, reflecting the equilibria involving soluble forms of both PuO_2^+ and PuO_2^{2+}, and quite possibly disproportionation reactions involving Pu^{4+}, which will precipitate as a polymeric hydroxide at pH = 6. The three solutions, which contained only PuO_2^{2+} initially, have slightly different solubility curves, but some trends are evident. The concentration of

soluble plutonium, drops exponentially over the first several days, and was measured to be ~5 x 10^{-5} M in two experiments, and ~1 x 10^{-5} M in one experiment, after several weeks. Photoacoustic spectra showed the soluble species were PuO_2^+ (λ_{max} = 569 nm) and a Pu(VI) species, probably $PuO_2(OH)^+$, (λ_{max} = 840.8 nm). PuO_2^+ is the dominant species in solution after a few days and is the only species present in significant amounts after a few weeks. The times at which PuO_2^+ becomes the major species in solution, and later essentially the only species in solution, depends on the initial concentration of PuO_2^{2+}. Quantification of plutonium(VI) (and the ratio of PuO_2^+/Pu(VI) based on the 840.8 nm spectral band is dependent on the molar absorptivity. If the absorbance band is assumed to correspond to a single mononuclear species and there is exactly one Pu(VI) species present, the molar absorptivity is ~284 Abs.(M*cm)$^{-1}$. Kim and Pashalidis[42] have also observed the absorbance band at 840.8 nm, and identified the species as $PuO_2(OH)^+$, with a molar absorptivity of 130 Abs.(M*cm)$^{-1}$, in a study where solid PuO_2CO_3 was dissolved in 0.1 M $NaClO_4$ under an argon atmosphere. They observed the $PuO_2(OH)^+$ species when the solution pH was 5.73, 6.24, and 7.1. (Absorbance bands corresponding to PuO_2^{2+} and $PuO_2(OH)_2$ were also present at 830.4 and 851 nm, respectively, with intensities varying as a function of pH.)

Table 29. Solubility and Speciation of Plutonium From Oversaturation in 0.100 M $NaClO_4$, pH = 6.0(1), T = 30.0(2), P_{CO_2} = 5.71%.

Initial Species, Concentration (M)	Duration of Experiment (days)	Concentration of Soluble Plutonium (M)	Fraction of PuO_2^+ as a Function of Time	
			(day)	(%)
Pu^{4+}, 4.75 x 10^{-5}	22	1.0(3) x 10^{-6}		none detected
PuO_2^+, 2.51 x 10^{-5}	52	2.1(1) x 10^{-5}	1-52	95-100
PuO_2^{2+}, 1.63 x 10^{-4}	43	6.3(9) x 10^{-5}	1, 3, 43	58, 68, 87
PuO_2^{2+}, 2.42 x 10^{-4}	120	3.1(5) x 10^{-6}	1, 24, 96	14, 75, 100
PuO_2^{2+}, 3.68 x 10^{-4}	150	8.5(1.3) x 10^{-6}	1, 7, 33	28, 63, 100

Clearly the criteria for "thermodynamically meaningful solubility studies" outlined in introduction were not met in this work because the solid phases were not defined or characterized, in addition the condition of true equilibrium is difficult to maintain. This research, especially the variability in the results of the three PuO_2^{2+} experiments, shows that solubility studies should be replicated and must be long term.

Results for the solubility and speciation of ^{242}Pu in the model for groundwater at pH 6.0, 30°C, with 1.93 mM total dissolved carbonate are compared with J-13 groundwater at pH = 7.0, 25°C, determined by Nitsche and Edelstein[7] in Table 30. Solubility levels for the initially Pu^{4+} and PuO_2^{2+} are in excellent agreement; the initially PuO_2^{+} solution had approximately twice the soluble plutonium as the J-13 groundwater. The results of the J-13 groundwater study indicated that regardless of the initial oxidation state, the only significant solution species present at steady state were PuO_2^{+} and PuO_2^{2+}, present at a 2:1 ratio, except in the initially Pu^{4+} experiment, where the ratio was 1:1; whereas PuO_2^{+} is clearly the only significant solution species present at steady state in the groundwater model solution. Differences between the two studies may be attributed to the differences in pH, plutonium isotopic compositions, and ionic compositions of the solutions, but the final oxidation state distributions were also measured using a different methods.

Table 30. Comparison of Plutonium Solubility and Speciation In Groundwater at pH = 7.0, 25°C, Determined by Nitsche and Edelstein[7] vs Groundwater Model Solution: 0.100 M $NaClO_4$, pH = 6.0(1), T = 30.0(2), P_{CO_2} = 5.71(6)%.

	J-13 Water, pH = 7.0		**Model Solution**, pH = 6.0	
Initial Species	Solubility (M), Time	Fraction Pu(V)	Solubility (M), Time	Fraction PuO_2^{+}
Pu^{4+}	$1.6 \pm 0.2 \times 10^{-6}$, 50 days	40 ± 5%	$1.0 \pm 0.3 \times 10^{-6}$, 22 days	not meas.
PuO_2^{+}	$8 \pm 3 \times 10^{-6}$, 48 days	68± 6%	$2.1 \pm 0.1 \times 10^{-5}$, 52 days	95 ± 5%
PuO_2^{2+}	$3 \pm 2 \times 10^{-5}$, 49 days	67± 6%	$9.2 \pm 1.5 \times 10^{-5}$, 24 days*	75 ± 5%
			$3.1 \pm 0.5 \times 10^{-5}$, 49 days	not meas.
			$8.5 \pm 1.3 \times 10^{-6}$, 150 days	100 ± 5%

*PuO_2^{2+} results listed are for the experiment where $C_i = 3.68 \times 10^{-4}$ M, which is most comparable to the J-13 study where $C_i = 3.9 \times 10^{-4}$ M.

Using a photoacoustic spectrometer which includes a dye laser to study solution behavior has some significant limitations. Among them are the narrow and specific spectral regions accessible using commercially available dyes, and the relatively long time between measurements in different regions necessitated by the changing of laser dyes and realignment of the optical components of the dye laser. The Spectra-Physics

company is developing a system, using a β-barium borate nonlinear crystal, which may soon serve as a solid-state replacement for the pulsed dye laser and allow measurement of spectra over several hundred nanometers.[43] This advancement would increase the amount of spectral data which could be obtained and reduce the time required for data acquisition, making speciation studies much more powerful.

References

(1) Patera, E. S.; Hobart, D. E.; Meijer, A.; Rundberg, R. S. *J. Radioanal. and Nucl.Chem., Articles* **1990**, *142(1)*, 331.

(2) Buddemeier, R. W.; Finkel, R. C.; Marsh, K. V.; Ruggieri, M. R.; Rego, J. H.; Silva, R. J. *Radiochim. Acta* **1991**, *52/53*, 275.

(3) The body of work in this area is extensive. The following reference is an actinide solubility study. Nitsche, H.; Müller, A.; Standifer, E. M.; Deinhammer, R. S.; Becraft, K.; Prussin, T.; Gatti, R. C. *Radiochimica Acta* **1992**, *58/59*, 27.

(4) Choppin, G. R. *Radiochim. Acta* **1988**, *43*, 82.

(5) Hobart, D. E. In *Actinides in the Environment*; Procedings of Robert A. Welch Foundation Conference on Chemical Research XXXIV. Fifty Years with Transuranium Elements; Houston, TX; 1990, 379.

(6) Nitsche, H. *Radiochim. Acta* **1991**, *52/53*, 3.

(7) Nitsche, H.; Edelstein, N. M. *Radiochimica Acta* **1985**, *39*, 23.

(8) Daniels, W. R. et al "Summary Report on Geochemistry of Yucca Mountain and Environs," Los Alamos National Laboratory, LA-9328-MS, 1982.

(9) Ogard, A. E.; Kerrisk, J. F. "Groundwater Chemistry Along Flow Paths Between a Proposed Repository Site and the Accessible Environment," Los Alamos National Laboratory, LA-10188-MS, 1984.

(10) Tucker, D. B.; Standifer, E. M.; Nitsche, H. *Lanth. and Act. Res.* **1988**, *2*, 279.

(11) Blaise, J.; Fred, M. S.; Carnall, W. T.; Crosswhite, H. M.; Crosswhite, H. In *Plutonium Chemistry*; 216 ed.; W. T. Carnall and G. R. Choppin, Ed.; American Chemical Society: Washington, D.C, 1983; pp 173.

(12) Cohen, D. *J. Inorg. Nucl. Chem.* **1961**, *18*, 211.

(13) Tam, A. C. *Rev. Mod. Phys.* **1986**, *58(2)*, 381.

(14) Braslavsky, S. E.; Heibel, G. E. *Chem. Rev.* **1992**, *92*, 1381.

(15) Schrepp, W.; Stumpe, R.; Kim, J. I.; Walther, H. *Appl. Phys. B* **1983**, *32*, 207.

(16) See for example: Beitz, J. V.; Bowers, D. L.; Doxtader, M. M.; Maroni, V. A.; Reed, D. T. *Radiochimica Acta* **1988**, *44/45*, 87.

(17) Klenze, R.; Kim, J. I. *Radiochimica Acta* **1988**, *44/45*, 77.

(18) Pollard, P. M.; Liezers, M.; McMillan, J. W.; Phillips, G.; Thomason, H. P.; Ewart, F. T. *Radiochimica Acta* **1988**, *44/45*, 95.

(19) Klenze, R.; Kim, J. I.; Wimmer, H. *Radiochimica Acta* **1991**, *52/53*, 97.

(20) Berg, J. M.; Tait, C. D.; Morris, D. E.; Woodruff, W. H. In *Actinide Speciation by Photothermal Spectroscopies: Instrumentation Development*; Scientific Basis for Nuclear Waste Management XIV; Boston, MA; 1991, 531.

(21) Russo, R. E.; Rojas, D.; Robouch, P.; Silva, R. J. *Rev. Sci. Instrum.* **1990**, *61(12)*, 3729.

(22) Torres, R. A.; Palmer, C. E. A.; Baisden, P. A.; Russo, R. E.; Silva, R. J. *Anal. Chem.* **1990**, *62*, 298.

(23) Nitsche, H.; Lee, S. C.; Gatti, R. C. *Radioanal. and Nucl. Chem.* **1988**, *124*, 171.

(24) Zolotov, Y. A.; Chmutova, M. K.; Palei, P. N. *Zh. Anal. Khim.* **1966**, *21(10)*, 1217.

(25) Bertrand, P. A.; Choppin, G. R. *Radiochim. Acta* **1982**, *31(3/4)*,

(26) Gehmecker, H.; Trautmann, N.; Herrmann, G. *Radiochim. Acta* **1986**, *40*, 11.

(27) Sekine, K.; Imai, T.; Kasai, A. *Talanta* **1987**, *34(6)*, 567.

(28) Schramke, J. A.; Rai, D.; Fulton, R. W.; Choppin, G. R. *J. Radioanal. and Nucl. Chem.* **1989**.

(29) Phal, D. G.; Kannan, S.; Ramakrishna, V. V.; Patil, S. K. *J. Radioanal. and Nucl. Chem., Articles* **1991**, *152(1)*, 137.

(30) Xi, R.; Gatti, R. C.; Roberts, K.; Nitsche, H. Lawerence Berkeley Laboratory,

(31) Katz, J. J.; Seaborg, G. T.; Morss, L. R. In *The Chemistry of the Actinide Elements*; Chapman and Hall: London, 1986; Vol. 1; pp 499-886.

(32) Hoffman, D. C. In *Collected Radiochemical and Geochemical Procedures*; 5th ed.; J. Kleinberg, Ed.; Los Alamos, NM, 1989; Vol. Report No. LA-1721; pp 194.

(33) Bennett, D. A. Ph. D. Thesis, University of California, Berkeley, 1990.

(34) Bennett, D. A.; Hoffman, D.; Nitsche, H.; Russo, R. E.; Torres, R. A.; Baisden, P. A.; Andrews, J. E.; Palmer, C. E. A.; Silva, R. J. *Radiochimica Acta* **1992**, *56*, 15.

(35) *Table of Isotopes*; 7th ed.; Browne, E.; Dairiki, J. M.; Doebler, R. E.; Shihab-Eldin, a. A.; Jardine, L. J.; Tuli, J. K.; Buyrn, A. B., Ed.; Wiley & Sons: New York, 1978.

(36) Nitsche, H.; Gatti, R. C.; Standifer, E. M.; Lee, S. C.; Müller, A.; Prussin, T.; Deinhammer, R. S.; Maurer, H.; Becraft, K.; Leung, S.; Carpenter, S. A. "Measured Solubilities and Speciations of Neptunium, Plutonium, and Americium in a Typical Groundwater (J-13) from the Yucca Mountain Region," Yucca Mountain Project Milestone Report, 3010-WBS 1.2.3.4.1.3.1, 1993.

(37) Schurig, D. A.; Klunder, G. L.; Silva, R. J.; Russo, R. E. *Submitted to Rev. Sci. Instrum.* **1992**.

(38) *Spectra-Calc*, Galactic Industries Corp., Salem, N.H., 1988.

(39) Fletcher, A. N.; Bliss, D. E. *Appl. Phys.* **1978**, *16*, 289.

(40) Okajima, S.; Reed, D. T.; Beitz, J. V.; Sabau, C. A.; Bowers, D. L. *Radiochim. Acta* **1991**, *52/53*, 111.

(41) Pashalidis, I.; Kim, J. I.; Lierse, C.; Sullivan, J. C. *Radiochim. Acta* **1993**, *61*, 29.

(42) Kim, J. I.; Pashalidis, I. Unpublished results, 1993.

(43) Spectra Physics New Product Information for the Master Oscillator-Power Oscillator, MOPO-700, 1993.

APPENDIX 1:

Tables of Crystal Data and Collection Parameters, Bond Lengths, Bond Angles, and Anisotropic Thermal Factors for Lead Hydroxamate Stuctures

Table A1.1 Crystallographic Data and Collection Parameters for the Crystal Structures.

Compound	(N-phenyltoluyl hydroxamato)$_4$Pb$_2$ • MeOH, **1**	L_4Pb_2• L (L = N-toluyl-*tert* butylhydroxamic acid), **2**	L_2(acetato)$_2Pb_4$ (L = N-toluyl-*tert* butylhydroxamic acid), **3**
Formula:	$PbO_5N_2C_{29}H_{28}$	$PbO_6N_3C_{36}H_{57}$	$Pb_2O_8N_2C_{28}H_{38}$
Formula weight:	691.75	835.06	944.95
Crystal Class:	triclinic	triclinic	triclinic
Space group:	P-1 (#2)	P-1 (#2)	P-1 (#2)
Z	2	2	2
a, Å	10.048(2)	11.651(3)	9.779(2)
b, Å	11.172(2)	12.929(3)	11.892(3)
c, Å	11.795(3)	13.138(4)	14.442(3)
α, (°)	101.17(2)	67.49(2)	70.54(2)
β, (°)	90.39(2)	78.26(2)	80.74(2)
γ, (°)	92.84(2)	89.31(2)	74.57(3)
V, Å^3	1297.2(9)	1790.1(9)	1521.6(7)
μ (cm^{-1})	65.90	47.92	111.78
ρ_{calc} (g/cm^3)	1.77	1.549	2.045
F(000)	676	848	896
Temperature (°C)	-117	-77	-95
Radiation (Mo K_a)	0.71073	0.71073	0.71073
θ range (°):	1.5 - 27.5	1.5 - 22.5	1.5 - 22.5
Scan mode:	ω-2θ	ω-2θ	ω-2θ
Crystal dim. (mm):	0.40 x 0.30 x 0.20	0.3 x 0.3 x 0.2	0.10 x 0.10 x 0.30
h,k,l range:	$0 \le h \le 12$, $-13 \le k \le 13$, $-14 \le l \le 14$	$0 \le h \le 12$, $-13 \le k \le 13$, $-14 \le l \le 14$	$0 \le h \le 10$, $-12 \le k \le 12$, $-15 \le l \le 15$
Reflections meas.:	6262	4937	4036
Unique reflections:	5936	4673	3967
Data(≥3.0 sigma):	5393	4160	2931
No. parameters:	447	443	350
Data/Parameter ratio:	12.1	9.4	8.4
R	0.022	0.021	0.029
R_w	0.027	0.027	0.034
GOF:	1.367	1.269	1.339

Table A2.1. Positional and Thermal Parameters and Their Estimated Standard Deviations for bis(N-phenyltoluylhydroxamato)-bis(μ-N-phenyltoluylhydroxamato)-dilead(II)-dimethanol solvate ($Pb_2O_{10}N_4C_{58}H_{56}$, **1**).

Atom	x	y	z	B(A2)
Pb1	0.04071(1)	0.39053(1)	0.35000(1)	1.480(2)
O1	-0.0809(2)	0.2453(2)	0.1901(2)	2.13(5)
O2	-0.1834(2)	0.3905(2)	0.3667(2)	1.93(4)
O3	0.0107(3)	0.5211(2)	0.2130(2)	2.07(5)
O4	0.0265(2)	0.5968(2)	0.4366(2)	1.85(4)
O5	0.2750(3)	0.7831(3)	0.4925(3)	3.62(6)
N1	-0.2526(3)	0.3559(3)	0.2630(2)	1.72(5)
N2	-0.0407(3)	0.6620(3)	0.3676(2)	1.68(5)
C1	-0.1968(3)	0.2782(3)	0.1782(3)	1.67(6)
C2	-0.2735(3)	0.2341(3)	0.0678(3)	1.62(6)
C3	-0.4038(3)	0.1855(3)	0.0650(3)	1.96(6)
C4	-0.4712(3)	0.1522(3)	-0.0397(3)	2.21(7)
C5	-0.4124(4)	0.1669(3)	-0.1424(3)	2.08(6)
C6	-0.2793(4)	0.2100(3)	-0.1391(3)	2.06(6)
C7	-0.2101(3)	0.2432(3)	-0.0344(3)	1.91(6)
C8	-0.4909(4)	0.1413(4)	-0.2537(4)	3.11(8)
C9	-0.3771(3)	0.4136(3)	0.2590(3)	1.56(5)
C10	-0.4624(3)	0.4130(3)	0.3495(3)	1.90(6)
C11	-0.5824(4)	0.4721(4)	0.3497(3)	2.32(7)
C12	-0.6137(4)	0.5297(4)	0.2601(3)	2.48(7)
C13	-0.5257(4)	0.5299(3)	0.1705(3)	2.32(7)
C14	-0.4062(3)	0.4730(3)	0.1699(3)	1.85(6)
C15	-0.0414(3)	0.6207(3)	0.2541(3)	1.68(6)
C16	-0.0950(3)	0.6949(3)	0.1738(3)	1.57(5)
C17	-0.0964(4)	0.8212(3)	0.1969(3)	1.97(6)
C18	-0.1325(4)	0.8842(3)	0.1125(3)	2.16(6)
C19	-0.1696(3)	0.8228(3)	0.0022(3)	2.02(6)
C20	-0.1713(3)	0.6969(3)	-0.0203(3)	1.92(6)
C21	-0.1326(3)	0.6323(3)	0.0624(3)	1.76(6)
C22	-0.2023(4)	0.8908(4)	-0.0929(3)	2.75(7)
C23	-0.1265(3)	0.7471(3)	0.4329(3)	1.62(5)
C24	-0.0696(4)	0.8447(3)	0.5117(3)	2.29(7)
C25	-0.1514(5)	0.9171(3)	0.5867(3)	2.90(8)
C26	-0.2878(5)	0.8925(4)	0.5822(3)	2.97(8)
C27	-0.3438(4)	0.7968(4)	0.5011(3)	2.57(7)
C28	-0.2631(4)	0.7234(3)	0.4265(3)	1.91(6)
C29	0.3053(5)	0.8714(4)	0.5905(4)	3.40(9)

Table A2.1. (cont.) Positional and Thermal Parameters and Their Estimated Standard Deviations for $Pb_2O_{10}N_4C_{58}H_{56}$, **1**.

Atom	x	y	z	B(A2)
H	0.228(6)	0.730(5)	0.504(5)	6(1)*
H3	-0.444(4)	0.177(3)	0.137(3)	2.2(8)*
H4	-0.555(4)	0.118(4)	-0.043(3)	2.6(9)*
H6	-0.229(5)	0.222(4)	-0.213(4)	4(1)*
H7	-0.117(4)	0.268(4)	-0.038(3)	2.4(8)*
H8A	-0.558(4)	0.190(4)	-0.253(4)	3(1)*
H8B	-0.532(5)	0.061(5)	-0.270(4)	5(1)*
H8C	-0.435(5)	0.150(5)	-0.320(4)	5(1)*
H10	-0.437(4)	0.385(3)	0.414(3)	1.5(7)*
H11	-0.627(4)	0.478(3)	0.409(3)	1.8(8)*
H12	-0.692(4)	0.568(4)	0.262(4)	2.9(9)*
H13	-0.546(4)	0.573(4)	0.112(3)	2.8(9)*
H14	-0.346(4)	0.479(3)	0.113(3)	2.0(8)*
H17	-0.065(4)	0.863(4)	0.267(3)	2.8(9)*
H18	-0.134(4)	0.967(4)	0.121(4)	3(1)*
H20	-0.204(4)	0.663(3)	-0.084(3)	2.1(8)*
H21	-0.134(3)	0.550(3)	0.043(3)	1.3(7)*
H22A	-0.274(5)	0.851(4)	-0.152(4)	4(1)*
H22B	-0.238(4)	0.972(4)	-0.057(3)	2.4(8)*
H22C	-0.123(5)	0.903(4)	-0.134(4)	5(1)*
H24	0.011(4)	0.855(3)	0.513(3)	2.1(8)*
H25	-0.112(4)	0.984(4)	0.637(4)	3(1)*
H26	-0.338(4)	0.945(4)	0.629(4)	4(1)*
H27	-0.436(4)	0.788(4)	0.503(4)	2.9(9)*
H28	-0.292(5)	0.654(4)	0.378(4)	4(1)*
H29C	0.344(6)	0.948(5)	0.571(5)	8(2)*
H29A	0.230(5)	0.899(5)	0.630(4)	5(1)*
H29B	0.372(5)	0.845(4)	0.647(4)	4(1)*

Starred atoms were included with isotropic thermal parameters.
The thermal parameter given for anisotropically refined atoms is the isotropic equivalent thermal parameter defined as:

$(4/3) * [a^2*\beta(1,1) + b^2*\beta(2,2) + c^2*\beta(3,3) + ab(\cos\gamma)*\beta(1,2) + ac(\cos\beta)*\beta(1,3) + bc(\cos\alpha)*\beta(2,3)]$

where a,b,c are real cell parameters, and $\beta(i,j)$ are anisotropic betas.

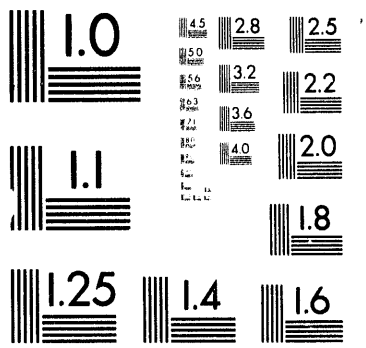
1.0
1.1
1.25
1.4
1.6
1.8
2.0
2.2
2.5
2.8
3.2
3.6
4.0
4.5
5.0
5.6
6.3
7.1
8.0
9.0
10.0
11.2
12.5
14.0
16.0
18.0
20.0
22.4
25.0
28.0
32.0
36.0

3 of 3

Table A2.2. Intramolecular Distances and Their Estimated Standard Deviations for $Pb_2O_{10}N_4C_{58}H_{56}$, **1**.

Atom 1	Atom 2	Distance (Å)	Atom 1	Atom 2	Distance (Å)
Pb1	Pb1'	4.008	C1	C2	1.494(4)
			C2	C3	1.390(5)
Pb1	O1	2.504(2)	C2	C7	1.386(5)
Pb1	O2	2.262(2)	C3	C4	1.381(5)
Pb1	O3	2.405(3)	C4	C5	1.386(5)
Pb1	O4	2.345(2)	C5	C6	1.397(5)
Pb1	O4'	2.589(2)	C5	C8	1.498(5)
			C6	C7	1.389(5)
O1	C1	1.254(4)	C9	C10	1.374(5)
O3	C15	1.264(4)	C9	C14	1.385(5)
			C10	C11	1.403(5)
O2	N1	1.382(3)	C11	C12	1.381(6)
O4	N2	1.386(4)	C12	C13	1.383(5)
			C13	C14	1.385(5)
O5	C29	1.387(5)	C15	C16	1.488(5)
			C16	C17	1.386(5)
N1	C1	1.337(4)	C16	C21	1.403(4)
N2	C15	1.329(4)	C17	C18	1.382(5)
			C18	C19	1.387(5)
N2	C23	1.430(4)	C19	C20	1.378(5)
N1	C9	1.439(4)	C19	C22	1.515(6)
			C20	C21	1.385(5)
			C23	C24	1.385(4)
			C23	C28	1.383(5)
			C24	C25	1.383(5)
			C25	C26	1.383(6)
			C26	C27	1.382(5)
			C27	C28	1.379(5)

Table A2.3. Intramolecular Angles and Their Estimated Standard Deviations for $Pb_2O_{10}N_4C_{58}H_{56}$, **1**.

Atom 1	Atom 2	Atom 3	Angle (°)	Atom 1	Atom 2	Atom 3	Angle (°)
O1	Pb1	O2	66.78(8)	C5	C6	C7	120.6(3)
O1	Pb1	O3	79.27(8)	C2	C7	C6	119.9(3)
O1	Pb1	O4	135.61(8)	N1	C9	C10	117.7(3)
O1	Pb1	O4'	121.04(8)	N1	C9	C14	120.8(3)
O2	Pb1	O3	85.34(9)	C10	C9	C14	121.3(3)
O2	Pb1	O4	82.34(8)	C9	C10	C11	118.9(3)
O2	Pb1	O4'	69.33(8)	C10	C11	C12	120.2(3)
O3	Pb1	O4	66.69(8)	C11	C12	C13	119.8(4)
O3	Pb1	O4'	133.37(8)	C12	C13	C14	120.5(4)
O4	Pb1	O4'	71.47(8)	C9	C14	C13	119.2(3)
Pb1	O1	C1	110.38(19)	O3	C15	N2	120.1(3)
Pb1	O2	N1	114.12(17)	O3	C15	C16	119.3(3)
Pb1	O3	C15	114.45(21)	N2	C15	C16	120.5(3)
Pb1	O4	Pb1'	108.53(9)	C15	C16	C17	124.6(3)
Pb1	O4	N2	112.60(15)	C15	C16	C21	116.8(3)
Pb1	O4'	N2	119.83(17)	C17	C16	C21	118.2(3)
C29	O5	H	114.0(39)	C16	C17	C18	121.0(3)
O2	N1	C1	118.1(3)	C17	C18	C19	121.0(3)
O2	N1	C9	114.18(23)	C18	C19	C20	118.1(3)
C1	N1	C9	127.7(3)	C18	C19	C22	121.5(3)
O4	N2	C15	117.6(3)	C20	C19	C22	120.3(3)
O4	N2	C23	112.24(24)	C19	C20	C21	121.8(3)
C15	N2	C23	128.2(3)	C16	C21	C20	119.9(3)
O1	C1	N1	120.5(3)	N2	C23	C24	118.6(3)
O1	C1	C2	120.6(3)	N2	C23	C28	119.9(3)
N1	C1	C2	118.9(3)	C24	C23	C28	121.1(3)
C1	C2	C3	122.4(3)	C23	C24	C25	118.9(3)
C1	C2	C7	117.6(3)	C24	C25	C26	120.3(3)
C3	C2	C7	120.0(3)	C25	C26	C27	120.3(4)
C2	C3	C4	119.4(3)	C26	C27	C28	119.9(4)
C3	C4	C5	121.6(3)	C23	C28	C27	119.5(3)
C4	C5	C6	118.3(3)	O5	C29	H29C	111.8(33)
C4	C5	C8	120.9(3)	O5	C29	H29A	112.8(29)
C6	C5	C8	120.7(3)	O5	C29	H29B	114.3(25)

Table A2.4. Anisotropic Thermal Factors[a] ($Å^2$) for $Pb_2O_{10}N_4C_{58}H_{56}$, **1**.

Atom	B(11)	B(22)	B(33)	B(12)	B(13)	B(23)	B(eqv.)
Pb1	1.247(4)	1.640(4)	1.707(4)	0.225(3)	-0.240(3)	0.678(3)	1.480(2)
O1	1.84(9)	2.33(9)	2.17(9)	0.55(8)	-0.26(8)	0.23(8)	2.13(5)
O2	2.20(9)	2.39(9)	1.11(7)	0.04(8)	-0.54(7)	0.10(7)	1.93(4)
O3	2.57(9)	1.98(8)	1.87(8)	0.67(8)	0.14(8)	0.74(7)	2.07(5)
O4	1.94(8)	2.04(8)	1.77(8)	0.41(7)	-0.49(7)	0.81(6)	1.85(4)
O5	3.9(1)	3.0(1)	3.9(1)	-1.0(1)	0.5(1)	0.6(1)	3.62(6)
N1	1.8(1)	2.0(1)	1.42(9)	0.16(9)	-0.26(8)	0.29(8)	1.72(5)
N2	1.9(1)	1.9(1)	1.42(9)	0.30(8)	-0.44(8)	0.66(7)	1.68(5)
C1	1.6(1)	1.8(1)	1.7(1)	0.11(9)	0.03(9)	0.60(9)	1.67(6)
C2	1.6(1)	1.5(1)	1.7(1)	0.30(9)	-0.18(9)	0.25(9)	1.62(6)
C3	1.7(1)	2.1(1)	2.1(1)	-0.1(1)	0.1(1)	0.5(1)	1.96(6)
C4	1.5(1)	2.0(1)	2.9(1)	0.1(1)	-0.3(1)	0.1(1)	2.21(7)
C5	2.3(1)	1.6(1)	2.3(1)	0.6(1)	-0.7(1)	0.0(1)	2.08(6)
C6	2.5(1)	2.0(1)	1.9(1)	0.6(1)	0.1(1)	0.4(1)	2.06(6)
C7	1.8(1)	2.0(1)	2.0(1)	0.2(1)	-0.1(1)	0.4(1)	1.91(6)
C8	3.2(2)	3.2(2)	2.6(1)	0.7(1)	-1.2(1)	-0.4(1)	3.11(8)
C9	1.5(1)	1.6(1)	1.6(1)	-0.09(9)	-0.47(9)	0.31(9)	1.56(5)
C10	2.0(1)	2.0(1)	1.8(1)	0.1(1)	0.0(1)	0.5(1)	1.90(6)
C11	1.8(1)	2.7(1)	2.3(1)	0.3(1)	0.2(1)	-0.0(1)	2.32(7)
C12	1.9(1)	2.5(1)	3.0(1)	0.8(1)	-0.4(1)	0.4(1)	2.48(7)
C13	2.5(1)	2.0(1)	2.5(1)	0.5(1)	-0.5(1)	0.6(1)	2.32(7)
C14	2.0(1)	1.6(1)	1.9(1)	0.1(1)	-0.1(1)	0.52(9)	1.85(6)
C15	1.6(1)	1.7(1)	1.9(1)	0.09(9)	-0.02(9)	0.72(9)	1.68(6)
C16	1.4(1)	1.8(1)	1.7(1)	0.14(9)	0.00(9)	0.87(8)	1.57(5)
C17	2.3(1)	1.8(1)	1.8(1)	0.0(1)	-0.2(1)	0.52(9)	1.97(6)
C18	2.6(1)	1.9(1)	2.2(1)	0.6(1)	0.3(1)	0.86(9)	2.16(6)
C19	1.9(1)	2.7(1)	1.8(1)	0.6(1)	0.3(1)	1.27(9)	2.02(6)
C20	1.8(1)	2.7(1)	1.3(1)	0.2(1)	-0.0(1)	0.4(1)	1.92(6)
C21	1.7(1)	1.8(1)	1.9(1)	-0.0(1)	-0.1(1)	0.62(9)	1.76(6)
C22	3.0(1)	3.5(1)	2.3(1)	1.3(1)	0.2(1)	1.6(1)	2.75(7)
C23	2.1(1)	1.4(1)	1.6(1)	0.15(9)	-0.31(9)	0.80(8)	1.62(5)
C24	2.7(1)	1.9(1)	2.3(1)	-0.3(1)	-0.5(1)	0.6(1)	2.29(7)
C25	4.7(2)	1.8(1)	2.1(1)	0.3(1)	-0.3(1)	0.2(1)	2.90(8)
C26	4.3(2)	2.4(1)	2.3(1)	1.3(1)	0.7(1)	0.6(1)	2.97(8)
C27	2.6(1)	2.7(1)	2.7(1)	0.4(1)	0.5(1)	1.2(1)	2.57(7)
C28	2.1(1)	1.8(1)	1.9(1)	-0.1(1)	-0.1(1)	0.65(9)	1.91(6)
C29	3.7(2)	2.7(2)	3.9(2)	0.1(1)	-0.9(2)	0.9(1)	3.40(9)

[a]The form of the anisotropic temperature factor is:
$\exp[-0.25\{h^2a^2B(1,1) + k^2b^2B(2,2) + l^2c^2B(3,3) + 2hkabB(1,2) + 2hlacB(1,3) + 2klbcB(2,3)\}]$ where a,b, and c are reciprocal lattice constants.

Table A2.5. Root-mean Square Amplitudes of Thermal Vibration for $Pb_2O_{10}N_4C_{58}H_{56}$, **1**.

Atom	Min.	Int'med.	Max.
Pb1	0.107	0.140	0.159
O1	0.137	0.161	0.190
O2	0.105	0.174	0.179
O3	0.131	0.158	0.192
O4	0.106	0.170	0.174
O5	0.165	0.216	0.253
N1	0.126	0.153	0.161
N2	0.103	0.160	0.167
C1	0.134	0.143	0.158
C2	0.127	0.141	0.159
C3	0.142	0.161	0.167
C4	0.137	0.158	0.200
C5	0.127	0.145	0.205
C6	0.145	0.153	0.185
C7	0.146	0.160	0.160
C8	0.144	0.185	0.251
C9	0.115	0.141	0.161
C10	0.147	0.158	0.161
C11	0.144	0.166	0.201
C12	0.131	0.183	0.209
C13	0.139	0.172	0.198
C14	0.138	0.154	0.166
C15	0.129	0.143	0.164
C16	0.116	0.136	0.166
C17	0.142	0.155	0.174
C18	0.131	0.162	0.196
C19	0.118	0.149	0.202
C20	0.126	0.151	0.185
C21	0.138	0.146	0.163
C22	0.125	0.178	0.239
C23	0.099	0.151	0.169
C24	0.150	0.155	0.200
C25	0.149	0.165	0.246
C26	0.154	0.166	0.248
C27	0.153	0.175	0.209
C28	0.137	0.155	0.173
C29	0.178	0.193	0.245

Table A3.1. Positional and Thermal Parameters and Their Estimated Standard Deviations for bis(N-toluyl-*tert*-butyl-hydroxamato)-bis(μ-N-toluyl-*tert*-butyl-hydroxamato)dilead(II)·N-toluyl-*tert*-butyl-hydroxamic acid ($Pb_2O_{12}N_6C_{72}H_{114}$, **2**).

Atom	x	y	z	B(A2)
Pb1	0.10149(1)	0.38698(1)	0.47439(1)	2.032(3)
O1	0.2712(3)	0.3535(2)	0.5413(2)	3.27(7)
O2	0.2046(3)	0.5540(2)	0.4704(2)	2.78(7)
O3	0.0102(3)	0.2210(2)	0.6296(3)	3.56(8)
O4	0.0146(3)	0.4214(2)	0.6301(2)	2.36(7)
O5	0.3881(3)	0.1810(2)	0.5306(3)	2.92(8)
O6	0.2091(3)	-0.0648(3)	0.6211(3)	3.85(8)
N1	0.3001(3)	0.4289(3)	0.5864(3)	2.56(8)
N2	-0.0512(3)	0.3313(3)	0.7204(3)	2.41(9)
N3	0.2925(3)	0.1103(3)	0.5410(3)	2.58(9)
C10	0.3325(4)	0.3706(3)	0.6920(3)	2.5(1)
C11	0.2471(4)	0.3211(4)	0.7864(4)	3.2(1)
C12	0.2773(5)	0.2600(4)	0.8884(4)	3.7(1)
C13	0.3931(4)	0.2463(4)	0.8960(4)	3.5(1)
C14	0.4279(6)	0.1794(5)	1.0057(5)	5.7(2)
C15	0.4774(4)	0.2946(4)	0.7979(4)	3.6(1)
C16	0.4489(4)	0.3567(4)	0.6967(4)	3.1(1)
C20	0.2603(4)	0.5308(4)	0.5472(3)	2.6(1)
C21	0.2828(4)	0.6217(4)	0.5906(3)	2.7(1)
C22	0.4003(4)	0.6190(4)	0.6257(4)	3.5(1)
C23	0.1806(5)	0.6096(4)	0.6888(4)	3.9(1)
C24	0.2811(5)	0.7365(4)	0.4939(4)	4.7(1)
C30	-0.0493(4)	0.2311(4)	0.7153(4)	2.8(1)
C31	-0.1137(5)	0.1227(4)	0.8105(4)	3.8(1)
C32A	-0.165(1)	0.1219(8)	0.9220(9)	6.9(3)
C32B	-0.244(1)	0.138(1)	0.850(1)	5.8(4)
C33A	-0.021(1)	0.0337(9)	0.824(1)	6.9(4)
C33B	-0.056(1)	0.100(1)	0.915(1)	7.8(5)
C34B	-0.096(2)	0.033(1)	0.770(1)	9.2(6)
C34A	-0.207(1)	0.084(1)	0.758(1)	8.9(4)
C40	-0.1223(4)	0.3667(4)	0.8023(3)	2.4(1)
C41	-0.2331(4)	0.3995(4)	0.7905(3)	2.5(1)
C42	-0.3020(4)	0.4344(4)	0.8684(4)	2.9(1)
C43	-0.2619(4)	0.4377(4)	0.9589(4)	2.9(1)
C44	-0.3374(5)	0.4720(4)	1.0454(4)	4.3(1)
C45	-0.1488(5)	0.4073(4)	0.9678(4)	3.6(1)
C46	-0.0781(4)	0.3737(4)	0.8897(4)	3.4(1)
C50	0.2366(4)	0.1493(3)	0.4489(3)	2.4(1)
C51	0.2958(4)	0.2260(4)	0.3446(4)	2.8(1)
C52	0.2404(4)	0.2659(4)	0.2554(4)	3.2(1)
C53	0.1254(4)	0.2333(4)	0.2663(4)	2.9(1)
C54	0.0660(5)	0.2777(4)	0.1682(4)	4.2(1)
C55	0.0649(4)	0.1589(4)	0.3712(4)	2.9(1)
C56	0.1187(4)	0.1169(3)	0.4617(4)	2.5(1)
C60	0.2799(4)	0.0038(4)	0.6216(4)	2.9(1)
C61	0.3545(4)	-0.0276(4)	0.7115(4)	3.0(1)

Table A3.1 (cont.). Positional and Thermal Parameters and Their Estimated Standard Deviations for $Pb_2O_{12}N_6C_{72}H_{114}$, **2.**

Atom	x	y	z	B(A2)
C62	0.3388(5)	0.0490(4)	0.7754(4)	4.5(1)
C63	0.3110(5)	-0.1471(4)	0.7963(4)	4.6(1)
C64	0.4839(5)	-0.0280(5)	0.6584(5)	4.6(1)
H5	0.363(4)	0.233(3)	0.542(3)	3.8*
H11	0.167(3)	0.328(3)	0.782(3)	4(1)*
H12	0.217(3)	0.227(3)	0.954(3)	4.8(9)*
H14A	0.360(4)	0.161(4)	1.077(4)	7.3*
H14C	0.470(4)	0.222(4)	1.030(4)	7.3*
H14B	0.432(4)	0.101(4)	1.023(4)	7.3*
H15	0.558(3)	0.285(3)	0.801(3)	4.6(8)*
H16	0.509(3)	0.390(3)	0.631(3)	4.0(9)*
H22C	0.463(3)	0.629(3)	0.563(3)	5(1)*
H22A	0.41(1)	0.68(1)	0.65(1)	5(5)*
H22B	0.404(4)	0.549(4)	0.685(4)	4.5*
H23A	0.192(4)	0.665(4)	0.718(4)	5.1*
H23B	0.109(4)	0.619(4)	0.663(4)	5.1*
H23C	0.177(4)	0.537(4)	0.747(4)	5.1*
H24A	0.295(5)	0.795(4)	0.518(4)	6.1*
H24B	0.341(5)	0.743(4)	0.430(4)	6.1*
H24C	0.207(5)	0.742(4)	0.474(4)	6.1*
H41	-0.262(4)	0.398(3)	0.729(3)	3.3*
H42	-0.379(4)	0.457(3)	0.859(3)	3.7*
H44C	-0.394(4)	0.527(4)	1.012(4)	5.6*
H44A	-0.377(4)	0.414(4)	1.106(4)	5.6*
H44B	-0.296(4)	0.515(4)	1.068(4)	5.6*
H45	-0.119(4)	0.410(4)	1.029(4)	4.6*
H46	0.000(4)	0.356(4)	0.896(4)	4.4*
H51	0.375(4)	0.251(4)	0.335(3)	3.7*
H52	0.283(4)	0.317(4)	0.185(4)	4.1*
H54A	0.035(4)	0.357(4)	0.162(4)	5.5*
H54B	0.010(4)	0.234(4)	0.178(4)	5.5*
H54C	0.126(4)	0.308(4)	0.095(4)	5.5*
H55	-0.015(4)	0.136(3)	0.381(3)	3.8*
H56	0.076(4)	0.066(3)	0.533(3)	3.2*
H62B	0.362(4)	0.124(4)	0.724(4)	5.8*
H62C	0.259(4)	0.044(4)	0.812(4)	5.8*
H62A	0.386(4)	0.027(4)	0.830(4)	5.8*
H63B	0.230(5)	-0.149(4)	0.830(4)	6.0*
H63C	0.321(4)	-0.197(4)	0.759(4)	6.0*
H63A	0.355(5)	-0.169(4)	0.853(4)	6.0*
H64A	0.529(4)	-0.048(4)	0.715(4)	6.0*
H64B	0.492(4)	-0.081(4)	0.624(4)	6.0*
H64C	0.511(4)	0.044(4)	0.603(4)	6.0*

Starred atoms were included with isotropic thermal parameters.
The thermal parameter given for anisotropically refined atoms is the isotropic equivalent thermal parameter defined as:

$(4/3) * [a^2*\beta(1,1) + b^2*\beta(2,2) + c^2*\beta(3,3) + ab(\cos\gamma)*\beta(1,2) + ac(\cos\beta)*\beta(1,3) + bc(\cos\alpha)*\beta(2,3)]$, where a,b,c are real cell parameters, and $\beta(i,j)$ are anisotropic betas.

Table A3.2. Intramolecular Distances and Their Estimated Standard Deviations for $Pb_2O_{12}N_6C_{72}H_{114}$, **2.**

Atom 1	Atom 2	Distance (Å)	Atom 1	Atom 2	Distance (Å)
Pb	Pb'	3.9133(4)	C10	C11	1.358(7)
Pb	O1	2.295(3)	C11	C12	1.386(7)
Pb	O2	2.463(3)	C12	C13	1.378(7)
Pb	O3	2.392(3)	C13	C14	1.506(8)
Pb	O4	2.296(3)	C13	C15	1.379(7)
Pb	O2'	3.625(3)	C10	C16	1.377(7)
Pb	O4'	2.815(3)	C15	C16	1.372(7)
			C20	C21	1.538(6)
O1	N1	1.397(5)	C21	C22	1.527(7)
O1	H5	1.885(3)	C21	C23	1.528(7)
O1	O5	2.637(4)	C21	C24	1.544(7)
			C30	C31	1.548(7)
O2	C20	1.250(5)	C31	C32A	1.466(13)
			C31	C32B	1.542(15)
O3	C30	1.250(6)	C32A	C32B	1.406(23)
			C31	C33A	1.556(15)
O4	N2	1.396(4)	C31	C33B	1.575(17)
			C32A	C33B	1.290(22)
O5	H5	0.780(3)	C33A	C33B	1.71(3)
O5	N3	1.402(5)	C31	C34A	1.582(15)
			C32B	C34A	1.610(25)
O6	C60	1.222(6)	C34B	C34A	1.46(3)
			C31	C34B	1.442(18)
N1	C10	1.430(6)	C33A	C34B	1.23(3)
N1	C20	1.335(6)	C40	C41	1.374(6)
			C41	C42	1.384(7)
N2	C30	1.323(6)	C42	C43	1.380(7)
N2	C40	1.438(6)	C43	C44	1.497(7)
			C43	C45	1.385(7)
N3	C50	1.412(6)	C40	C46	1.385(7)
N3	C60	1.366(6)	C45	C46	1.385(7)
			C50	C51	1.389(7)
			C51	C52	1.377(7)
			C52	C53	1.371(7)
			C53	C54	1.504(7)
			C53	C55	1.390(7)
			C50	C56	1.399(6)
			C55	C56	1.380(7)
			C60	C61	1.537(7)
			C61	C62	1.516(7)
			C61	C63	1.535(7)
			C61	C64	1.529(8)

Table A3.3. Intramolecular Angles and Their Estimated Standard Deviations for $Pb_2O_{12}N_6C_{72}H_{114}$, **2.**

Atom 1	Atom 2	Atom 3	Angle (°)	Atom 1	Atom 2	Atom 3	Angle (°)
O1	Pb	O2	65.20(11)	O1	Pb	O3	88.49(13)
O1	Pb	O4	89.15(11)	O1	Pb	O4'	135.66(10)
O2	Pb	O3	130.66(11)	O2	Pb	O4	71.19(10)
O2	Pb	O4'	70.67(10)	O3	Pb	O4	67.28(10)
O3	Pb	O4'	125.18(10)	O4	Pb	O4'	80.61(10)
Pb	O1	N1	114.27(24)	Pb	O1	H5	124.22(15)
Pb	O2	C20	112.4(3)	Pb	O3	C30	118.3(3)
Pb	O4	N2	116.32(23)	Pb	O4	Pb'	99.39(10)
Pb'	O4	N2	118.27(22)	N3	O5	H5	107.9(3)
O1	H5	O5	161.7(3)	O1	N1	C20	116.7(4)
O1	N1	C10	110.8(4)	O4	N2	C30	118.6(4)
C10	N1	C20	128.8(4)	C30	N2	C40	129.3(4)
O4	N2	C40	111.8(3)	O5	N3	C60	118.1(4)
O5	N3	C50	114.0(4)	N1	C10	C11	119.4(4)
C50	N3	C60	126.0(4)	C11	C10	C16	120.1(5)
N1	C10	C16	120.4(4)	C11	C12	C13	121.2(5)
C10	C11	C12	120.0(5)	C12	C13	C15	117.3(5)
C12	C13	C14	122.2(5)	C13	C15	C16	122.1(5)
C14	C13	C15	120.5(5)	O2	C20	C21	118.7(4)
O2	C20	N1	118.6(4)	C20	C21	C22	114.8(4)
N1	C20	C21	122.6(4)	C20	C21	C24	107.2(4)
C20	C21	C23	107.5(4)	C22	C21	C24	107.7(4)
C22	C21	C23	110.7(4)	O3	C30	N2	118.9(4)
C23	C21	C24	108.7(5)	N2	C30	C31	124.5(4)
O3	C30	C31	116.6(4)	C30	C31	C32B	111.9(6)
C30	C31	C32A	120.2(6)	C30	C31	C33B	106.7(7)
C30	C31	C33A	104.9(7)	C30	C31	C34A	105.2(6)
C30	C31	C34B	107.6(8)	C32A	C31	C33A	108.3(9)
C32A	C31	C32B	55.7(9)	C32A	C31	C34B	131.7(9)
C32A	C31	C33B	50.1(10)	C32B	C31	C33A	142.9(8)
C32A	C31	C34A	112.1(11)	C32B	C31	C34B	113.6(14)
C32B	C31	C33B	105.6(12)	C33A	C31	C33B	66.1(11)
C32B	C31	C34A	62.0(10)	C33A	C31	C34A	104.9(11)
C33A	C31	C34B	48.3(12)	C33B	C31	C34A	148.1(8)
C33B	C31	C34B	111.1(15)	N2	C40	C41	119.6(4)
C34B	C31	C34A	57.4(13)	C41	C40	C46	119.7(4)
N2	C40	C46	120.6(4)	C41	C42	C43	121.4(4)
C40	C41	C42	120.1(4)	C42	C43	C45	117.7(4)
C42	C43	C44	121.6(5)	C43	C45	C46	121.6(5)
C44	C43	C45	120.6(5)	N3	C50	C51	120.5(4)
C40	C46	C45	119.4(5)	C50	C51	C52	120.5(4)
N3	C50	C56	121.0(4)	C52	C53	C54	121.2(5)
C51	C52	C53	121.7(5)	C54	C53	C55	120.9(5)
C52	C53	C55	118.0(4)	C50	C56	C55	120.0(4)
C53	C55	C56	121.4(4)	O6	C60	C61	121.2(4)
O6	C60	N3	119.3(4)	C60	C61	C62	111.9(4)
N3	C60	C61	119.5(4)	C60	C61	C64	110.5(4)
C60	C61	C63	107.1(4)	C62	C61	C64	111.1(5)
C62	C61	C63	107.7(4)	C63	C61	C64	108.2(5)

Table A3.4. Anisotropic Thermal Factors[a] ($Å^2$) for $Pb_2O_{12}N_6C_{72}H_{114}$, **2.**

Atom	B(11)	B(22)	B(33)	B(12)	B(13)	B(23)	B(eqv.)
Pb1	2.563(6)	1.947(5)	1.791(5)	0.173(5)	-0.462(5)	-0.954(4)	2.032(3)
O1	3.2(1)	3.6(1)	4.9(1)	1.2(1)	-1.9(1)	-3.19(8)	3.27(7)
O2	4.0(1)	2.4(1)	2.0(1)	-0.4(1)	-0.7(1)	-0.94(8)	2.78(7)
O3	4.9(2)	2.4(1)	2.9(1)	-0.1(1)	1.1(1)	-1.37(9)	3.56(8)
O4	2.8(1)	1.9(1)	2.0(1)	-0.3(1)	0.3(1)	-0.80(8)	2.36(7)
O5	2.4(1)	2.3(1)	4.3(1)	0.0(1)	-0.9(1)	-1.34(9)	2.92(8)
O6	5.1(2)	1.9(1)	4.6(1)	-0.6(1)	-2.1(1)	-0.7(1)	3.85(8)
N1	2.9(1)	3.0(1)	3.0(1)	0.3(1)	-1.1(1)	-2.21(9)	2.56(8)
N2	2.6(2)	2.3(1)	1.9(1)	0.0(1)	0.2(1)	-0.8(1)	2.41(9)
N3	2.7(1)	1.9(1)	3.3(1)	-0.0(1)	-0.7(1)	-1.2(1)	2.58(9)
C10	2.4(2)	2.6(2)	3.0(2)	-0.1(1)	-0.6(1)	-1.7(1)	2.5(1)
C11	2.6(2)	4.0(2)	3.6(2)	0.2(2)	-0.3(2)	-2.3(1)	3.2(1)
C12	3.8(2)	4.2(2)	3.1(2)	-0.0(2)	0.1(2)	-1.9(1)	3.7(1)
C13	4.6(2)	3.0(2)	3.5(2)	0.0(2)	-1.6(2)	-1.6(1)	3.5(1)
C14	7.9(3)	5.0(3)	3.9(2)	-0.1(3)	-2.9(2)	-0.7(2)	5.7(2)
C15	2.6(2)	3.8(2)	4.7(2)	-0.0(2)	-1.4(2)	-1.8(2)	3.6(1)
C16	2.8(2)	3.4(2)	3.2(2)	-0.3(2)	-0.6(2)	-1.4(1)	3.1(1)
C20	2.6(2)	3.0(2)	2.0(2)	-0.3(2)	0.1(1)	-1.2(1)	2.6(1)
C21	3.2(2)	3.0(2)	2.5(2)	-0.4(2)	-0.4(1)	-1.8(1)	2.7(1)
C22	3.9(2)	3.3(2)	3.6(2)	-0.9(2)	-0.4(2)	-2.0(1)	3.5(1)
C23	3.7(2)	4.9(2)	4.6(2)	-0.1(2)	-0.7(2)	-3.5(1)	3.9(1)
C24	6.9(3)	3.0(2)	4.9(2)	-0.2(2)	-1.8(2)	-2.1(2)	4.7(1)
C30	3.3(2)	2.2(2)	2.4(2)	-0.0(2)	-0.3(2)	-0.5(1)	2.8(1)
C31	5.0(3)	2.0(2)	2.9(2)	0.2(2)	0.4(2)	0.0(2)	3.8(1)
C32A	11.1(8)	2.2(4)	3.7(4)	0.7(5)	3.9(5)	0.2(3)	6.9(3)
C32B	3.5(5)	3.0(5)	6.8(8)	-0.6(5)	1.3(6)	1.2(6)	5.8(4)
C33A	9.1(7)	3.4(5)	5.1(6)	2.3(5)	1.5(6)	0.1(4)	6.9(4)
C33B	8.6(8)	6.2(8)	4.8(7)	-1.8(7)	-3.2(6)	2.8(6)	7.8(5)
C34B	18(2)	0.9(4)	5.6(7)	-1.8(7)	3.2(9)	-1.1(4)	9.2(6)
C34A	10.5(7)	7.5(6)	6.1(6)	-6.2(5)	-2.9(5)	0.8(5)	8.9(4)
C40	2.8(2)	2.1(2)	1.8(2)	-0.1(1)	0.1(1)	-0.5(1)	2.4(1)
C41	2.7(2)	3.0(2)	1.8(2)	-0.0(2)	-0.4(1)	-0.9(1)	2.5(1)
C42	2.9(2)	3.5(2)	2.3(2)	0.6(2)	-0.4(1)	-1.2(1)	2.9(1)
C43	3.5(2)	3.0(2)	2.0(2)	0.4(2)	-0.1(2)	-1.1(1)	2.9(1)
C44	5.1(3)	5.1(2)	3.0(2)	0.9(2)	-0.2(2)	-2.4(2)	4.3(1)
C45	4.4(2)	4.6(2)	2.3(2)	0.6(2)	-1.1(2)	-1.8(1)	3.6(1)
C46	3.1(2)	4.9(2)	2.7(2)	0.9(2)	-1.0(1)	-1.8(1)	3.4(1)
C50	2.8(2)	2.0(2)	2.9(2)	0.7(1)	-0.8(1)	-1.3(1)	2.4(1)
C51	2.9(2)	2.2(2)	3.1(2)	0.2(2)	-0.1(2)	-1.0(1)	2.8(1)
C52	3.5(2)	2.7(2)	2.7(2)	0.5(2)	0.1(2)	-0.8(1)	3.2(1)
C53	4.3(2)	2.3(2)	2.8(2)	1.0(2)	-1.3(2)	-1.5(1)	2.9(1)
C54	5.2(3)	4.2(2)	3.4(2)	1.2(2)	-1.6(2)	-1.5(2)	4.2(1)
C55	3.2(2)	2.6(2)	3.6(2)	0.3(2)	-0.9(1)	-2.0(1)	2.9(1)
C56	2.6(2)	2.0(2)	2.7(2)	-0.1(1)	-0.3(1)	-0.9(1)	2.5(1)
C60	3.5(2)	2.5(2)	2.9(2)	0.4(2)	-0.5(2)	-1.2(1)	2.9(1)
C61	4.0(2)	2.7(2)	2.9(2)	0.5(2)	-1.1(2)	-1.4(1)	3.0(1)
C62	6.3(3)	3.8(2)	3.8(2)	0.3(2)	-1.2(2)	-1.9(2)	4.5(1)
C63	7.4(3)	3.0(2)	3.9(2)	-0.3(2)	-2.6(2)	-1.0(2)	4.6(1)
C64	4.2(2)	5.3(3)	4.8(2)	2.0(2)	-2.0(2)	-1.8(2)	4.6(1)

[a]The form of the anisotropic temperature factor is:
$\exp[-0.25\{h^2a^2B(1,1) + k^2b^2B(2,2) + l^2c^2B(3,3) + 2hkabB(1,2) + 2hlacB(1,3) + 2klbcB(2,3)\}]$ where a,b, and c are reciprocal lattice constants.

Table A3.5. Root-mean Square Amplitudes of Thermal Vibration for $Pb_2O_{12}N_6C_{72}H_{114}$, **2.**

Atom	Min.	Int'med.	Max.
Pb1	0.137	0.161	0.181
O1	0.140	0.178	0.270
O2	0.148	0.170	0.234
O3	0.146	0.175	0.289
O4	0.143	0.154	0.213
O5	0.158	0.176	0.234
O6	0.145	0.209	0.286
N1	0.116	0.189	0.218
N2	0.141	0.171	0.205
N3	0.144	0.186	0.206
C10	0.138	0.179	0.206
C11	0.173	0.189	0.237
C12	0.175	0.220	0.247
C13	0.167	0.205	0.249
C14	0.190	0.259	0.334
C15	0.160	0.222	0.245
C16	0.175	0.197	0.216
C20	0.146	0.175	0.212
C21	0.135	0.189	0.223
C22	0.155	0.207	0.255
C23	0.155	0.217	0.279
C24	0.168	0.245	0.300
C30	0.158	0.191	0.212
C31	0.144	0.210	0.282
C32A	0.135	0.191	0.456
C32B	0.135	0.232	0.383
C33A	0.183	0.233	0.419
C33B	0.151	0.290	0.433
C34A	0.176	0.265	0.485
C34B	0.090	0.246	0.531
C40	0.141	0.172	0.201
C41	0.150	0.183	0.199
C42	0.163	0.188	0.216
C43	0.151	0.193	0.220
C44	0.159	0.251	0.271
C45	0.150	0.231	0.245
C46	0.169	0.192	0.253
C50	0.134	0.183	0.200
C51	0.166	0.179	0.220
C52	0.174	0.180	0.240
C53	0.147	0.179	0.239
C54	0.196	0.222	0.266
C55	0.147	0.200	0.220
C56	0.157	0.178	0.195
C60	0.169	0.191	0.213
C61	0.166	0.191	0.226
C62	0.195	0.228	0.283
C63	0.191	0.194	0.319
C64	0.180	0.251	0.284

Table A4.1. Positional and Thermal Parameters and Their Estimated Standard Deviations for tetra(μ-N-toluyl-*tert*-butyl-hydroxamato)-tetra(μ-acetato)-tetralead(II) ($Pb_4O_{16}N_4C_{56}H_{76}$, **3**).

Atom	x	y	z	B(A2)
Pb1	0.04347(1)	-0.03601(1)	0.14121(1)	2.074(9)
Pb2	0.35570(1)	0.05529(1)	-0.09233(1)	2.42(1)
O1	0.1509(7)	0.1538(6)	0.0116(5)	2.8(2)
O2	0.3480(8)	0.2002(7)	0.0180(5)	3.9(2)
O3	0.1299(7)	-0.0806(5)	-0.0078(4)	1.9(2)
O4	0.0896(8)	-0.2424(6)	0.1609(5)	3.3(2)
O5	0.6476(8)	0.0836(7)	-0.1424(5)	3.6(2)
O6	0.5412(8)	0.0596(7)	-0.2519(5)	3.4(2)
O7	-0.3128(8)	-0.2521(6)	0.1965(5)	3.0(2)
O8	-0.1974(7)	-0.0829(6)	0.2021(5)	2.5(2)
N1	0.1782(9)	-0.2053(7)	0.0036(6)	2.6(2)
N2	-0.2044(9)	-0.1860(7)	0.2849(6)	2.5(2)
C1	0.222(1)	0.1952(8)	0.0556(6)	1.7(2)*
C2	0.1747(9)	0.2202(7)	0.1288(6)	1.0(2)*
C3	0.255(1)	-0.2259(9)	-0.0863(8)	2.8(3)
C4	0.394(1)	-0.2240(9)	-0.1015(8)	3.1(3)
C5	0.469(1)	-0.230(1)	-0.1913(9)	4.1(3)
C6	0.398(1)	-0.240(1)	-0.2639(8)	3.8(3)
C7	0.259(1)	-0.244(1)	-0.2447(8)	3.7(3)
C8	0.180(1)	-0.2358(9)	-0.1566(7)	2.9(3)
C9	0.473(2)	-0.250(1)	-0.361(1)	6.3(5)
C10	0.154(1)	-0.285(1)	0.0934(8)	3.2(3)
C11	0.195(2)	-0.425(1)	0.114(1)	8.1(6)
C12	0.284(2)	-0.479(1)	0.041(1)	6.9(5)
C13	0.176(2)	-0.485(1)	0.217(1)	8.9(6)
C14	0.031(3)	-0.448(2)	0.094(2)	8.9(9)
C14'	0.378(5)	-0.443(3)	0.153(3)	9(1)
C15	0.643(1)	0.0884(8	-0.2304(6)	1.5(2)*
C16	0.7380(9)	0.1213(8)	-0.2918(6)	1.3(2)*
C17	-0.168(1)	-0.1675(9)	0.3713(7)	2.5(3)
C18	-0.031(1)	-0.211(1)	0.3992(7)	3.2(3)
C19	0.002(1)	-0.191(1)	0.4825(9)	4.8(4)
C20	-0.102(1)	-0.132(1)	0.5380(8)	4.5(4)

Table A4.1 (cont.). Positional and Thermal Parameters and Their Estimated Standard Deviations for $Pb_4O_{16}N_4C_{56}H_{76}$, **3.**

Atom	x	y	z	B(A2)
C21	-0.239(1)	-0.084(1)	0.5032(8)	4.1(3)
C22	-0.272(1)	-0.102(1)	0.4220(8)	3.4(3)
C23	-0.068(2)	-0.116(1)	0.6324(9)	6.4(5)
C24	-0.264(1)	-0.2690(9)	0.2788(7)	2.6(3)
C25	-0.288(1)	-0.382(1)	0.3628(8)	4.0(3)
C26	-0.274(2)	-0.484(1)	0.322(1)	7.8(5)
C27	-0.188(2)	-0.427(1)	0.444(1)	10.6(6)
C28	-0.438(2)	-0.348(1)	0.406(1)	8.5(5)
H1	0.44154(1)	-0.21864(1)	-0.05090(1)	4.1*
H2	0.56794(1)	-0.22748(1)	-0.20264(1)	5.3*
H3	0.21363(1)	-0.25177(1)	-0.29461(1)	4.9*
H4	0.08138(1)	-0.23708(1)	-0.14511(1)	3.8*
H5	0.04125(1)	-0.25292(1)	0.36224(1)	4.1*
H6	0.09632(1)	-0.21919(1)	0.50131(1)	6.2*
H7	-0.31072(1)	-0.03691(1)	0.53809(1)	5.3*
H8	-0.36617(1)	-0.07074(1)	0.40192(1)	4.4*
H9	0.41090(1)	-0.25592(1)	-0.40083(1)	8.2*
H10	0.51220(1)	-0.17893(1)	-0.39382(1)	8.2*
H11	0.55186(1)	-0.32043(1)	-0.35029(1)	8.2*
H12	-0.29022(1)	-0.55419(1)	0.37515(1)	11.1*
H13	-0.34465(1)	-0.46066(1)	0.27699(1)	11.1*
H14	-0.18291(1)	-0.50085(1)	0.29120(1)	11.1*
H15	-0.21296(1)	-0.49612(1)	0.49363(1)	14.1*
H16	-0.09401(1)	-0.44730(1)	0.41826(1)	14.1*
H17	-0.19847(1)	-0.36319(1)	0.47358(1)	14.1*
H18	-0.46106(1)	-0.41465(1)	0.46027(1)	11.6*
H19	-0.45063(1)	-0.27908(1)	0.42976(1)	11.6*
H20	-0.50426(1)	-0.32663(1)	0.35752(1)	11.6*

Starred atoms were included with isotropic thermal parameters.
The thermal parameter given for anisotropically refined atoms is the isotropic equivalent thermal parameter defined as:

$(4/3) * [a^2*\beta(1,1) + b^2*\beta(2,2) + c^2*\beta(3,3) + ab(\cos\gamma)*\beta(1,2)$

$+ ac(\cos\beta)*\beta(1,3) + bc(\cos\alpha)*\beta(2,3)]$

where a,b,c are real cell parameters, and $\beta(i,j)$ are anisotropic betas.

Table A4.2. Intramolecular Distances and Their Estimated Standard Deviations for $Pb_4O_{16}N_4C_{56}H_{76}$, **3**.

Atom 1	Atom 2	Distance (Å)	Atom 1	Atom 2	Distance (Å)
Pb1	Pb1'	4.058(1)	Pb1'	Pb2	4.152(1)
Pb1	Pb2	4.229(1)	Pb2	Pb2'	3.859(1)
Pb1	O1	2.743(7)	Pb2	O1	2.566(8)
Pb1	O3	2.357(7)	Pb2	O2	2.689(8)
Pb1	O3'	2.554(6)	Pb2	O6	2.688(7)
Pb1	O4	2.303(8)	Pb2	O7	2.292(7)
Pb1	O8	2.518(7)	Pb2	O8'	2.276(7)
Pb1	O5'	2.923(8)	Pb2	O5	2.909(8)
			Pb2	O3	2.949(7)
			Pb2'	O5	3.238
			Pb2'	O2	3.595
O1	C1	1.290(12)	O3	N1	1.393(10)
O2	C1	1.270(12)	O8	N2	1.407(10)
O4	C10	1.253(13)	N1	C3	1.453(14)
O5	C15	1.259(12)	N1	C10	1.357(14)
O6	C15	1.248(12)	N2	C17	1.448(14)
O7	C24	1.286(13)	N2	C24	1.303(14)
C1	C2	1.183(13)	C1	C8	3.930(16)
C3	C4	1.345(16)	C1	C14	3.64(3)
C3	C8	1.394(16)	C1	C15	3.539(13)
C4	C5	1.396(17)	C2	C5	3.777(16)
C5	C6	1.398(18)	C2	C8	3.390(15)
C6	C7	1.348(17)	C2	C12	3.763(18)
C6	C9	1.498(18)	C2	C14	3.711(24)
C7	C8	1.397(16)	C2	C14	3.89(3)
C10	C11	1.533(17)	C2	C15	3.547(13)
C11	C12	1.467(20)	C2	C16	3.900(12)
C11	C13	1.423(21)	C2	C23	3.345(16)
C11	C14	1.78(3)	C3	C6	2.750(16)
C15	C16	1.224(13)	C3	C10	2.556(16)
C17	C18	1.371(15)	C3	C11	3.154(18)
C17	C22	1.373(16)	C3	C12	2.921(18)
C18	C19	1.397(17)	C3	C14	3.90(3)
C19	C20	1.377(19)	C3	C14'	3.72(5)
C20	C21	1.417(18)	C4	C7	2.724(17)
C20	C23	1.531(18)	C4	C9	3.797(19)
C21	C22	1.362(17)	C4	C10	3.372(17)
C24	C25	1.525(15)	C4	C11	3.843(20)
C25	C26	1.480(20)			
C25	C27	1.502(21)			
C25	C28	1.507(22)			

Table A4.3. Intramolecular Angles and Their Estimated Standard Deviations for $Pb_4O_{16}N_4C_{56}H_{76}$, **3.**

Atom 1	Atom 2	Atom 3	Angle (°)	Atom 1	Atom 2	Atom 3	Angle (°)
O3	Pb1	O3'	68.6(3)	Pb1	O3	Pb1'	111.4(3)
O3	Pb1	O4	67.89(24)	Pb1'	O8	Pb2	119.9(3)
O3	Pb1	O8	111.79(23)	Pb1	O1	Pb2	105.5
O3	Pb1	O4	109.5(3)				
O3	Pb1	O8	70.40(21)	Pb1	O3	N1	113.7(5)
O4	Pb1	O8	77.9(3)	Pb1'	O3	N1	114.9(5)
				Pb1	O8	N2	117.5(5)
O1	Pb2	O7	81.07(25)	Pb2	O8	N2	111.9(5)
O1	Pb2	O8	88.71(24)	Pb2	O1	C1	99.5(6)
O7	Pb2	O8	68.9(3)				
O7	Pb2	O2	73.77	Pb2	O1	C1	99.5(6)
O7	Pb2	O5	80.94	Pb1	O4	C10	121.1(7)
O7	Pb2	O6	72.56	Pb2	O7	C24	116.3(7)
O8	Pb2	O2	126.80				
O8	Pb2	O5	125.53	C4	C3	C8	122.8(11)
O8	Pb2	O6	82.20	C3	C4	C5	120.1(12)
O1	Pb2	O2	48.58	C4	C5	C6	119.0(12)
O1	Pb2	O5	130.88	C5	C6	C7	118.7(12)
O1	Pb2	O6	153.63	C5	C6	C9	121.6(13)
O2	Pb2	O5	82.52	C7	C6	C9	119.6(14)
O2	Pb2	O6	120.65	C6	C7	C8	123.9(12)
O5	Pb2	O6	45.07	C3	C8	C7	115.4(11)
				C10	C11	C12	120.4(13)
O3	N1	C3	111.0(8)	C10	C11	C13	110.5(14)
O3	N1	C10	118.1(9)	C10	C11	C14	99.6(14)
O8	N2	C17	110.3(8)	C12	C11	C13	125.9(14)
O8	N2	C24	118.9(8)	C12	C11	C14	96.8(17)
				C13	C11	C14	91.4(18)
N1	C10	O4	117.9(10)	C18	C17	C22	121.1(11)
N2	C24	O7	117.7(9)	C17	C18	C19	119.5(12)
C2	C1	O1	121.4(10)	C18	C19	C20	120.8(13)
C2	C1	O2	123.1(11)	C19	C20	C21	117.5(12)
C11	C10	O4	118.9(11)	C19	C20	C23	121.3(14)
C16	C15	O5	119.2(10)	C21	C20	C23	121.1(14)
C16	C15	O6	122.3(10)	C20	C21	C22	121.6(12)
C25	C24	O7	116.6(11)	C17	C22	C21	119.3(12)
O1	C1	O2	115.4(9)	C24	C25	C26	109.1(11)
O5	C15	O6	118.5(9)	C24	C25	C27	115.8(12)
				C24	C25	C28	105.9(11)
				C26	C25	C27	107.6(14)
				C26	C25	C28	109.5(14)
				C27	C25	C28	108.9(15)

Table A4.4. Anisotropic Thermal Factors[a] ($Å^2$) for $Pb_4O_{16}N_4C_{56}H_{76}$, **3.**

Atom	B(11)	B(22)	B(33)	B(12)	B(13)	B(23)	B(eqv.)
Pb1	1.89(2)	2.48(1)	1.99(1)	-0.79(1)	-0.16(1)	-0.63(1)	2.074(9)
Pb2	1.96(2)	3.06(2)	2.29(2)	-0.94(1)	-0.24(1)	-0.55(1)	2.42(1)
O1	2.2(3)	3.6(3)	3.0(3)	-1.4(2)	-0.2(2)	-0.7(2)	2.8(2)
O2	4.1(3)	5.0(3)	3.8(3)	-2.6(3)	-0.1(3)	-1.8(3)	3.9(2)
O3	1.9(3)	1.7(2)	2.2(2)	-0.1(2)	-0.3(2)	-0.9(2)	1.9(2)
O4	4.2(4)	2.3(3)	3.1(3)	-0.5(3)	1.0(3)	-1.0(2)	3.3(2)
O5	3.0(3)	4.2(4)	3.1(3)	-1.2(3)	-0.3(3)	-0.1(3)	3.6(2)
O6	2.9(3)	4.2(3)	3.1(3)	-0.6(3)	-0.1(3)	-1.3(3)	3.4(2)
O7	3.7(3)	2.4(3)	3.2(3)	-1.1(2)	-0.1(3)	-1.0(2)	3.0(2)
O8	2.4(3)	3.0(3)	2.1(3)	-1.2(2)	0.1(2)	-0.2(2)	2.5(2)
N1	2.8(4)	2.1(3)	2.9(3)	-0.2(3)	0.3(3)	-1.3(3)	2.6(2)
N2	3.1(4)	2.5(4)	1.5(3)	-0.8(3)	-0.1(3)	0.1(3)	2.5(2)
C3	2.1(5)	2.5(4)	3.4(5)	0.4(4)	0.5(4)	-1.2(4)	2.8(3)
C4	2.1(4)	3.7(4)	4.5(5)	-1.1(3)	-0.3(4)	-2.2(3)	3.1(3)
C5	3.2(5)	3.2(5)	6.1(6)	-1.4(4)	1.1(5)	-1.9(4)	4.1(3)
C6	3.6(6)	3.1(5)	4.3(5)	-0.4(4)	1.3(5)	-1.9(4)	3.8(3)
C7	4.1(6)	3.6(5)	3.9(5)	-0.6(4)	-0.5(4)	-2.0(4)	3.7(3)
C8	3.4(5)	2.8(4)	3.5(4)	-0.7(4)	-0.7(4)	-2.0(3)	2.9(3)
C9	9(1)	5.4(7)	4.4(6)	-1.4(7)	2.3(6)	-2.4(5)	6.3(5)
C10	3.2(5)	2.6(5)	3.7(5)	-0.3(4)	0.1(4)	-1.0(4)	3.2(3)
C11	13(1)	1.4(5)	6.2(8)	0.5(7)	2.2(9)	-0.2(5)	8.1(6)
C12	11(1)	2.1(5)	6.8(7)	-0.4(6)	2.5(8)	-2.3(5)	6.9(5)
C13	15(1)	2.5(6)	6.2(8)	-0.1(8)	1.8(9)	0.4(6)	8.9(6)
C14	7(1)	2.9(7)	19(2)	-3.2(7)	1(1)	-5.4(9)	8.9(9)
C14'	9(2)	2(2)	14(3)	4(2)	-9(2)	-2(2)	9(1)
C17	2.2(4)	2.7(4)	2.1(4)	-0.5(4)	0.7(4)	-0.4(3)	2.5(3)
C18	3.2(5)	3.7(5)	2.5(4)	-0.1(4)	-0.1(4)	-1.4(4)	3.2(3)
C19	4.0(6)	6.0(7)	4.3(5)	-0.5(5)	-1.5(5)	-1.4(5)	4.8(4)
C20	6.6(7)	4.7(6)	2.6(5)	-2.0(5)	-0.5(5)	-0.8(4)	4.5(4)
C21	3.7(6)	5.4(6)	3.8(5)	-1.3(5)	0.9(5)	-2.5(4)	4.1(3)
C22	3.4(5)	3.6(5)	3.0(4)	-0.7(4)	-0.6(4)	-0.7(4)	3.4(3)
C23	10(1)	7.1(7)	2.8(5)	-1.3(7)	-1.7(5)	-2.0(5)	6.4(5)
C24	2.6(5)	2.6(4)	2.4(4)	-1.0(4)	0.4(4)	-0.3(4)	2.6(3)
C25	5.4(6)	3.7(5)	2.9(5)	-2.3(4)	-0.1(5)	-0.3(4)	4.0(3)
C26	15(1)	4.1(6)	5.1(7)	-4.6(6)	-1.3(8)	-0.3(5)	7.8(5)
C27	16(1)	6.1(8)	8.3(8)	-6.1(7)	-6.9(8)	5.1(7)	10.6(6)
C28	10(1)	5.3(8)	7.6(9)	-2.7(7)	4.9(8)	-0.3(7)	8.5(5)

[a]The form of the anisotropic temperature factor is:
$\exp[-0.25\{h^2a^2B(1,1) + k^2b^2B(2,2) + l^2c^2B(3,3) + 2hkabB(1,2) + 2hlacB(1,3) + 2klbcB(2,3)\}]$ where a,b, and c are reciprocal lattice constants.

Table A4.5. Root-mean Square Amplitudes of Thermal Vibration in Angstroms for $Pb_4O_{16}N_4C_{56}H_{76}$, **3.**

Atom	Min.	Int'med.	Max.	Atom	Min.	Int'med.	Max.
Pb1	0.145	0.159	0.180	C10	0.175	0.202	0.227
Pb2	0.147	0.170	0.204	C11	0.131	0.263	0.469
O1	0.144	0.193	0.222	C12	0.134	0.264	0.418
O2	0.163	0.217	0.273	C13	0.168	0.285	0.477
O3	0.133	0.158	0.175	C14	0.028	0.294	0.502
O4	0.161	0.178	0.263	C14'	0.031	0.268	0.502
O5	0.183	0.196	0.257	C17	0.129	0.180	0.218
O6	0.186	0.198	0.233	C18	0.163	0.196	0.235
O7	0.161	0.199	0.220	C19	0.191	0.255	0.285
O8	0.141	0.178	0.213	C20	0.181	0.233	0.292
N1	0.138	0.190	0.208	C21	0.173	0.229	0.272
N2	0.126	0.198	0.202	C22	0.187	0.213	0.222
C3	0.121	0.200	0.231	C23	0.158	0.300	0.356
C4	0.134	0.194	0.248	C24	0.142	0.192	0.207
C5	0.173	0.197	0.294	C25	0.174	0.215	0.272
C6	0.147	0.215	0.274	C26	0.187	0.263	0.439
C7	0.174	0.223	0.244	C27	0.137	0.318	0.533
C8	0.126	0.204	0.229	C28	0.178	0.289	0.457
C9	0.186	0.265	0.369				

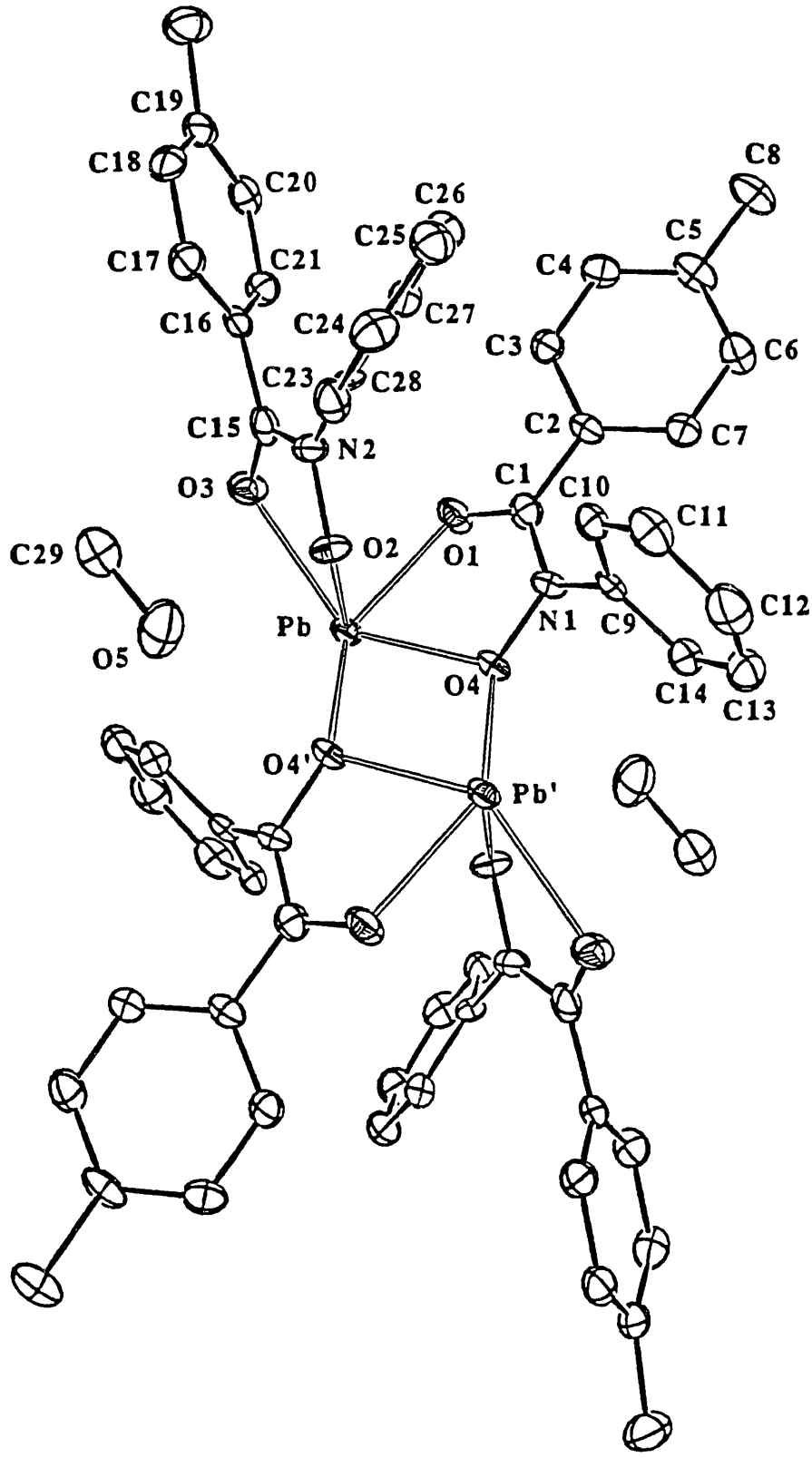

Figure A1.1. Fully labeled ORTEP view of bis(N-phenyltoluylhydroxamato)-bis(m-N-phenyltoluylhydroxamato)-dilead(II)-dimethanol solvate (Pb2O10N4C58H56, 1) with 50% probability ellipsoids. Hydrogen atoms omitted for clarity.

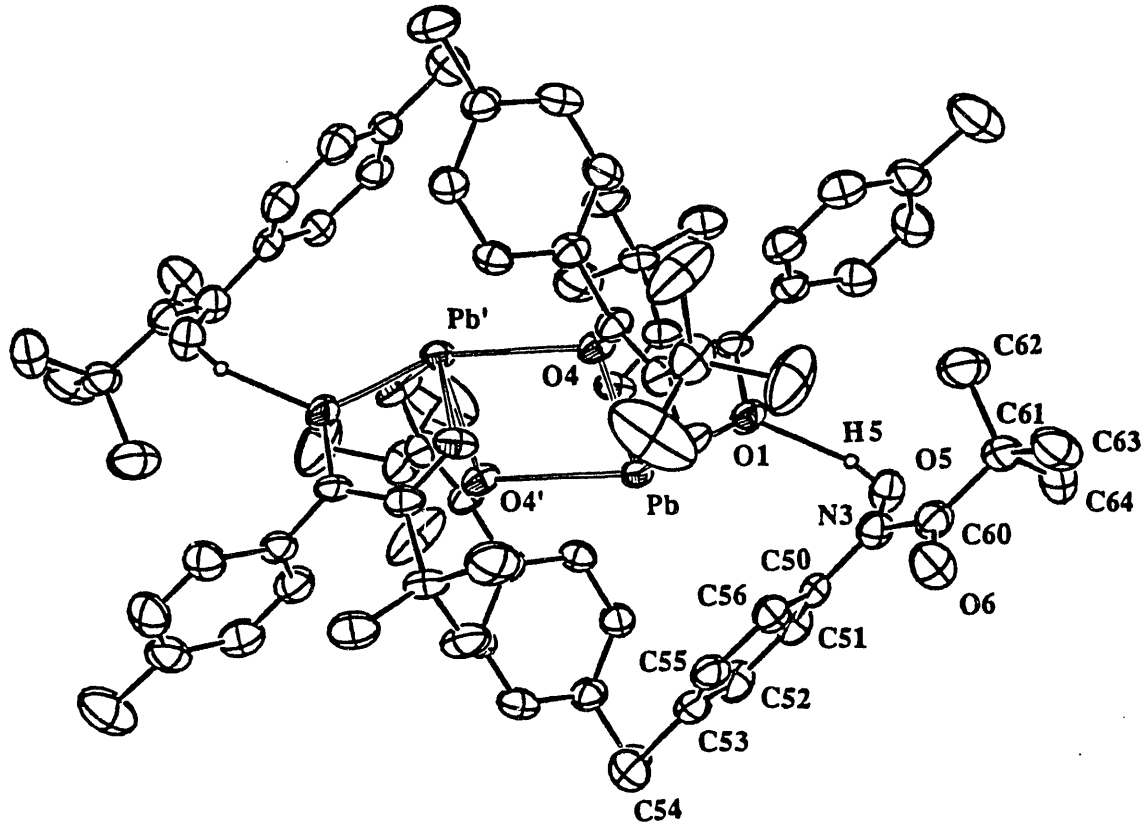

Figure A1.2. Partially labeled ORTEP view of bis(N-toluyl-*tert*-butyl-hydroxamato)-bis(μ-N-toluyl-*tert*-butyl-hydroxamato)dilead(II)·N-toluyl-*tert*-butyl-hydroxamic acid ($Pb_2O_{12}N_6C_{72}H_{114}$, **2**) with 50% probability ellipsoids Hydrogen atoms omitted for clarity.

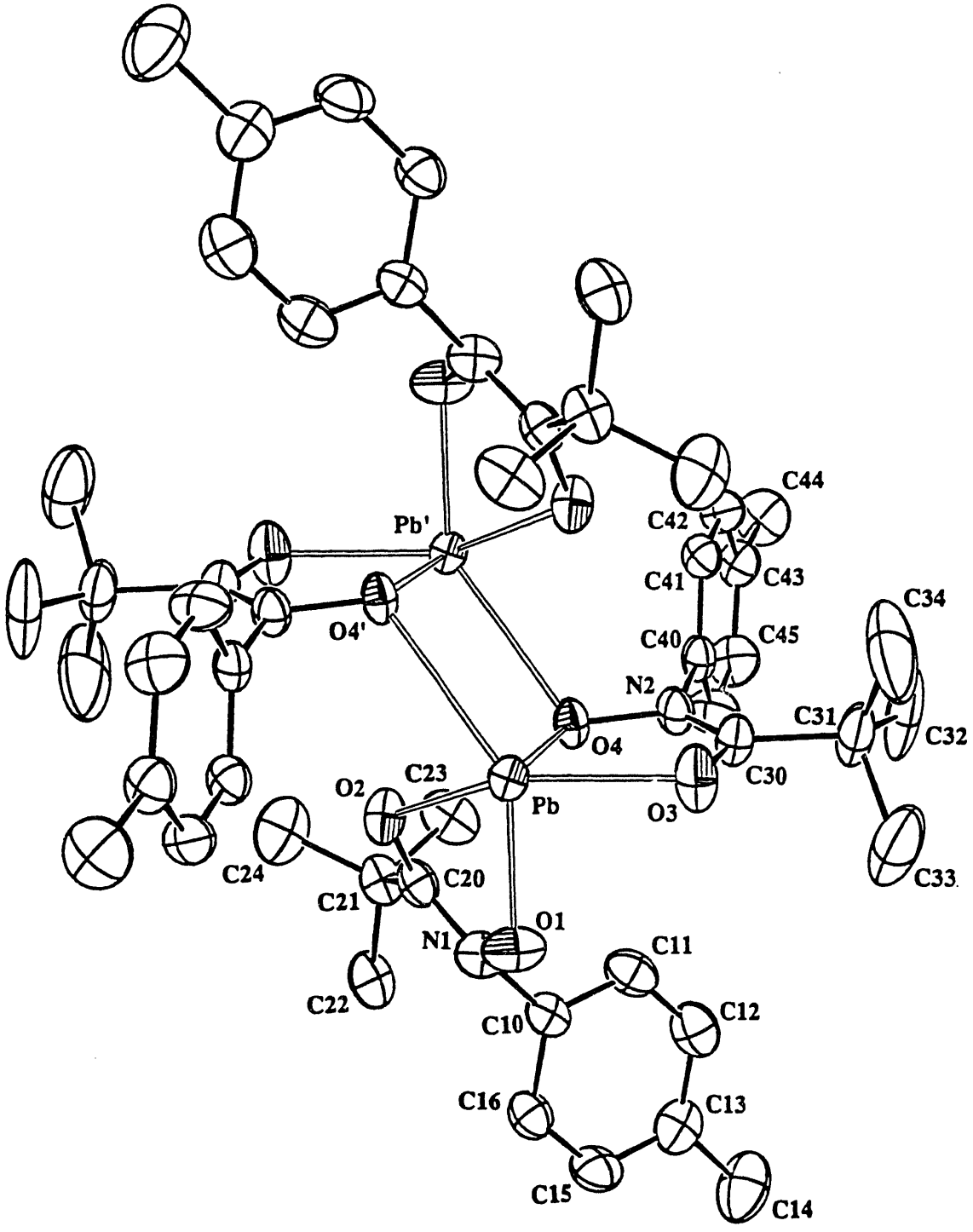

Figure A1.3. ORTEP view of the lead(II) dimer in $Pb_2O_{12}N_6C_{72}H_{114}$, **2** with 50% probability ellipsoids. Hydrogen atoms omitted for clarity.

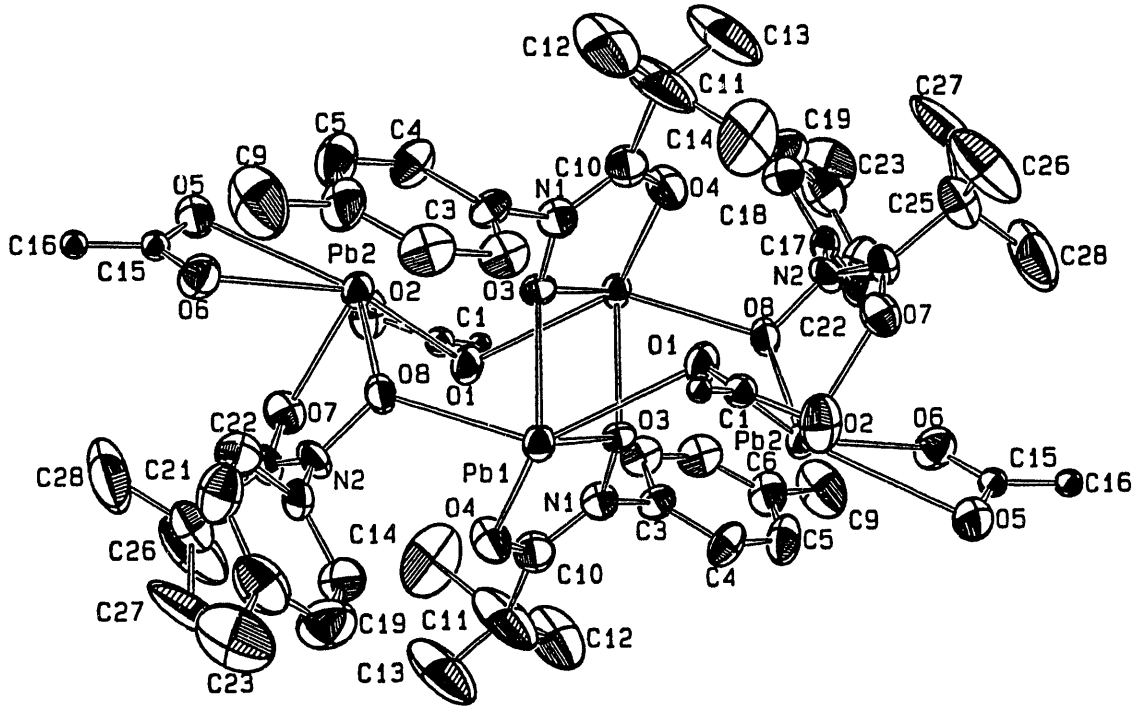

Figure A1.4. Fully labeled ORTEP view of tetra(μ-N-toluyl-*tert*-butyl-hydroxamato)-tetra(μ-acetato)-tetralead(II) ($Pb_4O_{16}N_4C_{56}H_{76}$, **3**) with 50% probability ellipsoids. Hydrogen atoms omitted for clarity.

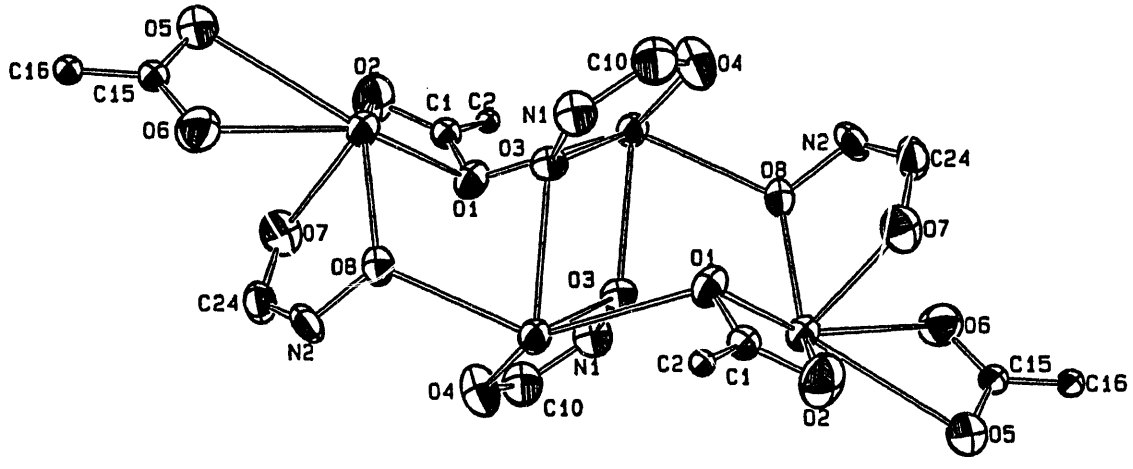

Figure A1.5. Fully labeled ORTEP view of the lead coordination sphere in $Pb_4O_{16}N_4C_{56}H_{76}$, **3** with 50% probability ellipsoids.

APPENDIX 2: Plutonium (IV)-Desferrioxamine B Solution Chemistry.

The determination of stability constants for the plutonium(IV)-DFO complexes has been introduced earlier in this dissertation. This appendix includes data collected in attempts to determine the formation constants, both by spectrophotometric competition titrations, and by direct titration, following the method used by Jarvis and Hancock.[1]

To establish the stoichiometry of plutonium(IV)-DFO complexes, spectra were obtained for Pu^{4+} in the presence of varying amounts of the ligand, at pH = 1, 3, and above 6. Spectra measured for solutions at pH = 1, shown in Figure A2.1, have increasing absorbances at ~400 and ~670 nm with increasing ligand concentration until a ligand to metal ratio of 1.5:1 is reached, indicating that at low pH a 3:2 complex is formed. At higher pH, shown in Figure A2.2, an absorbance band tailing into the UV increases with increasing ligand concentration. Unfortunately, these spectra were measured using a fiber optic spectrometer with fibers which absorb in the UV, precluding measurement of the absorbance band; therefore, it is difficult to conclude if the species present above pH 6 is a 1:1 or 3:2 ligand to metal species, or if there is a shift in the absorbance maxima corresponding to an equilibrium such as $Pu_X(DFO)_y$ --> $Pu_X(DFO)_y(OH)_z$.

Attermpting to reproduce the result of Jarvis and Hancock[1], a 1:1, DFO:Pu^{4+} solution was titrated with acid, from pH 5.0 to approximately 0.7. The spectra obtained, shown in Figures A2.3, differed substantially from those reported by Jarvis and Hancock. The spectrum measured at pH 5.0 contains a shoulder at ~360 nm. When the pH was decreased to 2.46 a band centered at 366 nm grew in, and at pH ~ 0.7 there are absorbance maxima at 38 and 410 nm. Most significantly, neither the spectra measured at high acid concentration, nor the spectrum Jarvis and Hancock report, corresponds to the uncomplexed metal in the presence of protonated ligand, appear to be Pu^{4+} plus H_3DFO. A similar set of acid titration spectra was collected with the ligand to metal ratio was 3:2; these data are shown in Figure A2.4. Again, as the pH was decreased a shoulder at 360 nm was red shifted, and when the acid concentration was quite high (1 and 3 M for the last two spectra) two absorbance maxima were present at 385 and 415 nm. For reference, the extinction coefficient spectra of Pu^{4+} in 0.1 M $HClO_4$, and of protonated and deprotonated forms of DFO are presented in Figure A2.5. The Pu^{4+} spectrum contains several distinct absorbance bands in the visible range. The protonated ligand has an absorbance maxima at 208 nm (ε ~ 40,000 Abs.*M^{-1}*cm^{-1}) and virtually no absorbance in the UV/visible range at wavelengths longer than 250 nm; and the deprotonated ligand has an absorbance band at 232 nm (ε = 23,000 Abs.*M^{-1}*cm^{-1}) with

virtually no absorbance at wavelengths longer than 273 nm. Clearly, a spectrum of a solution containing free Pu^{4+} in the presence of protonated DFO should look like a sum of the extinction coefficient spectra in Figure A2.5 and would contain characteristic Pu^{4+} absorbance bands in the visible region. A possible explanation for the spectra observed is decomposition of DFO in strong acid solutions, presumably via clevage at the amide groups. Decomposition of DFO under similar conditions has been postulated in the report of the solution structure of Ga^{3+}-DFO[2] and was reported to occur in a study of the Fe^{3+} complex.[3]

Two spectrophotometric titrations of Pu^{4+}-DFO, in which EDTA was used as a competitor, have been performed. One of the data sets, where the pH was varied from 4.8 to 7.9, is shown in Figure A2.6. The spectrum of the Pu^{4+}-EDTA complex contains relatively strong absorbance bands at 450 and 500 nm. Upon addition of DFO there is a strong absorbance in the UV; even when EDTA is present at concentrations where the EDTA to DFO ratio is 60 to 1 this change is observed. These data suggest that either the Pu^{4+}-DFO complex is so strong that no amount of EDTA can force the equilibrium back to Pu^{4+}-EDTA, or that a mixed ligand species is formed. As the pH is increased in Pu^{4+}/DFO/EDTA titrations to favor a Pu^{4+}-DFO species, the Pu^{4+}-EDTA bands disappear and a band at ~410 nm grows in. Unfortunately, the data could not be modeled with equilibria corresponding to simple competition, such as:

$$Pu^{4+} - EDTA \;\Leftrightarrow\; Pu^{4+} - DFO - EDTA \;\Leftrightarrow\; Pu^{4+} - DFO$$

Attempting to identify the stoichiometry of the species and the equilibria, spectra for Pu^{4+}-DFO as EDTA was added to the solution were measured. The spectra obtained, shown in Figure A2.7, show that as more EDTA is added the absorbance band tailing into the UV remains, the Pu^{4+} is not all present as the Pu^{4+}-EDTA complex, and addition of EDTA shifts the equilibrium from a Pu^{4+}-DFO species to a Pu^{4+}-DFO-EDTA species. Further additions of EDTA did not affect the spectrum. However, with the addition of base intensity of the UV band increased, the absorbance maxima shifted to ~410 nm and the band at ~500 nm disappeared, indicating a Pu^{4+}-DFO species is reformed and the equilibrium is reversible. The base titration is shown in Figure A2.9. A model which was consistent with the data and fit the competition spectrophotometric titration data shown in Figure A2.6 consists of:

$$Pu_2(DFO)_2(HEDTA)^+ + H_3DFO^+ \Leftrightarrow Pu_2(DFO)_2(HDFO) + H_2EDTA^{2-} + H^+$$

$$Pu_2(DFO)_2(HDFO) \Leftrightarrow Pu_2(DFO)_3^- + H^+$$

This model with the formation constants , $\log\beta_{2300} = 85.5$, $\log\beta_{2301} = 92.5$, and $\log\beta_{2211} = 85.7$, successfully fit the data while no other models would.

One of the complications of investigating equilibria involving a hexadentate ligand and a metal with a preferred coordination number of eight and large hydrolysis constants, is the possibility of hydroxo and/or aquo species. The use of EDTA as a competitor further complicates the system by adding the possibility of mixed ligand species. Use of bands which extend into the UV having absorbances with larger error and are ill defined with respect to band shape, adds more uncertainty to our analysis. In the future, the spectral region from 450 to 750 nm should be considered more carefully to monitor the appearance/disappearance of Pu^{4+}-EDTA absorbance bands, and to identify characteristic bands for one or more mixed ligand species, even if this requires the use of higher concentrations of Pu^{4+}.

References

(1) Jarvis, N. V.; Hancock, R. D. *Inorg. Chim. Acta* **1991**, *182*, 229.

(2) Borgias, B.; Hugi, A. D.; Raymond, K. N. *J. Am. Chem. Soc.* **1989**, *28*, 3538.

(3) Schwarzenbach, G.; Schwarzenbach, K. *Helv. Chim. Acta.* **1963**, *46*, 1390.

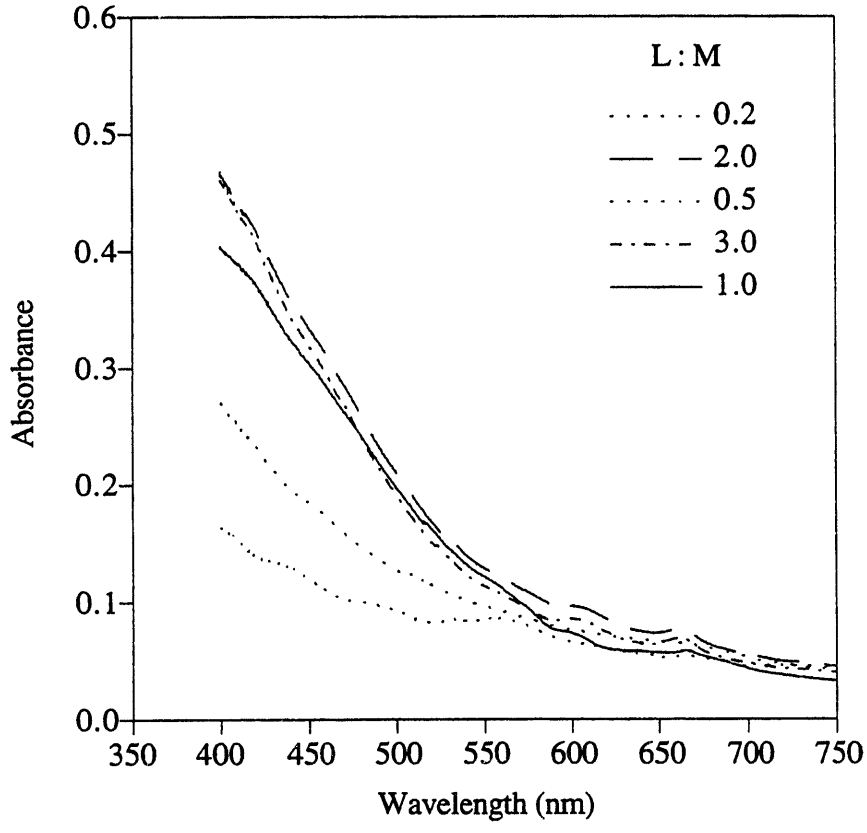

Figure A2.1. Visible spectra of Pu4+-DFO solutions where the pH is 1, [Pu4+] = 8.71 x 10-4 M, and [DFO] is varied from 1.74 x 10-4 to 1.74 x 10-3 M.

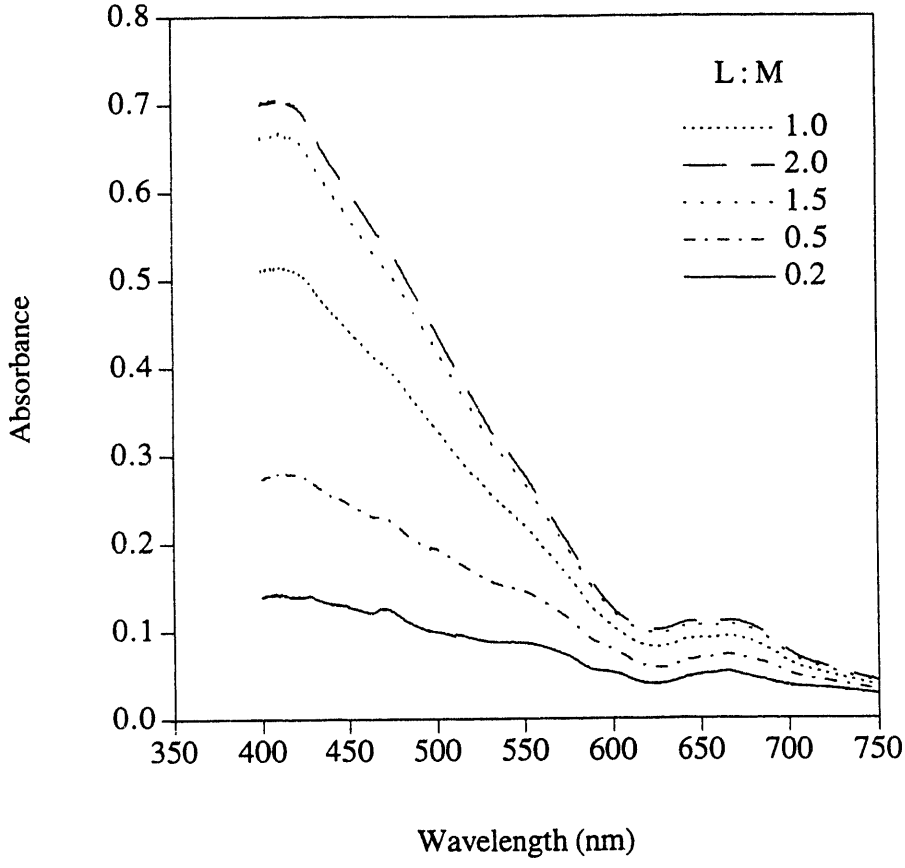

Figure A2.2. Visible spectra of Pu^{4+}-DFO solutions where the pH is >6, $[Pu^{4+}] = 6.33 \times 10^{-4}$ M, and [DFO] is varied from 1.27×10^{-4} to 1.90×10^{-3} M.

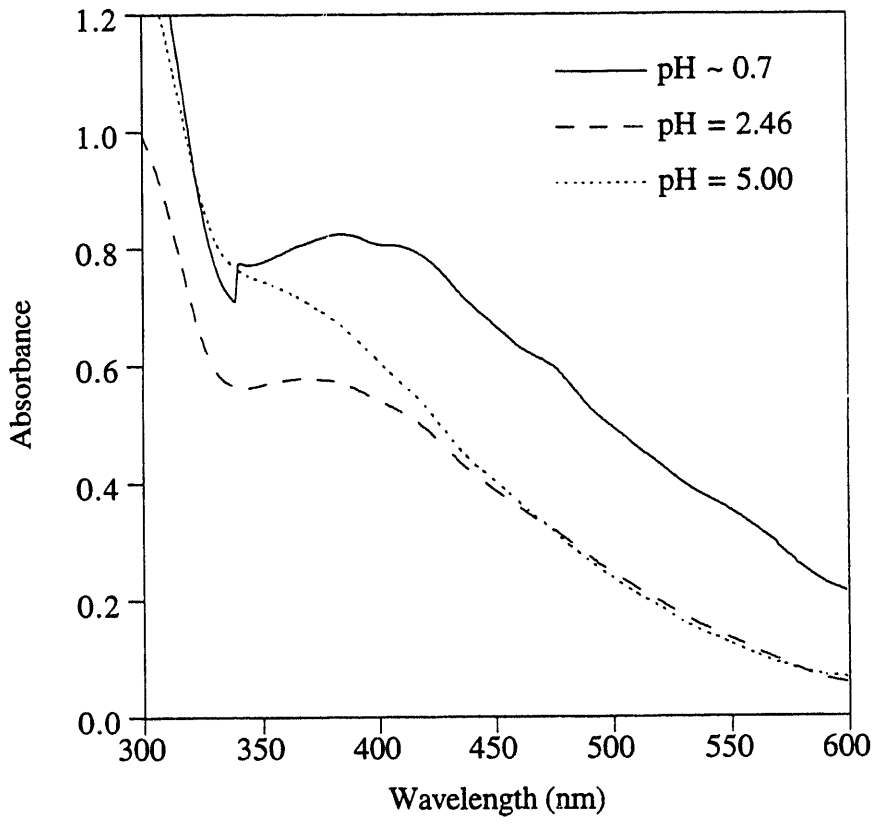

Figure A2.3. Titration of Pu^{4+}-DFO, where $[Pu^{4+}]$ = [DFO] = 1.13 mM and pH was increased from ~0.7 to 5.34.

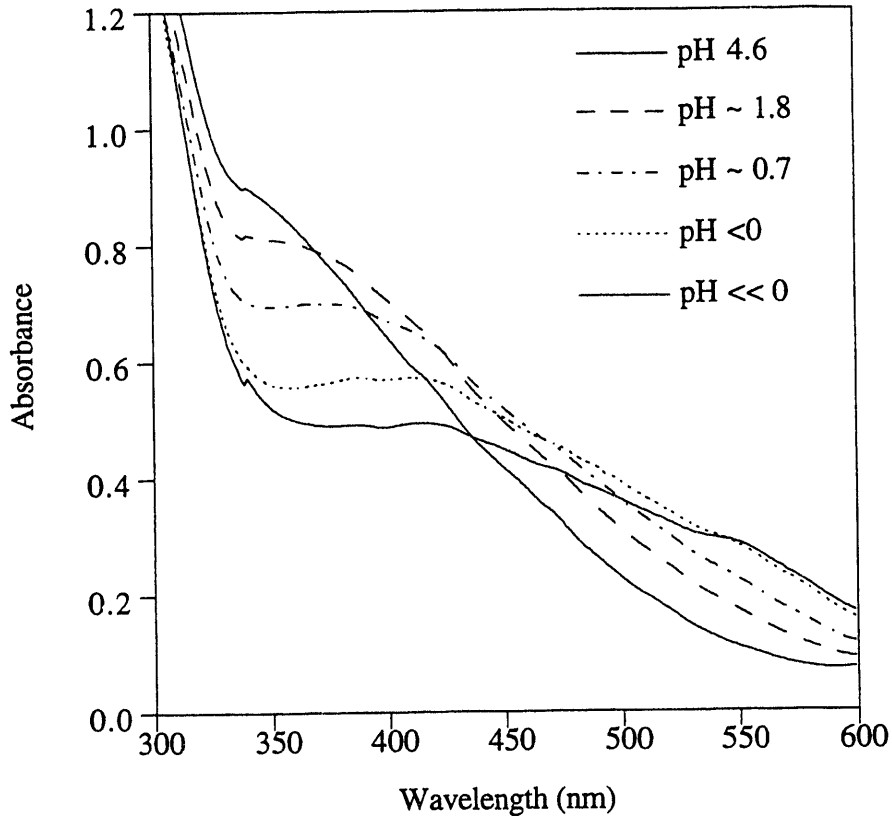

Figure A2.4. Titration of Pu^{4+}-DFO, where $[Pu^{4+}] = (2/3)[DFO] = 1.13$ mM and pH was decreased from 4.6 to ~0.7. The final acid concentration was ~3 M.

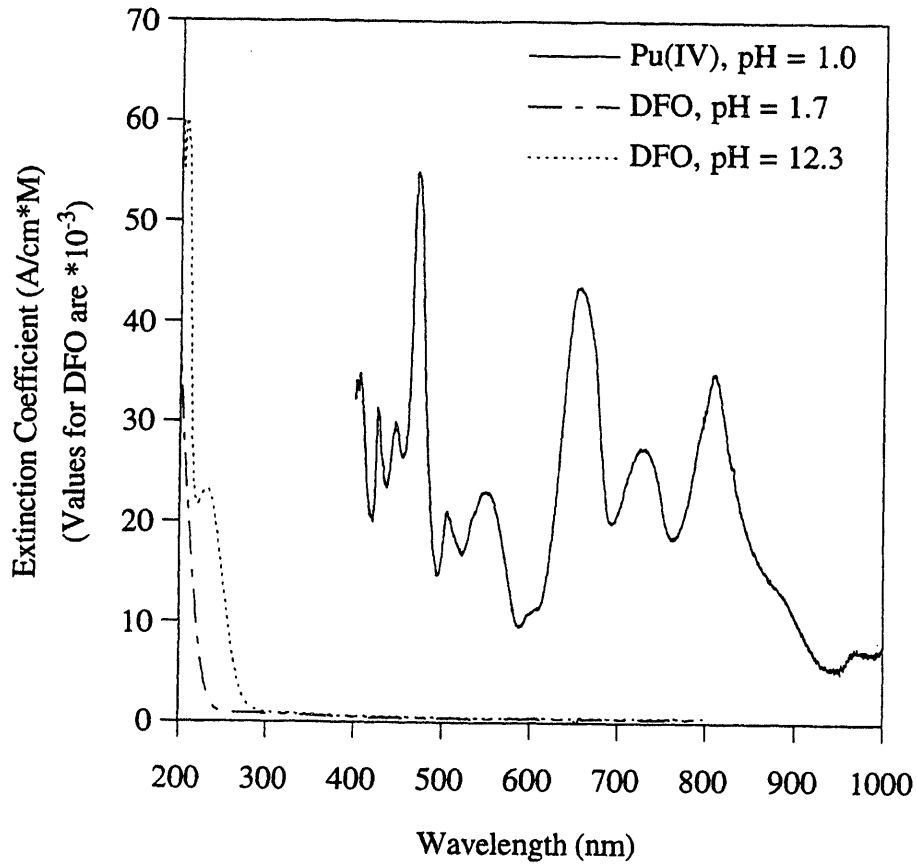

Figure A2.5. Extinction coefficient spectra of Pu^{4+} and protonated and deprotonated forms of DFO. The Pu^{4+} spectrum was generated from an absorbance spectrum of 1.96 mM Pu^{4+} in 0.1 M $HClO_4$ and the ligand spectra were generated from absorbance spectra of 5.0 x 10^{-4} M DFO solutions at pH 1.7 and 12.3.

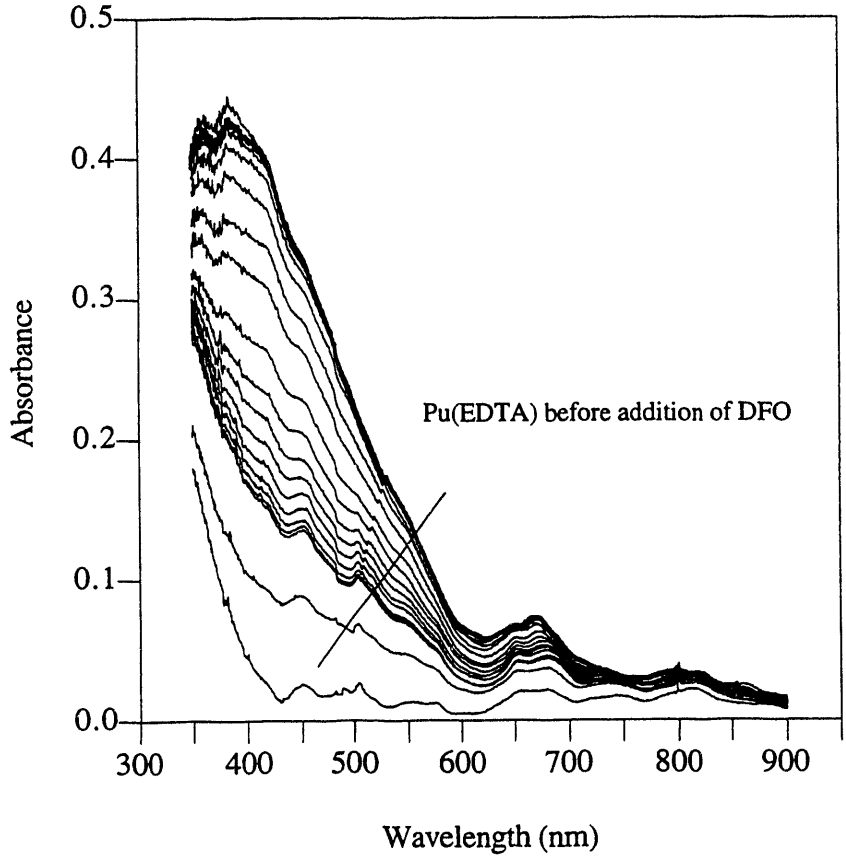

Figure A2.6. Ultra violet/visible spectra collected during a titration of Pu^{4+}/DFO/EDTA, where $[Pu^{4+}]$ = 0.62 mM, [DFO] = 0.931 mM, [EDTA] = 56.0 mM and pH was increased from 4.8 to 7.9.

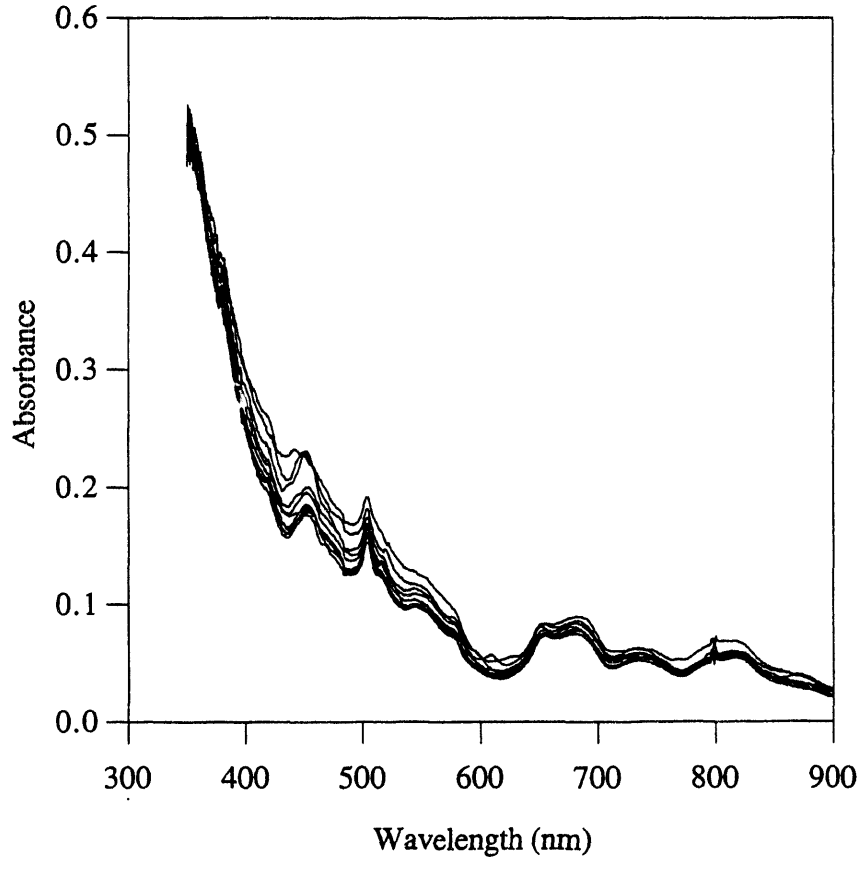

Figure A2.7. Ultra violet/visible spectra collected during a titration of Pu^{4+}/DFO with EDTA, where [Pu^{4+}] = 0.62 mM, [DFO] = 0.931 mM, pH = 2.0 to 2.7, and [EDTA] was varied from 0.931 mM to 56.0 mM.

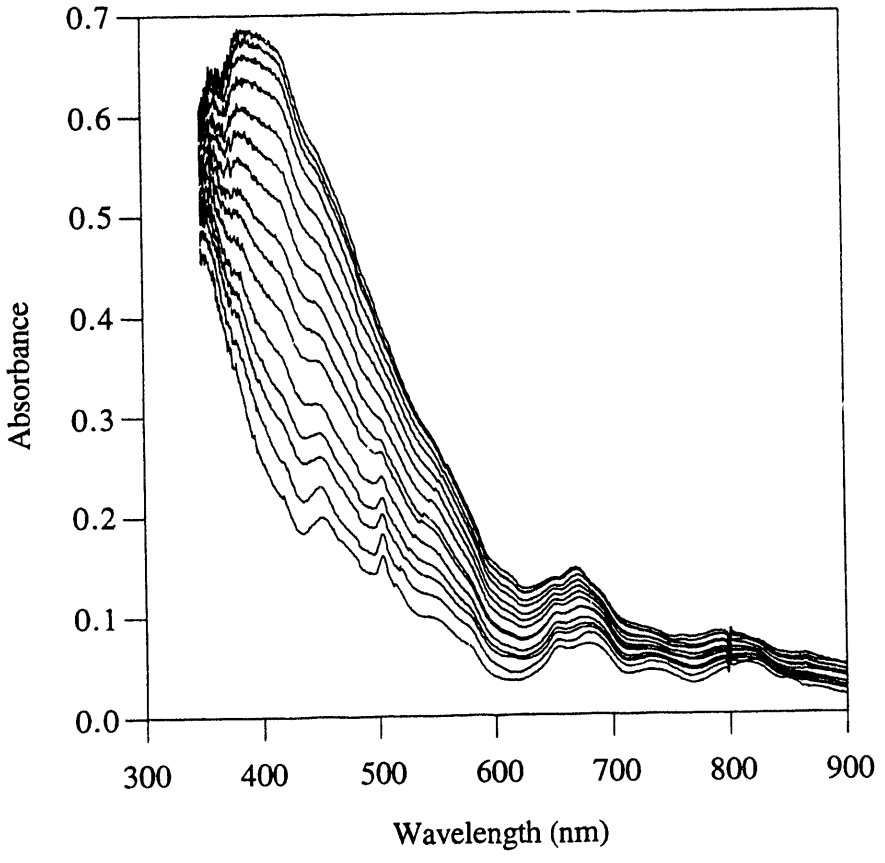

Figure A2.8. Ultra violet/visible spectra collected during a base titration of Pu^{4+}/DFO/EDTA,
where $[Pu^{4+}]$ = 0.62 mM, [DFO] = 0.931 mM, [EDTA] = 56.0 mM and pH was increased from 2.7 to 7.8.

DATE
FILMED
2/3/94
END